22

0-315-12338-9

National Library of Canada — Bibliothèque nationale du Canada

Canadian Theses Division — Division des thèses canadiennes

Ottawa, Canada
K1A 0N4

60249

PERMISSION TO MICROFILM — AUTORISATION DE MICROFILMER

• Please print or type — Écrire en lettres moulées ou dactylographier

Full Name of Author — Nom complet de l'auteur

LAW HIN-SUM

Date of Birth — Date de naissance	Country of Birth — Lieu de naissance
NOV 5 1951	HONG KONG

Permanent Address — Résidence fixe

#105 12415 LANSDOWNE DR. EDMONTON ALBERTA
T6H 4L4

Title of Thesis — Titre de la thèse

MASS TRANSFER DUE TO A CONFINED LAMINAR IMPINGING TWO-DIMENSIONAL JET

University — Université

U. OF ALBERTA

Degree for which thesis was presented — Grade pour lequel cette thèse fut présentée

Ph. D.

Year this degree conferred — Année d'obtention de ce grade	Name of Supervisor — Nom du directeur de thèse
1982	MASLIYAH, J. H

Date	Signature
Oct. 14 1982	Hin-Sum Law

NL-91 (4/77)

THE UNIVERSITY OF ALBERTA

MASS TRANSFER DUE TO A CONFINED LAMINAR IMPINGING TWO-DIMENSIONAL JET

by

HIN-SUM LAW

A THESIS

SUBMITTED TO THE FACULTY OF GRADUATE STUDIES AND RESEARCH

IN PARTIAL FULFILMENT OF THE REQUIREMENTS FOR THE DEGREE

OF DOCTOR OF PHILOSOPHY

DEPARTMENT OF CHEMICAL ENGINEERING

EDMONTON, ALBERTA

FALL 1982

THE UNIVERSITY OF ALBERTA

RELEASE FORM

NAME OF AUTHOR HIN-SUM LAW

TITLE OF THESIS MASS TRANSFER DUE TO A CONFINED LAMINAR IMPINGING TWO-DIMENSIONAL JET

DEGREE FOR WHICH THESIS WAS PRESENTED DOCTOR OF PHILOSOPHY

YEAR THIS DEGREE GRANTED FALL 1982

Permission is hereby granted to THE UNIVERSITY OF ALBERTA LIBRARY to reproduce single copies of this thesis and to lend or sell such copies for private, scholarly or scientific research purposes only.

The author reserves other publication rights, and neither the thesis nor extensive extracts from it may be printed or otherwise reproduced without the author's written permission.

(SIGNED) Hin-Sum Law......

PERMANENT ADDRESS:

#105 12415 Lansdowne Dr.

Edmonton Alberta

T6H 4L4

DATED October 7 1982

THE UNIVERSITY OF ALBERTA

FACULTY OF GRADUATE STUDIES AND RESEARCH

The undersigned certify that they have read, and recommend to the Faculty of Graduate Studies and Research, for acceptance, a thesis entitled MASS TRANSFER DUE TO A CONFINED LAMINAR IMPINGING TWO-DIMENSIONAL JET submitted by HIN-SUM LAW in partial fulfilment of the requirements for the degree of DOCTOR OF PHILOSOPHY.

J. Masliyah
Supervisor

David Wilson

C Kiparissides

....

Arun S. Mujumdar
External Examiner

Date Oct 7/82

To My Wife

Julie

ABSTRACT

Local mass transfer due to the impingement of a confined laminar two-dimensional air jet on a flat surface has been studied. The influence of the jet Reynolds number and the jet-to-plate spacing on the local mass transfer were investigated. The range of Reynolds number was 100 to 400 with the slot width, b, taken as the characteristic length. The jet-to-plate spacings were 2b, 4b and 12b. Experimental mass transfer studies were made using a swollen polymer method coupled with laser holography interferometric techniques.

The local Sherwood number along the impingement plate was found to exhibit a local minimum and a local maximum in the region away from the jet centre. The locations of the extrema points were a function of the jet Reynolds number and jet-to-plate spacing.

A two-dimensional numerical study was also made simulating the experimental set-up. The momentum and transport equations were numerically solved using hybrid differencing schemes (upstream-weighted and upstream schemes). The numerical study confirmed the presence of the local extrema in the Sherwood number. Contours of the flow stream function indicated that the presence of the Sherwood number extrema is due to flow recirculation in the region between the confinement plate and the impingement surface.

Excellent agreement was obtained between the measured local Sherwood numbers and those computed using the numerical solution of the transport equations.

ACKNOWLEDGEMENT

The author wishes to acknowledge the assistance given by the following during the course of this work:

1. Professor Jacob H. Masliyah, the author's supervisor, for providing the valuable advice and necessary guidance to complete this work. His effort is deeply appreciated.
2. Dr. K. Nandakumar, for several helpful discussions of the general numerical problem.
3. Jerry Moser, for the design and construstion of the hologram-recording system at the initial stage of this work.
4. Keith Faulder and the staff of the workshop, for the invaluable assistance of the experimental equipment throughout this work.
5. Don Sutherland and the staff of the instrument shop, for their contributions throughout this work.

The author would also like to offer his sincere thanks to his officemate, Dr. John Ivory, for his friendship and encouragement during the long course of this work.

Table of Contents

LIST OF TABLES

LIST OF FIGURES

LIST OF PHOTOGRAPHIC PLATES

1. INTRODUCTION

Jet impingement flows are frequently used for their excellent heat and mass transfer characteristics, where localized and controlled surface transfer is desirable. The drying of textiles, veneer, paper or film material, the annealing of metal and plastic sheets, the tempering of glass, and the cooling of gas turbine blades and miniature electronic components are some of its more important practical applications.

Heat and mass transfer characteristics of the various types of impinging jets have been studied rather extensively. Under technically realistic conditions, these studies have been mainly concerned with relatively high velocities so that the flow, developing from the exit of the nozzle from which the jet issues is turbulent. The case of heat and mass transfer in impinging flow with a jet that is laminar at the nozzle exit has recieved lesser attention. This is especially true for the case of two-dimensional jet. Within the knowledge of the author, there has been only one publication dealing with the laminar two-dimensional impinging jet in the presence of the confinement plates. Van Heiningen et. al. (96) predicted numerically the flow field and impingement heat transfer due to a laminar two-dimensional jet with an upper confinement plate, including the effect of uniform suction at the impingement plate. No experimental results of either heat or mass transfer due to a confined laminar impinging two-dimensional jet are available.

Reasonably accurate analogy exists between heat and mass transfer provided that the mass transfer rate is low and the normal surface velocity is nearly zero. In such a case, a single transport process, either heat or mass transfer, can be studied in isolation. Usually determination of local heat transfer coefficients is not very reliable owing to the relatively large errors involved in the heat transfer sensors. Therefore, it is more convenient to resort to mass transfer studies rather than heat transfer experimentation. According to the analogy for stagnation flows, it is possible to use the usual $(Pr/Sc)^{0.4}$ factor to convert the fairly precise mass transfer measurements presented by the Sherwood number, into heat transfer measurements presented by the Nusselt number.

The present work is concerned with a confined two-dimensional jet having an initially laminar fully developed profile at the nozzle exit. Impingement mass transfer due to this jet has been studied both experimentally and numerically in order to emphasize not only the engineering applications but also the macroscopic nature of the transport phenomenon. A set of empirical equations which are obtained from the mass transfer experiments can be used immediately for engineering designs. On the other hand, numerical predictions verified by the experimental results provide a complete understanding of the flow and mass transfer characteristics.

1.1 OBJECTIVES OF THE WORK

In this work it was desired to:

1. examine experimentally the effects of the jet Reynolds number and jet-to-plate spacing on the local mass transfer due to the impingement of a confined laminar two-dimensional jet,
2. study the effect of the presence of confinement plates by comparing the experimental results from this work to those obtained by other investigators using unconfined two-dimensional jets,
3. develop a numerical model which would predict the flow field and the mass transfer due to a confined laminar two-dimensional jet, and finally
4. investigate numerically the effect of nozzle exit velocity profile, (i.e. flat and parabolic velocity profiles), on the flow and mass transfer characteristics of a confined laminar impinging two-dimensional jet.

1.2 CHAPTER CONTENTS

A brief review of related literature in impinging jet flow, heat and mass transfer is given in Chapter 2. The choice of experimental techniques is discussed in Chapter 3 with experimental set-up and procedure given in Chapter 4. Calibration and validity of the experimental set-up are given in Chapter 5. The theoretical development which leads to the finite difference equations is presented in Chapters 6 and 7. The adopted numerical procedure is given in Chapter 8 and the validity of the numerical solutions are tested in Chapter 9. Both experimental and numerical results are discussed in Chapter 10 where the effects of jet Reynolds number, jet-to-plate spacing, nozzle exit velocity profile and presence of confinement plates are studied.

Finally, conclusions are drawn in Chapter 11 and recommendations for further study are outlined in Chapter 12.

2. LITERATURE REVIEW

Detailed investigations of the flow field, heat and mass transfer due to single as well as multiple impinging jets have been given by numerous authors. Because of the large number of possible governing parameters, it is hardly surprising that disparity exists between the results and correlations of different investigators. A complete list of literature, together with suitable editorial comment, are of themselves a major undertaking. Therefore, no attempt will be made to review all literature in this area in detail. Only the more relevant references dealing with a single laminar impinging jet similar to the one studied in this work will be reviewed in detail.

In general, there are two types of impinging jets:

1. liquid jet (or free jet): liquid to gas, i.e. water to air referred to as "water jet".
2. submerged jet: liquid to liquid or gas to gas, i.e. air to air referred to as "air jet".

The two types of jets differ substantially from each other. For a liquid jet, entrainment is negligible and the jet forms a free surface at ambient pressure imposed by the surrounding gas. This is the reason why it is also called a "free jet". For a submerged jet, entrainment is important and there is a substantial amount of mixing between the jet and the surrounding fluid.

There are only few studies of impinging jets that deal with liquid jets (11,58,63,98). On the other hand, impinging submerged jets are studied in more detail. In particular, turbulent submerged jets are studied in detail due to their wide industrial applications. Although literature survey of turbulent impinging submerged jets is not the main objective in this chapter, a brief review will also be given here.

For a single turbulent impinging submerged jet, numerous investigations have been made for both axisymmetric (12,14,16,18,20,22,23,24,31,33,39,64,66,67,68,70,86,87,95) and two-dimensional (6,9,10,18,19,42,101,102) cases. Different variables such as jet flow rate, size of the nozzle and jet-to-plate spacing have been considered. For more detail on the studies of single turbulent impinging submerged jet, the reader is referred to the literature reviews given by Cartwright and Russell (10), Gauntner et. al. (21) and Martin (48).

For multiple turbulent impinging submerged jets, numerous investigations have been made for both axisymmetric (20,33,41,59) and two-dimensional (19,42) cases. An additional variable to those mentioned above for a single submerged jet is the spacings between adjacent jets. For more detail on the studies of multiple turbulent impinging submerged jets, the reader is referred to the literature review given by Martin (48).

Another interesting topic in the study of turbulent impinging submerged jets is the impingement heat transfer with crossflow. A few investigators have studied the impingement heat transfer with crossflow for single (8,89), and multiple (17,40,56,57) axisymmetric submerged jets. Their studies were concerned with the effect of jet-to-plate spacing, jet flow rate and controlled crossflow flow rate on the impingement heat transfer.

Turbulent submerged jets have been studied rather extensively as mentioned above. However, laminar submerged jets have recieved lesser attention. Most studies of laminar submerged jets deal with a single jet.

2.1 FLOW CHARACTERISTICS OF A SINGLE LAMINAR IMPINGING SUBMERGED JET

The flow pattern produced by a single submerged jet (laminar or turbulent, confined or unconfined) impinging normally on a flat plate can generally be subdivided into three characteristic regions: the free jet region, the stagnation flow region and the wall jet region (15,21,48). The flow field of an unconfined laminar impinging submerged jet is shown schematically in Figure 2.1. The flow field of a confined laminar impinging submerged jet is very similar to the one shown in Figure 2.1 and will be discussed later in this Section.

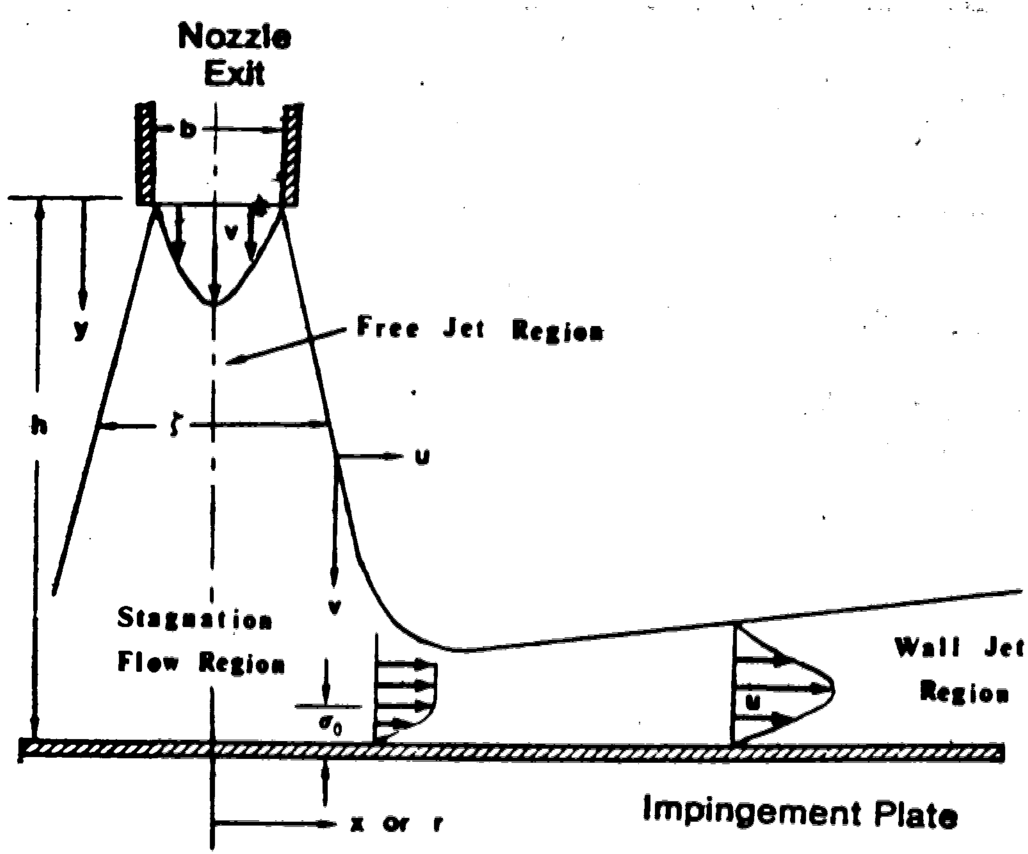

FIGURE 2.1 : FLOW FIELD OF AN UNCONFINED LAMINAR IMPINGING SUBMERGED JET

2.1.1 UNCONFINED SUBMERGED JET

Most of the studies of a laminar impinging submerged jet deal with an unconfined jet. In this case, no confinement plates of any kind are present.

2.1.1.1 FREE JET REGION

The free jet region is defined as a region of the submerged jet not influenced by the impingement plate. A submerged jet has been examined at some length (32,78). In general, near the nozzle exit, the jet is decelerated by tangential shear stress. At the same time, the surrounding still fluid is accelerated producing a "mixing region". The width of the mixing region increases continuously, and at some distance downstream it is wide enough to have penetrated to the centerline of the jet. Up to this point the centerline velocity is practically unaffected by mixing and is substantially equal to the nozzle exit velocity. Beyond the end of the so called "potential core" the centerline velocity decays as the jet shares its momentum with more entrained fluid.

Extensive reviews of literature concerning laminar submerged jets were presented by Schlichting (78). He studied the decay of centerline velocity and the spread of the jet for both axisymmetric and two-dimensional cases by applying the boundary layer theory. For the sake of simplicity, Schlichting assumed the jet exit is infinitely small and the velocity at the exit is infinity in order to retain a finite volumetric flow rate as well as a finite momentum. For a laminar two-dimensional submerged jet, the decay of centerline velocity, $v|_{x=0}$, and the spread of the jet, ζ, are given by

$$(v/\bar{v}_j)|_{x=0} = d_1 (y/b)^{-1/3} \tag{2.1}$$

$$\zeta/b = e_1 (y/b)^{2/3} \tag{2.2}$$

where b is the slot width, and d_1 and e_1 are constants. Their values depend on the flux of momentum at the jet nozzle exit. For a laminar axisymmetric submerged jet, the decay of centerline velocity and the spread of the jet are given by

$$(v/\bar{v}_j)|_{r=0} = d_2 (y/d)^{-1} \tag{2.3}$$

$$\zeta/d = e_2 (y/d) \tag{2.4}$$

where r is the radial coordinate, d is the nozzle diameter, and d_2 and e_2 are constants. Their values are dependent on the flux of momentum at the jet nozzle exit.

The length of potential core has been investigated by several researchers for jets of finite size. The core length in general is defined as the distance from the nozzle exit to a position where the centerline velocity is 98% of its initial value, $(v/\bar{v}_j)|_{x=0}=0.98$ (22), or the centerline pressure head is 95% of its initial value, $(v/\bar{v}_j)^2|_{x=0}=0.95$ (48). Core lengths of about 4b for turbulent two-dimensional submerged jets (48,101), or 4d for turbulent axisymmetric submerged jets (15,22,48) are to be expected. For laminar submerged jets, core lengths are expected to be longer and depend upon the jet Reynolds number. Since the behavior of turbulence increases the rate of mixing between the jet and surrounding fluid, the core length decreases sharply. According to Hrycak et. al.'s (32) experiment for an axisymmetric air jet, the core length is about 15d at Re_d =500 and increases with jet Reynolds number to a maximum value of about 20d at Re_d=1000.

2.1.1.2 STAGNATION FLOW REGION

As the submerged jet approaches the impingement plate, the axial velocity component, v, is decelerated and transformed into an accelerated streamwise velocity, u. At the stagnation point, the velocity is zero and the pressure attains a local maximum. Stagnation flow of this type is a typical boundary layer flow with the influence of viscosity being restricted to a thin layer near the impingement plate. The axial extent of the stagnation flow region can be measured as the distance from the impingement plate where the axial centerline velocity drops to 98% of that in the undisturbed submerged jet at the same distance from the jet nozzle exit (22). In other words, it is where the submerged jet flow deflection begins. For a turbulent axisymmetric submerged jet, the beginning of stagnation flow region is about 1.2d away from the impingement plate (18,22,32).

Within the knowledge of the author, no such measurement has been reported for a laminar submerged jet.

Schlichting (78) studied analytically the stagnation regions of laminar axisymmetric and two-dimensional flows against an infinite plate. The velocity components of the inviscid flow within the stagnation flow region are linearly proportional to the distance from the stagnation point. For two-dimensional stagnation flow, these velocity components are given by

$$v/\bar{v}_j = a_1 (h - y)/b \qquad (2.5)$$

$$u/\bar{v}_j = a_1 (x/b) \qquad (2.6)$$

where a_1 is a constant value. For axisymmetric stagnation flow, the velocity components are given by

$$v/\bar{v}_j = 2a_2 (h - y)/d \qquad (2.7)$$

$$u/\bar{v}_j = a_2 (r/d) \qquad (2.8)$$

where a_2 is constant value. The viscous boundary layer thickness, δ_o, is defined as the distance from the impingement plate where the streamwise velocity, u, reaches 99% of the value of the inviscid flow in either Equations 2.6 or 2.8 depending on the geometry of the stagnation flow. The boundary thickness is given by Schlichting (78) as

$$\delta_o/b = 2.38 / (a_1 Re_b)^{0.5} \qquad (2.9)$$

for two-dimensional stagnation flow, and

$$\sigma_0/d = 1.95 / (a_1 Re_d)^{0.5} \qquad (2.10)$$

for axisymmetric stagnation flow.

2.1.1.3 WALL JET REGION

The wall jet is the boundary layer flow formed by deflection of the submerged jet through the stagnation flow region. Due to the exchange of momentum with the surrounding fluid, the fluid which is accelerated in the stagnation flow region must eventually decelerate in the wall jet region. Therefore, the streamwise velocity, u, initially increases linearly in the stagnation region mentioned above must reach a maximum value at a certain distance downstream and finally decreases in the wall jet region. For a laminar axisymmetric jet, this maximum value is located at about 1d away from the stagnation point for Re_d=1. As the jet Reynolds number increases, this location moves further away from the stagnation point (45).

The wall jet has the characteristic of zero velocity at both the impingement plate and the outer jet edge, and hence it exhibits a maximum velocity. The flow pattern in the wall jet region can be divided into two parts according to the location of the maximum velocity: an inner layer which has features common to the ordinary boundary layer and an outer layer which has features common to a submerged jet.

Important parameters in the analysis of flow characteristics of wall jets are the growth of the wall jet boundary layer and the decay of the maximum velocity. The boundary layer thickness of the wall jet, σ, generally used is defined as the thickness in wall jet outer layer where the streamwise velocity is 50% of the maximum velocity.

The first complete theoretical analysis was performed by Glauert (25) who studied both laminar and turbulent, two-dimensional and axisymmetric wall jets. Since then numerous investigations of turbulent (7,10,14,25,48,60,61, 70,83,84) and laminar (25,71,79,82) wall jets have been reported. For a laminar two-dimensional wall jet, the decay of maximum velocity, u_{max}, and the growth of the wall jet boundary layer, σ, are given by (25,82)

$$u_{max} / \bar{v}_j = f_1 \ (x/b)^{-0.5} \qquad (2.11)$$

$$\sigma/b = g_1 \ (x/b)^{0.75} \qquad (2.12)$$

where f_1 and g_1 are constants. For a laminar axisymmetric wall jet, the decay of the maximum velocity and the growth of the wall jet boundary layer are given by (25,71,79)

$$u_{max} / \bar{v}_j = f_2 \ (r/d)^{-1.5} \qquad (2.13)$$

$$\sigma/b = g_2 \ (r/d)^{1.25} \qquad (2.14)$$

where f_2 and g_2 are constants.

2.1.2 CONFINED SUBMERGED JET

The confined two-dimensional submerged jet used in this study is a submerged jet with a confinement plate parallel to and at a distance, h, from the impingement plate. The length of this confinement plate is the same as that of the impingement plate. In addition, two spacers are used to fit between the impingement and the confinement plates so as to form a rectangular channel to which the jet flow would be confined. No such confined submerged jet has been studied. Actually, only a few investigators (34,45,77,96) who studied a laminar impinging submerged jet numerically, considered the effect of the presence of a confinement plate. In all these studies, the submerged jet was only partially confined by a confinement plate parallel to the impingement plate. Such a jet, with no spacers between the impingement and the confinement plates, is referred to as "semi-confined" submerged jet by the investigators.

For a semi-confined submerged jet, the flow field is very similar to that shown in Figure 2.1 for an unconfined submerged jet except a recirculation region is induced between the impingement plate and the confinement plate (45,77,96). This recirculation region can affect the spread of the submerged jet in the free jet region. The inertial effects of the upper part of this recirculation derives the greater part of its momentum from the jet in the wall jet region (96). An interesting result was observed by Van Heiningen et. al. (96) in their study of a semi-confined laminar two-dimensional air jet is that the jet contracts slightly below the nozzle exit for an initially parabolic jet velocity profile.

The effects of the velocity profile at the nozzle exit on the spread of a submerged jet and the decay of centerline velocity in the free jet region were noted by Van Heiningen et. al. (96) and Li (45) in their numerical studies of semi-confined laminar two-dimensional and axisymmetric submerged jets, respectively. A submerged jet issuing with a flat velocity profile spreads and decays faster than that with a parabolic velocity profile. For the case of flat velocity profile, the momentum just inside the free streamline is an order of magnitude greater than that of the surrounding fluid just outside the free streamline. Therefore interaction occurs immediately between the high momentum fluid at the outer edge of the jet and the still fluid surrounding it, causing a higher rate of spread of the jet. This spreading effect is less important for the submerged jet with a parabolic velocity profile. As mentioned above, the jet actually contracts slightly below the nozzle exit in this case.

2.2 HEAT AND MASS TRANSFER DUE TO A SINGLE LAMINAR IMPINGING SUBMERGED JET

Heat and mass transfer characteristics of laminar impinging axisymmetric submerged jets have been studied rather extensively. The theoretical and experimental results are well correlated. However, heat and mass transfer chacteristics of laminar impinging two-dimensional submerged jets have recieved lesser attention. In this section, laterature related to confined and unconfined submerged jets will be reviewed separately with emphasis on the two-dimensional case.

2.2.1 UNCONFINED SUBMERGED JET

Most of the studies of heat and mass transfer due to unconfined laminar impinging submerged jets cover both the stagnation flow and the wall jet regions. But there are also a few studies which cover the wall jet region only (79,82). In these studies, correlations for heat and mass transfer in terms of simple governing parameters of the flow were obtained. In general, at a given jet Reynolds number, the heat and mass transfer characteristics in the stagnation flow region are very much affected by the jet-to-plate spacing, but those in the wall jet region are not so much affected.

2.2.1.1 UNCONFINED AXISYMMETRIC SUBMERGED JET

Scholtz and Trass (79) studied mass transfer due to a laminar impinging axisymmetric submerged jet both theoretically and experimentally. Their theoretical expression, which has been experimentally verified for mass transfer in the wall jet region is given by

$$Sh_d = c_1 \; Re_d^{0.75} \; (r/d)^{-1.25} \tag{2.15}$$

where $c_1 = c_2 \; (-g'(0))$ (2.16)

and $(-g'(0)) = \Gamma(Sc + 1/3)/(\Gamma(Sc) \; \Gamma(1/3))$ (2.17)

$(-g'(0))$ is defined as a dimensionless gradient of concentration at the wall. c_2 is a constant and its value is dependent on the exterior flux of momentum flux defined as by Glauert (25). For a flat velocity profile at nozzle exit, c_2=0.426. On the other hand, for a parabolic velocity profile, c_2=0.458. For comparison with the theoretical expression of Equation 2.15, experimental data were obtained by measuring the shrinkage of coatings of acetanilide and benzoic acid in the range of $1000 \le Re_d \le 3000$ and $970 \le Sc \le 4400$. Agreement with theory was good.

Later, Scholtz and Trass (80,81) have given a theoretical solution in the stagnation flow region of a laminar axisymmetric submerged jet with a parabolic velocity profile at nozzle exit. The solution for inviscid flow in the body of impinging jet was first obtained (80) and then was used as the boundary condition to solve the viscous boundary layer flow near the impingement plate (81). For impinging jet with a parabolic velocity profile at nozzle exit, the Sherwood number in the stagnation flow region was given by

$$Sh_d / Re_d^{0.5} = 1.6484\ Sc^{0.361} - 1.0808\ (r/d)^2\ Sc^{0.361} + \cdots \quad (2.18)$$

for $h/d=0.5$, $r/d \le 0.5$ and $1 \le Sc \le 10$. By setting $r=0$, the stagnation point Sherwood number is given by

$$Sh_d^{\circ} = 1.6484\ Re_d^{0.5}\ Sc^{0.361} \quad (2.19)$$

In a similar manner, the mass transfer from the impingement plate in the stagnation flow region using an impinging jet with a flat velocity profile at the nozzle exit was calculated by Scholtz and Trass (81). The results indicated that, at a given jet Reynolds number, the mass transfer at the stagnation point is less than half that observed for a jet with a parabolic velocity profile at nozzle exit. However, no experimental data were obtained to confirm this theoretical finding.

Mass transfer experimental data were obtained by Scholtz and Trass (81) from measurement of the sublimation rates of a naphthalene coating exposed to air jet with a parabolic velocity profile at nozzle exit ($Sc=2.45$). For the ranges of $570 \le Re_d \le 1970$ and $0.5 \le h/d \le 6$, good agreement was reported between the experiment results and the theoretical expression of Equation 2.18. In addition, a smooth transition from the stagnation flow region to the wall jet region was observed in the region of $0.5 \le r/d \le 2.25$. Experimental data in this transition region were correlated in terms of jet Reynolds number as

$$Sh_d = 1.05\ Re_d^{\text{[illegible]}}\ (r/d)^{-\text{[illegible]}} \qquad (2.20)$$

for $570 \leq Re_d \leq 1970$ and $Sc = 2.45$.

A typical curve showing the variation of local Sherwood number on the impingement plate for an unconfined laminar axisymmetric submerged jet can be plotted from the correlations for different regions in Equations 2.15, 2.18 and 2.20. Since the dependence of local Sherwood number on Reynolds number differ in the stagnation flow, transition and wall jet regions, the relationship between the local Sherwood number in these regions on a plot of Sh_d versus r/d will depend on Re_d. A typical variation of the local Sherwood number on the impingement plate for an unconfined laminar axisymmetric submerged jet with a parabolic velocity profile at nozzle exit is shown in Figure 2.2 for $Re_d = 1740$ and $Sc = 2.45$.

Kapur and Macleod (36,37,38) have applied the techniques of holographic interferometry to the profilometric measurement of mass transfer rates at solid-fluid surface exposed to an unconfined laminar impinging axisymmetric air jet. Experimental results for the wall jet region in the range of $255 \leq Re_d \leq 1870$ were in excellent agreement with the theoretical predictions of Scholtz and Trass (79). Mass transfer coefficients near the stagnation point were also reported for $Re_d = 1340$ and

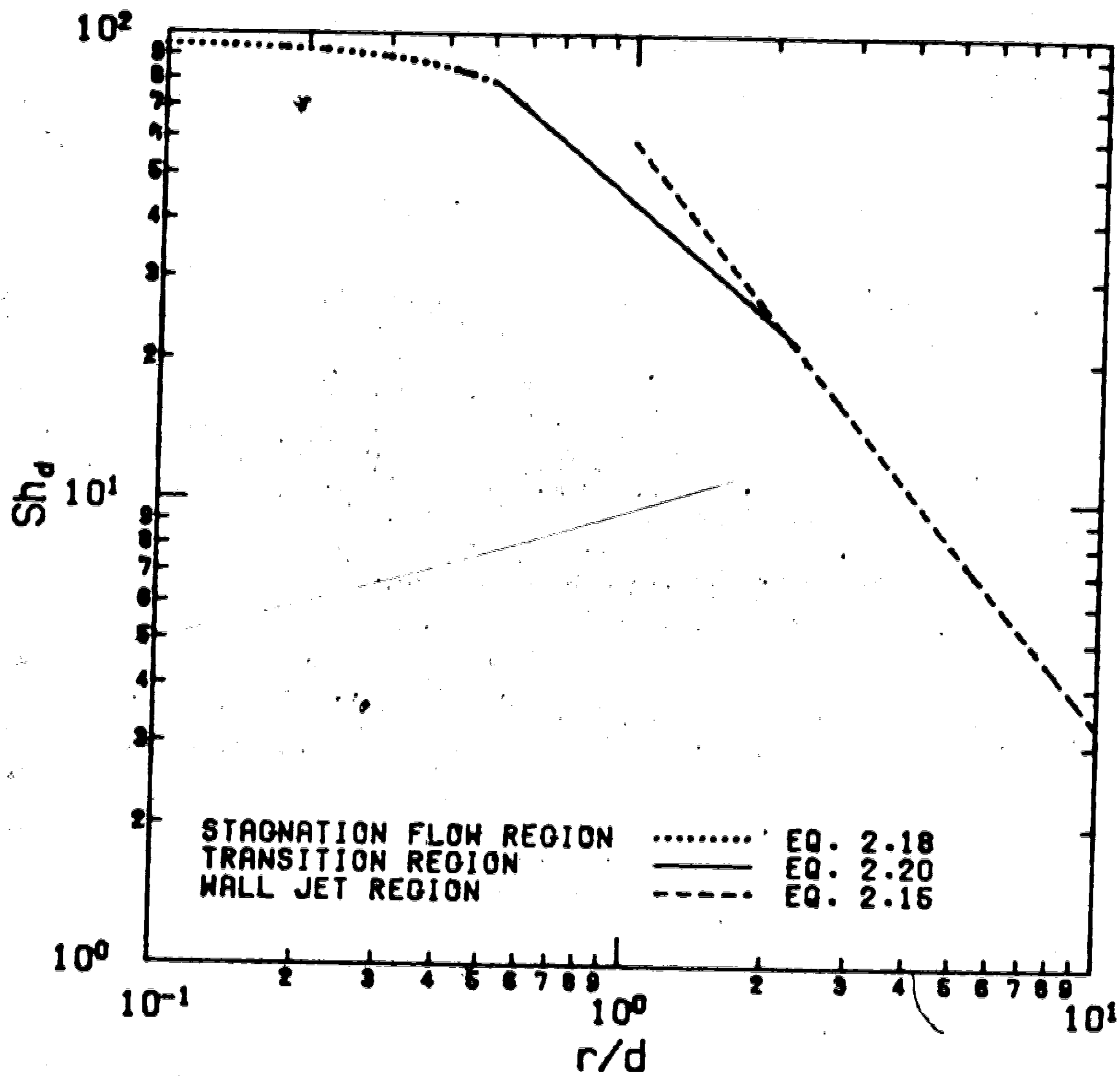

FIGURE 2.2 : VARIATION OF LOCAL SHERWOOD NUMBER ON IMPINGEMENT PLATE FOR AN UNCONFINED LAMINAR AXISYMMETRIC SUBMERGED JET WITH INITIAL PARABOLIC PROFILE (Re_d=1740, Sc=2.45)

h/d=0.5d, 1d and 1.5d. Within the narrow range of the jet-to-plate spacings used, the mass transfer coefficients in the stagnation flow region were found by Kapur and Macleod to be independent of jet-to-plate spacing.

Masliyah and Nguyen carried out a number of investigations on mass transfer due to laminar axisymmetric (50,51), square (50,51), rectangular (50,52) and two-dimensional (53) air jets by using a laser holography interferometric technique. In their study of axisymmetric jet, experimental results for the wall jet region of Re_d =1145 and 1420 were found to be dependent on $Re_d^{0.5}$ and $(r/d)^{-1.25}$. The exponents of Re_d and (r/d) were in good agreement with the theoretical findings by Scholtz and Trass (79).

2.2.1.2 UNCONFINED TWO-DIMENSIONAL SUBMERGED JET

Schwarz and Caswell (82) studied the heat transfer characteristics of a laminar two-dimensional wall jet by solving the flow equations analytically for a wall jet as developed by Glauert (25). Their correlation for mass transfer in the wall jet region is given by

$$Sh_b = c_3 \, Re_b^{0.75} \, (x/b)^{-0.75} \qquad (2.21)$$

where $c_3 = c_4 \, (-g'(0))$ (2.22)

c_4 is a constant whose value is dependent on the exterior flux of momentum flux as defined by Glauert (25). For a flat velocity profile at nozzle exit, c_4=0.446. On the other hand, for a parabolic velocity profile, c_4=0.465.

Gardon and Akfirat (19) studied experimentally the heat transfer characteristics of unconfined impinging two-dimensional air jets for both laminar and turbulent cases. Although the nozzle exit velocity profile of the jet was not specified, due to the short nozzles used by Gardon and Akfirat, the nozzle exit velocity profile was most likely flat. In their studies of a single unconfined laminar two-dimensional jet (Re_b=450, 650 and 950), their main interest was the effects of jet Reynolds number and jet-to-plate spacing on the stagnation point Nusselt number. For jet-to-plate spacing less than the length of the potential core of the submerged jet (0.5<h/b<5), Nusselt numbers at the stagnation point depend on the jet Reynolds number only. They are approximately proportional to $Re_b^{0.33}$. At large jet-to-plate spacings, stagnation point Nusselt numbers varied with $(h/b)^{-0.}$[illegible] for Re_b=450. However, when Reynolds number was increased to 650 and 950, this monotonic decreasing behavior of stagnation point Nusselt numbers with increasing jet-to-plate spacing does not exist. Instead, a maximum of stagnation point Nusselt numbers occurs when jet-to-plate spacing is in the range of 10<h/b<15. The behavior was explained by Gardon and Akfirat (18) and it is caused by the penetration of mixing induced turbulence to the centerline of initially laminar jets. The interactions between the centerline turbulence and the approaching centerline velocity in the stagnation flow region is the reason why this non-monotonic behavior of the stagnation point Nusselt numbers was observed. It is because the centerline turbulence increases with increasing jet-to-plate spacing and the approaching centerline velocity decreases with increasing jet-to-plate spacing due to the decay of centerline velocity. Gardon and Akfirat (19) concluded that for small jet-to-plate spacings, it is likely that the potential core velocity will be independent of the jet-to-plate spacing, and the stagnation point Nusselt numbers should show a corresponding trend. Once the core has been engulfed by the mixing region, the decay of the centerline velocity would tend to decrease the heat transfer rate at the stagnation point, but centerline turbulence would have an opposite effect. At lower Reynolds numbers the former should be more important, whereas at the higher Reynolds numbers the influence from centerline turbulence should become more important instead.

Miyazaki and Silberman (58) have analysed theoretically the flow friction and heat transfer characteristics on a heated or cooled flat plate with unconfined laminar impinging two-dimensional jet with initial flat profile. A potential flow solution was obtained to provide the distribution of the main-stream velocity. The boundary layer and energy equations were then solved numerically by a finite difference method. The correlation obtained by Miyazaki and Silberman in terms of mass transfer variables at the stagnation point is given by

$$Sh_b^o = 0.506\ Re_b^{0.5}\ Sc^{0.373} \qquad (2.23)$$

for $h/b \geq 1.5$ and $0.7 \leq Sc \leq 10$. Variations of local Nusselt numbers on the impingement plate were also evaluated, though no correlations were given. For $h/b \geq 1.5$, Nusselt number exhibits a maximum at the stagnation point and remains constant within the stagnation flow region. Away from the stagnation flow region, Nusselt number decreases monotonically and finally tends to vary proportionally with $x^{-0.5}$ as for the flow over a flat plate.

Sparrow and Wong (91) studied the impingement mass transfer due to an unconfined laminar two-dimensional submerged jet with initial parabolic velocity profile. By using the naphthalene sublimation technique ($Sc=2.5$), variation of the local mass transfer coefficient on the impingement plate was determined for Re_b=150, 300, 450, 650 and 950, and h=2b, 5b, 10b, 15b and 20b. In general, the local mass transfer coefficient was found to decrease monotonically with increasing distance from the stagnation point, but correlations were not given. Sparrow and Wong also studied the effect of jet-to-plate spacing on the stagnation point Sherwood number. The non-monotonic behavior of stagnation point transfer coefficients with increasing jet-to-plate spacing mentioned by Gardon and Akfirat (19) for higher Reynolds numbers was again observed. Stagnation point Sherwood numbers measured by Sparrow and Wong (91) were converted into Nusselt numbers by using the analogy between heat and mass transfer, $Nu_b = (Pr/Sc)^{0.4} Sh_b$, in order to compare with the stagnation point Nusselt numbers measured by Gardon and Akfirat (19). The results of Sparrow and Wong are about 30% higher than those of Gardon and Akfirat. The main cause of this different is the nature of the initial velocity profiles of these two studies. Similar observation is made by Scholtz and Trass (81) for an unconfined impinging axisymmetric submerged jet that the mass transfer at the stagnation point for a jet with initial flat velocity profile is less than that for a jet with initial parabolic velocity profile.

Sparrow and Lee (90) analysed fluid flow and heat and mass transfer characteristics associated with the impingement of an unconfined laminar two-dimensional submerged jet with an initial parabolic velocity profile. The velocity field within the impinging jet was solved within the framework of an inviscid flow model and the results were used as input for the analysis of the boundary layer heat or mass transfer on the impingement plate. The transfer coefficients were found insensitive to the jet-to-plate spacing within the range investigated, which was $0.375 \leq h/b \leq 1.5$. The dependence of stagnation point Sherwood number on Reynolds number was given as

$$Sh_b^o = 1.4\ Re_b^{0.5} \tag{2.24}$$

for Sc=2.5. Fair agreement between Equation 2.24 and the experimental data of Sparrow and Wong (91) for h/b=2 was obtained.

In the experimental study of an unconfined laminar impinging two-dimensional air jet with initial parabolic velocity profile by Masliyah and Nguyen (53), a regression equation for the local Sherwood number was given as

$$Sh_b = 0.55\ Re_b^{0.55}\ (x/b)^{-0.73} \qquad (2.25)$$

for Sc=2.85, $90 \leq Re_b \leq 300$ and $1 \leq x/b \leq 30$. All the experimental data reported were taken with jet-to-plate spacing equal to 4b. They also pointed out that the experimental results with a jet-to-plate spacing equal to 8b gave similar results. An overall general agreement between Equation 2.25 and the experimental results from Sparrow and Wong (91) was obtained. In addition, the exponent, -0.73, of (x/b) in Equation 2.25 is in fair agreement with the theoretical analysis of Schwarz and Caswell (82) for a two-dimensional wall jet, which is -0.75. However, their exponents of Reynolds number do not agree.

It would be appropriate to conclude that there are no unified correlations of the variation of local Sherwood number for unconfined two-dimensional submerged jet. In general a typical distribution of local Sherwood number on impingement plate for the two-dimensional case is similar to that for the axisymmetric case. A plot is shown in Figure

2.3 for Re_b=400 and Sc=2.85 by using the correlations of Equations 2.21 2.24 and 2.25 and assuming that the local Sherwood number in the stagnation flow region remains constant.

2.2.2 CONFINED SUBMERGED JET

Heat and mass transfer due to a confined laminar impinging submerged jet have been studied numerically. All studies cover both the stagnation flow and the wall jet regions.

2.2.2.1 CONFINED AXISYMMETRIC SUBMERGED JET

Saad et. al. (77) have simulated the flow and heat transfer characteristics of a semi-confined laminar impinging axisymmetric air jet. The vorticity-stream function formulation of the Navier-Stokes and the energy equations were solved numerically. Effects of uniform suction and nozzle exit velocity profile on the flow and heat transfer characteristics were studied. Saad et. al. also observed the finding of Scholtz and Trass (81) concerning the effect of the initial velocity profile even with the presence of a confinement plate. By comparing their results with the experimental data obtained by Scholtz and Trass (81) who used an unconfined axisymmetric jet, Saad et. al. showed that the presence of a confinement plate has only a minor influence on the stagnation point heat transfer for the range of $2 \le h/d \le 4$ and $450 \le Re_d \le 2500$.

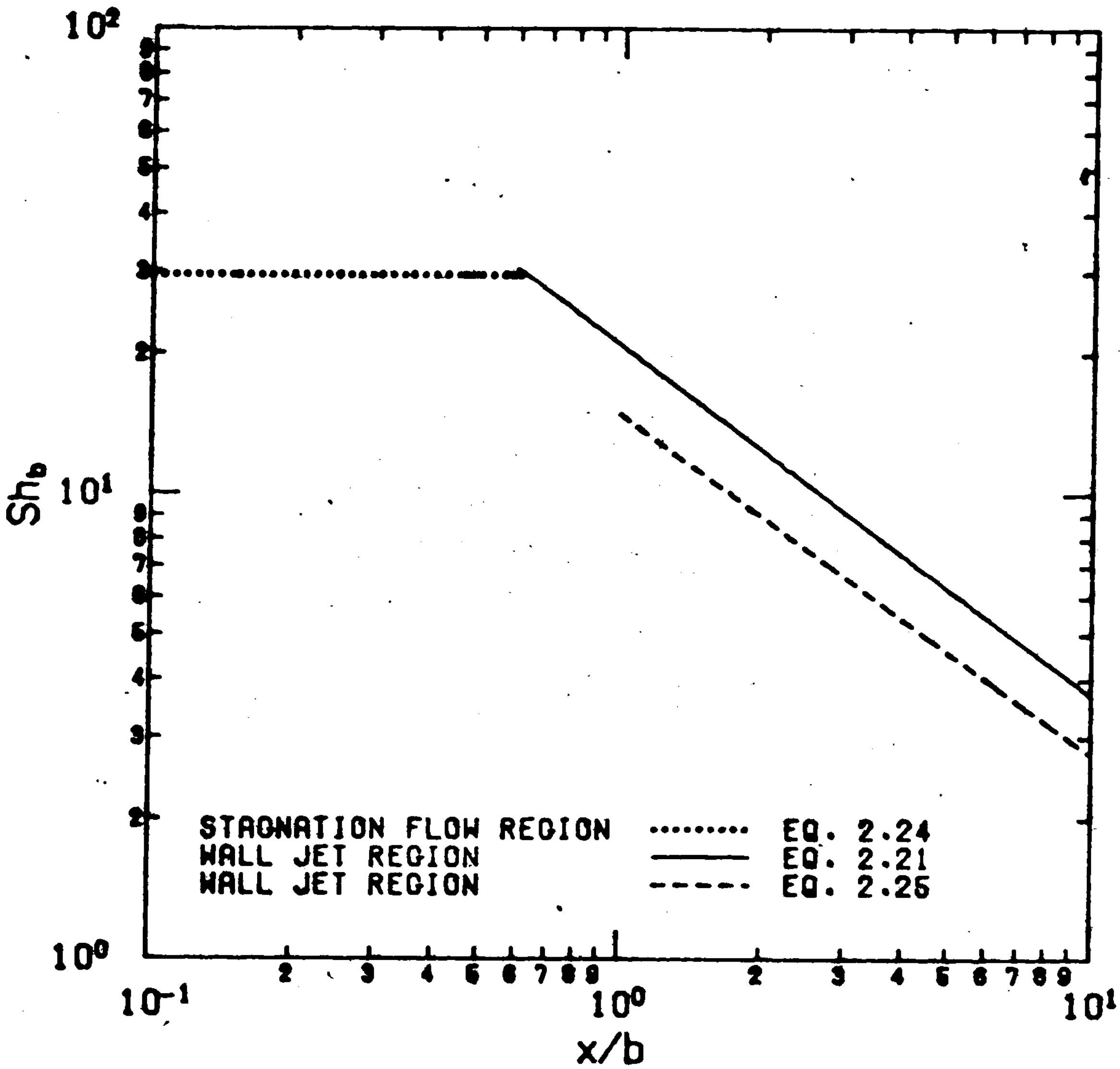

FIGURE 2.3 : VARIATION OF LOCAL SHERWOOD NUMBER ON IMPINGEMENT PLATE FOR AN UNCONFINED LAMINAR TWO-DIMENSIONAL SUBMERGED JET WITH INITIAL PARABOLIC PROFILE (Re_b=400, Sc=2.85)

Other numerical studies of semi-confined laminar axisymmetric jets included the studies by Huang et. al. (34) and Li (45). Huang et. al. (34) have numerically solved the Navier-Stokes equations in their primitive form with the energy equation for a semi-confined laminar axisymmetric swirling jet. Li (45) has studied numerically the simultaneous heat and mass transfer under a semi-confined laminar impinging axisymmetric jet.

2.2.2.2 CONFINED TWO-DIMENSIONAL SUBMERGED JET

Only one study of heat transfer due to a laminar impinging two-dimensional submerged jet by Van Heiningen et. al. (96), considered the effect of the presence of a confinement plate. By using the same numerical technique as Saad et. al.'s (77), Van Heiningen studied the effects of uniform suction and nozzle exit velocity profile on the flow and heat transfer characteristics. They found that for a jet-to-plate spacing equal to 4b and $100 \leq Re_b \leq 950$, the stagnation point Nusselt number for an initial parabolic velocity profile was between 1.5 and 2 times the value for an initial flat velocity profile. For a flat velocity profile, similar behaviors of skin friction factors and Nusselt numbers along the impingement plate mentioned by Miyazaki and Silberman (58) were also observed, although the results obtained by Miyazaki and Silberman were consistently higher than those obtained by Van Heiningen et. al.. This difference as pointed out by Van Heiningen et. al. is due to the assumption of potential flow for the flow outside the boundary layer used by Miyazaki and Silberman. For the case of a parabolic velocity profile, Sherwood numbers measured by Sparrow and Wong (91) were converted into Nusselt numbers by using the analogy between heat and mass transfer as mentioned above in order to compare with the numerical results from Van Heiningen et. al.. Good agreement was obtained both in the stagnation flow and in the wall jet regions indicating that the presence of a confinement plate has only a minor effect on the heat and mass transfer characteristics. It is worthwhile to mention that the effect of jet-to-plate spacing was not studied by Van Heiningen et. al. as only one jet-to-plate spacing of 4b was used in their study.

3. BASIC EXPERIMENTAL TECHNIQUES

Measurement techniques used to study problems in heat and mass transfer are numerous and often quite complex. Mass transfer techniques have usually been used to avoid the errors inherent in heat transfer measurements; for example, conduction errors in a forced convection heat transfer system even with near-ideal design often cannot be reduced to a sufficiently low level due to the finite conductivity of even the best of insulators. Mass transfer techniques, if properly utilized, do not have an analogous conduction error and for this reason, they are very valuable when precise local measurements are required.

A novel profilometric technique for determining local mass transfer coefficients at solid surface was first described by Macleod and Todd (47). Instead of a volatile or soluble surface coating (i.e., naphthalene coating) customarily employed in profilometric work, the coating used is composed of non-volatile polymer capable of absorbing volatile or soluble swelling agents. Rates of transfer of swelling agent to or from the surface by the experimental fluid stream can then be evaluated from measurements of the swelling or shrinking rate of the coating. In most practical cases, the polymer coating swelling or shrinkage is of order of 10^{-6}m and consequently mechanical means for these measurements are difficult and unreliable. Holographic interferometry in the conjunction with the swollen polymer technique of Macleod and Todd (47) proposed by Kapur and Macleod (36,37,38) and Masliyah and Nguyen (50,51,52,53) was found to be a powerful and convenient means for measuring such a small change in polymer coating thickness. The unique advantage of this optical method is that it does not influence the process examined. In addition, instead of point by point measurements, information about a whole field of interest can be obtained by the evaluation of photographs.

3.1 SWOLLEN POLYMER TECHNIQUE

The essence of the swollen polymer technique is to coat the flat surface under study with a thin layer of an non-volatile silicon polymer and to swell this coating in a bath of ethylsalicylate. Transfer of ethylsalicylate from the polymer coating when the coating is subjected to an air jet results in local changes in the degree of swelling. These changes cause the polymer coating to shrink (47). It has been shown that the local shrinkage of the polymer coating over a known time within the "constant rate period" provides an accurate measure of the local mass transfer coefficients over the surface (47,51). In other words, in order for the swollen polymer technique to be useful in mass transfer studies, it is essential that a "constant rate period" is maintained while measurements of mass transfer are taken.

Macleod and Todd (47) have pointed out in their study of this technique that the following important conditions hold within the constant rate period:

1. Swollen polymers having virtually zero heats of mixing, exhibited no total volume change on swelling, i.e., the swollen polymer volume is the sum of the volumes of the dry polymer and that of the pure swelling agent. Thus, the shrinkage of the polymer coating is proportional to the amount of swelling agent transferred from the coating.
2. Although the vapor pressure of the swelling agent over the surface depends both on temperature and on the composition of the coating, and must change as volatilization proceeds at constant temperature, it is reasonable to assume that a change in the partial vapor pressure of up to 5% at the polymer coating during an experiment has a negligible effect on the determination of mass transfer coefficients compared with other sources of error. The so called "constant rate period" is defined as the time period when the vapor pressure remains within 5% of its initial value during volatilization. Within this period, the partial vapor pressure of the swelling agent at the surface can be assumed to be effectively the same as the vapor pressure of the pure swelling agent. Such a constant rate period

was found experimentally and theoretically to be as high as 2500 s.

3. The overall resistance to mass transfer is predominantly in the gas phase.
4. The effect of diffusion of the swelling agent parallel to the surface from regions of low mass transfer to regions of high mass transfer can be neglected. The behavior of the coating at any given point is therefore governed by the local mass transfer in the direction normal to the polymer coating only.

Because of all these conditions mentioned above the swollen technique is a powerful technique in the profilometric determination of local mass transfer coefficients.

The practical advantages of the swollen polymer technique are summarized as follows:

1. The coating itself can be used repeatedly; for each new experiment it can be re-activated by re-immersion in the swelling agent bath.
2. The Schmidt number of the system can be varied; this can be accomplished by a changing the swelling agent alone, without changing the experimental fluid or the polymer coating.
3. Because the mass transfer rate is independent of the coating thickness, no uniformity of thickness other than that implied by the need for hydraulic smoothness at the polymer surface of the coating is required.
4. Unlike the surface of a subliming solid, the surface of

the shrinking polymer maintains a nearly constant optical quality. It is therefore possible to record its shrinkage by fairly standard techniques of holographic interferometry.

It is propriate to mention that the swollen polymer technique is not suitable for determining local mass transfer coefficients for a curved surface and also when the local mass transfer rate is high.

3.2 LASER HOLOGRAPHY INTERFEROMETRIC TECHNIQUE

Many optical methods have been used in heat and mass transfer studies; reviews of this methods have been presented by Hauf and Grigull (29) and Goldstein (26). Up to a decade ago, the most common methods used were Mach-Zehnder and Michelson interferometry. In 1948, Gabor invented a new optical recording technique which he called "image formation by reconstructed wavefronts" at that time. Not until two years later, the word "holography" was apparently first applied by Roger (43) to describe this new photographic procedure. In contrast to ordinary photography, by which only the amplitude of the reflected light from the object is recorded, holography allows the recording and reconstruction not only the amplitude but also the phase distribution of wavefronts. As holography demands a highly coherent light source, there is a technological break-through after the invention of the laser about twenty years ago; since then, the holographic techniques have played an important role in the studies of heat and mass transfer (54).

The general theory of holography is so comprehensive that for a detailed description the reader is referred to the literature (13,43,44,73). In this work, only the principles necessary for understanding the holographic measurement techniques are mentioned.

To record a hologram of an object, a beam from a coherent monochromatic light source (usually a laser) is split into two separate beams. One beam, so called the "object beam or wave", illuminates the object, and the reflected scattered light falls directly onto a photographic plate. The other beam, so called "reference beam or wave", travels by a separate path bypassing the object, and falls on the same area of the photographic plate. If both these two waves are mutually coherent, they will interact and form a stable interference pattern. This interference pattern can therefore map an exposure pattern across the surface of the photosensitive emulsion on the photographic plate. When the photographic plate is developed and fixed, the plate with a pattern of dark fringes is called "hologram". The fringe pattern which in general consists of about 1000 lines per millimeter, contains all the visual information about the object. The amplitude of the light from the object is recorded in the form of different contrast of the fringes since the intensity of light incident on the emulsion will be the square of the sum of the amplitudes from the reference and the object waves. The phase of the light from the object is recorded in the spatial variation of the fringe pattern since when the pathlengths between the reference and the object waves differ by one-half wavelength, interference will be destructive and no light energy will be available to expose the emulsion.

When the hologram is illuminated by the reference wave, the fringe pattern acts like a diffraction grating. A number of light waves are generated by the interaction of the light with the grating. The "zero order" wave propagates in the same direction as the incident light. Beyond the two first order waves, second, third and higher order waves also occur. One of the first order waves travels in the same direction as the original object wave and it is responsible for the virtual image of the original object. The other first order wave is responsible for the real image of the object which usually appears unsharp and highly distorted. Since the scattered light from one point of the object is recorded in each part of the hologram, this point can be seen even through only a small fraction of the plate. It can therefore be observed from various angles, limited only by the size of the hologram. Thus, in the reconstruction stage, a truly three-dimensional picture of the image is obtained.

Making use of these recording properties, several exposures can be made on the same photographic plate. Illuminating this multiple exposed hologram with the reference wave after processing, the object waves due to different exposures will all be reconstructed and if they differ only slightly from one another they can interfere with each other to form fringes. This is the basic idea of holographic interferometry.

Normally holographic interferometry is made using a double exposure. The interference fringe pattern from the two reconstructed object waves after two different exposures can be photographed and therefore can be analysed at any time.

3.2.1 DOUBLE EXPOSURE HOLOGRAPHIC INTERFEROMETRY

In double exposure holographic interferometry, a hologram of the object, which in this work is the polymer coating, is made before subjecting the polymer coating to the air jet. After the polymer coating is subjected to the air jet, a second exposure is made onto the same photographic plate. After processing the photographic plate, the double exposed hologram is repositioned and illuminated by the reference wave. Now both object waves, the first one is due to the original undisturbed polymer coating and the second is due to the shrunk coating, are reconstructed. The interference from these two object waves forms fringes indicating the change in thickness of the polymer coating between the two exposures. These interference fringes, so called "frozen fringes", are contours of equal coating shrinkage or equal mass transfer and can be photographed with a 35mm camera.

The main difference of this technique from classical interferometry, such as Mach-Zehnder and Michelson interferometry, is that the object wave is compared to itself. Since both waves pass through the same optical set-up, any imperfections of mirrors and lenses are eliminated. Another advantage of this technique is that it can provide a complete record of the local mass transfer coefficients at all points on the surface. No other technique of heat or mass transfer measurement hitherto reported has this capability. Therefore, mass transfer data can be provided both in precision and completeness.

However, there are also some drawbacks. The photographic process of this technique, particularly at the initial stages, requires a high degree of specialized skill. Its success is greatly dependent on the correct choice of several optical and photographic processing variables, such as ratio of beam intensities, length of exposure and conditions of hologram development. More importantly, in this technique it is difficult to identify the order of any particular fringe. The "frozen fringe" pattern on the double exposed hologram only provides information about differences between the shrinkage of the coating at different points. The actual value of the shrinkage can only be found if the order of fringe at a given point is known. This shortcoming can be overcome by real time holographic interferometry.

3.2.2 REAL TIME HOLOGRAPHIC INTERFEROMETRY

Real time holographic interferometry can be done by using a precise and adjustable hologram mount. After the first exposure, the hologram is processed and replaced in its original position. The "reference image", which is actually the image of the object before the mass transfer experiment, is then reconstructed continuously by illuminating the hologram with the reference wave. Then the mass transfer experiment is started, the reconstructed light can be superimposed onto the changing object wave. The changes of the interference pattern can then be continuously observed and the order of any particular fringe at any given time can be easily determined by counting fringes at a given location as they appear in real time.

Another apparent advantage of this technique is that it is possible to distinguish between a monotonic and a "U" type coating shrinkage between which the double exposure technique fails to distinguish. In double exposure technique, the appearance of "frozen fringes" is simply due to change in depth regardless of whether such a change is a shrinkage or a rise. But in real time technique, the ability to determine the order of each fringe gives a complete information on how the coating shrinkage proceeds. Therefore a "U" type coating shrinkage can be easily observed and recorded.

The optical set-up used in this work which is suitable for both double exposure and real time holographic interferometry will be discussed in Chapter 4.

4. EXPERIMENTAL SET-UP AND PROCEDURE

The experimental set-up in this work is shown in Figure 4.1 which includes the optical set-up for recording a hologram and also the experimental apparatus for the mass transfer experiment due to an impinging submerged jet. With the hypothenuse surface of a right-angle glass prism as the mass transferring surface, where the polymer coating is applied, it becomes possible to have the entire optical set-up to be located behind the mass transferring surface. Since both the prism and the polymer coating are transparent, the mass transferring surface can be observed from the optical system all the time during the progress of the experiment. Therefore, such an arrangement is suitable not only for double exposure holographic interferometry but also for real time holographic interferometry.

4.1 OPTICAL SET-UP

A concrete table with a concrete slab of size 2.74 x 1.37 x 0.13m is used as the working surface for the optical set-up. The function of heavy slab is to prevent floor vibration from being transmitted to the optical components.

The optical components include:

1. a Spectra Physics model 125A 50mW He-Ne laser which is

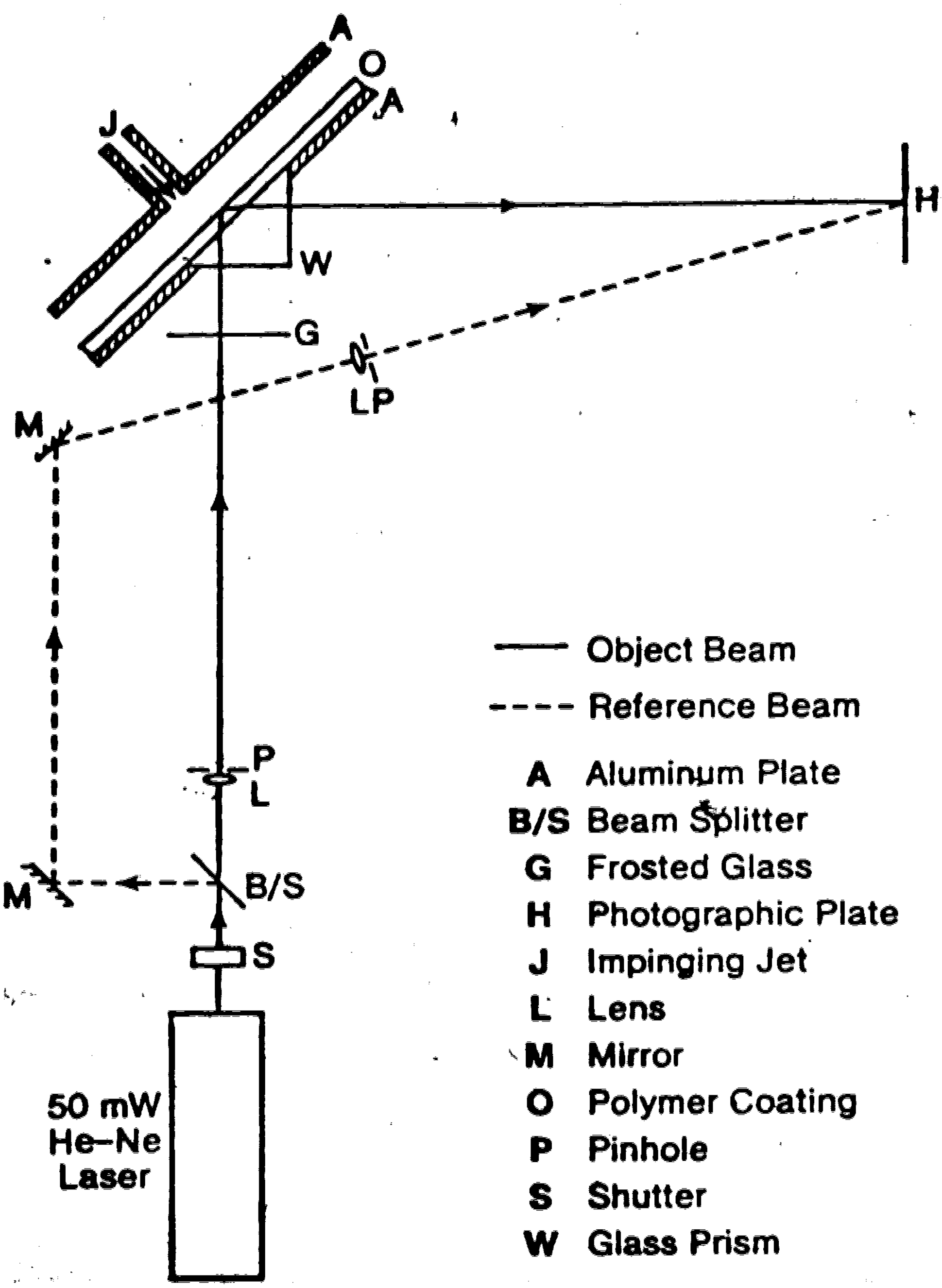

FIGURE 4.1 : ARRANGEMENT FOR THE EXPERIMENTAL SET-UP

used as the source of the monochromatic coherent light of wavelength equal to 632.8×10^{-9}m,

2. a Prontor-Press shutter which is used to set the exposure time for making a hologram,
3. an Elomag beam splitter-attenuator, model VBA-200, which is a variable reflectivity aluminum mirror for use in splitting the laser beam into the reference and the object beams and in adjusting the ratio of the beam intensities,
4. a Spectra Physics model 332 spatial filter and expanding lens assembly (expanding lens L3, aperture A3) mounted on a Spectra Physics model 306A precision optical mount with base and vertical post which is used to eliminate spatial noise and produce a smooth intensity profile across the expanded object beam,
5. two Spectra Physics model 386-11 utility mirror mounts (includes model 564 mirrors) which are used to reflect the reference beam in order that the reference beam can travel bypassing the object,
6. a Spectra Physics model 332 spatial filter and expanding lens assembly (expanding lens L4, aperture A4) mounted on a Spectra Physics model 306A precision optical mount with base and vertical post which is used to eliminate spatial noise and produce a smooth intensity profile across the expanded reference beam,
7. a piece of 0.3 x 0.2m frosted glass mounted on a heavy metal base, of which its reconstructed image from the

hologram is used as a white background for the interference fringes,

8. a photographic plate holder which is designed to hold a half size Agfa-Gevaert 10E75 AH (0.1016 x 0.0635m) photographic plate for double exposure holographic technique, or an Elomag immersion-type X-Y micropositionable photographic plate holder, model MPH-45W, including PC-45 plate carriage which is used to hold and to reposition a full size Agfa-Gevaert 10E75 (0.1016 x 0.127m) photographic plate for real time holographic technique. Photographs of these holographic plate holders are shown in Plate 4.1.

The positions of the optical components and the polymer coating surface are determined according to the Holo-Diagram technique (1,2,3,4). The polymer coating is placed along the ellipse whose foci are the beam splitter and the center of the photoghaphic plate and away from the line joining the two foci. In this work, the distance between the beam splitter and the center of the photographic plate is fixed at approximately 1.2m. The length of the object surface, which is the hypothenuse of a right-angle glass prism is 0.125m. Because of the geometry of the optical set-up in this work, the angle of illumination and observation of the object surface is restricted to 45° by use of the right-angle prism. Abramson (1) has mentioned that in holographic interferometry, if the object is illuminated and looked upon in a direction that makes an angle β, to the

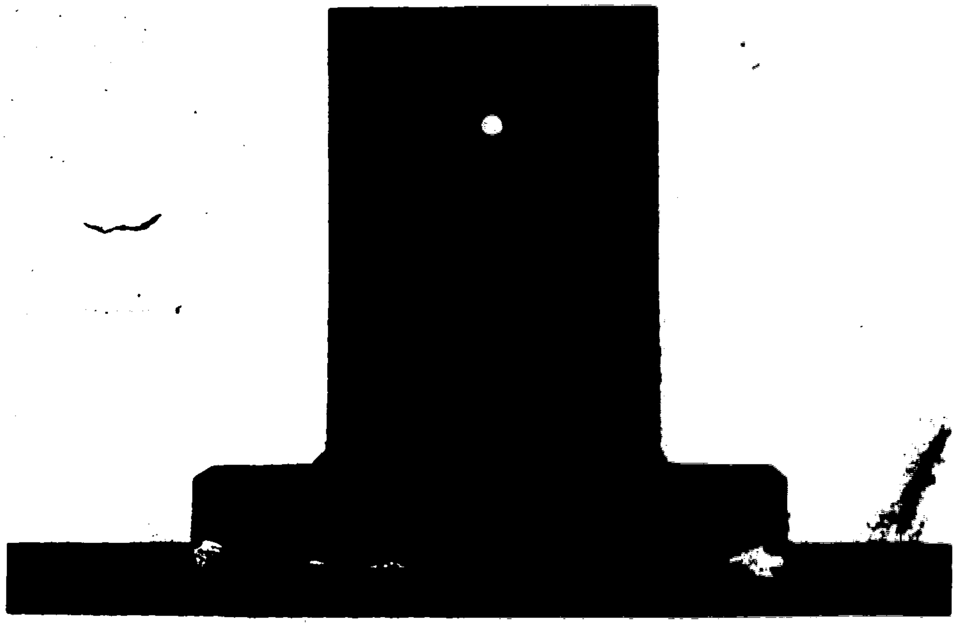

(a) DOUBLE EXPOSURE HOLOGRAPHY

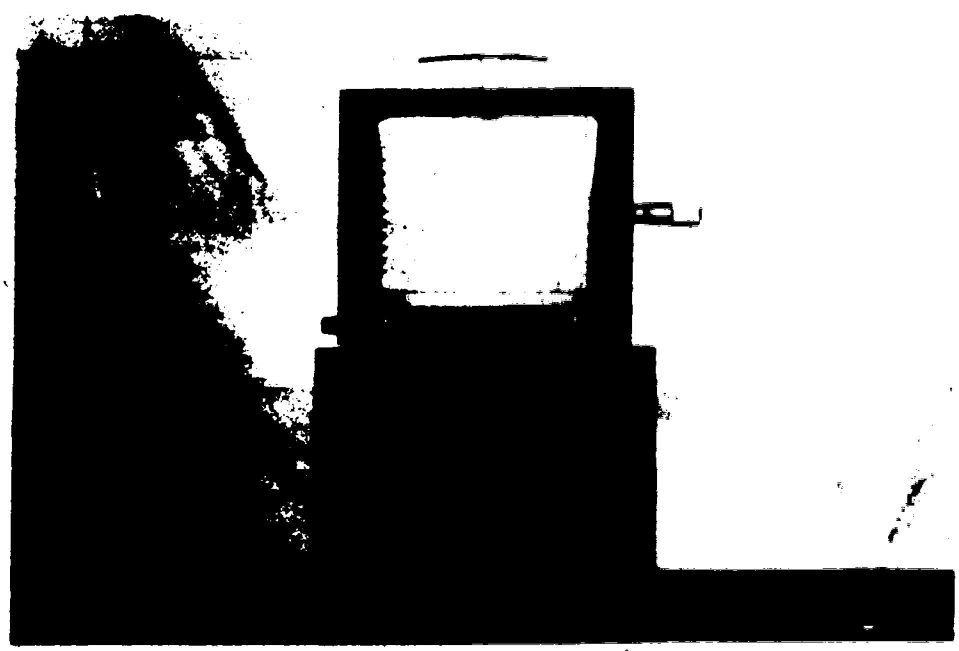

(b) REAL TIME HOLOGRAPHY

PLATE 4.1 : PHOTOGRAPHS OF HOLOGRAPHIC PLATE HOLDERS

object surface, the distance between two dark fringes will correspond to a difference in thickness of half the wavelength of the light used multipled by a constant k_1. Abramson defined the constant k_1 as the reciprocal of cos β_1. In this work, the value of k_1 can be easily evaluated as 1.414 or the reciprocal of cos 45°. According to the Holo-Diagram, the object in this work must be placed along the ellipse passing through the point at which the k_1 value is 1.414 and the distances to both the two foci are equal. Due to the finite length of the object surface, the light that is reflected from its different parts must travel different distances. In other words, the k_1 values along the object surface at different parts are always different. Consequently, the pattern of fringes moves relatively to the object when viewed from different directions (2). In this work, the length of the object is only 0.125m compared to the distance which is 1.2m between the two foci, therefore the movement of the fringe pattern is not serious. In addition, this shortcoming can be overcome by looking at and photographing the fringe pattern at a fixed direction all the time. This can be accomplished by mounting an aluminum plate with a 0.013m diameter hole at the center on the photographic plate holder (see Plate 4.1). The fringe pattern is then viewed through the circular hole.

The positions of the two mirrors are adjusted so that the path lengths of the object and the reference beams, measured from the beam splitter to the center of the photographic plate have the same value. Consequently, the maximum coherent length of the laser is utilized so as to give the maximum object field of depth.

An overall view of the optical set-up is shown in the photographs in Plate 4.2.

To record a hologram of the polymer coating from this optical set-up, the laser beam with diameter about 0.002m is split into a reference and a object beams. The ratio of beam intensitives can be altered at any time by rotating the mirror of the beam splitter-attenuator to different surface reflectivities. The reference beam is directed by two mirrors bypassing the polymer coating and is expanded by the spatial filter and expanding lens assembly. The expanded reference beam falls on the photographic plate. The object beam is expanded by the spatial filter and expanding lens assembly so that it is wide enough to cover the whole object. The object beam travels through the prism and the polymer coating and it experiences a total internal reflection at the surface of the coating. Finally, the object beam leaves the prism and falls on the photographic plate. The interference pattern generated by over-lapping object and reference beams is recorded to form the hologram.

In both the double exposure holographic technique and the real time holographic technique, on reconstruction of the hologram, the object images recorded before and after the change in coating thickness interfere with each other to form fringes. The absolute magnitude of the change of

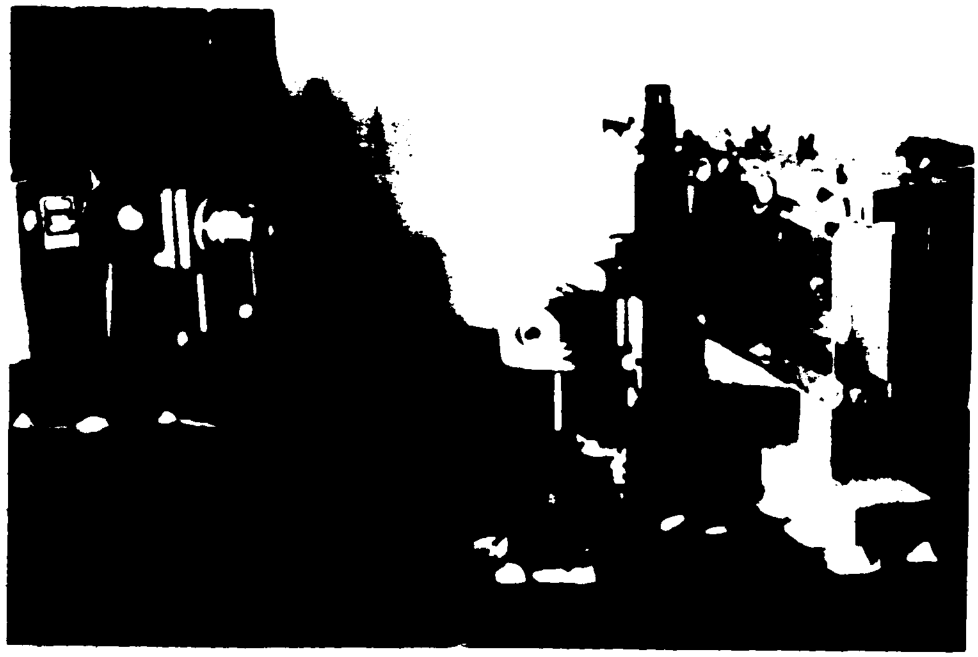

(a)

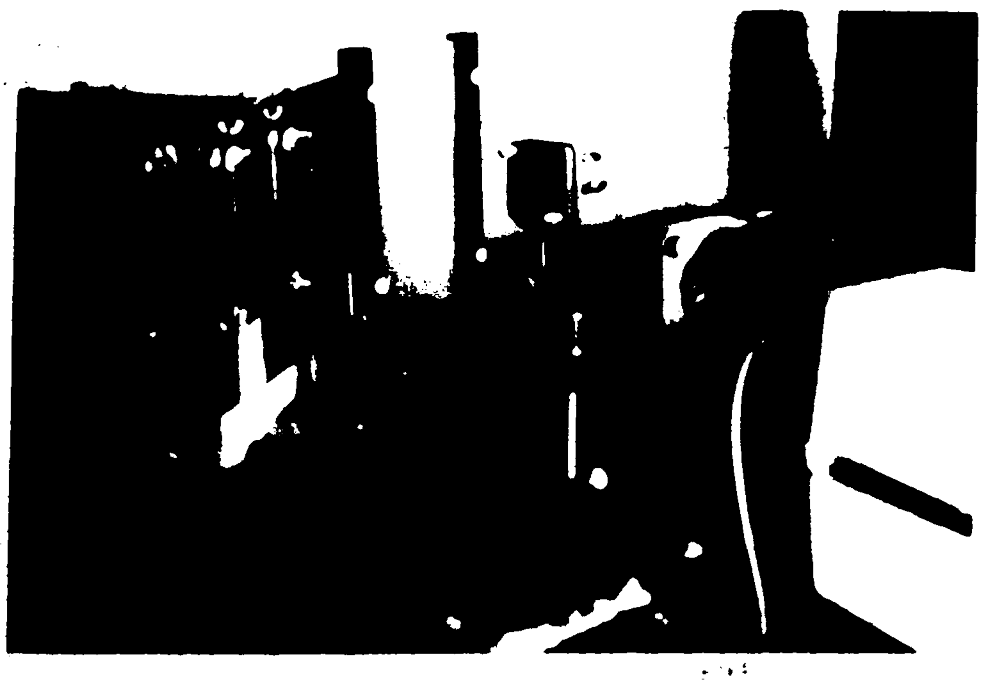

(b)

PLATE 4.2 : OVERALL VIEW OF THE OPTICAL SET-UP

coating thickness is given by

$$r' = n\, B\, \lambda \qquad (4.1)$$

where r' is the displacement of a given object point from a fixed point, λ is the wavelength of light, and n is the fringe order of the point under consideration. B is, in general, a function of spatial position of the object point relative to the beam splitter and the photographic plate. In this work, all the positions of the optical components remained the same, therefore B is considered a constant. By simple geometrical manipulations, B can be easily evaluated from the optical set-up by calculating the difference in the path lengths of a light ray before and after a change of coating thickness. Figure 4.2 shows the paths of a light ray before and after a mass transfer experiment for a given change of coating thickness, r'. The change in the light path length between a-a and b-b is the same between c-c and d-d, and is given by

$$2r'(n_s - n_p \sin \beta_1 \sin \beta_2) / \cos \beta_2 \qquad (4.2)$$

where n and n are refractive index of the swollen polymer and the glass prism respectively (n_s=1.428 and n_p=1.5). The angle β_1 as shown in Figure 4.2 is equal to 45°. The angle $\beta_2 = \sin^{-1} (n_p \sin \beta_1 / n_s)$ is calculated as 47°58'. As the appearance of a fringe is due to a change of light path

7

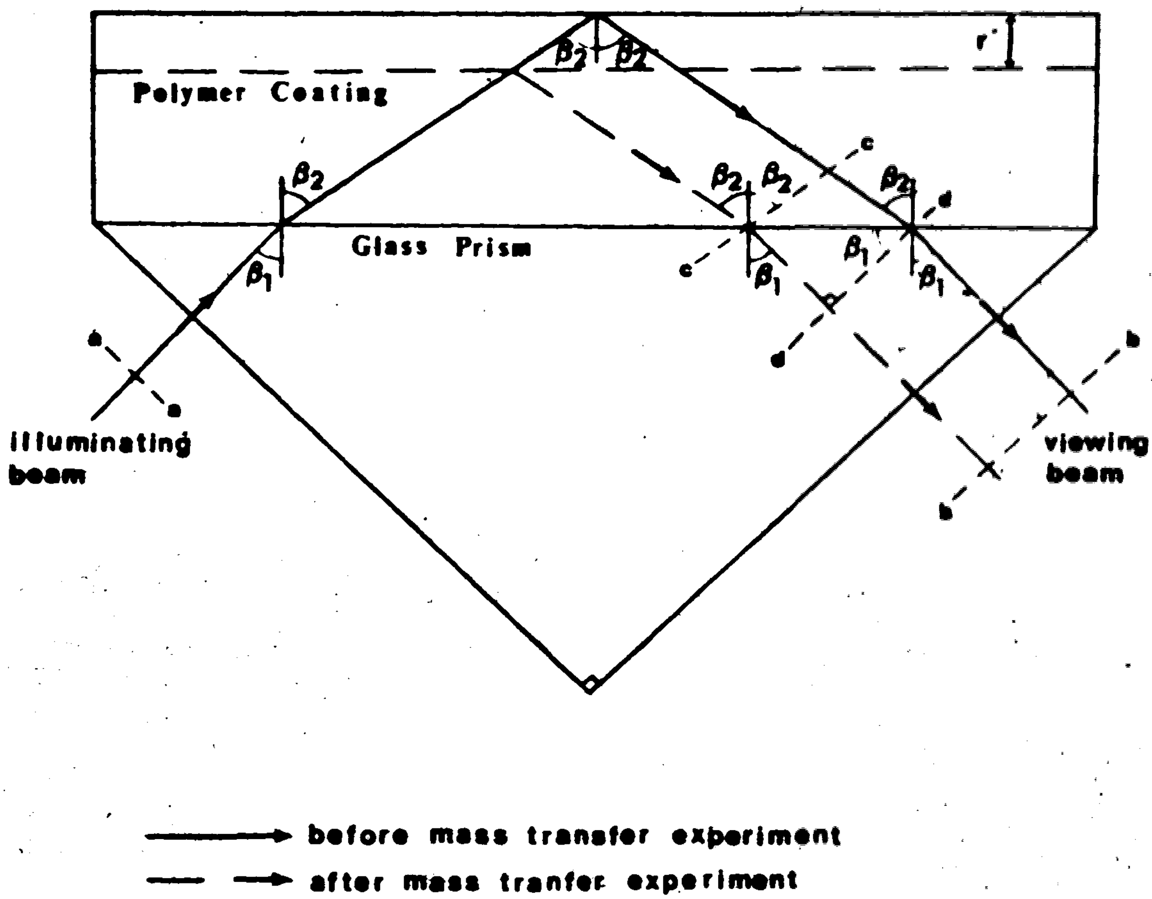

FIGURE 4.2 : LIGHT PATH LENGTH BEFORE AND AFTER MASS TRANSFER EXPERIMENT

lengths of $n\lambda/2$, then the change of coating thickness r' for nth fringe is given by

$$r' = n\lambda \cos \beta_2 \,/\, 4(n_s - n_p \sin \beta_1 \sin \beta_2) \qquad (4.3)$$

Comparing Equations 4.1 and 4.3, the constant B is given by

$$B = \cos \beta_2 \,/\, 4(n_s - n_p \sin \beta_1 \sin \beta_2) \qquad (4.4)$$

Hence, by knowing the incident angle β_1 and the refractive angle β_2, the value of B can be calculated by using Equation 4.4. If the value of B is known and the fringe order n is determined, the absolute magnitude of the polymer coating shrinkage at a given point can be evaluated.

4.2 MASS TRANSFER EXPERIMENTAL SET-UP

The mass transfer experimental set-up is shown in the photographs in Plate 4.3 and it includes the following: an impingement plate, a confinement plate from which a slot jet issues, a top spacer and also a bottom spacer.

1. The mass transferring surface is the hypothenuse surface of a right-angle glass prism (0.089 x 0.125m) which is fitted into a window cutting of an aluminum plate. The aluminum plate, 0.149 x 0.625m, has a thickness of 0.012m. The surface of the prism together with the

(a)

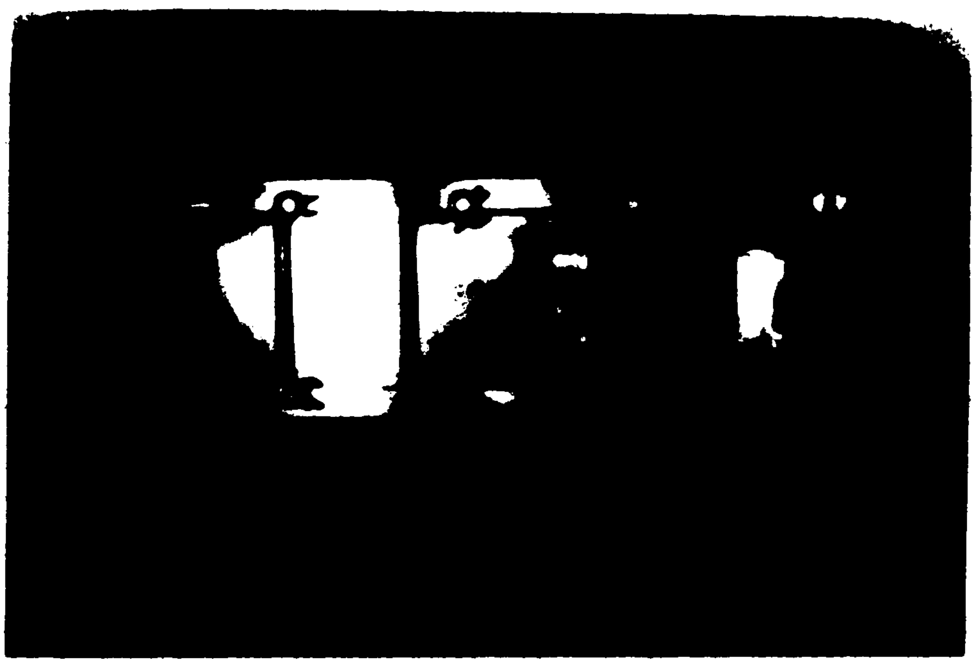

(b)

PLATE 4.3 : THE OVERALL VIEW OF THE MASS TRANSFER EXPERIMENTAL SET-UP

aluminum plate form one flat surface. This surface is then coated with a thin layer of silicone rubber to form the impingement plate. The front and top views of this impingement plate are shown in Figure 4.3.

2. An aluminum plate having a thickness of 0.012m and the same size as the impingement plate is attached normally to the nozzle of an aluminum slot tube. The aluminum tube with dimensions 0.0015 x 0.132 x 0.4m is long enough to provide a fully developed parabolic velocity profile at the nozzle exit for the highest Reynolds number used in this work. The large ratio of plate span (0.132m) to nozzle width (0.0015m) minimizes end effects and leads to a situation of nearly a two-dimensional jet. The front and top views of the confined plate and the aluminum tube are shown in Figure 4.4.

3. Three sets of spacers are used so as to obtain three different jet-to-plate spacings. A set of spacers includes two aluminum plates of the equal width. One aluminum plate is mounted on top of the impingement plate and the confinement plate, so called top spacer. Another aluminum plate is mounted on the bottom, so called bottom spacer. The gaps between the impingement plate and the confinement plate for these three sets of spacers are 0.003m, 0.006m, and 0.018m, respectively. These correspond to jet-to-plate spacings of 2b, 4b and 12b.

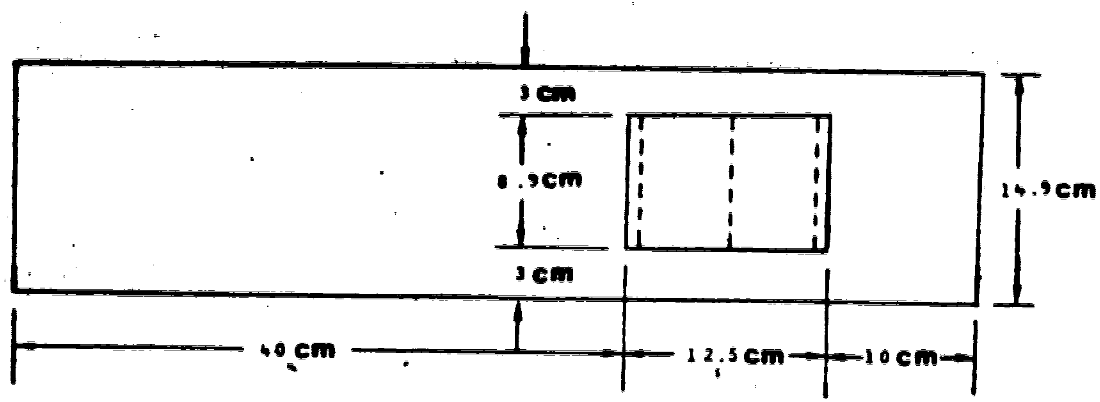

(a) FRONT VIEW

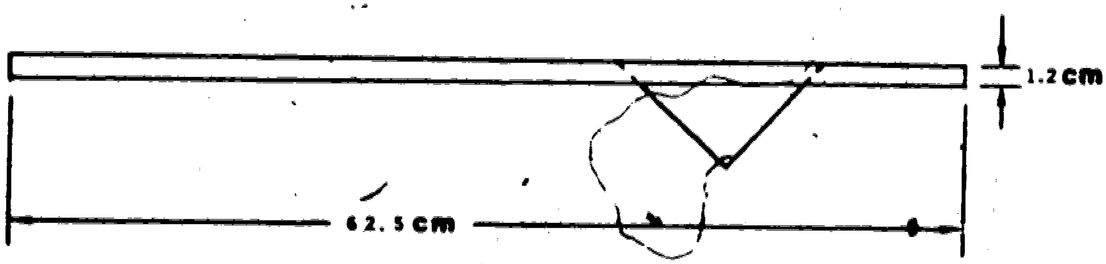

(b) TOP VIEW

FIGURE 4.3 : FRONT AND TOP VIEWS OF IMPINGEMENT PLATE

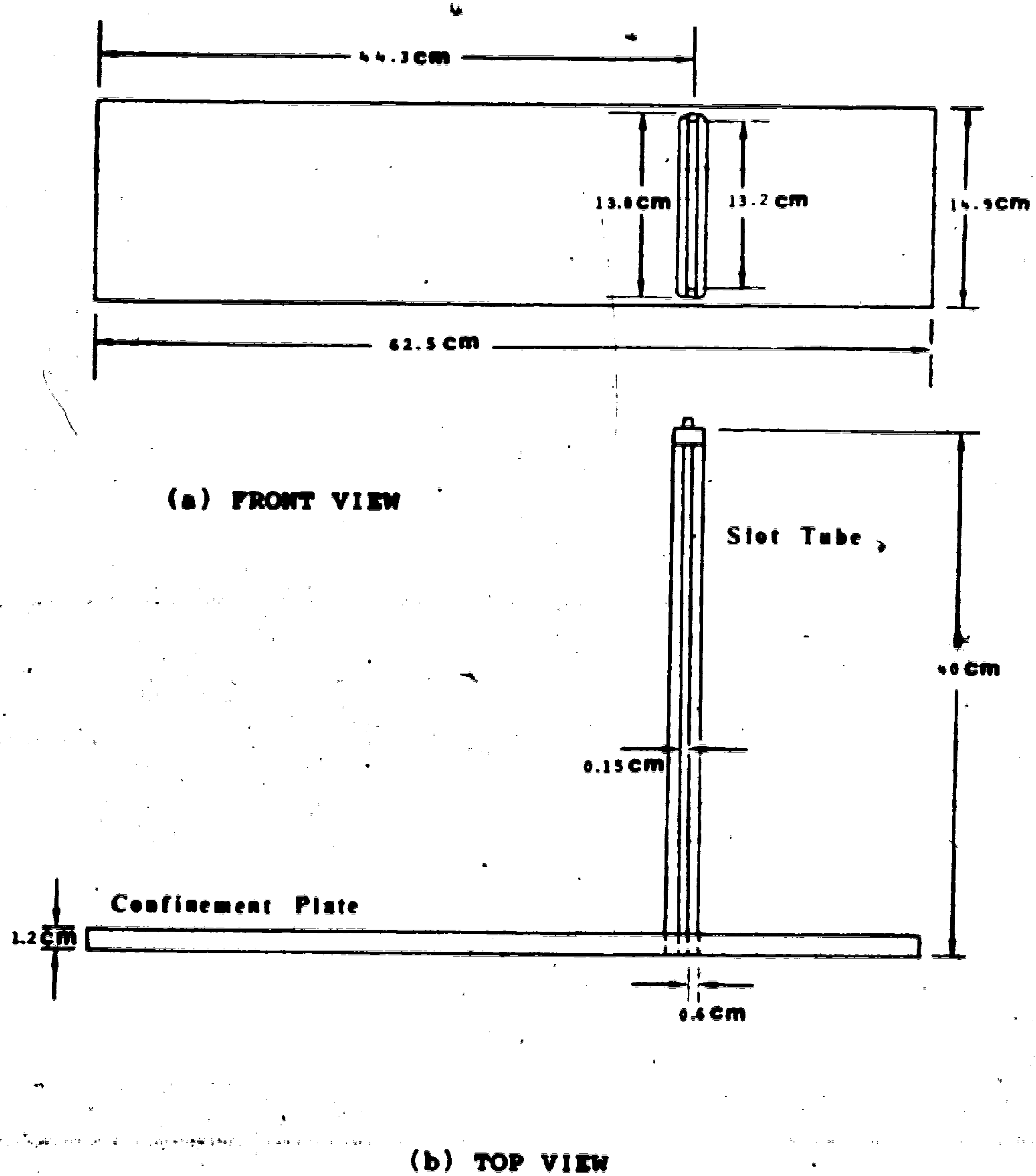

FIGURE 4.4 : FRONT AND TOP VIEWS OF CONFINEMENT PLATE WITH SLOT TUBE

The mass transfer experimental set-up is mounted on a heavy metal base as shown in Plate 4.3. The spacers are used to fit between the impingement and the confinement plates so as to form a rectangular channel in which the jet flow would be confined. With such an arrangement of the aluminum slot tube and the impingement plate, the air impinges normally on the impingement surface at a line which is 0.043m from one edge of the glass prism and 0.082m from the other. Since only the mass transfer on the hypothenuse surface of the prism can be studied by holographic interferometry, the location of the slot nozzle allows the effective downstream distance for which mass transfer can be measured to be 55b.

Before each experiment, the impingement plate is easily repositioned with the help of the top and bottom spacers. The impingement plate and the top spacer can be removed after each experiment while the confinement plate and the bottom spacer remained on the heavy metal base.

4.3 EXPERIMENTAL PROCEDURE

The experimental procedure for double exposure holographic interferometry is discussed in Sections 4.3.1 to 4.3.4, while the experimental procedure for real time holographic interferometry is discussed in Section 4.3.5.

4.3.1 PREPARATION OF POLYMER COATING

The polymer coating is formed as follows:

1. Liquid silicone primer, SS-4120, from General Electric is applied by bushing uniformly on the cleaned mass transferring surface. It is important to allow the primer to dry in air for at least one hour before the polymer is applied.
2. Ten parts of liquid polymer rubber, RTV-615A silicone rubber, and one part of catalyst RTV-615B (both from General Electric) are mixed throughly in a styrofoam cup to about 0.1 kg of mixture.
3. The polymer mixture is poured evenly on the mass transferring surface with the mass transferring surface being horizontal.
4. In order to obtain a uniform coating thickness, the freshly coated surface is allowed to semi-harden at room temperature for about ten hours.
5. The semi-harden surface is then cured in the oven at 65°C for three hours.

For complete swelling of a fresh polymer coating with ethylsalicylate it took at least ten hours, while re-swelling a partially exhausted coating after an experimental run required about three hours of immersion in the swelling agent bath.

The refractive index of silicone rubber swollen to various degrees was found by Masliyah and Nguyen (51). It is evident that the refractive index is a weak function of the degree of swelling when the swollen polymer is near its equilibrium value.

4.3.2 MAKING OF DOUBLE EXPOSURE HOLOGRAM

Each full sized Agfa-Gevaert 10E75 AH photographic plate (0.1016 x 0.127m) is cut into two halves (0.1016 x 0.0635m) in the dark room by using a glass cutter and an aluminum guiding plate. To avoid damage to the emulsion side of the photographic plate, an incision is made only on the back side with minimum stress.

The 50 mW He-Ne laser is turned on at least half an hour before an experimental run. By rotating the mirror of the beam splitter-attenuator to the reading of 110, the intensity of the object beam is selected as about three times the intensity of the reference beam. The shutter is then set at 1/30 s. The selections of the exposure time and the intensity ratio between the two beams were found by trial and error, and remained the same for all the experimental runs.

The impingement plate is removed from the swelling bath and is dried carefully by using clean tissue paper. The impingement plate is then placed on top of the bottom spacer and is mounted with the confinement plate and the top spacer to form a rectangular channel. The laboratory temperature and pressure are measured, and the laboratory lights are then switched off. The photographic plate is placed in the plate holder.

Since handling the mounting of the rectangular channel and the photographic plate can create a temperature gradient, the equipment is left for several minutes in order to equilibrate with the laboratory. The shutter is then activated with an exposure time of 1/30 s and the first exposure is made on the photographic plate. The mass transfer experiment is then started. Air is supplied from a compressed air cylinder and its volumetric flow rate is measured by a rotameter. Two rotameters are used in this work, Fischer & Porter Co. Rotameter and Brook Rotameter. Each rotameter covers a different range of volumetric air flow rate. The calibrations of these two rotameters are given in Appendix B. After a given period of time, the air flow is stopped. The shutter is reactivated with the same exposure time to obtain a second exposure on the photographic plate.

4.3.3 PROCESSING OF HOLOGRAM

The exposed photographic plate is removed from the plate holder for processing. The processing sequence is as follows:

The photographic plate is

1. developed with Kodak D-19 developer solution for 2 to 3 minutes,
2. stopped with Kodak indicator stop bath for half a minute,
3. fixed with Kodak rapid fixed solution for 2 minutes,

4. washed with tap water,
5. and finally dried by spraying methanol on the photographic plate.

4.3.4 PHOTOGRAPHING OF RECONSTRUCTED IMAGE

To record the virtual image of a double exposed hologram, the following procedure is used.

1. The double exposed hologram, after processing, is repositioned in the photographic plate holder.
2. The intensity of the reference beam is selected as about one half of that of the object beam by rotating the mirror of the beam splitter-attenuator to the reading of 60. In other words, the intensity of the reference beam is higher than that when the double exposed hologram was made.
3. The object beam is then blocked off.
4. A Nikon F2A Photomic camera with Nikon Motor Drive MD-3 and Micro-Nikkor 105mm f/4 Lens is placed behind the hologram and the view guiding aluminum plate. The lens aperture is normally set at f/4 and exposure time varied from 8 to 20 seconds. Focusing the camera on the reconstructed virtual image, the photograph of this image can then be taken.
5. Kodak Tri-X pan film (TX 402) with ASA speed of 400, a fast black and white film, is used.

The processing of the Tri-X pan film is proceeded in room temperature as follows:

The film is

1. developed with Kodak D-76 developer solution for 7 minutes,
2. stopped with Kodak indicator stop bath for half a minute,
3. fixed with Kodak fixer solution for 4 minutes,
4. washed with running tap water,
5. and finally dried by hanging in a dust free room.

4.3.5 PROCEDURE FOR REAL TIME HOLOGRAPHIC INTERFEROMETRY

In this work, real time holographic interferometry is used for qualitative study only. This technique is used for determining the order of a particular fringe of the "frozen fringe" pattern obtained from double exposed hologram.

For real time holographic interferometry, an immersion-type X-Y micropositionable photographic plate holder, model MPH-45W, is used instead of the simple plate holder used in double exposure holographic interferometry. A full size Agfa-Gevaert 10E75 (0.1016 x 0.127m) photographic plate is placed in the PC-45 plate carriage and is allowed to normalize in the plate holder water cell for approximately 15 minutes. This operation pre-sensitizes the emulsion and also allows strain release, swelling, or other emulsion excursions to occur prior to exposure. The mass transfer set-up is prepared as previously discussed. The shutter is activated with an exposure time of 1/60 s. This exposure time is half of that of the double exposure holographic interferometry because the photographic emulsion becomes more sensitive while soaking in water. But the intensity ratio between the reference and the object beams is maintained the same as that of the double exposure holographic interferometry. The plate carriage with the photographic plate is then removed from the water cell for processing. The processing sequence is as previous Section 4.3.3 except in this case the developing time is shorter.

The hologram after processing is placed back into the water cell to within one fringe alignment by using the precision X-Y controls on the plate holder. With both the reference and object beams striking the hologram, the fringes which occur between the holographic virtual image and the actual subject image can be eliminated by adjusting the plate position with the precision X-Y controls. When no interference fringes on the object are observed, this indicates that the photographic plate is repositioned in its original position. The mass transfer experiment is then proceeded with. The shrinkage of the polymer coating can be viewed behind the hologram as real time interference fringes across the image. The order of any particular fringe can be determined by counting fringes at a given location on the impingement plate as they appear in real time.

5. CALIBRATION AND VALIDITY OF THE EXPERIMENTAL SET-UP

Mass transfer characteristics due to an unconfined laminar impinging two-dimensional air jet is studied by measuring the local Sherwood number along the impingement plate. Local Sherwood number in this work is defined by

$$Sh_b = k\ b\ /\ D \tag{5.1}$$

or

$$Sh'_b = k'\ b\ /\ D \tag{5.2}$$

where k and k' are the local mass transfer coefficients, and D is the diffusion coefficient. The local mass transfer coefficients k and k' are defined by

$$N = k\ (p_s - p_j)\ \rho^*\ Mw\ /\ P \tag{5.3}$$

and

$$N = k'\ (p_s - p_s)\ \rho^*\ Mw\ /\ P \tag{5.4}$$

where N is mass flux, ρ^* is the molar density of the gas mixture, Mw is the molecular weight of swelling agent, and P is the total pressure. The partial vapor pressures of the swelling agent, p_s, p_j and p_s are located at the coating surface, the jet nozzle exit and in the bulk flow, respectively.

For an unconfined air jet, the partial vapor pressures of the swelling agent at the jet nozzle exit and in the bulk flow are equal to zero (p_j=p_s=0). It leads to k=k' from

Equations 5.3 and 5.4. However, for an confined air jet, p_s is no longer equal to zero and it is not easy to measure in the experimental set-up of this work. Therefore, only the Sherwood numbers evaluated from Equation 5.1 are investigated in the experimental study for confined air jet. On the other hand, p_s can be evaluated numerically. Both the Sherwood numbers evaluated from Equations 5.1 and 5.2 are investigated in the numerical study.

For both confined and unconfined air jet, $p_j=0$ and the partial vapor pressure of the swelling agent at the coating surface, p_s, is that of its vapor pressure, $P°$, during the "constant rate period" and Equation 5.3 simplifies to

$$N = k\ P°\ \rho°\ Mw\ /\ P \qquad (5.5)$$

The mass flux, N, can also be given as

$$N = r'\ \rho_s\ /\ T \qquad (5.6)$$

where r' is the change of coating thickness given by Equation 4.1, ρ_s is the density of the swollen polymer and T is the duration of the mass transfer experiment. The product $r'\rho_s$ is the mass of swelling agent transfered per unit area, since the swollen polymer volume is the sum of the volume of the dry polymer and that of the pure swelling agent (47). Substituting Equation 4.1 into Equation 5.6, one obtains

$$N = n B \lambda \rho_s / T \qquad (5.7)$$

Define $A = B \lambda \rho_s$, then Equation 5.7 becomes

$$N = A (n / T) \qquad (5.8)$$

where A is a constant for a given mass transfer experimental and optical set-up. Constant A is also referred to as the calibration constant of the experimental set-up. Combining Equations 5.1, 5.5 and 5.8, one obtains

$$\begin{aligned} Sh &= (A P / \rho^{\circ} P^{\circ} Mw) (b / D) (n / T) \\ &= G (n / T) \end{aligned} \qquad (5.9)$$

where G is dependent only on the physical properties of working fluids.

Therefore, to evaluate the local Sherwood number it is necessary to know the physical properties under the operating conditions, the local fringe order and the duration of the experimental run.

5.1 CALIBRATION PROCEDURE

In order to evaluate the mass flux of the swelling agent, it is necessary to know the value of the constant A of Equation 5.8. The calibration constant A can be obtained by studying the mass transfer due to an unconfined laminar impinging axisymmetric air jet with initial parabolic velocity profile using the same optical set-up as shown in Figure 4.1.

This calibration is made using the theoretical expression obtained by Scholtz and Trass (79) for an unconfined laminar impinging axisymmetric submerged jet in the wall jet region given by Equation 2.15 as

$$Sh_d = c_1 \, Re_d^{0.75} \, (r/d)^{-1.25} \qquad (5.10)$$

where $c_1 = 0.458 \; \Gamma(Sc + 1/3) / (\Gamma(Sc) \; \Gamma(1/3))$ (5.11)

for initial parabolic velocity profile. Equation 5.10 has been shown by Scholtz and Trass (79) to be fairly accurate in the wall jet region. Equating Equations 5.9 and 5.10 by using the nozzle diameter, d, instead of the slot width, b, as the characteristic length in Equation 5.9 for the case of axisymmetric and rearranging, yields

$$n = (c_1 \, D \, \rho^{\circ} \, P^{\circ} \, Mw \, / \, d \, A \, P) \, (T \, Re_d^{0.75} \, (r/d)^{-1.25}) \qquad (5.12)$$

If a mass transfer experiment is performed using an unconfined impinging axisymmetric air jet with initial parabolic velocity profile, then a plot of n versus $(T \, Re_d^{0.75} \, (r/d)^{-1.25})$ in the wall jet region gives as its slope $(c,\ D\ \rho^{\circ}\ P^{\circ}\ Mw\ /\ d\ A\ P)$. The constant A can then be evaluated from the knowledge of the physical properties of the system.

The experimental set-up and procedure for an unconfined axisymmetric jet are similar to those for a confined two-dimensional jet mentioned in Chapter [illegible]. Here, the confinement plate and slot tube referred to in Chapter 4 is replaced by a circular tube with a diameter equal to 0.003m. This tube is mounted on a heavy stand. The tube is set perpendicular to the mass transferring surface with a jet-to-plate spacing of 1.5d. Double exposure holographic interferometry is used throughtout this calibration. Experimental runs with durations equal to 90s, 180s and 360s and for Re_d=1210 and 1470 are made. The average operating temperature and pressure of the experimental runs were 20.7°C and 93.87kPa, respectively.

The "frozen fringe" pattern for run no. CJ14-1.5B for Re_d=1470 and T=90s is shown in Plate 5.1a. The "frozen fringe" pattern for run no. CJ14-6A for Re_d=1470 and T=360s is shown in Plate 5.1b. Determination of fringe order of these "frozen fringe" patterns is rather simple. In Plate 5.1a, the outer bright region is considered to be the zeroth order fringe where no mass transfer as yet has occured. Since in this case the zeroth order fringe is known, the determination of the order of other fringes is straightforward. By counting the fringe order from the outer zeroth order fringe towards the stagnation point, it is

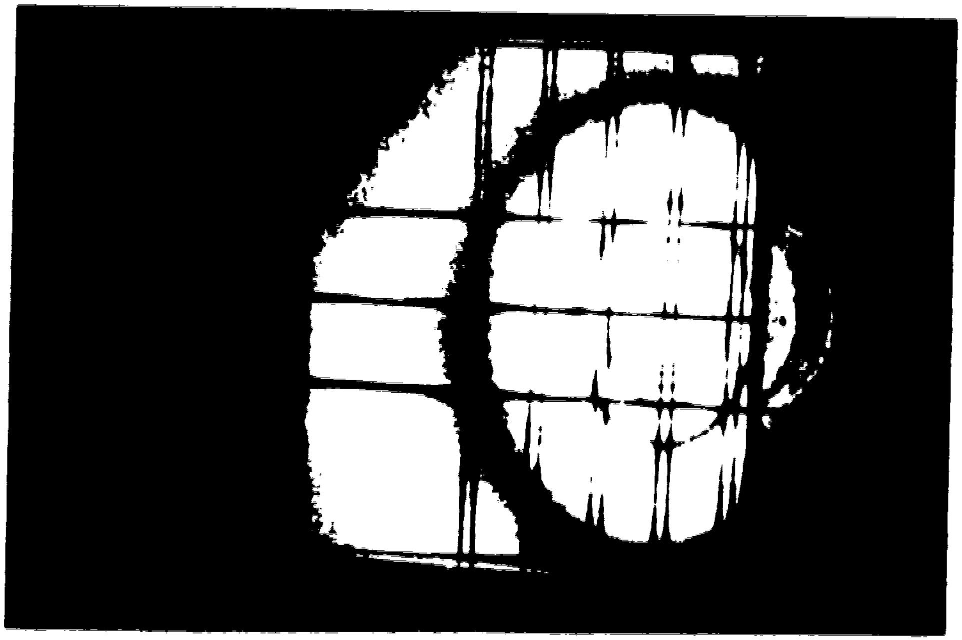

(a) T = 90s

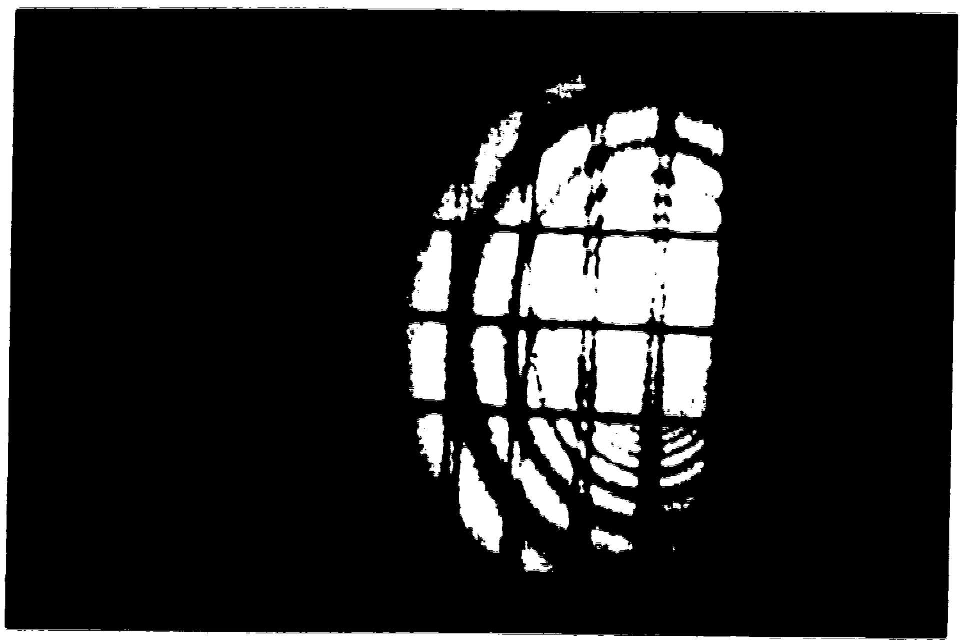

(b) T = 360s

PLATE 5.1 : CONTOURS OF EQUAL MASS TRANSFER RATE FOR AN UNCONFINED AXISYMMETRIC AIR JET (Re_d=1470)

possible to label all the fringes. It is thus this short duration experiment that gives the base on which the long duration experiment, such as the one shown in Plate 5.1b, are interpreted. In each experimental run, the variation of the local fringe order, n, with dimensionless radial distance, r/d, is determined. Experimental results of local fringe order, n, and dimensionless radial distance, r/d, are given in Appendix C.

A confirmation of the "constant rate period" can be obtained by combining all the experimental runs for a given Reynolds number in the form of n/T (51). A plot of n/T versus r/d for Re_d=1470 is shown in Figure 5.1. Here, the data for different duration collapse onto one curve indicating that the driving force, in this case, the swelling agent vapor pressure at the coating surface, P', is the same for both the shortest and for the longest mass transfer experiment.

A plot of Equation 5.12 is given in Figure 5.2. The slope of the least squares linear regression is 634.08s^{-1} which gives A as 1.614x10^{-4} kg/m^2 using physical properties in Appendix A evaluated at average operating conditions of 20.7°C and 93.87kPa.

It is possible to proceed in a different manner to obtain a calibration constant A. Using the appropriate data, Equation 4.4 gives B=0.2615. Since the calibration constant, A, is defined as $B\lambda\rho_s$, by using the values of swollen coating density, ρ_s, and the wavelength of the light, λ, in

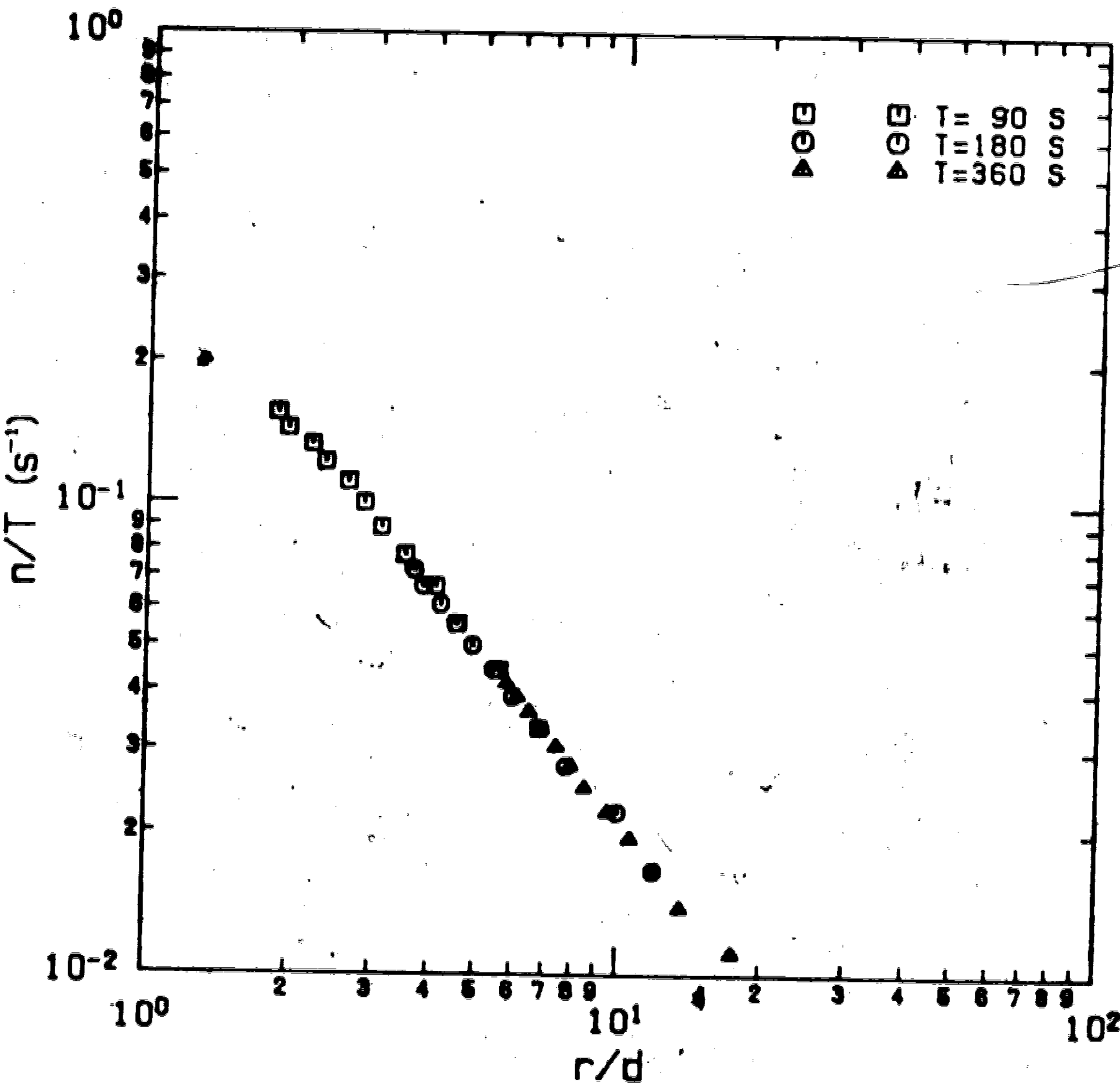

FIGURE 5.1 : VARIATION OF n/T WITH DIMENSIONLESS RADIAL DISTANCE FOR Re_d=1470

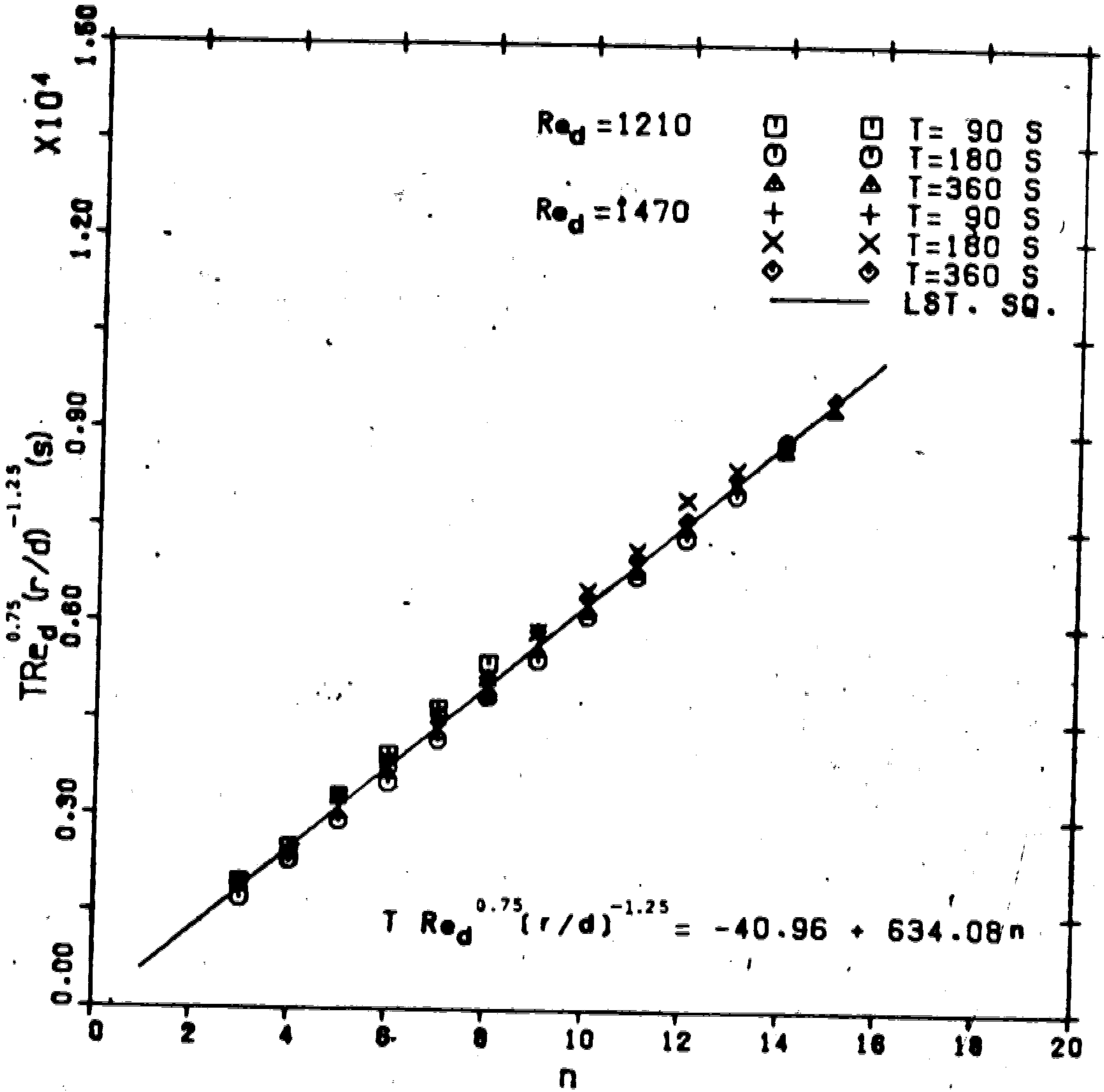

FIGURE 5.2 : CALIBRATION PLOT USING AN UNCONFINED AXISYMMETRIC AIR JET

Appendix A, A becomes 1.67×10^{-4} kg/m^2.

The agreement between the two methods for evaluating the constant A is within 3.3%. This agreement confirms the success of the method based on optical analysis mentioned in Section 4.1. This also indicates that the coating surface is reasonably smooth throughtout the region of interest during the experimental period. The value of A as obtained from an unconfined axisymmetric air jet is used for the evaluation of local Sherwood number throughtout the experimental study of this work

5.2 TEST OF CALIBRATION VALIDITY

The validity of the value of calibration constant A evaluated in Section 5.1 is tested by studying the mass transfer due to an unconfined laminar impinging two-dimensional air jet with an initial parabolic velocity profile. The same optical set-up as shown in Figure 4.1 is used. Local Sherwood numbers in the wall jet region evaluated by using Equation 5.9 with $A = 1.614 \times 10^{-4}$ kg/m^2 are compared with the regression equation given by Masliyah and Nguyen (53)

$$Sh_b = 0.55\ Re_b^{0.55}\ (x/b)^{-0.73} \qquad (5.13)$$

for an unconfined impinging two-dimensional air jet

(Sc=2.85).

The experimental set-up and procedure for an unconfined two-dimensional jet are similar to those for an unconfined axisymmetric jet mentioned in Section 5.1, except a plexiglass slot tube with dimensions 0.0015 x 0.075 x 0.35m is used. This tube is mounted on a heavy stand and set perpendicular to the mass transferring surface with a jet-to-plate spacing of 4b. Double exposure holographic interferometry is used. Experiemental runs with durations equal to 120s, 240s and 480s and for Re_b=94 and 204 are made. The average operating temperature and pressure of the experimental runs were 20.7°C and 93.98kPa, respectively. Under these operating conditions, Sc=2.74.

The "frozen fringe" pattern for run no. SJ1-2A for Re_b=94 and T=120s is shown in Plate 5.2a. The "frozen fringe" pattern for run no. SJ1-4F for Re_b=94 and T=240s is shown in Plate 5.2b. In both cases, the zeroth order fringes are no longer on the mass transferring surface. A simple trial and error method introduced by Masliyah and Nguyen (51) when the zeroth order fringe cannot be identified is used to determine the fringe order in this case. In their study of unconfined axisymmetric air jet, Masliyah and Nguyen pointed out that, according to Equation 5.12, a plot of log(n) versus log(r/d) for experiments with various durations of a given Reynolds number gave curves which are parallel to each other. Similar behavior of fringe order with dimensionless streamwise distance for the

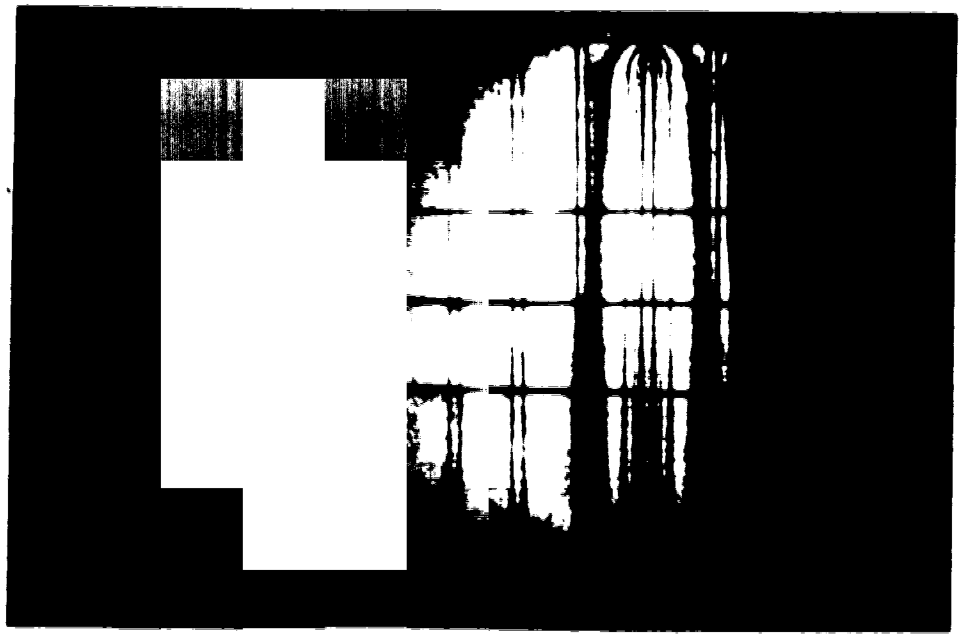

a T = 120s

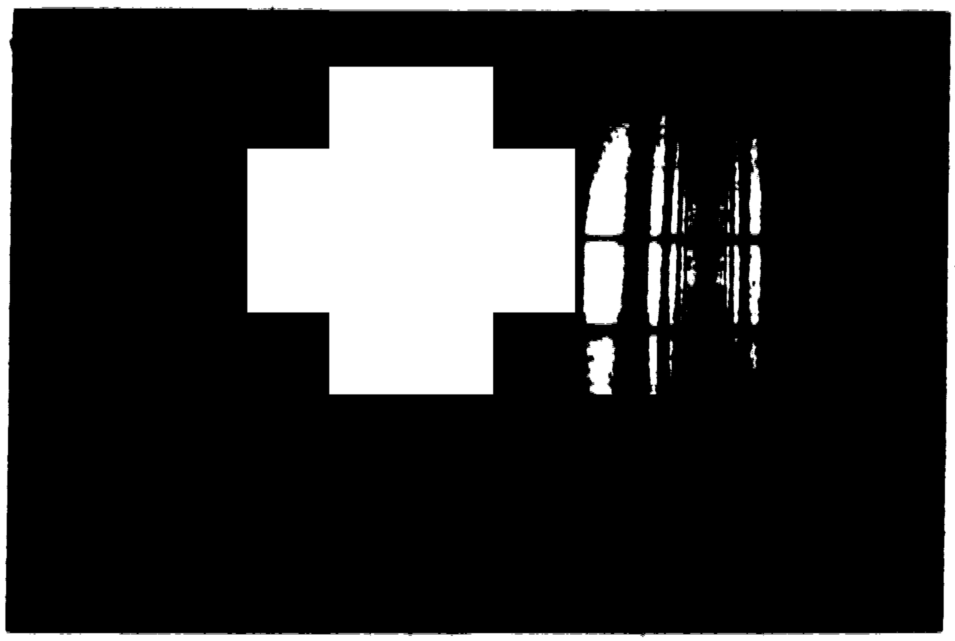

(b) T = 240s

PLATE 5.2 : CONTOURS OF EQUAL MASS TRANSFER RATE FOR AN UNCONFINED TWO-DIMENSIONAL AIR JET (Re_b=94)

two-dimensional case is expected. By choosing the correct local fringe order, the curves from a plot of log(n) versus log(x/b) for experiments with various durations of a given Reynolds number should therefore parallel to each other. Such a plot for an unconfined two-dimensional air jet is shown in Figure 5.3 for Re_b=94. Using such trial and error method, the outer darken regions in both Plates 5.2a and 5.2b are determined to be the first order fringes. By counting the fringe order from the outer first order fringe towards the stagnation point, it is possible to label all the fringes. As soon as the local fringe order is known, local Sherwood number can be easily determined by using Equation 5.9. In each experimental run, the variation of local Sherwood number, Sh_b, with dimensionless streamwise distance, x/b, are determined. Experimental results of local Sherwood number, Sh_b, and dimensionless streamwise distance, x/b, are given in Appendix D.

It is worthwhile to mention that the regression equation given by Masliyah and Nguyen (53), Equation 5.13, is only valid for Sc=2.85 which is slightly different from the Sc=2.74 of this work. Considering the effect of Schmidt number on local Sherwood number by using the correlation given by Scholtz and Trass, Equation 5.11, Equation 5.13 becomes

$$Sh_b = 0.54\ Re_b^{0.58}\ (x/b)^{-0.73} \qquad (5.14)$$

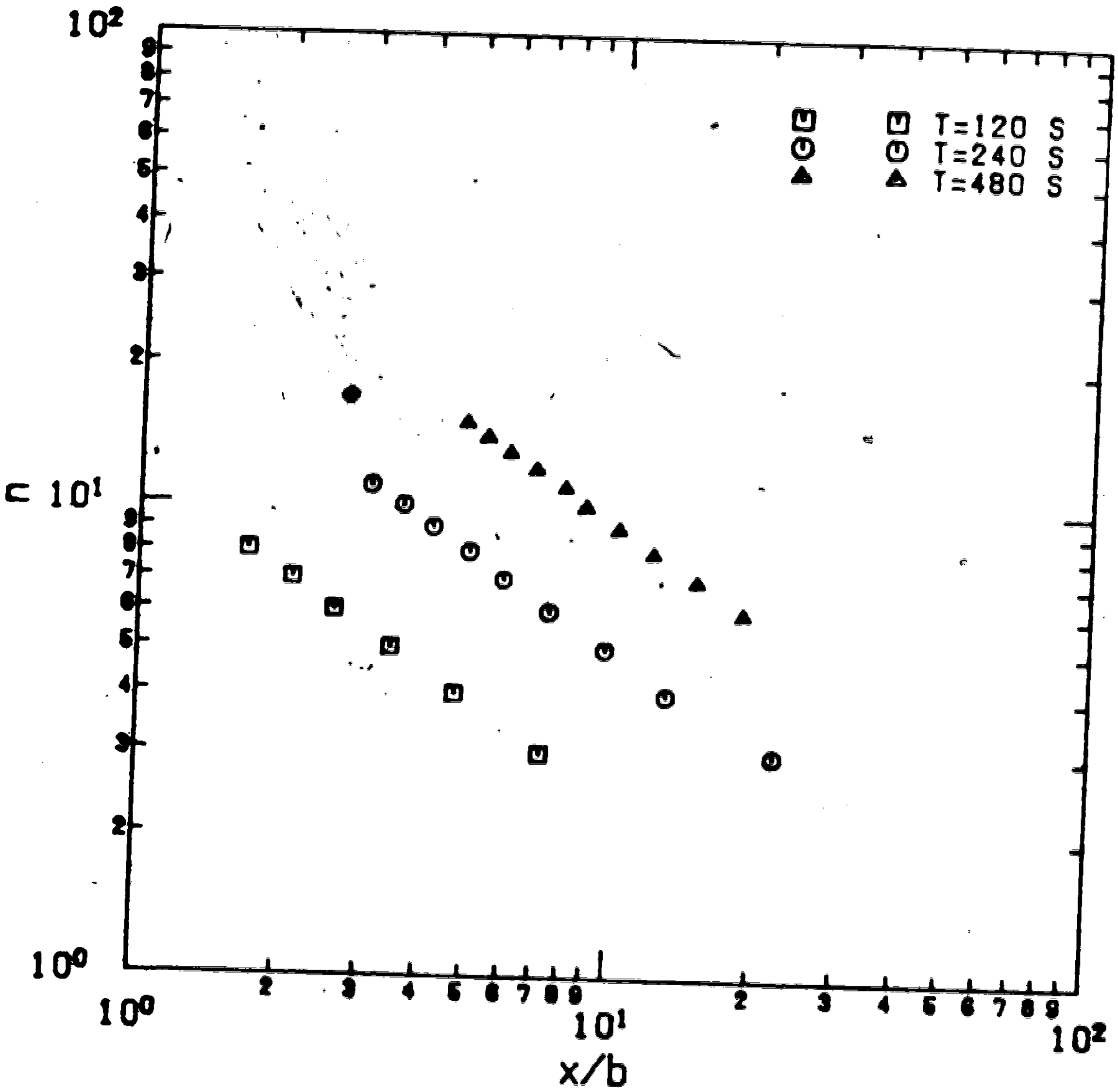

FIGURE 5.3 : VARIATION OF FRINGE ORDER WITH DIMENSIONLESS STREAMWISE DISTANCE FOR Re_b=94

for Sc=2.74.

A plot to test the validity of the experimental loc- Sherwood numbers for an unconfined two-dimensional air is shown in Figure 5.4. For a perfect fit with Equation 5.14, all data points should lie on a straight line having a slope of unity. From Figure 5.4, although it is observed that the data points are consistently above the perfect fit line, there are still within the scattered range (±9%) of the experimental data obtained by Masliyah and Nguyen (53). Therefore, the validity of the calibration constant A is reaffirmed.

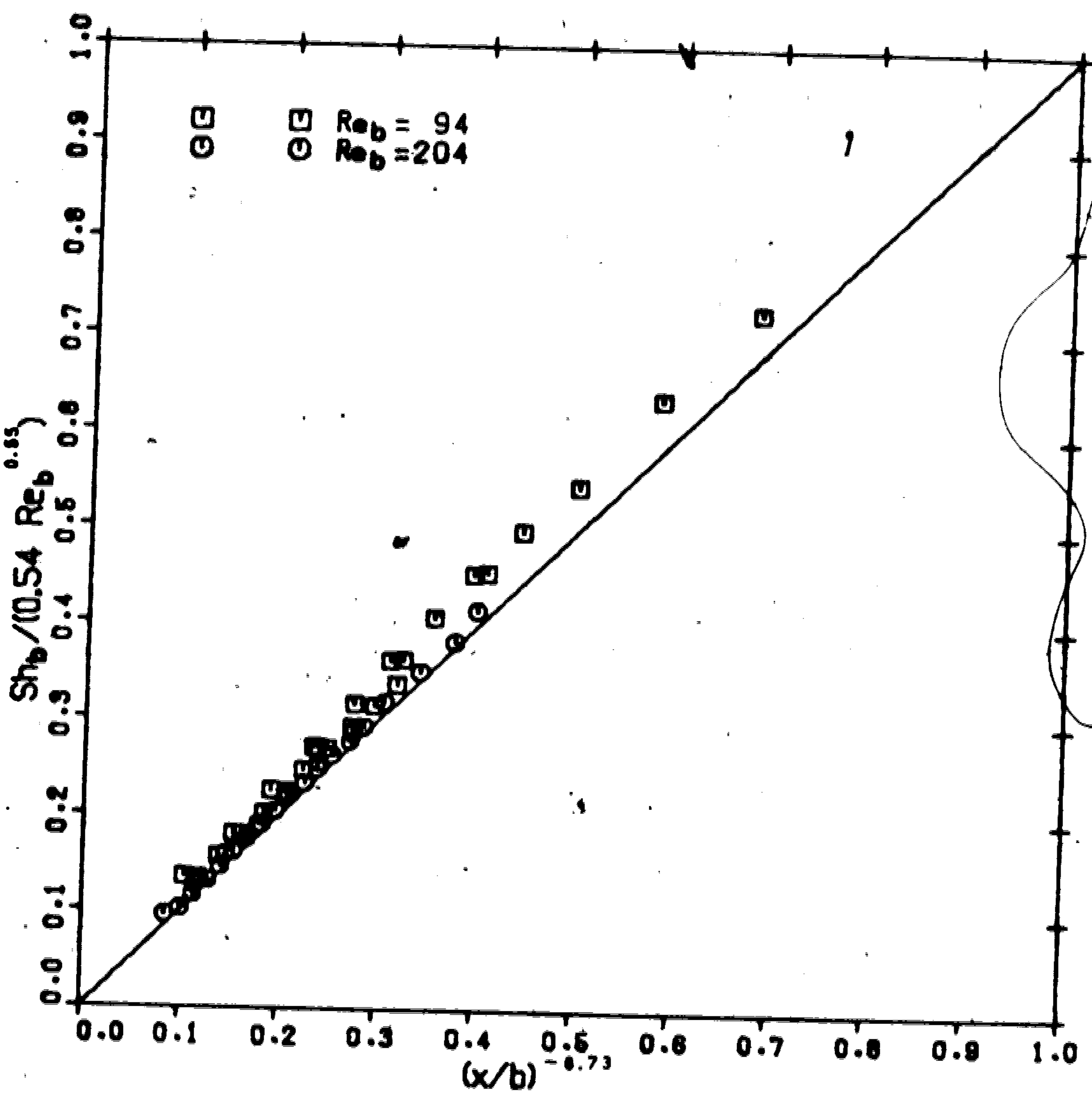

FIGURE 5.4 : COMPARISON OF MASS TRANSFER DATA DUE TO AN UNCONFINED IMPINGING TWO-DIMENSIONAL AIR JET WITH EQUATION 5.14

6. NUMERICAL MODEL-MATHEMATICAL FORMULATION

A two-dimensional numerical model is used to simulate the experimental set-up. The impinging jet system considered in this work is shown in Figure 6.1. The air jet issues from a two-dimensional slot tube of width b with an average velocity of $\bar{v}_j$. The confinement plate is located parallel to and at a distance h from the impingement plate. The impingement is normal to the impingement plate. For the description of the flow and the concentration fields, a two-dimensional rectangular coordinate system is used with the origin at the center of the jet nozzle exit. The x-coordinate is parallel to the impingement plate and the y-coordinate is normal to it. The outflow region is chosen at a location sufficiently far away from the stagnation flow region to ensure that the velocity and the concentration profiles at this location are developing as those for parallel plates.

The governing equations for this two-dimensional impinging jet system are presented in Section 6.1. The boundary conditions for this system are presented in Section 6.2.

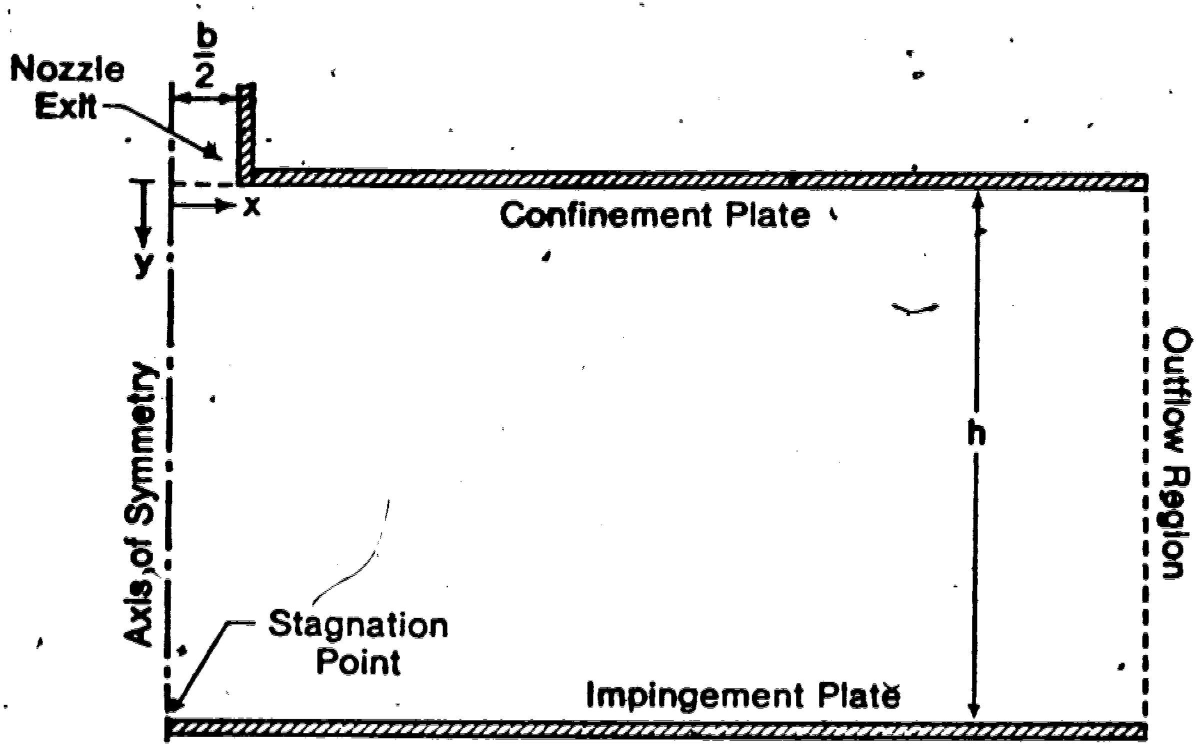

FIGURE 6.1 : COORDINATE SYSTEM AND BOUNDARIES OF THE IMPINGING JET SYSTEM

6.1 GOVERNING EQUATIONS

The pressure gradient is so small that the change of density at each point in the system can be neglected. Therefore, air can be treated as an incompressible Newtonian fluid, even though it is a compressible fluid itself. The two-dimensional momentum and transport equations can be reduced to the corresponding vorticity-stream function form with the assumption of steady state, incompressible viscous Newtonian fluid flow with constant physical properties. The pertinent equations are (69):

$$\frac{\partial(u\ \omega)}{\partial x} + \frac{\partial(v\ \omega)}{\partial y} = \left(\frac{\partial^2 \omega}{\partial x^2} + \frac{\partial^2 \omega}{\partial y^2}\right) \qquad (6.1)$$

$$\frac{\partial^2 \psi}{\partial x^2} + \frac{\partial^2 \psi}{\partial y^2} = \omega \qquad (6.2)$$

$$\frac{\partial(u\ c)}{\partial x} + \frac{\partial(v\ c)}{\partial y} = D\left(\frac{\partial^2 c}{\partial x^2} + \frac{\partial^2 c}{\partial y^2}\right) + R \qquad (6.3)$$

where ω is the vorticity and is defined by

$$\omega = \frac{\partial u}{\partial y} - \frac{\partial v}{\partial x} \qquad (6.4)$$

ψ is stream function and is defined by

$$\frac{\partial \psi}{\partial Y} = u \quad \text{and} \quad \frac{\partial \psi}{\partial x} = -v \qquad (6.5)$$

c is the molar concentration of the swelling agent, and R is the molar rate of production of the swelling agent per unit volume. For a system without chemical reaction, R=0.

When dimensionless variables are introduced as follows:

$$L = h / b$$
$$U = u / \bar{v}_j$$
$$V = v / \bar{v}_j$$
$$X = x / b$$
$$Y = y / b$$
$$C = (c - c_j) / (c_s - c_j)$$
$$\Omega = \omega (b / \bar{v}_j)$$
$$\Psi = \psi / (b \, \bar{v}_j)$$
$$Re_b = b \, \bar{v}_j / \nu$$
$$Sc = \nu / D \qquad (6.6)$$

then the above equations becomes:

$$\frac{\partial (U \, \Omega)}{\partial X} + \frac{\partial (V \, \Omega)}{\partial Y} = \frac{1}{Re_b} \left(\frac{\partial^2 \Omega}{\partial X^2} + \frac{\partial^2 \Omega}{\partial Y^2} \right) \qquad (6.7)$$

$$\frac{\partial^2 \Psi}{\partial X^2} + \frac{\partial^2 \Psi}{\partial Y^2} = \Omega \qquad (6.8)$$

$$\frac{\partial(U\ C)}{\partial X} + \frac{\partial(V\ C)}{\partial Y} = \frac{1}{Re_b\ Sc}\left(\frac{\partial^2 C}{\partial X^2} + \frac{\partial^2 C}{\partial Y^2}\right) \qquad (6.9)$$

$$\text{where } \frac{\partial\Psi}{\partial Y} = U \quad \text{and} \quad \frac{\partial\Psi}{\partial X} = -V \qquad (6.10)$$

The objective of the numerical study is to solve Equations 6.7, 6.8 and 6.9 for Ω, Ψ and C.

6.2 BOUNDARY CONDITIONS

Because the governing equations are elliptic in nature, boundary conditions must be specified at all the boundaries. The boundaries are classified in five regions: the nozzle exit, the confinement plate, the impingement plate, the axis of symmetry and the outflow region.

6.2.1 NOZZLE EXIT

For an initial parabolic velocity profile at the nozzle exit, the velocity components are

$$V = 1.5\ (1 - 4\ X^2)$$
$$U = 0 \qquad (6.11)$$

From these velocity components, one can show that

$$\Psi = -1.5\ X + 2\ X^3 \qquad (6.12)$$

$$\Omega = .12\,X \qquad (6.13)$$

where the stream function, ψ, at the axis of symmetry ($X=0$) is taken as zero.

For an initial flat velocity profile at nozzle exit, the velocity components are

$$V = 1$$
$$U = 0 \qquad (6.14)$$

From these velocity components, one can show that

$$\psi = -X \qquad (6.15)$$
$$\Omega = 0 \qquad (6.16)$$

The boundary condition for the concentration at the nozzle exit is

$$C = 0 \qquad (6.17)$$

for an air jet.

6.2.2 CONFINEMENT PLATE

Because the confinement plate is impermeable, the value of the stream function does not change along the plate. This value can be determined by substituting $X=0.5$ in Equations 6.12 and 6.15 for the case of parabolic and flat velocity profile, respectively. For both cases, the boundary condition of the stream function at the confinement plate is

$$\Psi = -0.5 \qquad (6.18)$$

The boundary condition for the vorticity at the confinement plate is evaluated by using no-slip boundary condition (96). This boundary condition is given in finite difference form and will be discussed in Chapter 7.

The boundary condition for the concentration is

$$\partial C / \partial Y = 0 \qquad (6.19)$$

due to no mass transfer occurring at the plate.

6.2.3 IMPINGEMENT PLATE

Again, because the impingement plate is impermeable, the value of stream function does not change along the plate. The stream function can be arbitrary set to zero to give

$$\Psi = 0 \qquad (6.20)$$

The boundary condition for the vorticity at the impingment plate is the same as that of the confinement plate.

The boundary condition for the concentration is given by

$$C = 1 \quad (6.21)$$

6.2.4 AXIS OF SYMMETRY

The axis of symmetry is given by X=0 and the stream function is a constant along it. Arbitrarily the constant is set to zero to give

$$\Psi = 0 \quad (6.22)$$

The boundary condition of vorticity can be easily determined by setting $U=\partial V/\partial X=\partial U/\partial Y=0$ and noting that $V(X,Y)=V(-X,Y)$. The vorticity along X=0 is then given by

$$\Omega = 0 \quad (6.23)$$

Since the concentration is also symmetric on both sides of the axis, it leads to

$$\partial C / \partial X = 0 \quad (6.24)$$

along the axis of symmetry.

6.2.5 OUTFLOW REGION

This boundary is located sufficiently far from the jet such that the flow is nearly fully developed where the influence of the impinging zone is not felt. Usually, a fully developed flow is assumed at this boundary (96). If, instead a <u>developing</u> flow profile for the parallel plates channel is assumed, the outflow boundary can then be located anywhere in the x-direction as long as it is far enough and not influenced by the impinging jet flow. With an assumption of a <u>developing</u> flow profile at the outflow boundary, this boundary can be located closer to the stagnation point than that with an assumption of a fully developed flow profile. In other words, the number of grid points in x-direction can then be minimized.

The developing stream function and vorticity profiles are derived from the developing velocity profile given by Sparrow et. al. (92) for their study of velocity development for the parallel-plate channel. By using only the most dominant term in their solution series, the stream function and the vorticity at the outflow region are given by

$$\psi = \psi_{fd} + \frac{1}{\alpha_1^2 L} \left[\frac{\sin\left[\alpha_1 (2(Y/L)-1)\right]}{\cos \alpha_1} \left(\frac{L}{2\alpha_1}\right) - Y + \frac{L}{2} \right] e^{-8\alpha_1^2 (X/L)/Re_b} \qquad (6.25)$$

and

$$\Omega = \Omega_{fd} - \frac{2}{\alpha_1 L^2} \left\{ \frac{\sin\left[\alpha_1 (2(Y/L)-1)\right]}{\cos \alpha_1} \right\} e^{-8\alpha_1^2 (X/L)/Re_b} \tag{6.26}$$

where α_1=4.49341. The subscript "fd" denotes fully developed flow, where

$$\Psi_{fd} = 1.5\ (Y/L)^2 - (Y/L)^3 - 0.5 \tag{6.27}$$

$$\Omega_{fd} = 3\ (1 - 2\ (Y/L))\ /\ L^2 \tag{6.28}$$

The developing concentration profile is analogous to the developing temperature profile for parallel plates given by McCuen (62) and Shah and London (85). The boundary conditions used in this work are similar to those of the fundamental solution of the third kind in their work. The concentration at the outflow region is given by

$$C = C_{fd} + \sum_{i=1}^{\infty} E_i\ Y_i\ e^{-\lambda_i^2 (X/2L)/(Re_b\ Sc)} \tag{6.29}$$

where Y_i's are functions of Y. E_i's and λ_i's are eigenconstants and eigenvalues, respectively and they are evaluated at the confinement plate for the first four terms in the series as (62,85):

λ_1 = 3.117 and $E_1 Y_1$ = -1.2480

λ_2 = 9.714 and $E_2 Y_2$ = +0.3831

$$\lambda_3 = 16.260 \quad \text{and} \quad E_3Y_3 = -0.2263$$
$$\lambda_4 = 22.810 \quad \text{and} \quad E_4Y_4 = +0.1605 \qquad (6.30)$$

Due to the oscillating behavior of the series in Equation 6.29 (from the values of E_iY_i's), there is no dominant term in this series. The fully developed concentration profile is given by

$$C_{fd} = 1 \qquad (6.31)$$

The finite difference form of the boundary conditions in the outflow region will be discussed in Chapter 7.

The location of the outflow region boundary is chosen depending on the jet Reynolds number and jet-to-plate spacing. It is given in Table 6.1.

TABLE 6.1 : LOCATION OF OUTFLOW REGION BOUNDARY

L	Re_b	X
2	100 - 400	74
4	100 - 400	74
12	100 - 300	170
	400	186

7. NUMERICAL FORMULTION

Initially the numerical technique used in this work was similar to the method introduced by Joseph, Smith and Adler (35) which is that of the Marker-and-Cell (MAC) method used by other investigators dealing with numerical studies (5,28,30,65,72, 93,99). The method is to solve the unsteady state primitive equations. A steady state solution is obtained by advancing the velocities and pressure from one time interval to another until the solution no longer changes with time. This numerical technique was later abandoned due to the failure to obtain a converged solution for higher Reynolds number unless the time interval was steadily reduced. Large CPU time was required in order to obtain a steady state solution.

The second numerical technique used in this work was the central finite-difference representation of the steady state vorticity transport equation. This numerical technique was again abandoned due to the failure to obtain a converged solution for $Re_b>100$. Severe under-relaxation was required for the run of $Re_b=100$. Converged solution for $Re_b=100$ was not obtained until after 2700 iterations.

The third and successful numerical technique used in this work is the hybrid differencing schemes, so called "upstream-weighted" and "upstream" differencing schemes, introduced by Raithby and Torrance (69). The detail of derivations of the general finite-difference equations is given in Section 7.1. The derivations of the finite-difference equations at the boundaries are given in Section 7.2. The finite-difference equations for "upstream-weighted" and "upstream" differencing schemes is discussed in Section 7.3. Finally, the stability properties of the finite-difference equations are discussed in Section 7.4.

7.1 FINITE-DIFFERENCE EQUATIONS

The governing equations are:

$$\frac{\partial(U\,\phi)}{\partial X} + \frac{\partial(V\,\phi)}{\partial Y} = a\left(\frac{\partial^2\phi}{\partial X^2} + \frac{\partial^2\phi}{\partial Y^2}\right) \qquad (7.1)$$

$$\frac{\partial^2\Psi}{\partial X^2} + \frac{\partial^2\Psi}{\partial Y^2} = \Omega \qquad (7.2)$$

$$\text{where } \frac{\partial\Psi}{\partial Y} = U \quad \text{and} \quad \frac{\partial\Psi}{\partial X} = -V \qquad (7.3)$$

Equation 7.1 is a more general equation than Equations 6.7 and 6.9. The variable ϕ represents vorticity, Ω, in Equation 6.7 and concentration, C, in Equation 6.9. The coefficient a for these two cases becomes $(Re_b)^{-1}$ and $(Re_b\ Sc)^{-1}$, respectively.

The region of interest is represented by a rectangular grid network shown in Figure 7.1 with grid lines parallel to the X and Y coordinates. Grid lines in X and Y directions are designated by i and j, respectively. As shown in Figure 7.1, the total numbers of node (the intersection of the grid lines) in X and Y directions are nx and ny, respectively. The numbers of node cover the jet nozzle exit is nj.

For the time being, let us restrict our attention to the region surrounding the typical node (i,j) shown in Figure 7.2. The variables Ω, Ψ and C are defined at each node, while the velocity components, U and V, are defined at points midway between these nodes. In other words, the velocity components are on the boundaries of the control volume. The control volume of a node is the region bounded by the dashed lines shown in Figure 7.2, the sides of which lie midway between the neighbouring nodes. One of the advantages of using such a finite-difference grid is that it simplifies the computation of mass flux into and out of the control volume, since the velocity components are located at the control volume boundary itself.

The finite-difference equations of the velocity components are obtained as follows

$$[\Psi(i+1,j+1) + \Psi(i,j+1) - \Psi(i+1,j-1) - \Psi(i,j-1)]/4 = U(i+1/2,j)\ \Delta Y(j) \quad , \qquad (7.4)$$

$$[\Psi(i+1,j+1) + \Psi(i+1,j) - \Psi(i-1,j+1) - \Psi(i-1,j)]/4 = -\ V(i,j+1/2)\ \Delta X(i) \qquad (7.5)$$

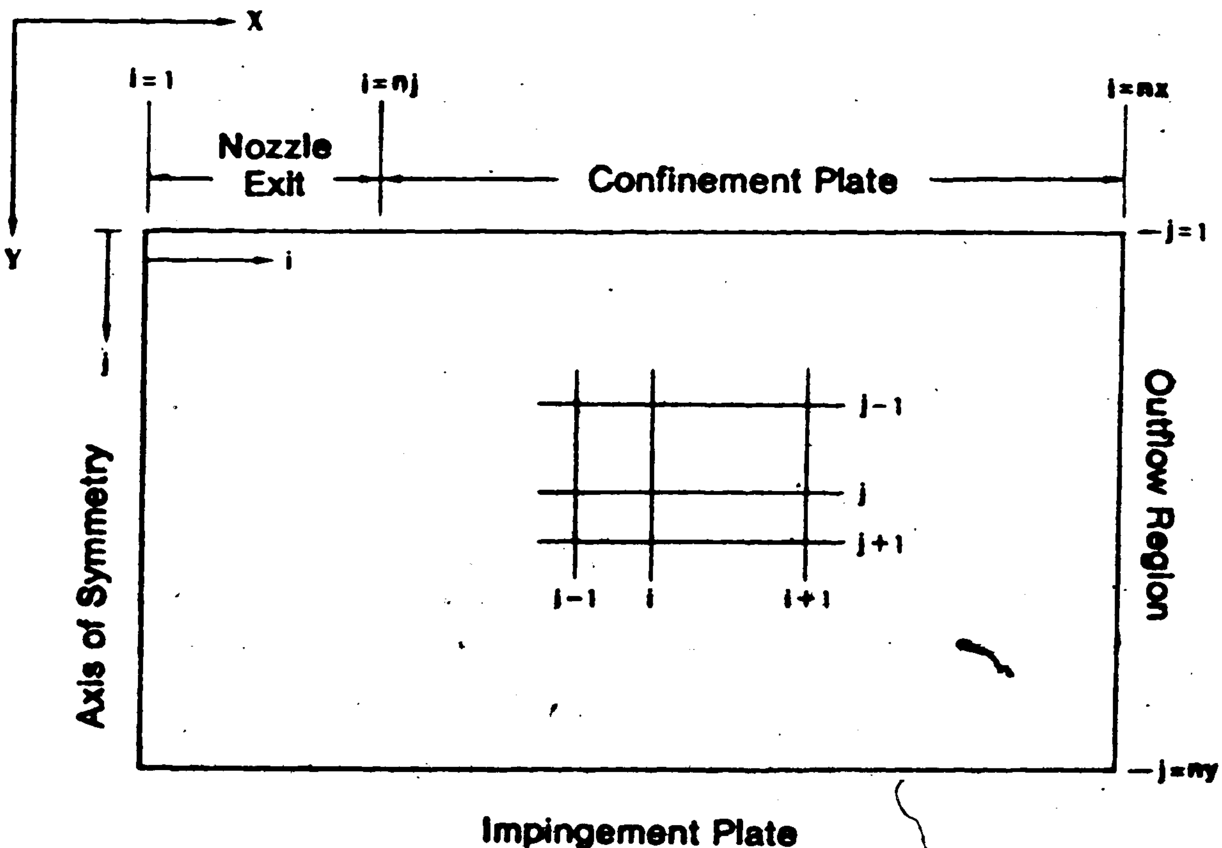

FIGURE 7.1 : GRID NETWORK OF THE IMPINGING JET SYSTEM

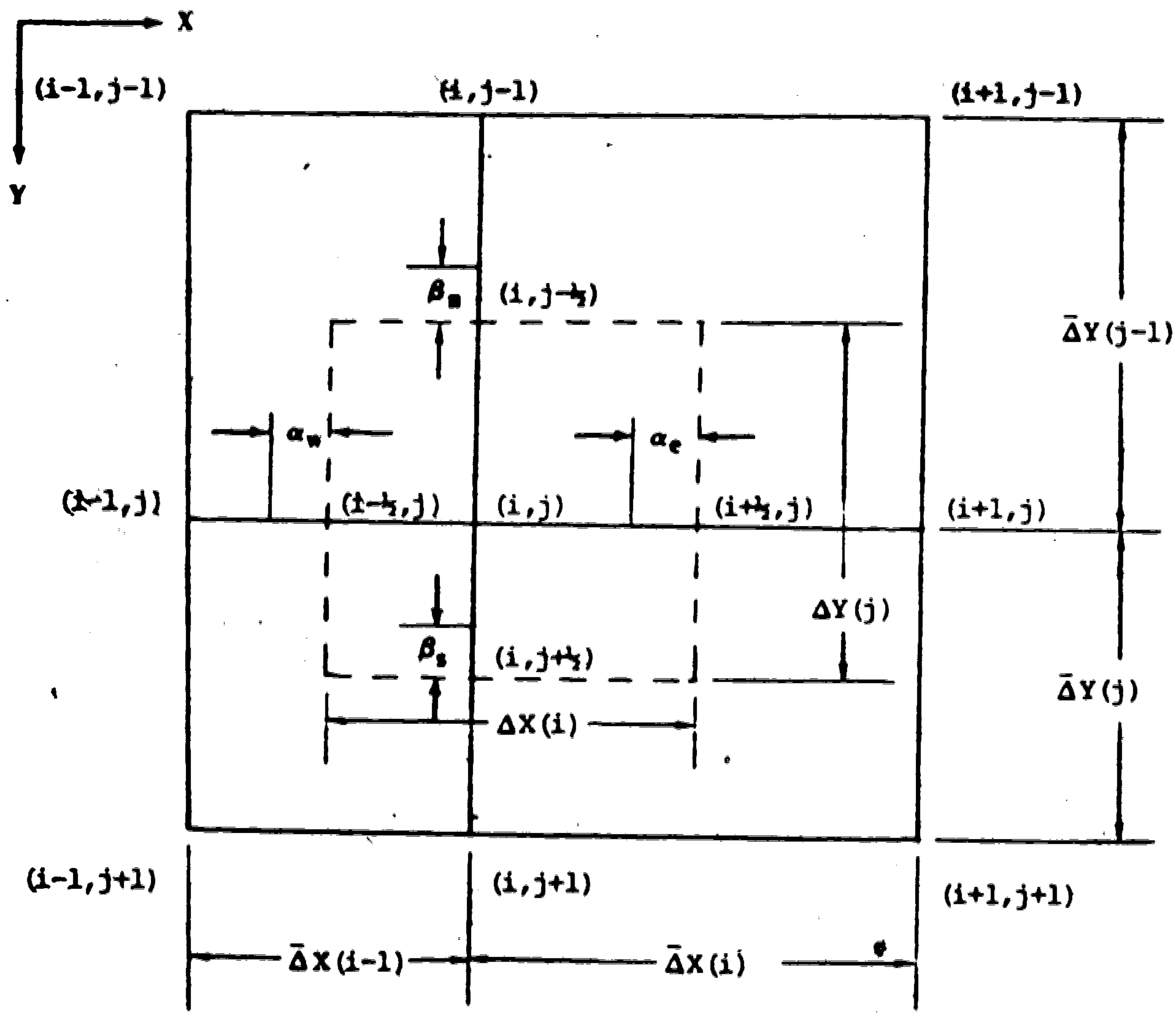

FIGURE 7.2 : GRID NETWORK AND CONTROL VOLUME SURROUNDING TYPICAL NODE (i,j)

such that U(i+1/2,j) is the mean velocity in the X-direction in the region bounded by grid lines passing through nodes (i+1,j+1), (i,j+1), (i,j-1) and (i+1,j-1), and V(i,j+1/2) is the mean velocity in the Y-direction in the region bounded by the grid lines passing through nodes (i+1,j+1), (i-1,j+1), (i-1,j) and (i+1,j). With these approximate equations, the mass balance is satisfied exactly over the control volume. From Equations 7.4 and 7.5, one obtains

$$[U(i+1/2,j) - U(i-1/2,j)]\,\Delta Y(j) + [V(i,j+1/2) - V(i,j-1/2)]\,\Delta X(i) = 0 \qquad (7.6)$$

Dividing by $\Delta X(i)\ \Delta Y(j)$, Equation 7.6 becomes the central finite-difference representation of the equation of continuity over the control volume of node (i,j).

The convective term $\partial(U\ \phi)/\partial X$ of Equation 7.1 is represented as the difference between two fluxes, one through the right hand side boundary, the (i+1/2) face, and one through the left hand side boundary, the (i-1/2) face, of the control volume shown in Figure 7.2. The flux, $U\phi$, through the right hand side boundary is approximated by $U(i+1/2,j)\phi(i+1/2-\alpha_e,j)$, where $\phi(i+1/2-\alpha_e,j)$ is equal to the "true" value of the variable ϕ half-way between nodes (i,j) and (i+1,j) and is located at $(i+1/2-\alpha_e,j)$ if one linearly interpolates between $\phi(i,j)$ and $\phi(i+1,j)$ (69). Since both $\phi(i,j)$, $\phi(i+1/2-\alpha_e,j)$ and $\phi(i+1,j)$ lie on the same straight line, therefore

$$(0.5 + \alpha_e)\ \phi(i,j) + (0.5 - \alpha_e)\ \phi(i+1,j) = \phi(i+1/2-\alpha_e, j) \qquad (7.7)$$

Proceeding similarly at the left hand side boundary, using the parameter α_w, the flux, $U\phi$, is approximated by $U(i-1/2,j)\phi(i-1/2-\alpha_w,j)$ where

$$(0.5 + \alpha_w)\ \phi(i-1,j) + (0.5 - \alpha_w)\ \phi(i,j) = \phi(i-1/2-\alpha_w, j) \qquad (7.8)$$

Therefore, the convective term in X-direction becomes

$$\frac{\partial(U\ \phi)}{\partial X} = [U(i+1/2,j)\ \phi(i+1/2-\alpha_e,j) - U(i-1/2,j)\ \phi(i-1/2-\alpha_w,j)]\ /\ \Delta X(i) \qquad (7.9)$$

The convective term $\partial(V\ \phi)/\partial Y$ of Equation 7.1 is represented as the difference between fluxes, one through the top boundary, the (j-1/2) face, and one through the bottom boundary, the (j+1/2) face, of the control volume shown in Figure 7.2. Similarly, the convective term in the Y-direction becomes

$$\frac{\partial(V\ \phi)}{\partial Y} = [V(i,j+1/2)\ \phi(i,j+1/2-\beta_s) - V(i,j-1/2)\ \phi(i,j-1/2-\beta_n)]\ /\ \Delta Y(j) \qquad (7.10)$$

where $(0.5 + \beta_s)\ \phi(i,j) + (0.5 - \beta_s)\ \phi(i,j+1)$

$$= \phi(i,j+1/2-\beta_s) \tag{7.11}$$

$$(0.5 + \beta_n)\ \phi(i,j-1) + (0.5 - \beta_n)\ \phi(i,j) = \phi(i,j-1/2-\beta_n) \tag{7.12}$$

Note that all α's and β's are unknowns and are to be determined.

The finite-difference equations for the diffusion terms $a(\partial^2\phi/\partial X^2)$ and $a(\partial^2\phi/\partial Y^2)$ of Equation 7.1 were introduced by Raithby and Torrance (69) as follows

$$a\frac{\partial^2\phi}{\partial X^2} = \frac{a}{\Delta X(i)}\ \{\ (1-\gamma_e)\ [\frac{\phi(i+1,j) - \phi(i,j)}{\bar{\Delta}X(i)}] - (1-\gamma_w)\ [\frac{\phi(i,j) - \phi(i-1,j)}{\bar{\Delta}X(i-1)}]\ \} \tag{7.13}$$

in the X-direction, and

$$a\frac{\partial^2\phi}{\partial Y^2} = \frac{a}{\Delta Y(j)}\ \{\ (1-\delta_s)\ [\frac{\phi(i,j+1) - \phi(i,j)}{\bar{\Delta}Y(j)}] - (1-\delta_n)\ [\frac{\phi(i,j) - \phi(i,j-1)}{\bar{\Delta}Y(j-1)}]\ \} \tag{7.14}$$

in the Y-direction, where γ's and δ's are weighting factors to be determined. The advantage of using these weighting factors is that they retain flexibility similar to that for the convective terms.

Considering the flux crossing the common boundary between two adjacent control volumes, conservation requires that α_e and γ_e for the control volume of node (i,j) must equal α_w and γ_w for the control volume of the node (i+1,j). Similarly, β_s and δ_s for the control volume of the node (i,j) must equal β_n and δ_n for the control volume of the node (i,j+1). Therefore, α_e, γ_e, α_w, γ_w, β_s, δ_s, β_n and δ_n in the previous expressions can be replaced by the notations $\alpha(i+1,j)$, $\gamma(i+1,j)$, $\alpha(i,j)$, $\gamma(i,j)$, $\beta(i,j+1)$, $\delta(i,j+1)$, $\beta(i,j)$ and $\delta(i,j)$, respectively.

By introducing all the foregoing flux terms into Equation 7.1, one obtains the following explicit equation at each interior node

$$\Phi(i,j) = \{m_1\ \Phi(i-1,j) + m_2\ \Phi(i+1,j) + m_4\ \Phi(i,j-1) + m_5\ \Phi(i,j+1)\} \ /\ m_3 \quad (7.15)$$

The coefficients of Equation 7.15 are defined by

$$m_1 = [1 - \gamma(i,j)]\ \xi(i,j) + 0.5\ [U(i-1/2,j)\ \Delta Y(j)] + \alpha(i,j)\ |U(i-1/2,j)\ \Delta Y(j)|$$

$$m_2 = [1 - \gamma(i+1,j)]\ \xi(i+1,j) - 0.5\ [U(i+1/2,j)\ \Delta Y(j)] + \alpha(i+1,j)\ |U(i+1/2,j)\ \Delta Y(j)|$$

$$m_3 = \{|U(i+1/2,j)\ \Delta Y(j)|\ \alpha(i+1,j) + |U(i-1/2,j)\ \Delta Y(j)|\ \alpha(i,j) + |V(i,j+1/2)\ \Delta X(i)|\ \beta(i,j+1)$$

$$[illegible](i,j-1/2)\ \Delta X(i)|\ \beta(i,j)\}$$
$$+ \{[1-\gamma(i+1,j)]\ \xi(i+1,j) + [1-\gamma(i,j)]\ \xi(i,j)$$
$$+ [1-\delta(i,j+1)]\ \eta(i,j+1) + [1-\delta(i,j)]\ \eta(i,j)\}$$
$$m_4 = [1-\delta(i,j)]\ \eta(i,j) + 0.5\ [V(i,j-1/2)\ \Delta X(i)]$$
$$+ \beta(i,j)\ |V(i,j-1/2)\ \Delta X(i)|$$
$$m_5 = [1-\delta(i,j+1)]\ \eta(i,j+1) - 0.5\ [V(i,j+1/2)\ \Delta X(i)]$$
$$+ \beta(i,j+1)\ |V(i,j+1/2)\ \Delta X(i)| \qquad (7.16)$$

with
$$\xi(i,j) = \frac{a\ \Delta Y(j)}{\bar{\Delta}X(i-1)} \quad \text{and} \quad \eta(i,j) = \frac{a\ \Delta X(i)}{\bar{\Delta}Y(j-1)} \qquad (7.17)$$

As mentioned above, the sign of both elements in the products $\alpha(i,j)\ U(i-1/2,j)$, $\alpha(i+1,j)\ U(i+1/2,j)$, $\beta(i,j)\ V(i,j-1/2)$, and $\beta(i,j+1)\ V(i,j+1/2)$ must be the same. Therefore the products are all positive quantities and can be written as noted in Equation 7.16 with the understanding that all α's and β's used in this work are positive number.

The finite-difference approximations of the vorticity-stream function relation are derived from the central difference approximations for non-uniform grid network, where

$$\frac{\partial^2\Psi}{\partial X^2} = 2\ \left\{\frac{\bar{\Delta}X(i-1)\ \Psi(i+1,j) + \bar{\Delta}X(i)\ \Psi(i-1,j)}{\bar{\Delta}X(i)\ \bar{\Delta}X(i-1)\ [\ \bar{\Delta}X(i) + \bar{\Delta}X(i-1)]} - \frac{[\ \bar{\Delta}X(i) + \bar{\Delta}X(i-1)]\ \Psi(i,j)}{\bar{\Delta}X(i)\ \bar{\Delta}X(i-1)\ [\ \bar{\Delta}X(i) + \bar{\Delta}X(i-1)]}\right\} \qquad (7.18)$$

$$\text{and} \quad \frac{\partial^2 \psi}{\partial Y^2} = 2 \left\{ \frac{\bar{\Delta}Y(j-1)\ \psi(i,j+1) + \bar{\Delta}Y(i)\ \psi(i,j-1)}{\bar{\Delta}Y(j)\ \bar{\Delta}Y(j-1)\ [\ \bar{\Delta}Y(j) + \bar{\Delta}Y(j-1)]} - \frac{[\ \bar{\Delta}Y(j) + \bar{\Delta}Y(j-1)]\ \psi(i,j)}{\bar{\Delta}Y(j)\ \bar{\Delta}Y(j-1)\ [\ \bar{\Delta}Y(j) + \bar{\Delta}Y(j-1)]} \right\} \qquad (7.19)$$

By introducing Equations 7.18 and 7.19 into Equation 7.2, one obtains the following explicit equation for the stream function at each interior node

$$\psi(i,j) = \{n_1\ \psi(i-1,j) + n_2\ \psi(i+1,j) + n_4\ \psi(i,j-1) + n_5\ \psi(i,j+1) - \Omega(i,j)\} \;/\; n_3 \qquad (7.20)$$

The coefficients of Equation 7.20 are defined by

$$n_1 = 2 \;/\; \{\ \bar{\Delta}X(i-1)\ [\ \bar{\Delta}X(i) + \bar{\Delta}X(i-1)]\}$$
$$n_2 = 2 \;/\; \{\ \bar{\Delta}X(i)\ [\ \bar{\Delta}X(i) + \bar{\Delta}X(i-1)]\}$$
$$n_3 = 2 \left\{ \frac{1}{\bar{\Delta}X(i)\ \bar{\Delta}X(i-1)} + \frac{1}{\bar{\Delta}Y(j)\ \bar{\Delta}Y(j-1)} \right\}$$
$$n_4 = 2 \;/\; \{\ \bar{\Delta}Y(j-1)\ [\ \bar{\Delta}Y(j) + \bar{\Delta}Y(j-1)]\}$$
$$n_5 = 2 \;/\; \{\ \bar{\Delta}Y(j)\ [\ \bar{\Delta}Y(j) + \bar{\Delta}Y(j-1)]\} \qquad (7.21)$$

The distributions of vorticity, stream-function and concentration inside the region of interest can then be obtained by solving Equations 7.15 and 7.20 using an iterative method. The values of the parameters α, β, γ and δ can be specified depending on the differencing scheme used.

These values will be given later in this chapter. Procedure of the iterative method is discussed in Chapter 8. Since the variables Ω, Ψ and C are evaluated at nodes, for consistency in analysing the numerical results, the velocity components U and V are also evaluated at the nodes by using the following equations:

$$U(i,j) = [\Psi(i,j+1) - \Psi(i,j-1)] \;/\; 2\,\Delta Y(j) \qquad (7.22)$$

$$V(i,j) = -[\Psi(i+1,j) - \Psi(i-1,j)] \;/\; 2\,\Delta X(i) \qquad (7.23)$$

The velocity components obtained from Equations 7.22 and 7.23 are used instead of those evaluated from Equations 7.4 and 7.5 during the iterations.

7.2 BOUNDARY CONDITIONS

The finite-difference equations at the boundaries will be discussed for the five different regions mentioned above separately.

7.2.1 NOZZLE EXIT

This boundary is defined as $1 \le i < nj$ and $j=1$ in Figure 7.2. For an initial parabolic velocity profile,

$$V(i,1) = 1.5\,(1 - 4\,X(i)^2)$$

$$U(i,1) = 0$$

$$\Psi(i,1) = -1.5\ X(i) + 2\ X(i)^3$$
$$\Omega(i,1) = 12\ X(i) \quad (7.24)$$

and for an initial flat velocity profile,

$$U(i,1) = 1$$
$$V(i,1) = 0$$
$$\Psi(i,1) = -X(i)$$
$$\Omega(i,1) = 0 \quad (7.25)$$

The boundary condition for the concentration for both parabolic and flat velocity profiles are

$$C(i,1) = 0 \quad (7.26)$$

7.2.2 CONFINEMENT PLATE

This boundary is defined as $nj \le i < nx$ and $j=1$ in Figure 7.2. The boundary condition for the stream-function at the confinement plate is

$$\Psi(i,1) = -0.5 \quad . \quad (7.27)$$

The boundary condition of the vorticity at the confinement plate is approximated by a finite-difference expression with truncation error less than $O(\bar{\Delta}Y)^3$ which embodies the no-slip conditions, $\partial\Psi/\partial Y=U=0$ and $\partial^2\Psi/\partial Y^2=\partial U/\partial Y =\Omega(i,1)$ at the boundary. The finite-difference equation at this boundary is derived using Taylor series as

$$\Omega(i,1) = 2\left\{\frac{[\Psi(i,2) - \Psi(i,1)]\,[\bar{\Delta}Y(2) + \bar{\Delta}Y(1)]^2}{\bar{\Delta}Y(1)^2\,\bar{\Delta}Y(2)\,[\bar{\Delta}Y(1) + \bar{\Delta}Y(2)]^2} - \frac{[\Psi(i,3) - \Psi(i,1)]\,[\bar{\Delta}Y(1)]^2}{\bar{\Delta}Y(1)^2\,\bar{\Delta}Y(2)\,[\bar{\Delta}Y(1) + \bar{\Delta}Y(2)]^2}\right\} \quad (7.28)$$

The boundary condition for the concentration at the confinement plate is approximated by using a forward finite-difference expression with truncation error less than $O(\bar{\Delta}Y)^2$. For $\partial C/\partial Y=0$ at the boundary, the finite-difference equation becomes:

$$C(i,1) = \left\{\frac{[\bar{\Delta}Y(1) + \bar{\Delta}Y(2)]^2\,C(i,2) - \bar{\Delta}Y(1)^2\,C(i,3)}{[\bar{\Delta}Y(1) + \bar{\Delta}Y(2)]^2 - \bar{\Delta}Y(1)^2}\right\} \quad (7.29)$$

7.2.3 IMPINGEMENT PLATE

This boundary is defined as $1 \le i < nx$ and $j = ny$ in Figure 7.2. The boundary condition of stream-function is given by

$$\Psi(i,ny) = 0 \quad (7.30)$$

The boundary condition of the vorticity is similar to that at the confinement plate. The finite-difference equation for vorticity at this boundary is derived using

Taylor series as

$$\Omega(i,ny) = 2 \{\frac{[\Psi(i,ny-1) - \Psi(i,ny)] [\bar{\Delta Y}(ny-1) + \bar{\Delta Y}(ny-2)]^2}{\bar{\Delta Y}(ny-1)^2 \ \bar{\Delta Y}(ny-2) [\bar{\Delta Y}(ny-1) + \bar{\Delta Y}(ny-2)]^2}$$

$$- \frac{[\Psi(i,ny-2) - \Psi(i,ny)] \ \bar{\Delta Y}(ny-1)^2}{\bar{\Delta Y}(ny-1)^2 \ \bar{\Delta Y}(ny-2) [\bar{\Delta Y}(ny-1) + \bar{\Delta Y}(ny-2)]^2}\} \tag{7.31}$$

The boundary condition of the concentration is given by

$$C(i,ny) = 0 \tag{7.32}$$

7.2.4 AXIS OF SYMMETRY

This boundary is defined as i=1 and 1<j<ny in Figure 7.2. The boundary conditions of stream-function and vorticity are given by

$$\Psi(1,j) = 0$$
$$\Omega(1,j) = 0 \tag{7.32}$$

For the boundary condition of the concentration, a boundary control volume surrounding a boundary node (1,j) is introduced. Referring to Figure 7.2, the node (i,j) becomes (1,j) and $\bar{\Delta X}(1)=\bar{\Delta X}(0)=\Delta X(1)$. The index i≥1 will refer to the variables inside the system, and i<1 will refer to the variables outside the system. Equation 7.15 is now applied to the nodes on this boundary. Variables such as $V(1,j+1/2)$, $\beta(1,j+1)$, $\delta(1,j+1)$ and $\eta(1,j+1)$ can be evaluated at the boundary. Due to the fact that this boundary can be considered as a plane of symmetry, the variables outside the field can be evaluated as follows

$$\begin{aligned} \Psi(0,j) &= -\Psi(2,j) \\ U(1/2,j) &= -U(3/2,j) \\ C(0,j) &= C(2,j) \end{aligned} \qquad (7.34)$$

Therefore the concentration at this boundary, $C(1,j)$, can be evaluated from Equation 7.15 similarly to that of the interior node.

7.2.5 OUTFLOW REGION

This boundary is defined as i=nx and 1<j<ny in Figure 7.2. The finite-difference equations for fully developed stream-function, vorticity and concentration are given by

$$\begin{aligned} \Psi_{fd}(j) &= 1.5\ (Y(j)/L)^2 - (Y(j)/L)^3 - 0.5 \\ \Omega_{fd}(j) &= 3\ [1 - 2\ (Y(j)/L)]\ /\ L^2 \end{aligned}$$

and

$$C_{fd}(j) = 1 \qquad (7.35)$$

The finite-difference equations for the stream-function and vorticity at this boundary can be obtained from Equations 6.25 and 6.26. After rearrangement, they become, respectively

$$\Psi(nx,j) = \Psi_{fd}(j) + [\Psi(nx-1,j) - \Psi_{fd}(j)]\ Z_1 \quad (7.36)$$

$$\Omega(nx,j) = \Omega_{fd}(j) + [\Omega(nx-1,j) - \Omega_{fd}(j)]\ Z_1 \quad (7.37)$$

with $Z_1 = \exp\{-8\ \alpha_1^2\ [\ \Delta\bar{X}(nx-1)]\ /\ (L\ Re_b)\}$ (7.38)

The finite-difference equation for the concentration at this boundary can be obtained from Equation 6.29 by approximating the ratio of the series for $X=X(nx)$ and $X=X(nx-1)$ as the ratio of the first term of these series, where

$$C(nx,j) = C_{fd}(j) + [C(nx-1,j) - C_{fd}(j)]\ Z_2 \quad (7.39)$$

with $Z_2 = \exp\{-\ \lambda_1\ [\ \Delta\bar{X}(nx-1)]\ /\ (2\ L\ Re_b\ Sc)\}$ (7.40)

7.3 FINITE-DIFFERENCING SCHEMES

Three finite-differencing schemes are used in this work, namely, a central differencing scheme (C.D.S.), an upstream differencing scheme (U.D.S.) and an upstream-weighted differencing scheme (U.W.D.S.).

7.3.1 CENTRAL DIFFERENCING SCHEME (C.D.S.)

Setting $\alpha(i,j)=\beta(i,j)=\gamma(i,j)=\delta(i,j)=0$ in the finite-difference equations of Section 7.1 results in a central differencing scheme with truncation error $O(\Delta X^2, \Delta Y^2)$.

7.3.2 UPSTREAM DIFFERENCING SCHEME (U.D.S.)

Setting $\alpha(i,j)=\beta(i,j)=0.5$ and $\gamma(i,j)=\delta(i,j)=0$ in the finite-difference equations in Section 7.1 results in an upstream differencing scheme. This differencing scheme was used by Torrance (94) and Raithby and Torrance (69), and is similar to the "upwind differences" used by Runchal et. al. (74,75,76). In this case, the variables Ω, Ψ and C in the system are determined to a large extent by the values of the corresponding variables prevailing immediately upstream.

7.3.3 UPSTREAM-WEIGHTED DIFFERENCING SCHEME (U.W.D.S.)

In this case, the parameters $\alpha(i,j)$, $\beta(i,j)$, $\gamma(i,j)$ and $\delta(i,j)$ are determined from the exact solution to the local <u>one-dimensional</u> <u>transport</u> <u>equations</u> between nodes. Consider the transport equation of the variable ϕ in the X-direction between nodes (i-1,j) and (i,j), the one-dimensional equation governing the variation of the variable ϕ with X between nodes (i-1,j) and (i,j) is

$$U(i-1/2,j)\ \frac{d\phi}{dX} = a\ \frac{d^2\phi}{dX^2} \qquad (7.41)$$

The exact solution of Equation 7.41 is given by

$$\frac{\phi - \phi(i-1,j)}{\phi(i,j) - \phi(i-1,j)} = \frac{\exp\{U(i-1/2,j)\ [X-X(i-1)]/a\} - 1}{\exp\{U(i-1/2,j)\ [\bar{\Delta}X(i-1)]/a\} - 1}$$

(7.42)

Locally exact solutions of the form of Equation 7.42 were introduced by Spalding (88) and Raithby and Torrance (69). The value of ϕ at (i-0.5,j), where $X=X(i-1)+(\bar{\Delta}X(i-1)/2)$, can be evaluated from Equation 7.42. This "true" value of the variable ϕ is equal to $\phi(i-1/2-\alpha(i,j),j)$ of Equation 7.8. Therefore, from Equations 7.8 and 7.42, with $\alpha_w=\alpha(i,j)$, one obtains

$$\alpha(i,j) = \frac{1}{2} - \frac{\exp(Rw/2) - 1}{\exp(Rw) - 1} \qquad (7.43)$$

$$\text{where } Rw = |U(i-1/2,j)|\ \bar{\Delta}X(i-1)\ /\ a \qquad (7.44)$$

Similarly,

$$\beta(i,j) = \frac{1}{2} - \frac{\exp(Rs/2) - 1}{\exp(Rs) - 1} \qquad (7.45)$$

$$\text{where } Rs = |V(i,j-1/2)|\ \bar{\Delta}Y(j-1)\ /\ a \qquad (7.46)$$

The absolute signs are introduced since α's and β's are always positive numbers, and for stability reasons are chosen to match the signs of local mean velocities. From Equation 7.13, the first derivative of ϕ in X-direction at (i-1/2) is given by

$$\left.\frac{d\phi}{dx}\right|_{i-1/2} = [1 - \gamma(i,j)]\ \frac{[\phi(i,j) - \phi(i-1,j)]}{\bar{\Delta}X(i-1)} \qquad (7.47)$$

Since by introducing the parameter $\gamma(i,j)$, the finite-difference equation should yield the same result as the locally exact solution. The right hand side of Equation 7.47 can be evaluated from Equation 7.42. After rearrangement, one obtains

$$\gamma(i,j) = 1 - \frac{Rw \exp(Rw/2)}{\exp(Rw) - 1} \tag{7.48}$$

Similarly,

$$\delta(i,j) = 1 - \frac{Rs \exp(Rs/2)}{\exp(Rs) - 1} \tag{7.49}$$

Clearly, in the limit of Rw approaching zero both $\alpha(i,j)$ and $\gamma(i,j)$ approach zero and the finite-difference equations reduce to central differencing scheme. On the other hand, for large Rw, $\alpha(i,j)$ approaches 0.5 and $\gamma(i,j)$ approaches 1. This limit implies that upstream differencing scheme is used for the convection term and that the diffusion term is dropped. Similarly, $\beta(i,j)$ and $\delta(i,j)$ approach the same value with respect to the value of Rs.

7.4 STABILITY OF THE FINITE-DIFFERENCE EQUATIONS

The finite-difference equations derived in Section 7.1 are a set of non-linear algebraic equations to be solved iteratively.

For a set of linear algebraic equations with constant coefficients such as

$$K(i) = \sum_{\text{all } i} f(i,j)\ K(j) + g(i) \qquad (7.50)$$

The matrix theory states that such a set will converge to a solution in a successive substitution method when the matrix f(i,j) is "diagonally dominant" (45,74). This condition can be expressed as $\sum_{\text{all } i} |f(i,j)| \leq 1$, for all i, and for at least one i such that the inequality holds.

For non-linear equations, the above conditions are often sufficient, although they may not be the necessary conditions (27). Therefore, in order for Equation 7.15 to satisfy the conditions for convergence, the following

$$\left|\frac{m_1}{m_3}\right| + \left|\frac{m_2}{m_3}\right| + \left|\frac{m_4}{m_3}\right| + \left|\frac{m_5}{m_3}\right| \leq 1 \qquad (7.51)$$

must hold for all the interior nodes and with strict inequatity for at least one node.

The stability of the finite-difference equations for the three finite differencing schemes will be discussed separately.

7.4.1 CENTRAL DIFFERENCING SCHEME (C.D.S.)

For the central differencing scheme, $\alpha(i,j)=\beta(i,j)=\gamma(i,j)=\delta(i,j)=0$, one can immediately observe from Equation 7.16 that convergence of Equation 7.15 is not always assured: the sum of the terms on left hand side of Equation 7.51, because of the presence of the velocity terms in the numerator, is not bounded. As long as all the coefficients in Equation 7.16 are positive, the sum of these terms is unity. However, once this is not true, the sum of these terms may well exceed unity. In the region near the jet nozzle exit, the velocity in the Y-direction, V, is large. For the case of high Reynolds numbers, the coefficient m_s in Equation 7.16 becomes negative. Such a coefficient may lead to non-convergence or numerical instabilities.

7.4.2 UPSTREAM DIFFERENCING SCHEME (U.D.S.)

For the upstream differencing scheme, $\alpha(i,j)=\beta(i,j)=0.5$ and $\gamma(i,j)=\delta(i,j)=0$, one can immediately observe from Equation 7.16 that all the coefficients are always positive and hence the sum of the terms on the left hand side of Equation 7.51 will always be unity. Therefore, the upstream differencing scheme has a better chance of convergence.

7.4.3 UPSTREAM-WEIGHTED DIFFERENCING SCHEME (U.W.D.S.)

For the upstream-weighted differencing scheme, $\alpha(i,j)$, $\beta(i,j)$, $\gamma(i,j)$ and $\delta(i,j)$ are unknowns and are depended on the local velocity components and the grid size by studying Equations 4.43, 4.45, 4.48 and 4.49. The limit values of these parameters were shown in Section 7.3, where $\alpha(i,j)$ and $\beta(i,j)$ vary from 0 to 0.5 and $\gamma(i,j)$ and $\delta(i,j)$ vary from 0 to 1 with Rw and Rs increasing.

In order to have a better chance of convergence, all the coefficients in Equation 7.16 should be positive such that the sum of the terms on the left hand side of Equation 7.51 is unity. Since a negative coefficient occurs only when the local velocities are large, let us examine the coefficients for such cases. In the region of interest, the largest U occurs near the stagnation flow region and the largest V occurs near the jet nozzle exit. Therefore the values of $\alpha(i,j)$ and $\gamma(i,j)$ are close to 0.5 and 1 near the stagnation flow region, respectively. On the other hand, the values of $\beta(i,j)$ and $\delta(i,j)$ are close to 0.5 and 1 near the jet nozzle exit, respectively. From Equation 7.16, all the coefficients should be positive for both cases with m_2 approaching zero for the first case and m_1 approaching zero for the second case.

Once again, all the coefficients in Equation 7.16 are always positive. The convergence properties of this differencing scheme should be similar to those for the upstream differencing scheme.

8. COMPUTATIONAL PROCEDURE

The grid design used for the numerical computations is discussed in Section 8.1, followed by a detailed presentation of the method of solution in Section 8.2. The selection of the convergence criteria is discussed in Section 8.3. Finally, the construction of the computer program is given in Section 8.4.

8.1 GRID DESIGN

A non-uniform grid is used in the numerical computations. The grid size and the arrangement are known to be important factors in determining not only the accuracy of the solution, but also the convergence characteristics.

Due to relatively large gradients of velocity and concentration along the impingement plate, the gridlines parallel and adjacent to this plate must be very closely spaced. On the other hand, gridlines parallel and adjacent to the axis of symmetry are also closely spaced in order to ensure accurate calculation of the variables within the stagnation flow region.

In this work, different grid networks are designed for the numerical runs for the three different jet-to-plate spacings (L=2,4 and 12). These grid networks are results of numerous trials and are given in Table 8.1 Tests for the accuracy of these grid networks will be given in Chapter 9.

TABLE 8.1 : GRID NETWORKS FOR DIFFERENT L AND Re

L	Re_b	nx	ny
2	100 - 400	55	25
4	100 - 400	55	25
12	100 - 300	67	25
	400	69	25

8.1.1 GRID ARRANGEMENT IN X-DIRECTION

The finest grid spacings are adjacent to the axis of symmetry. In such a region, nine nodes are used to cover a distance [illegible] b/2 (nj=9). The grid spacings are then increased in steps [illegible] a factor of 2 in the X-direction. The largest grid spacings appear in the outflow region which are 128 times the finest one. The grid arrangement in X-direction are listed in Table 8.2.

The distance in X-direction which is covered by grid network is a function of nx, the total number of nodes in X-direction used. In other words, the location of the outflow region boundary is a function of nx. For the grid networks with nx=55, 67 and 69 as shown in Table 8.1, the outflow region boundaries are located at X=74, 170 and 186,

TABLE 8.2 : GRID ARRANGEMENT IN X-DIRECTION

i	X	RELATIVE SPACING
1	0	
2	0.0625	1
3	0.125	1
4	0.1875	1
5	0.25	1
6	0.3125	1
7	0.375	1
8	0.4375	1
9	0.5	1
10	0.625	2
11	0.75	2
12	1	4
13	1.25	4
14	1.5	4
15	2	8
16	2.5	8
17	3	8
18	3.5	8
19	4	8
20	4.5	8
21	5	8
22	5.5	8
23	6	8
24	6.5	8
25	7	8
26	7.5	8
27	8	8
28	8.5	8
29	9	8
30	9.5	8
31	10	8
32	10.5	8
33	11	8
34	11.5	8
35	12	8
36	13	16
37	14	16
38	15	16
39	16	16
40	17	16
41	18	16
42	19	16
43	20	16
44	22	32
45	24	32
46	26	32
47	28	32
48	30	32
49	34	64
50	38	64
51	42	64
52	50	128
53	58	128
54	66	128
55	74	128
56	82	128
57	90	128
58	98	128
59	106	128
60	114	128
61	122	128
62	130	128
63	138	128
64	146	128
65	154	128
66	162	128
67	170	128
68	178	128
69	186	128

respectively (see Table 8.2). These locations of the outflow region boundaries are also mentioned above in Table 6.1.

8.1.2 GRID ARRANGEMENT IN Y-DIRECTION

Since finer grid spacings must be located adjacent to the impingement plate, this can be achieved with a coordinate stretching transformation of some kind. One of the most commonly used transformation is that of an exponential stretch. Choose

$$Y = \frac{[1 - \exp(-b_1 Y')]}{[1 - \exp(-b_1 L)]} L \qquad (8.1)$$

such that the Y'-coordinate is transformed into the stretched Y-coordinate. b_1 is an arbitrary constant used to adjust the "stretch". Equation 8.1 satifies the boundary conditions of Y(1)=0, Y'(1)=0 and Y(ny)=L, Y'(ny)=L.

In this work, b_1 is choosen as 0.75, 0.25 and 0.075 for numerical runs of L=2, 4 and 12, respectively. Numerical runs with b_1=1.0 for L=2 and b_1=0.75 for L=4 are also made for the case of an initial parabolic velocity profile. The grid arrangements in Y-direction for three different jet-to-plate spacings are listed in Tables 8.3, 8.4 and 8.5 for L=2, 4 and 12, respectively. A total of 25 nodes are used in Y-direction (ny=25) throughtout all the numerical runs. Sample runs with ny=17 for L=2 and 4, and also with ny=33 for L=12 are only used for the purpose of testing the

TABLE 8.3 : GRID ARRANGEMENT IN Y-DIRECTION FOR L=2

$b_1 = 0.75$

j	Y	RELATIVE SPACING
1	0	4.216
2	0.156	3.973
3	0.303	3.703
4	0.440	3.486
5	0.569	3.297
6	0.691	3.081
7	0.805	2.892
8	0.912	2.730
9	1.013	2.568
10	1.108	2.378
11	1.196	2.270
12	1.280	2.108
13	1.358	2.000
14	1.432	1.865
15	1.501	1.757
16	1.566	1.649
17	1.627	1.568
18	1.685	1.459
19	1.739	1.350
20	1.789	1.297
21	1.837	1.216
22	1.882	1.135
23	1.924	1.054
24	1.963	1.000
25	2.000	

$b_1 = 1$

j	Y	RELATIVE SPACING
1	0	6.852
2	0.185	6.296
3	0.355	5.815
4	0.512	5.333
5	0.656	4.889
6	0.788	4.519
7	0.910	4.148
8	1.022	3.815
9	1.125	3.519
10	1.220	3.259
11	1.308	2.963
12	1.388	2.741
13	1.462	2.519
14	1.530	2.333
15	1.593	2.111
16	1.650	1.963
17	1.703	1.815
18	1.752	1.667
19	1.797	1.519
20	1.838	1.407
21	1.876	1.296
22	1.911	1.185
23	1.943	1.111
24	1.973	1.000
25	2.000	

TABLE 8.4 : GRID ARRANGEMENT IN Y-DIRECTION FOR L=4

b_1 = 0.25

j	Y	RELATIVE SPACING
1	0	2.606
2	0.258	2.506
3	0.506	2.404
4	0.744	2.293
5	0.971	2.212
6	1.190	2.121
7	1.400	2.030
8	1.601	1.949
9	1.794	1.869
10	1.979	1.788
11	2.156	1.727
12	2.327	1.646
13	2.490	1.576
14	2.646	1.525
15	2.797	1.455
16	2.941	1.394
17	3.079	1.343
18	3.212	1.283
19	3.339	1.232
20	3.461	1.182
21	3.578	1.131
22	3.690	1.091
23	3.798	1.040
24	3.901	1.000
25	4.000	

b_1 = 0.75

j	Y	RELATIVE SPACING
1	0	17.679
2	0.495	15.571
3	0.931	13.750
4	1.316	12.143
5	1.656	10.714
6	1.956	9.464
7	2.221	8.357
8	2.455	7.357
9	2.661	6.500
10	2.843	5.607
11	3.000	5.179
12	3.145	4.464
13	3.270	3.964
14	3.381	3.464
15	3.478	3.071
16	3.564	2.714
17	3.640	2.393
18	3.707	2.107
19	3.766	1.857
20	3.818	1.643
21	3.864	1.464
22	3.905	1.250
23	3.940	1.143
24	3.972	1.000
25	4.000	

TABLE 8.5 : GRID ARRANGEMENT IN Y-DIRECTION FOR L=12

$b_1 = 0.075$

j	Y	RELATIVE SPACING
1	0	2.369
2	0.744	2.283
3	1.461	2.201
4	2.152	2.118
5	2.817	2.038
6	3.457	1.965
7	4.074	1.895
8	4.669	1.822
9	5.241	1.755
10	5.792	1.691
11	6.323	1.631
12	6.835	1.570
13	7.328	1.510
14	7.802	1.455
15	8.259	1.405
16	8.700	1.350
17	9.124	1.299
18	9.532	1.255
19	9.926	1.204
20	10.304	1.162
21	10.669	1.121
22	11.021	1.080
23	11.360	1.038
24	11.686	1.000
25	12.000	

accuracy of the numerical solutions using a particular grid network.

8.2 METHOD OF SOLUTION

The finite-difference equations used to discretize the governing equations and the associated boundary conditions shown in Chapter 7 constitute a system of strongly non-linear algebraic equations. For a nx x ny grid network, there are (nx-2) x (ny-2) algebraic equations for each of the three variables, Ψ, Ω and C making a total of 3 x (nx-2) x (ny-2) equations to be solved. Because of the difficulty in solving a strongly non-linear system of equations, a linear algorithm is used such that the non-linear coefficients are updated periodically. The Gauss-Seidel iteration method coupled with the conventional successive over relaxation (SOR) method is used. This method has been established that an optimum relaxation factor exists which yields the maximum rate of convergence for linear problems. However, for a non-linear problem the relaxation factor varies not only from node to node but also with every iteration. An estimation of this relaxation factor is not worthwhile from a computational efficiency point of view. In such cases a constant value is used which is chosen based on numerical experimentation. In this work, the proper relaxation factors for the stream-function and the concentration are 1.7 and 0.7, respectively. While for the vorticity, the relaxation factor is in the range of 0.1 to 0.4.

A modified scheme of calculations, presented by Wilkes (100) is used during the iteration procedure. This modified scheme has been observed by Masliyah and Nandakumar (49) to have a stabilizing effect on the convergence characteristics and it is twice as fast as the conventional SOR method. The depiction of this scheme is shown in Figure 8.1. The grid network is divided into two subgrids. The circles refer to subgrid 1 and the crosses refer to subgrid 2. The iteration is carried out in two steps, one subgrid being covered first and the other next. In the first half of iteration, the nodes of the subgrid 1 are computed using the neighbouring four nodes of the subgrid 2 as given by Equations 7.15 and 7.20, together with

$$S_n^{(1)}(i,j) = S_{n-1}^{(1)}(i,j) + w\,[S_n^{(1)'}(i,j) - S_{n-1}^{(1)}(i,j)] \tag{8.2}$$

where $S_n^{(1)}(i.j)$ is the value of $S(i,j)$ (represented variables Ω, Ψ and C) at the nth iteration belonging to subgrid 1, $S_n^{(1)'}(i,j)$ is the value of $S(i,j)$ computed using the four neighbouring nodes of subgrid 2 and w is a constant relaxation factor. Therefore, all the nodes in subgrid 1 are computed first and only points belonging to subgrid 2 are used.

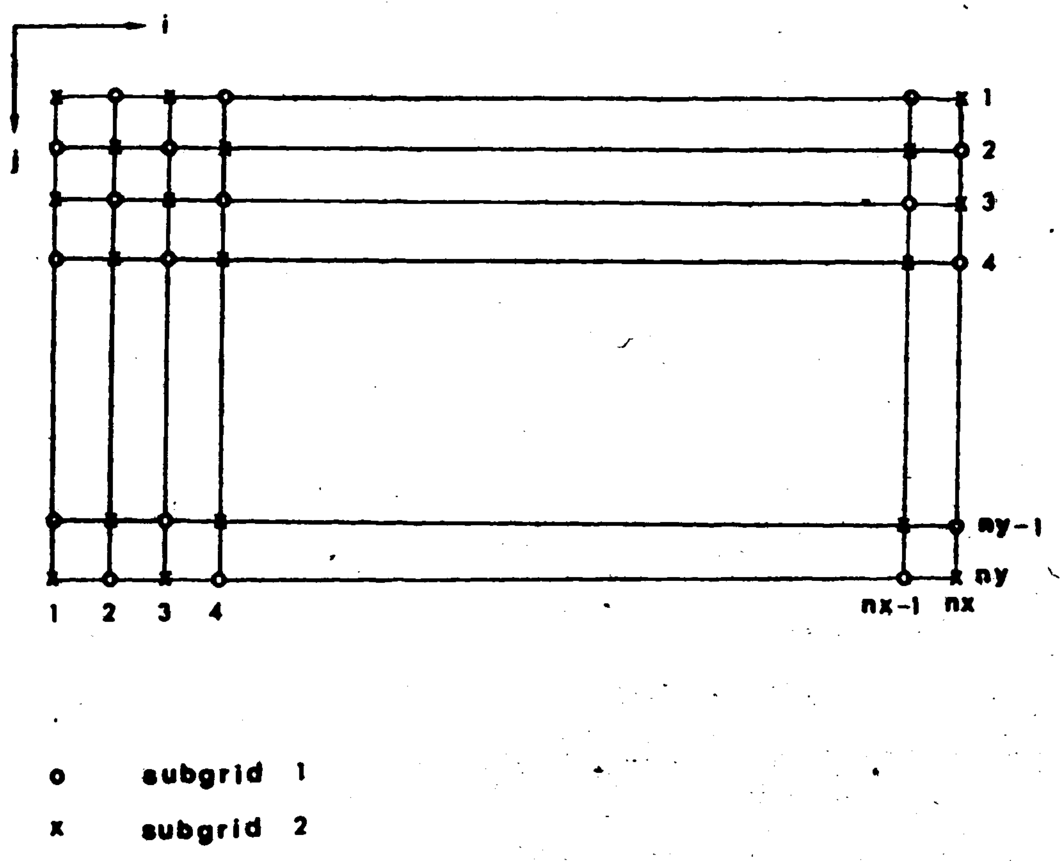

FIGURE 8.1 : SUBGRIDS USED FOR THE ITERATIVE SCHEME

In the next half of iteration, nodes of subgrid 2 are evaluated using the neighbouring four nodes which belong to subgrid 1. The válues of these four nodes in subgrid 1 computed in the first half iteration are used. In this second half iteration, the same relaxation factor, w, is used. This completes one full iteration.

Equations 7.4, 7.5, 7.15 and 7.16 are solved simultaneously to obtain the velocity, vorticity and stream-function distributions. The summary of the procedure used in solving the stream-function and vorticity transport equations is listed below

1. For a low Reynolds number case (Re_b=1), arbitrary constant values are used for the starting values of stream-function and vorticity. For the cases of higher Reynolds number the converged solution obtained for a lower Reynolds number is used as the initial starting values.
2. Any variable which is a constant is computed before entering the iteration loop.
3. Within the iteration loop, U(i+1/2,j) and V(i,j+1/2) are computed from Equations 7.4 and 7.5 using the guessed values of the stream-function.
4. The parameters α, β, γ and δ for upstream-weighted differencing scheme (U.W.D.S.) are then evaluated. One may notice that these parameters for central differencing scheme (C.D.S.) and upstream differencing scheme (U.D.S.) are constants and can be evaluated

before entering the iteration loop. Even for the case of U.W.D.S., the values of these parameters do not need frequent updating (69). In this work, these parameters are updated after every 50 iterations.

5. The non-linear coefficients m_1, m'_2, m_3, m_4 and m_5 are updated using Equation 7.16. Then the vorticity at each interior node is iterated in the manner mentioned above using Equation 7.15.
6. Next, the stream-function is iterated in the same manner at all interior nodes using Equation 7.20. This iteration is carried out three times in order to get a smooth solution in the manner suggested by Masliyah and Nandakumar (49).
7. The vorticity boundary conditions at both the impingement and confinement plates are updated. The vorticity and stream-function boundary conditions at the outflow region are also updated.
8. The modified variables are treated as improved guesses and steps 3 to 7 are then repeated until the process satisfied specified convergence criteria.

One cycle for steps 3 through 7 is refered to being one iteration. The convergence criterion is tested at the end of each iteration.

It is found that a relatively large number of iterations is required for a converged solution. For example, for Re_b=100 and L=4, 1353 iterations are needed to obtain the converged solution. In this case, the converged solution of $Re_b=1$ and $L=4$ is used as the initial guess. The CPU time used for this run is approximately 110 s on Amdahl 470/V8 computer.

After the converged solutions of vorticity and stream-function are obtained, the velocity components are evaluated at each interior node using Equations 7.22 and 7.23. In addition, an important variable, the local skin friction factor, is evaluated along the impingement plate from the flow field. The local skin friction factor, C_f, is defined as

$$C_f = \tau_s / (0.5 \rho \bar{v}_j^2) \qquad (8.3)$$

where ρ is the density of air and τ_s is the shear stress at the impingement plate. The shear stress at the impingement plate (y=h) is given by

$$\tau_s = - \left. \left(\frac{\partial u}{\partial y} + \frac{\partial v}{\partial x}\right) \right|_{y=h} \qquad (8.4)$$

Since the impingement plate is impermeable, implies that $v=(\partial v/\partial x)=0$ at the impingement plate. Introducing the dimensionless variables of Equation 6.6 and combining Equations 8.3 and 8.4, yields

$$C_f = - \frac{2}{Re_b} \left. \left(\frac{\partial U}{\partial Y}\right) \right|_{Y=L}$$

$$C_f = -\frac{2}{Re_b}\,\Omega\bigg|_{Y=L} \qquad (8.5)$$

By using Equation 8.5, the local skin friction factor can then be evaluated from the vorticity at the impingement plate and the jet Reynolds number.

The transport equation of the swelling agent is solved to obtained the concentration distribultion. The procedure is mainly the same as mentioned above except in this case the velocity components are known, therefore the coefficients m_1, m_2, m_3, m_4 and m_5 do not vary with iteration. In other words, the system of algebraic equations to be solved is linear.

After the converged solution of concentration is obtained, the bulk flow concentration is evaluated. The bulk flow concentration, c_B, is defined as

$$c_B = \left(\int_0^h u\ c\ dy\right) / (\bar{u}_o\ h) \qquad (8.6)$$

where $\bar{u}_o$ is the average velocity in the outflow region and is equal to $0.5\bar{v}_j b/h$ for the jet system in this work. Introducing the dimensionless variables of Equation 6.6, yields

$$C_B = 2\int_0^L U\ C\ dY \qquad (8.7)$$

In addition, the local Sherwood number is also evaluated along the impingement plate from the concentration field. The definitions of the Sherwood number are given in Equations 5.1 and 5.2. Rewriting the definitions of the local mass transfer coefficients k and k' in Equations 5.3 and 5.4 using ideal gas law and Dalton's law, yields

$$N = k\ (c_s - c_j)\ Mw \qquad (8.8)$$

$$\text{and} \quad N = k'\ (c_s - c_s)\ Mw \qquad (8.9)$$

According to Fick's law, the mass transfer of swelling agent from the impingement plate is described by

$$N = -D\ Mw\ \left(\frac{\partial c}{\partial y}\right)\Bigg|_{y=h} \qquad (8.10)$$

Introducing the dimensionless variables of Equation 6.6 and combining Equations 8.8 and 8.10, and also Equations 8.9 and 8.10, yield

$$Sh_b = -\left(\frac{\partial C}{\partial Y}\right)\Bigg|_{Y=L} \qquad (8.11)$$

$$Sh'_b = -\left(\frac{\partial C}{\partial Y}\right)\Bigg|_{Y=L} / \ (C_s - C_s) \qquad (8.12)$$

By using Equations 8.11 and 8.12, the local Sherwood numbers can then be evaluated from the gradient of concentration at the impingement plate.

8.3 CONVERGENCE CRITERION

Convergence of the numerical results is assumed when the maximum absolute difference between two consecutive iterations, defined as

$$\epsilon = \max_{ij} |S_n(i,j) - S_{n-1}(i,j)| \quad (8.13)$$

is less than 10^{-4} for vorticity and stream-function, and 10^{-6} for concentration. The suitability of these convergence criteria is confirmed by numerical experimentation. Once the convergence criterion is met, further iterations have no significant effect on the local skin friction factor and local Sherwood number along the impingement plate.

8.4 OUTLINE OF THE COMPUTER PROGRAM

A main program with four subroutines is used in the numerical study. The first subroutine, ITER1, is used to compute the stream-function and the vorticity distributions. After the converged solutions of the stream-function and the vorticity are obtained from ITER1, the second subroutine, CALC1, is used to compute the velocity components at all the nodes instead of midway points. In this subroutine, the local skin friction factor along the impingement plate is also evaluated. The third subroutine, ITER2, is used to compute the concentration distribution. After the converged solution of the concentration is obtained from ITER2, the fourth subroutine, CALC2, is used to compute the bulk flow concentration and the local Sherwood number along the impingement plate.

Only the computational procedure of subroutine ITER1 is shown in Figure 8.2 in the form of a flow diagram. The computational procedure of subroutine ITER2 is very similar to that of subroutine ITER1. The computational procedures of subroutines CALC1 and CALC2 are straightforward calculations only.

The program is listed in Appendix F, together with a typical output listing.

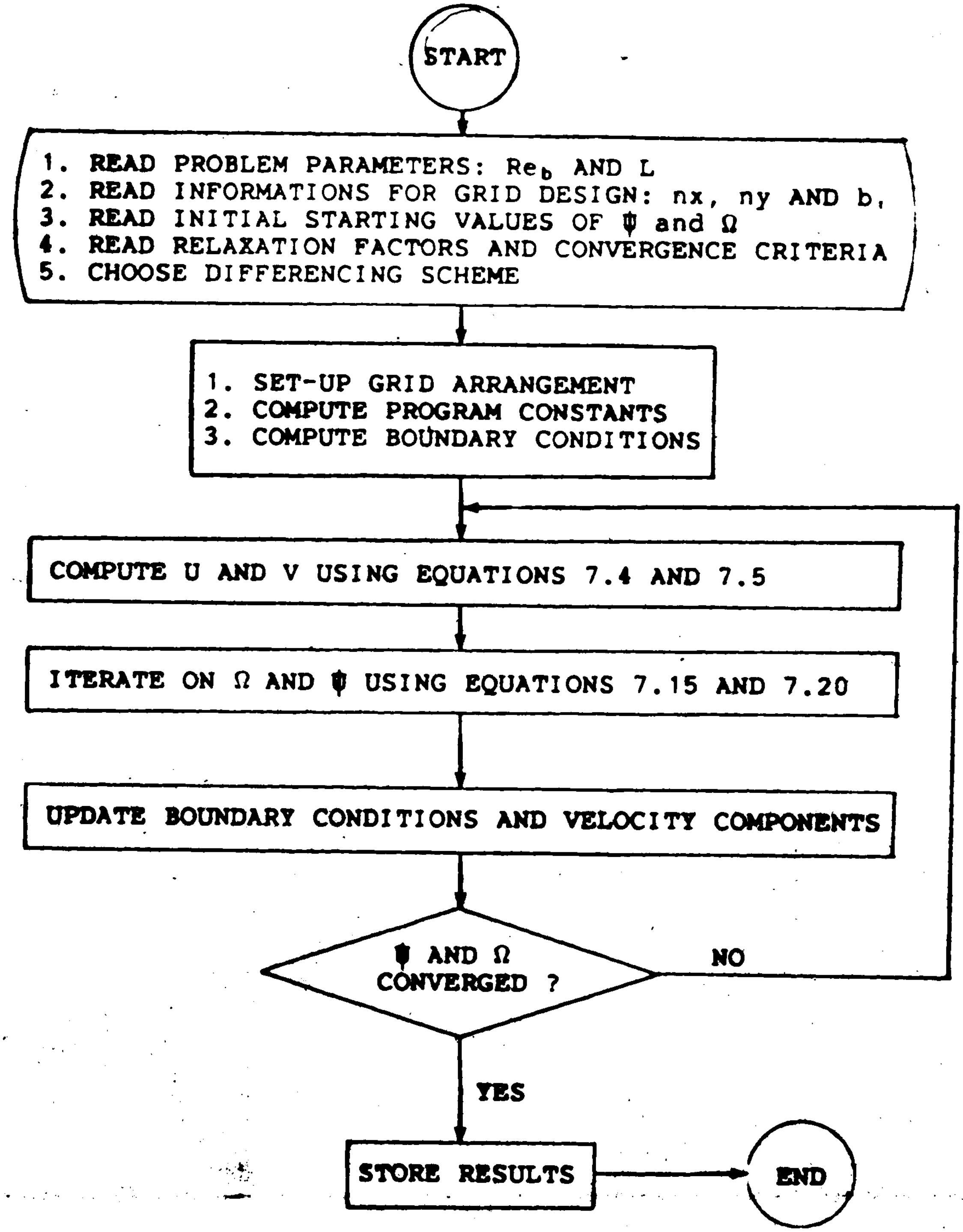

FIGURE 8.2 : COMPUTATIONAL FLOW DIAGRAM FOR SUBROUTINE ITER1

9. VALIDITY OF THE NUMERICAL SOLUTION

Accuracy of numerical solution is dependent on the choice of grid network and differencing scheme. The influences of grid network and differencing scheme on the numerical solution are studied separately in Sections 9.1 and 9.2, respectively.

9.1 INFLUENCE OF GRID NETWORK

The influences of the grid network on the numerical solutions for three different jet-to-plate spacings (L=2, 4 and 12) are studied separately.

For L=2, numerical runs for different Reynolds number using two different grid networks of 55 x 17 and 55 x 25 with b_1=0.75 are made. The differencing scheme used is U.W.D.S.. The skin friction factor evaluated along the impingement plate from these two grid networks are plotted in Figure 9.1 for Re_b=100, 200, 300 and 400 with an initial parabolic velocity profile. There is little difference between the values of $C_f Re_b$ obtained from the two different grid networks for Re_b=100 and 200. For Re_b=300 and 400, disagreement between the values of $C_f Re_b$ obtained from these two grid networks is found only in a small region near the stagnation flow region with a maximum difference of

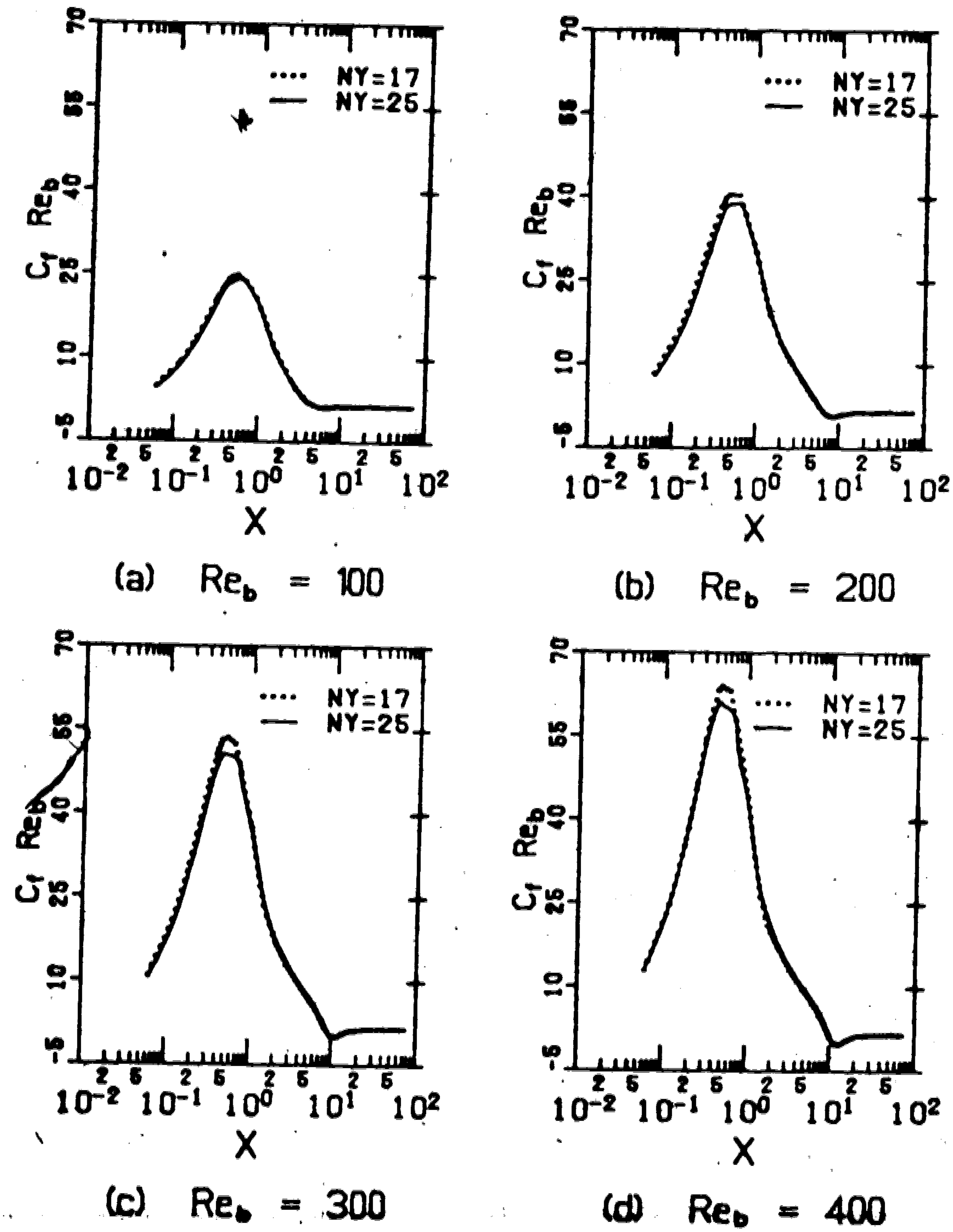

FIGURE 9.1 : INFLUENCE OF GRID NETWORK ON THE NUMERICAL SOLUTIONS FOR L=2 USING U.W.D.S.

approximately 5% only. Therefore, a conclusion can be made that both grid networks are suitable for the computation for the case of L=2. In all subsequent computations for the case of L=2, the network of 55 x 25 with the smaller grid size is used.

For L=4, numerical runs for different Reynolds number using two grid networks of 55 x 17 and 55 x 25 with b_1=0.25 are made. Again, the differencing scheme used is U.W.D.S.. The skin friction factors evaluated along the impingement plate from these two networks are plotted in Figure 9.2 for Re_b=100, 200, 300 and 400 with an initial parabolic velocity profile. There is little difference between the values of $C_f Re_b$ obtained from these two grid networks for Re_b=100. But for the Re_b=200, 300 and 400, disagreement is found mainly in the stagnation flow region with the worst case occured for Re_b=400. The maximum differences are 6%, 15% and 20% for Re_b=200, 300 and 400, respectively. Therefore, the two grid network are only suitable when $Re_b \leq 200$. But the network of 55 x 17 with the coarser grid size is no longer suitable for high Reynolds numbers. In all subsequent computations for the case of L=4, the network of 55 x 25 with the finer grid size is used.

From the conclusion above, it is obvious that a grid network of 55 x 17 will be too coarse for the case of L=12 because of the large jet-to-plate spacing. For L=12, numerical runs for Re_b=100, 200 and 300 using two different grid networks of 67 x 25 and 67 x 33, and for Re_b=400 using

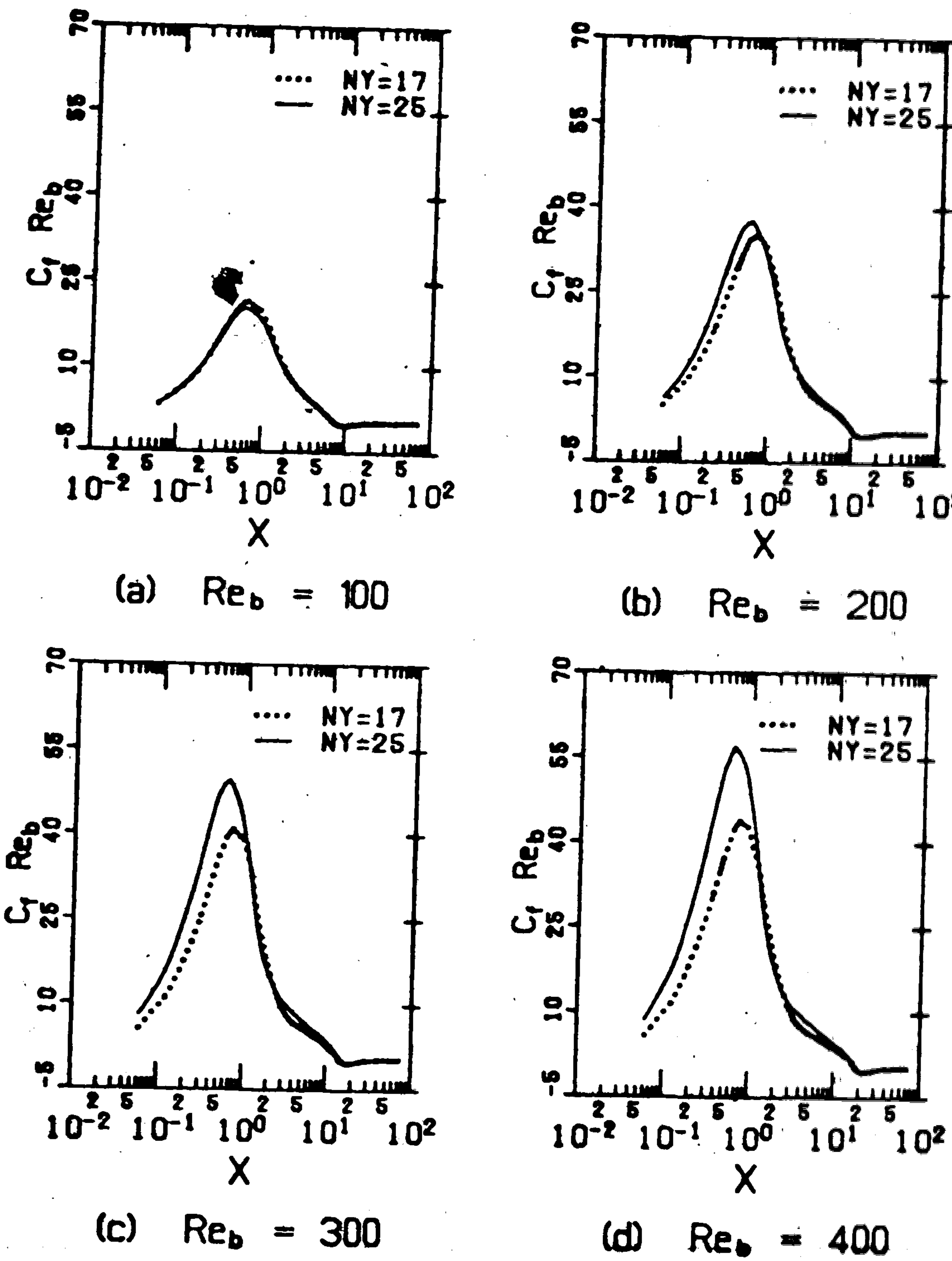

FIGURE 9.2 : INFLUENCE OF GRID NETWORK ON THE NUMERICAL SOLUTIONS FOR L=4 USING U.W.D.S.

two grid networks of 69 x 25 and 69 x 33 are made. For all these grid networks, the value of b, is chosen to be 0.075. The differencing scheme used is U.W.D.S.. Unfortunately, for Re_b=400, no converged solution can be obtained using the grid network of 69 x 33. The skin friction factors evaluated along the impingement plate from the two grid networks of 67 x 25 and 67 x 33 are plotted in Figure 9.3 for Re_b=100, 200 and 300 with an initial parabolic profile. There is again little difference between the values of $C_f Re_b$ obtained from these two grid networks for Re_b=100. For the cases of Re_b=200 and 300, disagreement is found mainly in the stagnation flow region. In all subsequent computations for the case of L=12, the network of 67 x 25 or 69 x 25 with the coarser grid size is used simply because a converged solution can be obtained from this network for all Reynolds numbers. It is noted that in order to obtain a converged solution for the case of L=12, a little sacrifice on the accuracy of the numerical solution in the stagnation flow region cannot be avoided.

For a particular numerical run in this work, only one grid network is used. These grid networks for different jet-to-plate spacing and Reynolds number are listed in Table 8.1.

The influence of grid arrangement on the numerical solution is not as obvious as that of the grid network. For L=2, numerical solutions of flow and concentration fields evaluated from grid network of 55 x 25 with b,=0.75 and 1

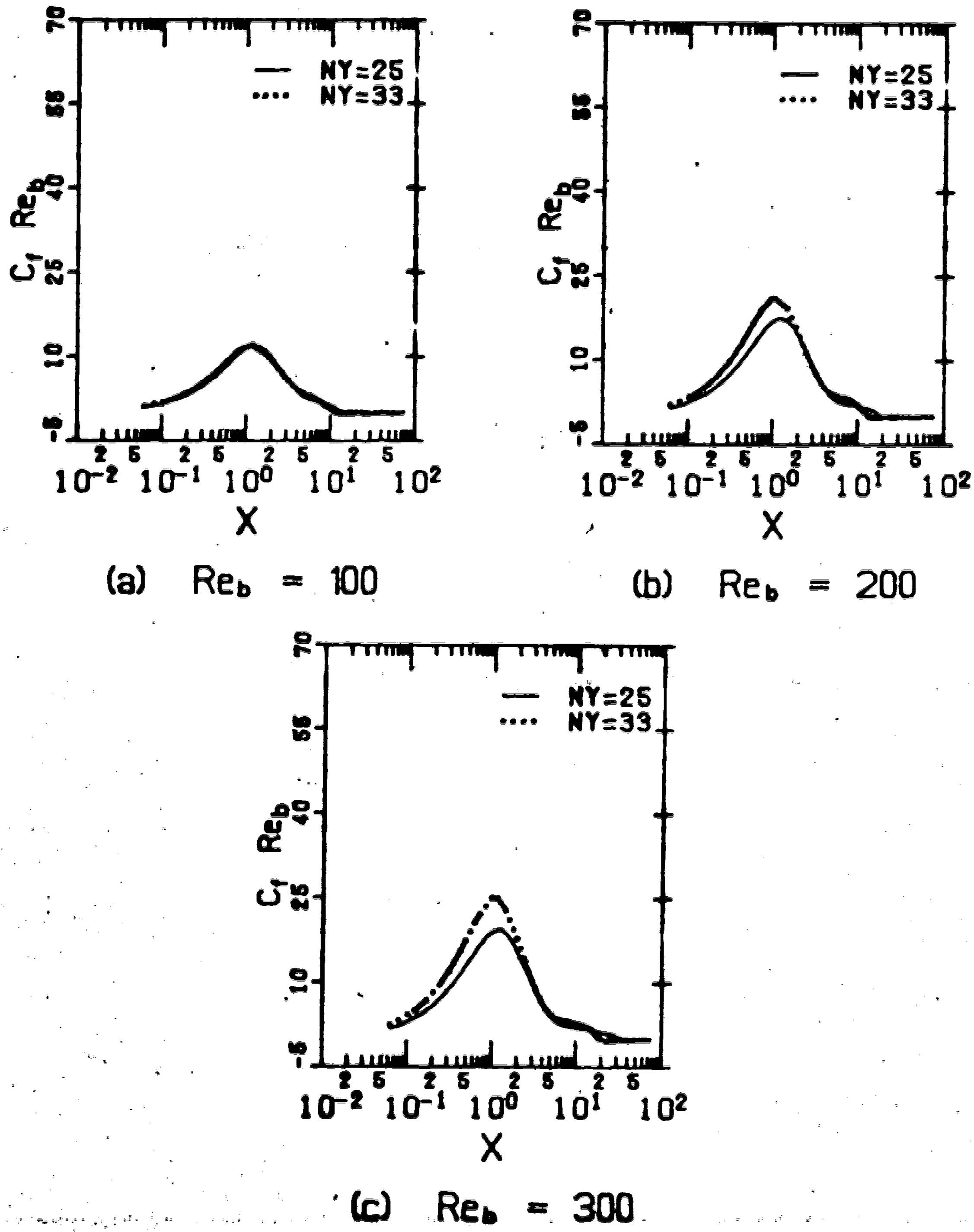

FIGURE 9.3 : INFLUENCE OF GRID NETWORK ON THE NUMERICAL SOLUTIONS FOR L=12 USING U.W.D.S.

are nearly the same for all Reynolds numbers. The variables such as local skin friction factor and local Sherwood number evaluated along the impingement plate from the two different grid arrangements are nearly the same for all Reynolds numbers. For L=4, numerical solutions of flow and concentration fields evaluated from grid network of 55 x 25 with b_1=0.25 and 0.75 are also nearly the same for all Reynolds numbers. Only in evaluating the local skin friction factor and the local Sherwood number along the impingement plate, this disagreement in these two arrangements is found near the stagnation flow region. In this work, the variables evaluated from the grid network of 55 x 25 with b_1=0.75 are used because these variables should be more accurate due to the finer grid spacings adjacent to the impingement plate. For L=12, only one grid arrangement with b_1=0.075 is used for both the grid network of 67 x 25 and the grid network of 69 x 25.

9.2 INFLUENCE OF DIFFERENCING SCHEME

The influence of differencing scheme on the numerical solution is studied briefly for the case of L=2. To conserve on the computational costs, a grid network of 55 x 17 with b_1=0.75 is used. This grid network was found in Section 9.1 to be suitable for the computations for the case of L=2. Numerical runs with an initial parabolic velocity profile are made using three different differencing schemes (C.D.S., U.D.S. and U.W.D.S.). Converged solutions are obtained for all runs using U.D.S. and U.W.D.S., while the converged solutions can only be obtained for $Re_b \leq 200$ using C.D.S..

The comparisons of the converged local skin friction factors obtained from the numerical runs using the three differencing schemes are shown in Figure 9.4 for $Re_b = 100$, 200, 300 and 400. It is found that the differencing scheme has little effect on the solutions except in a small region near the stagnation flow region. In the range of disagreement, some of the observations by Raithby and Torrance (69) on comparison of differencing schemes are confirmed. According to their study, solutions from the C.D.S. are the most accurate solutions compared to the exact solutions as long as converged solutions can be found. Although U.D.S. gives converged solutions for all cases, in the range where C.D.S. can be used, U.D.S. is inferior. Furthermore, U.W.D.S. also gives converged solutions for all cases and the solutions obtained from U.W.D.S. are better than those from U.D.S.. These observations are confirmed as shown in Figures 9.4(a) and 9.4(b) by assuming the solutions from the C.D.S. are the most accurate solutions in this work. The disagreements between the solutions of C.D.S. and U.D.S. are the largest in both cases which indicate that the solutions of U.D.S. are worse than those of U.W.D.S..

Since the solutions of C.D.S. are the best, it is logical to use C.D.S. as long as it gives a converged

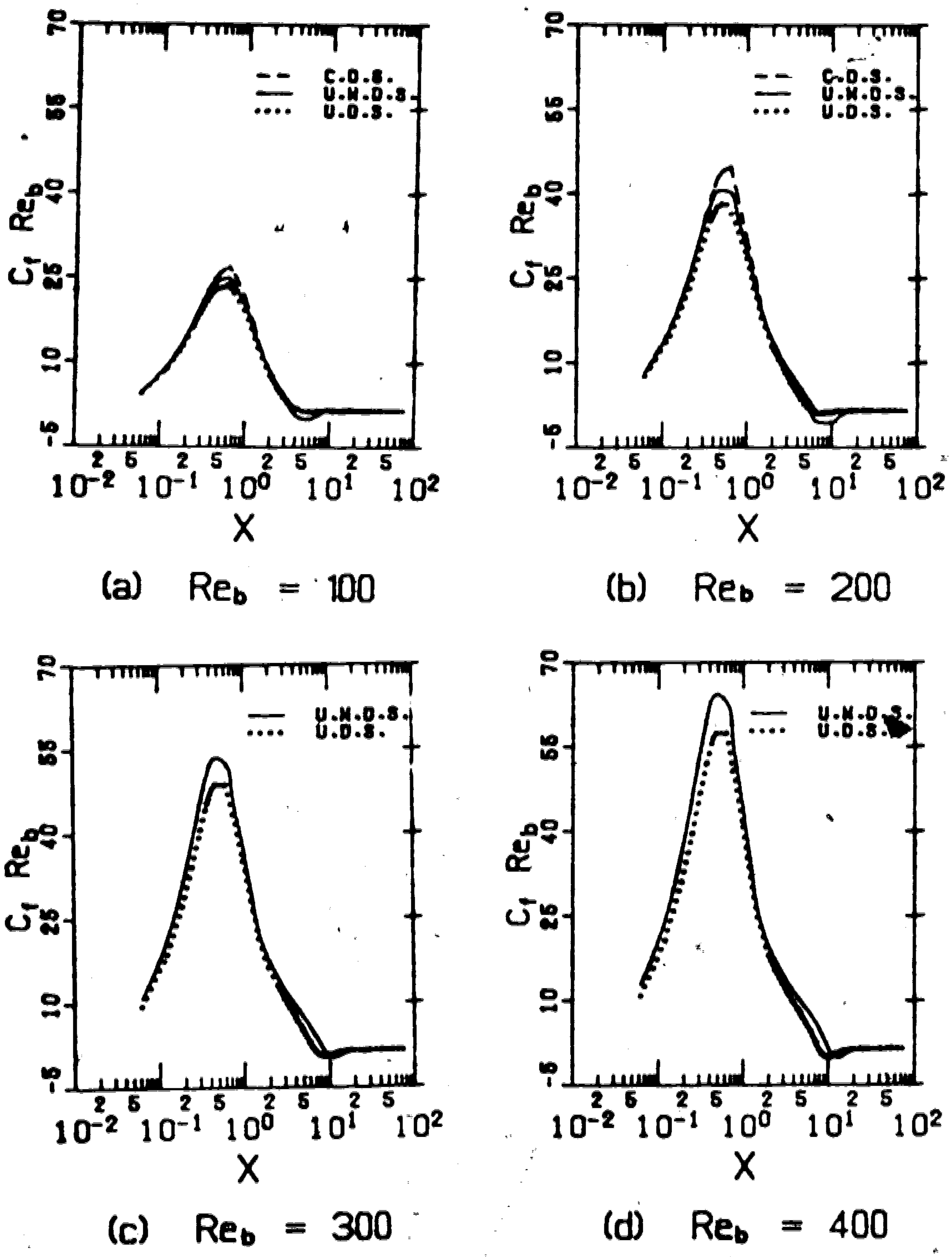

FIGURE 9.4 : INFLUENCE OF DIFFERENCING SCHEME ON THE NUMERICAL SOLUTIONS FOR L=2 USING A GRID NETWORK OF 55 x 17

solution. But unfortunately, the numerical solutions obtained by using C.D.S. for the chosen grid network of 55 x 25 did not give a converged solution. Therefore, in all subsequent numerical computations, only U.W.D.S. and U.D.S. are used while U.W.D.S. is expected to give a better solution for all cases.

10. RESULTS AND DISCUSSIONS

Experimental and numerical results for a confined air jet are both discussed in this chapter. Results are given for two different categories: flow characteristics and mass transfer characteristics. Flow characteristics can only be studied numerically in this work. While mass transfer characteristics are studied both experimentally and numerically. Experimental results in this case are used to verify the numerical predictions of the two-dimensional model.

10.1 FLOW CHARACTERISTICS

The flow behavior for different jet Reynolds numbers, jet-to-plate spacings and nozzle exit velocity profiles are studied numerically. A listing of the numerical runs is given in Appendix G. In this section, only the numerical results using the upstream-weighted differencing scheme (U.W.D.S.) are presented.

10.1.1 STREAMLINE CONTOURS

The flow field is studied qualitatively by observing the streamline contours from the numerical solution. The contours of the stream-function for L=2, 4 and 12 with an initial parabolic velocity profile are shown in Figures 10.1, 10.2 and 10.3, respectively. The contours of the stream-function for L=4 with an initial flat velocity profile are shown in Figure 10.4. The jet nozzle exit is at the upper left hand corner with the main flow travelling from left to right. The upper horizontal streamline represents the confinement plate and the lower horizontal streamline represents the impingement plate.

For the case of an initial parabolic profile, in general, a primary vortex rotating in the counter-clockwise direction is found near the confinement plate with its size increasing with jet Reynolds number. With the exception of the case of low Reynolds numbers for L=2, a second vortex rotating in clockwise direction is found near the impingement plate. This secondary vortex is much smaller than the first one in size and it is also weaker in terms of rotational intensity. The variation of the location of the vortex centre with the jet Reynolds number is shown in Figure 10.5. It can be observed that the centers of both the primary and secondary vortices move downstream with increase in Reynolds number.

For the case of an initial flat profile, only the primary vortex is found near the confinement plate. This vortex behaves as the primary vortex for the case of an initial parabolic profile except it is smaller in size and also weaker in terms of rotational intensity. The variation of the location of the primary vortex centre with the jet

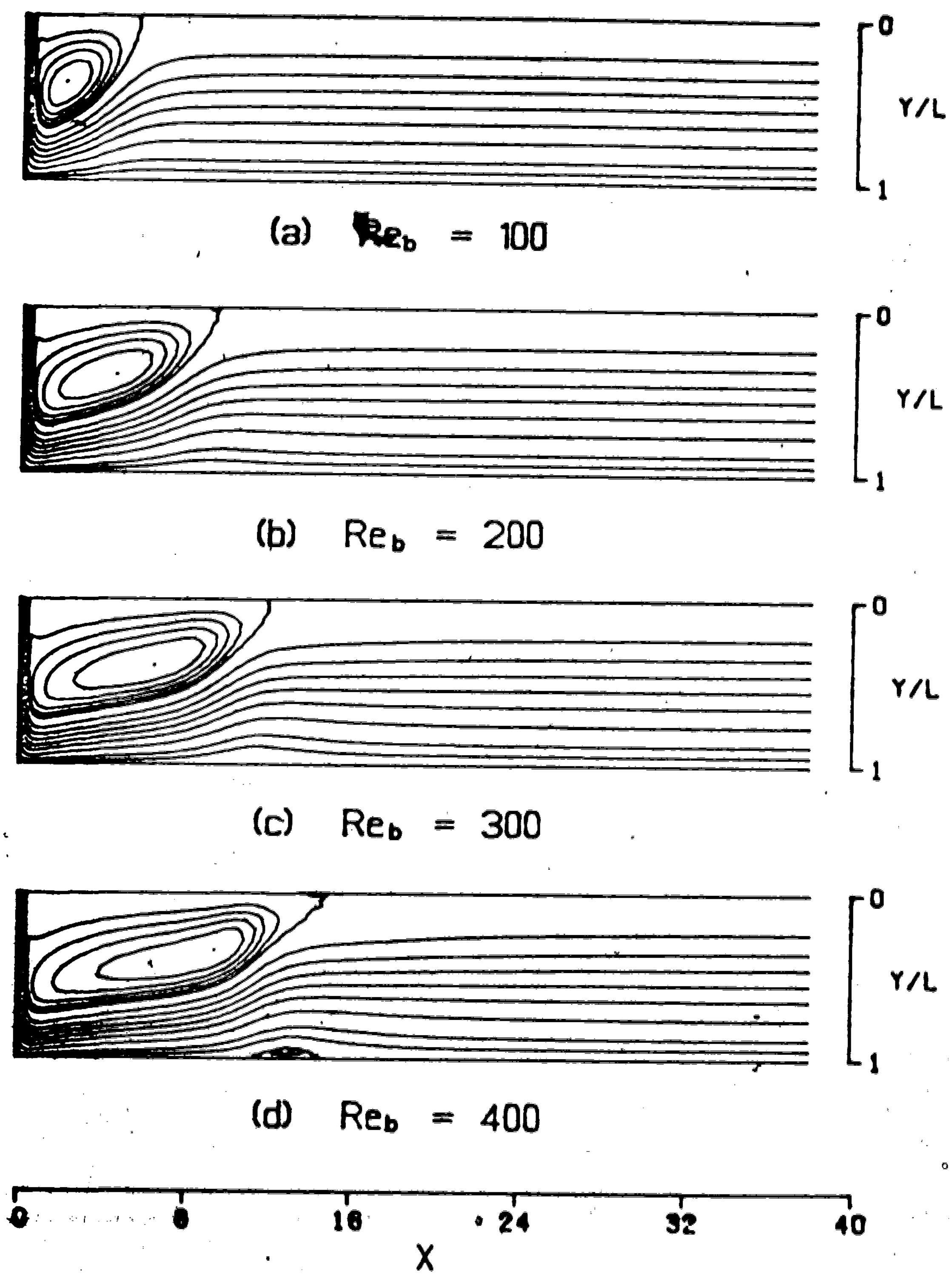

FIGURE 10.1 : CONTOURS OF STREAM-FUNCTION FOR L=2 WITH AN INITIAL PARABOLIC VELOCITY PROFILE

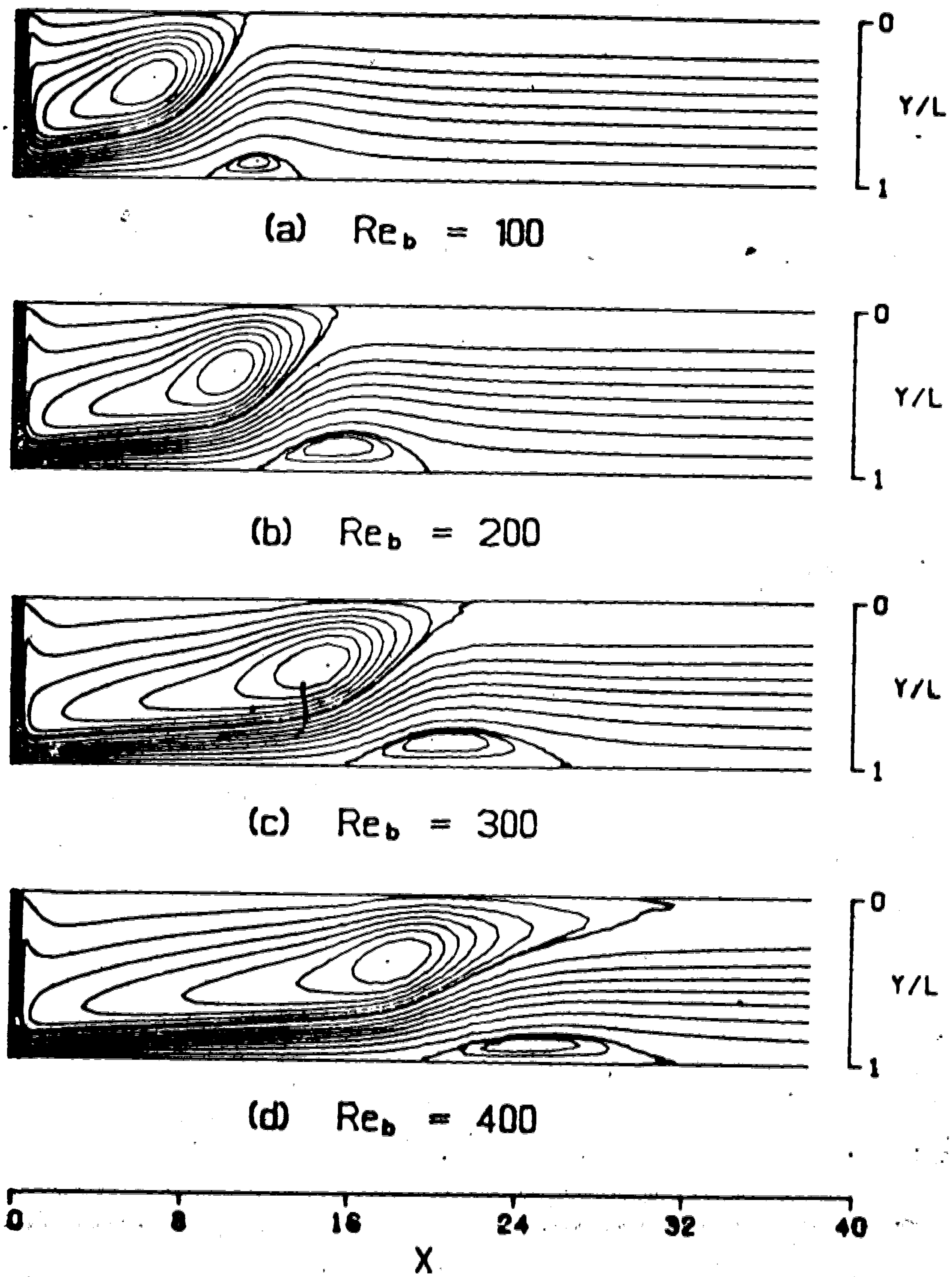

FIGURE 10.2 : CONTOURS OF STREAM-FUNCTION FOR L=4 WITH AN INITIAL PARABOLIC VELOCITY PROFILE

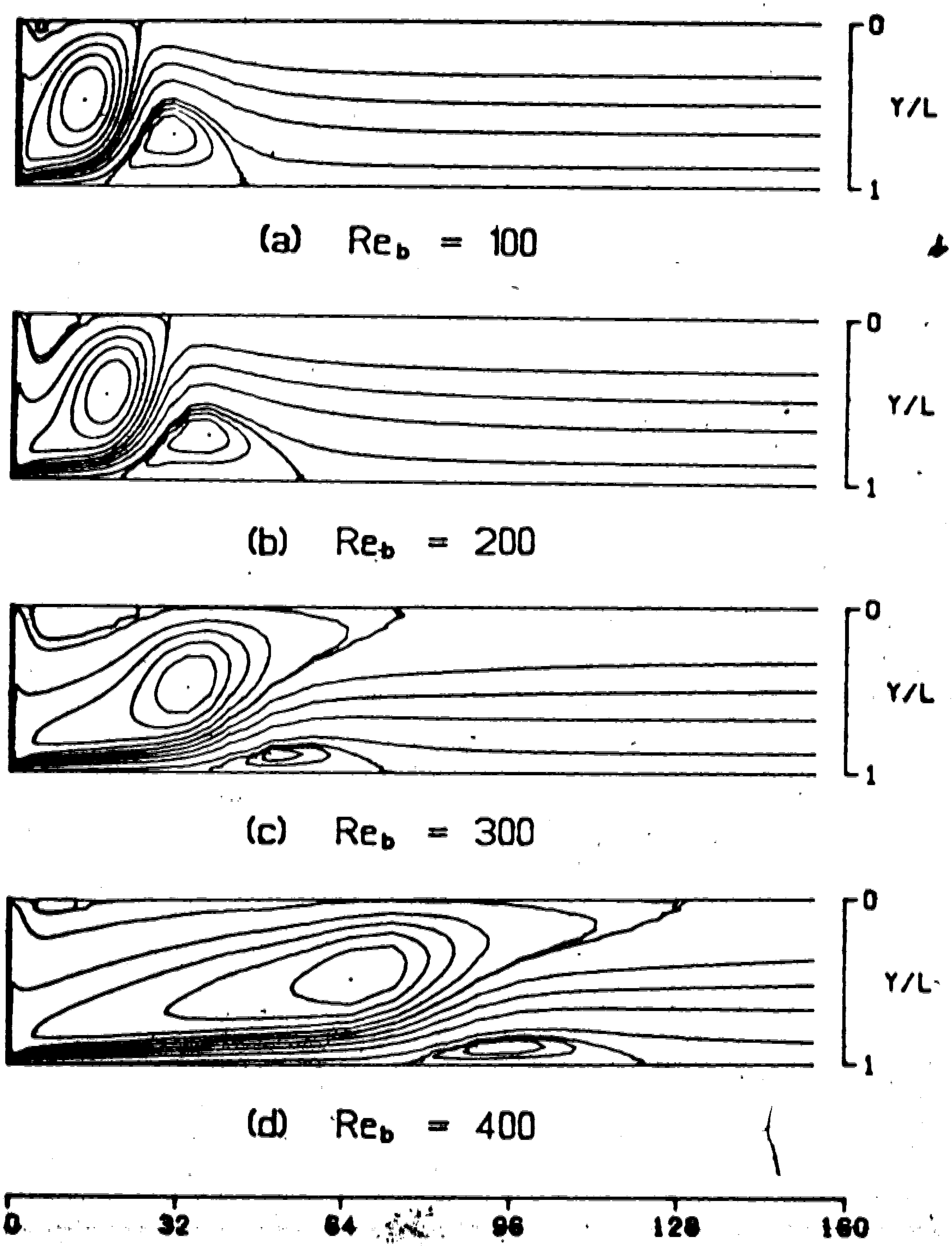

FIGURE 10.3 : CONTOURS OF STREAM-FUNCTION FOR L=12 WITH AN INITIAL PARABOLIC VELOCITY PROFILE

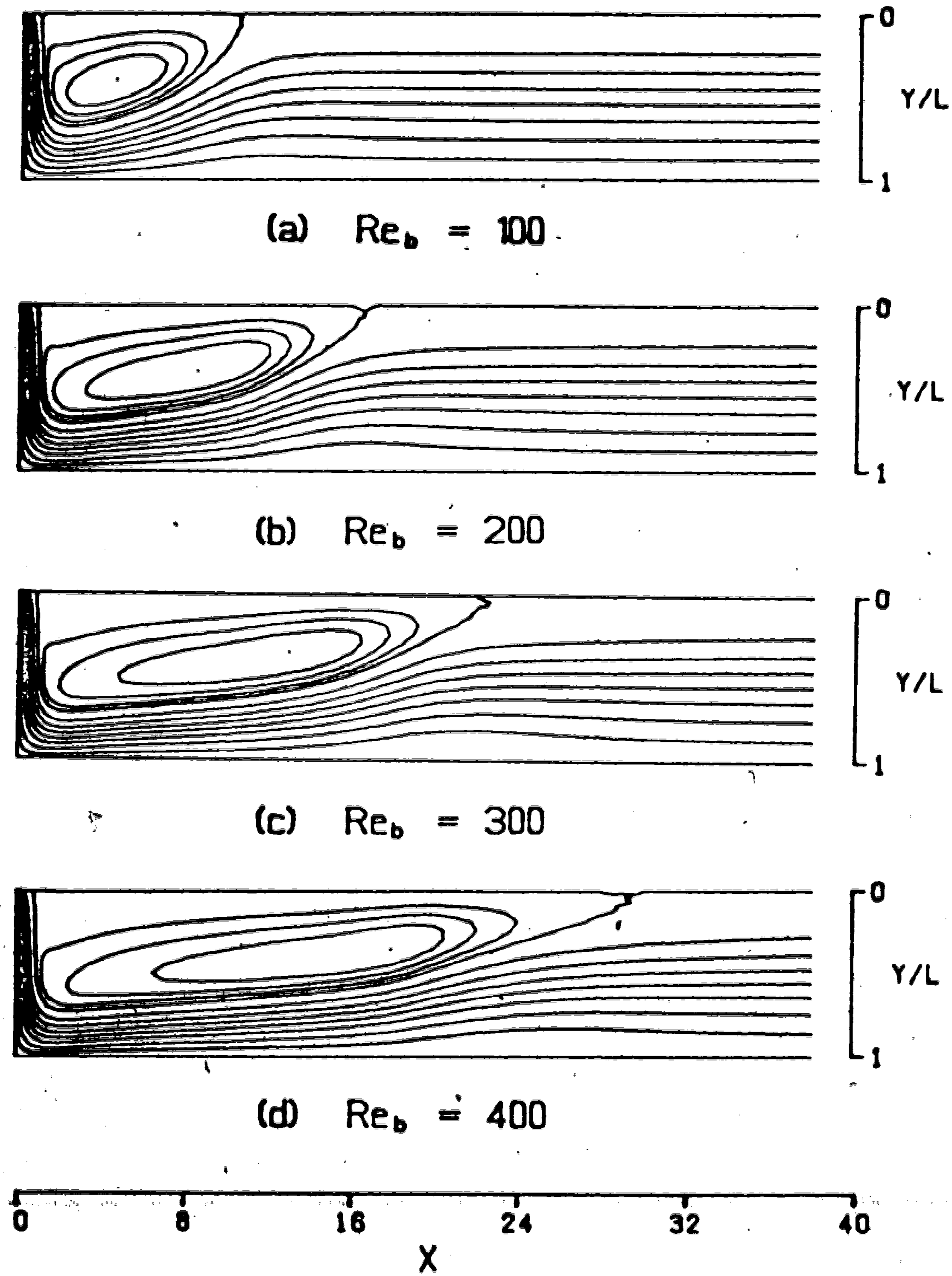

FIGURE 10.4 : CONTOURS OF STREAM-FUNCTION FOR L=4 WITH AN INITIAL FLAT VELOCITY PROFILE

7

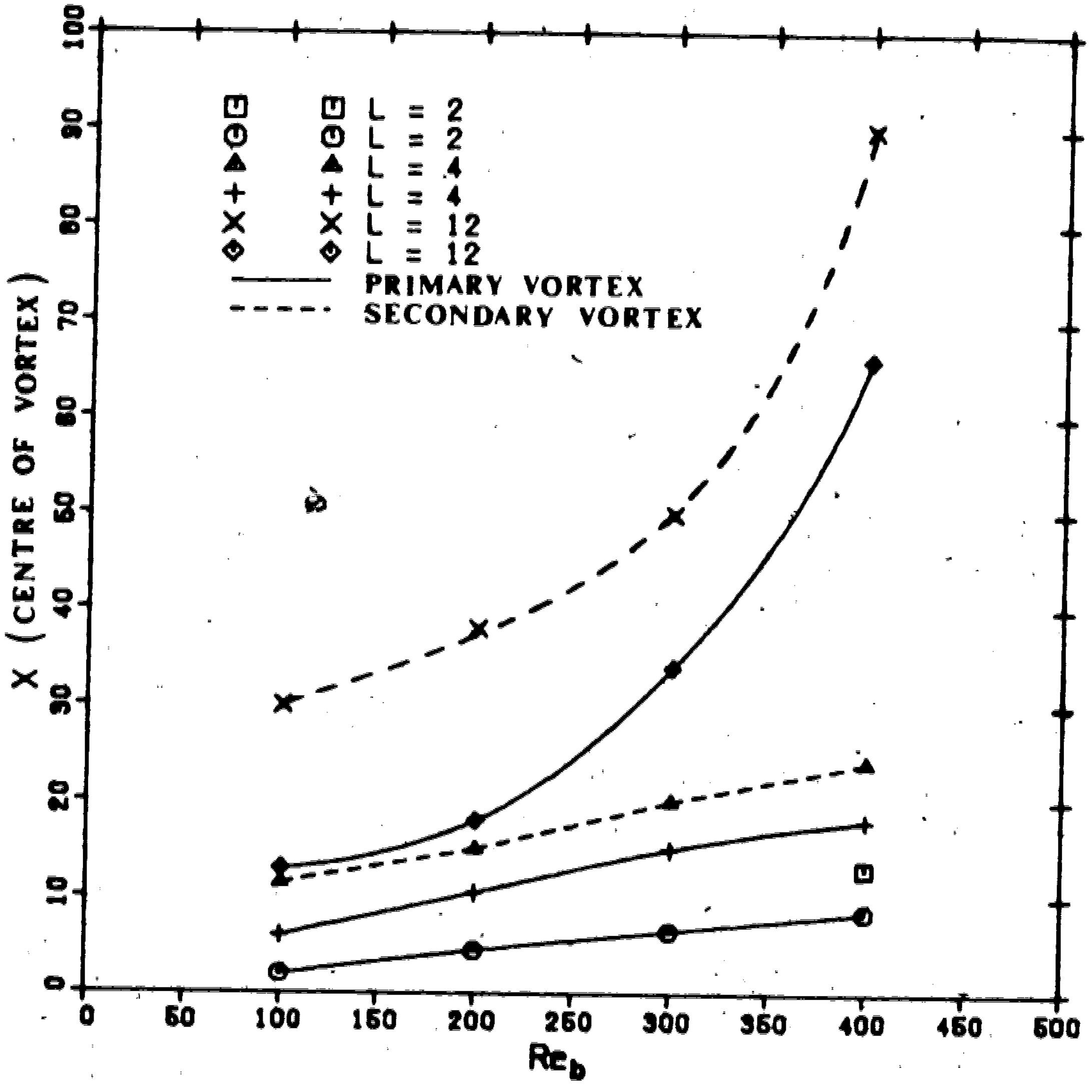

FIGURE 10.5 : VARIATION OF VORTEX CENTRE WITH REYNOLDS NUMBER FOR THE CASE OF PARABOLIC PROFILE

Reynolds number is shown in Figure 10.6. Again, the primary vortex move downstream with increase in Reynolds number.

A blow-up of the contours of stream-function for L=2, 4 and 12 with an initial parabolic profile are shown in Figures 10.7, 10.8 and 10.9, respectively, while that for L=4 with an initial flat profile is shown in Figure 10.10. The centre of the jet nozzle exit is at the upper left hand corner with the main flow travelling from left to right. The corresponding values of stream-function for each streamline numbered are listed as follows:

1. $\psi = 0$
2. $\psi = -0.09$
3. $\psi = -0.21$
4. $\psi = -0.33$
5. $\psi = -0.45$
6. $\psi = -0.5$
7. $\psi < -0.5$ (circulating flow)
8. $\psi < -0.5$ (circulating flow)

where streamline #1 represents the axis of symmetry and the impingement plate, and streamline #6 represents the confinement plate and the outermost free streamline of the submerged jet.

The spreading effect of the jet under the the influence of the confinement plate can be studied from the outermost free streamline (#6) in Figures 10.7, 10.8, 10.9 and 10.10.

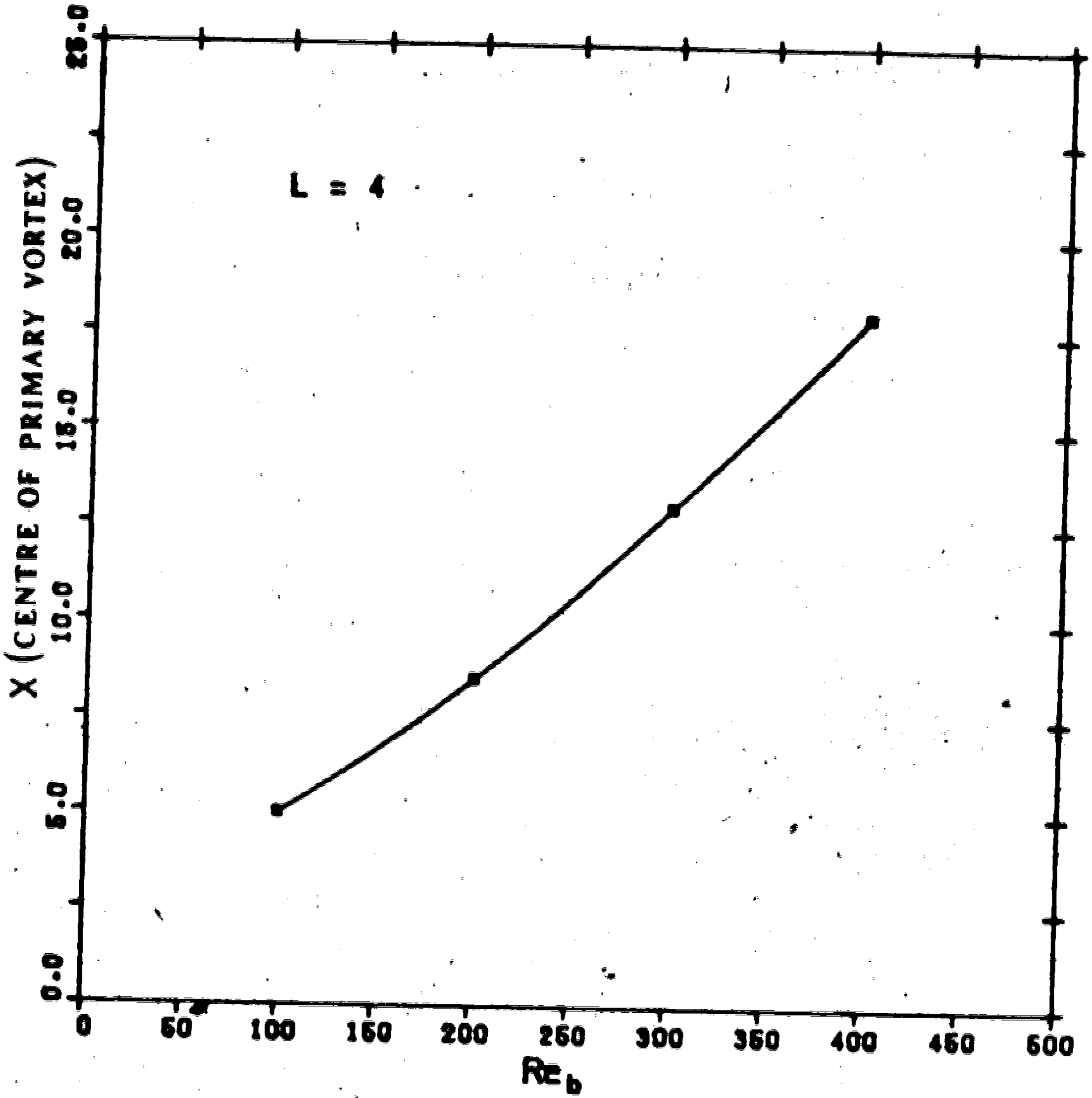

FIGURE 10.6 : VARIATION OF PRIMARY VORTEX CENTRE WITH REYNOLDS NUMBER FOR THE CASE OF FLAT PROFILE

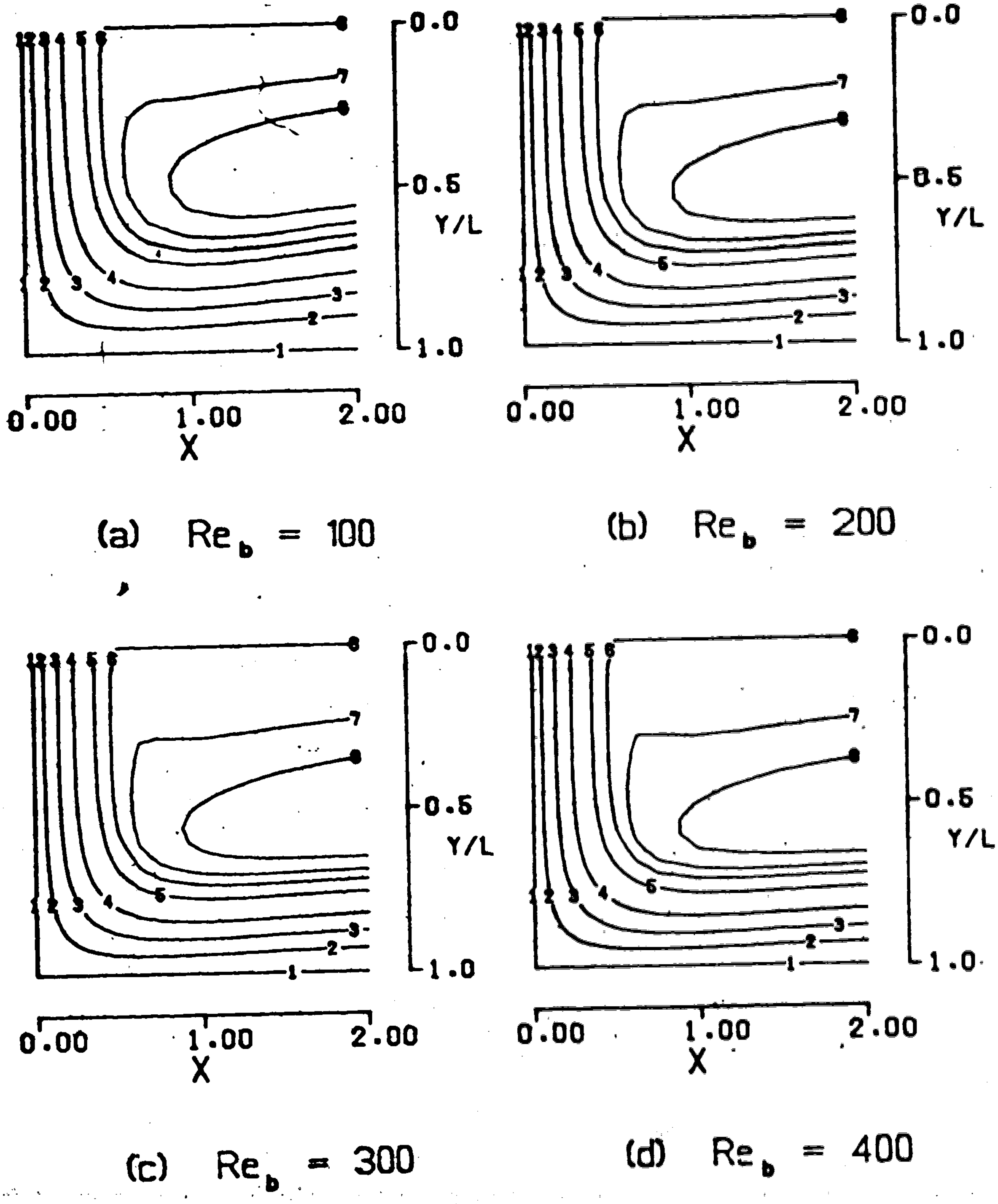

FIGURE 10.7 : CONTOURS OF STREAM-FUNCTION FOR L=2 NEAR THE STAGNATION POINT WITH AN INITIAL PARABOLIC VELOCITY PROFILE

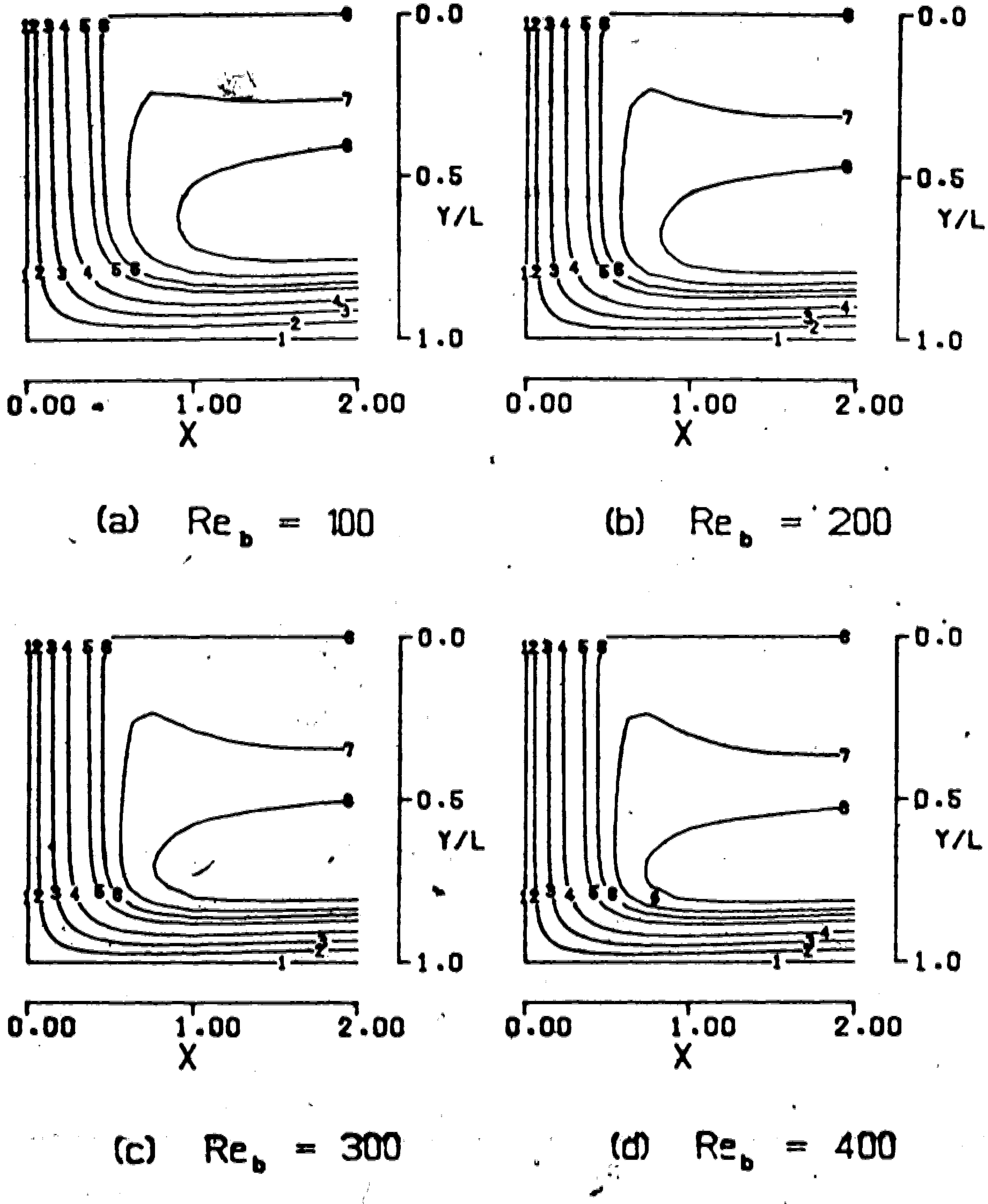

FIGURE 10.8 : CONTOURS OF STREAM-FUNCTION FOR L=4 NEAR THE STAGNATION POINT WITH AN INITIAL PARABOLIC VELOCITY PROFILE

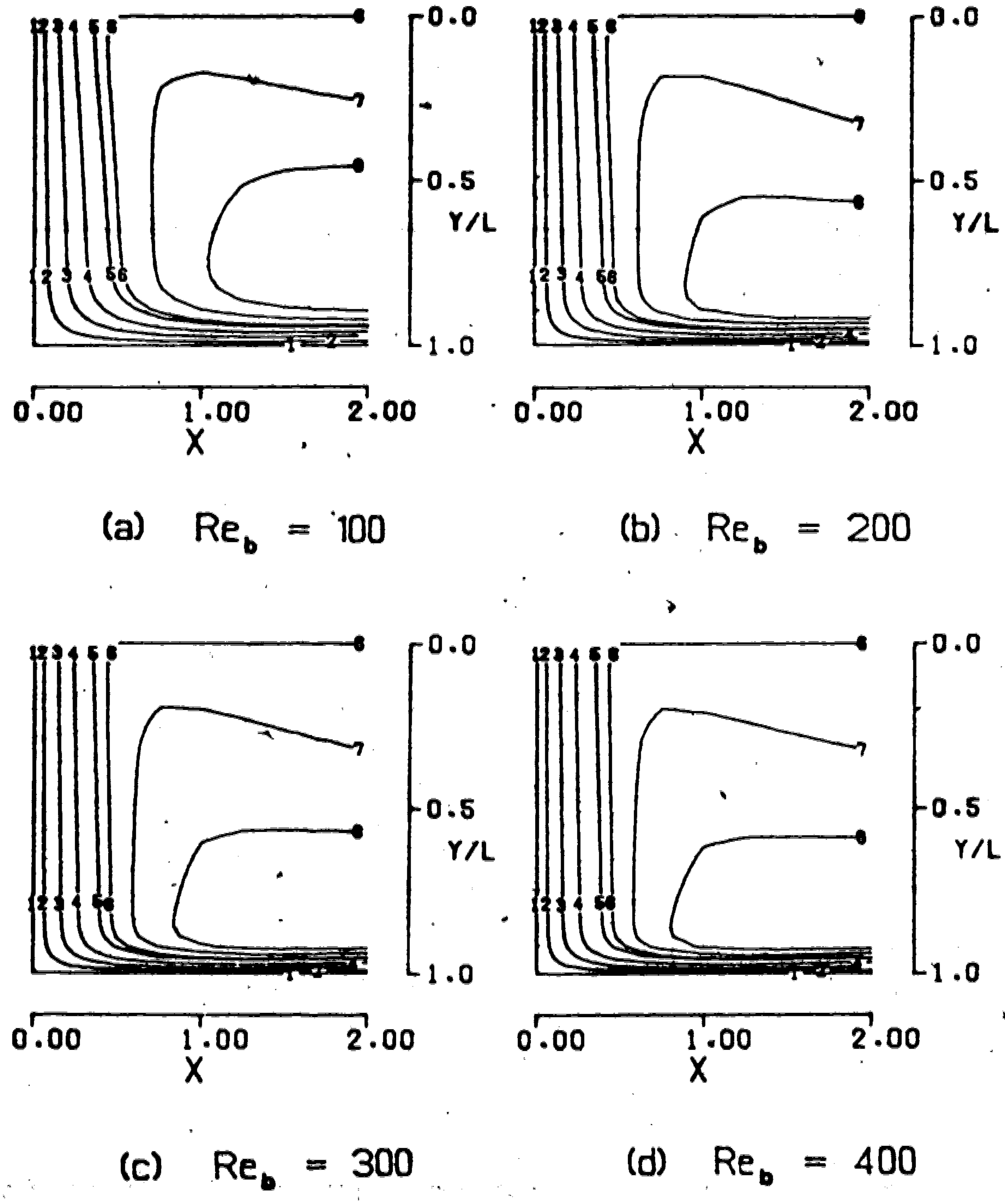

FIGURE 10.9 : CONTOURS OF STREAM-FUNCTION FOR L=12 NEAR THE STAGNATION POINT WITH AN INITIAL PARABOLIC VELOCITY PROFILE

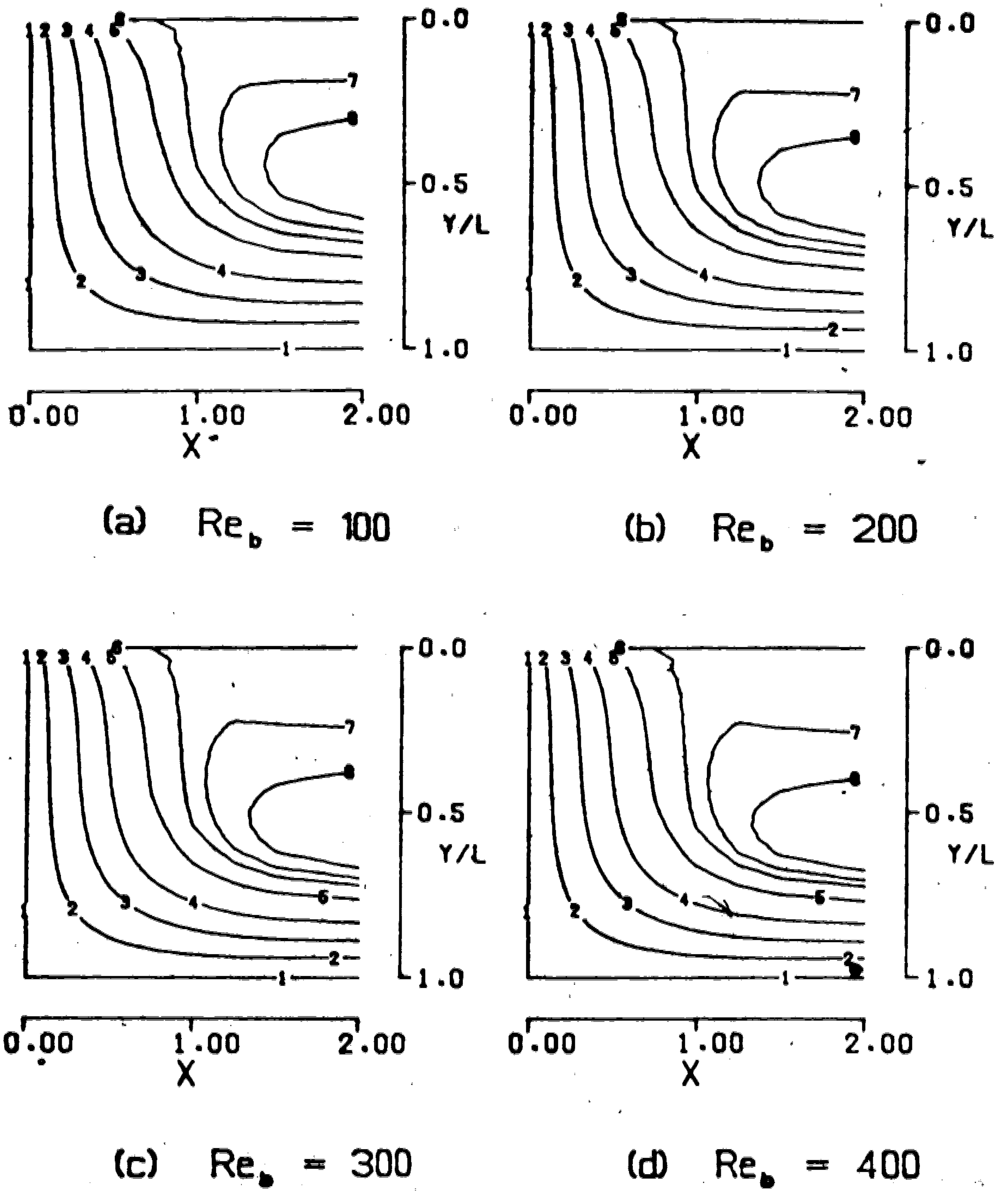

FIGURE 10.10 : CONTOURS OF STREAM-FUNCTION FOR L=4 NEAR THE STAGNATION POINT WITH AN INITIAL FLAT VELOCITY PROFILE

The jet contracts slightly below the nozzle exit for an initial parabolic profile, while for an initial flat profile, the jet expands continuously. Similar spreading effects were observed by Van Heiningen et. al. (96) in their study of semi-confined air jet with different initial velocity profiles. The explanations of these spreading behaviors have already been given in Section 2.1.2.

From the outermost free streamlines in Figures 10.8 and 10.10, it is found that the free streamline is significantly closer to the impingement plate for an initial parabolic profile. This is due to the higher momentum of the initial parabolic profile jet. Same observation has also been made by Van Heiningen et. al. (96).

10.1.2 AXIAL VELOCITY PROFILE

Typical axial velocity profiles at various positions in Y-direction for different jet Reynolds numbers for a confined jet are shown in Figures 10.11, 10.12 and 10.13 for L=2, 4 and 12 with an initial parabolic profile, and for L=4 with an initial flat profile in Figure 10.14. In all cases the initial velocity at nozzle exit (Y=0) are plotted. The axial velocities are normalized by the centerline axial velocity at the nozzle exit, $(V_j)|_{x=0}$.

The spreading of the jet as it approachs the impingement plate (Y=L) is obvious for all cases. This spreading is more dramatic for the jet with an initial flat profile than that with an parabolic profile.

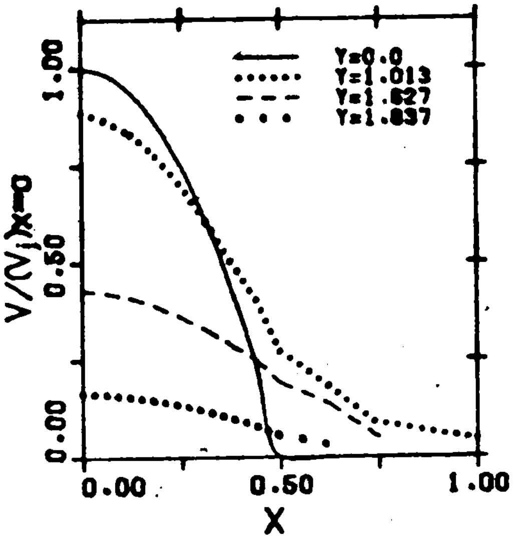

(a) Re_b = 100

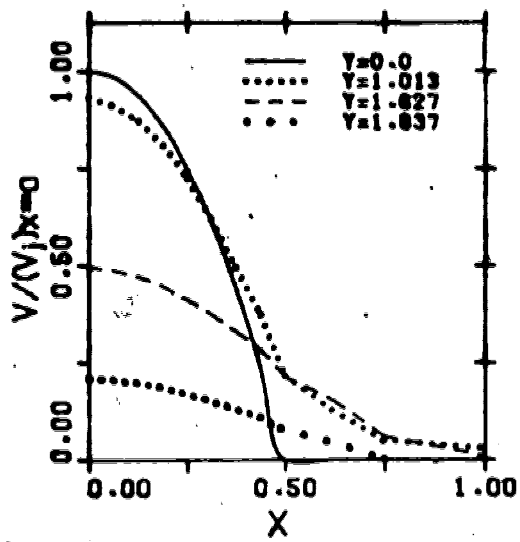

(b) Re_b = 200

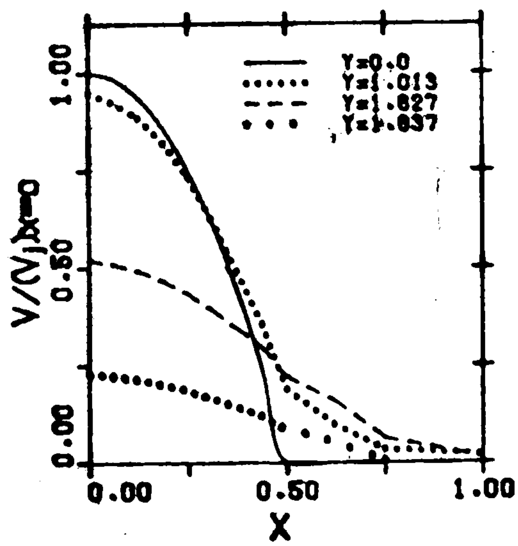

(c) Re_b = 300

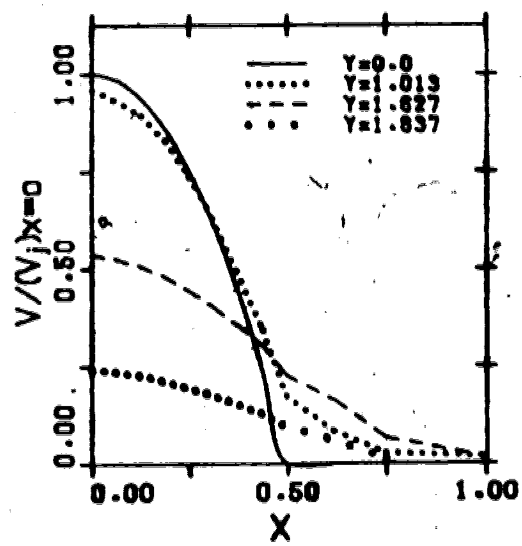

(d) Re_b = 400

FIGURE 10.11 : AXIAL VELOCITY PROFILES FOR L=2 WITH AN INITIAL PARABOLIC VELOCITY PROFILE

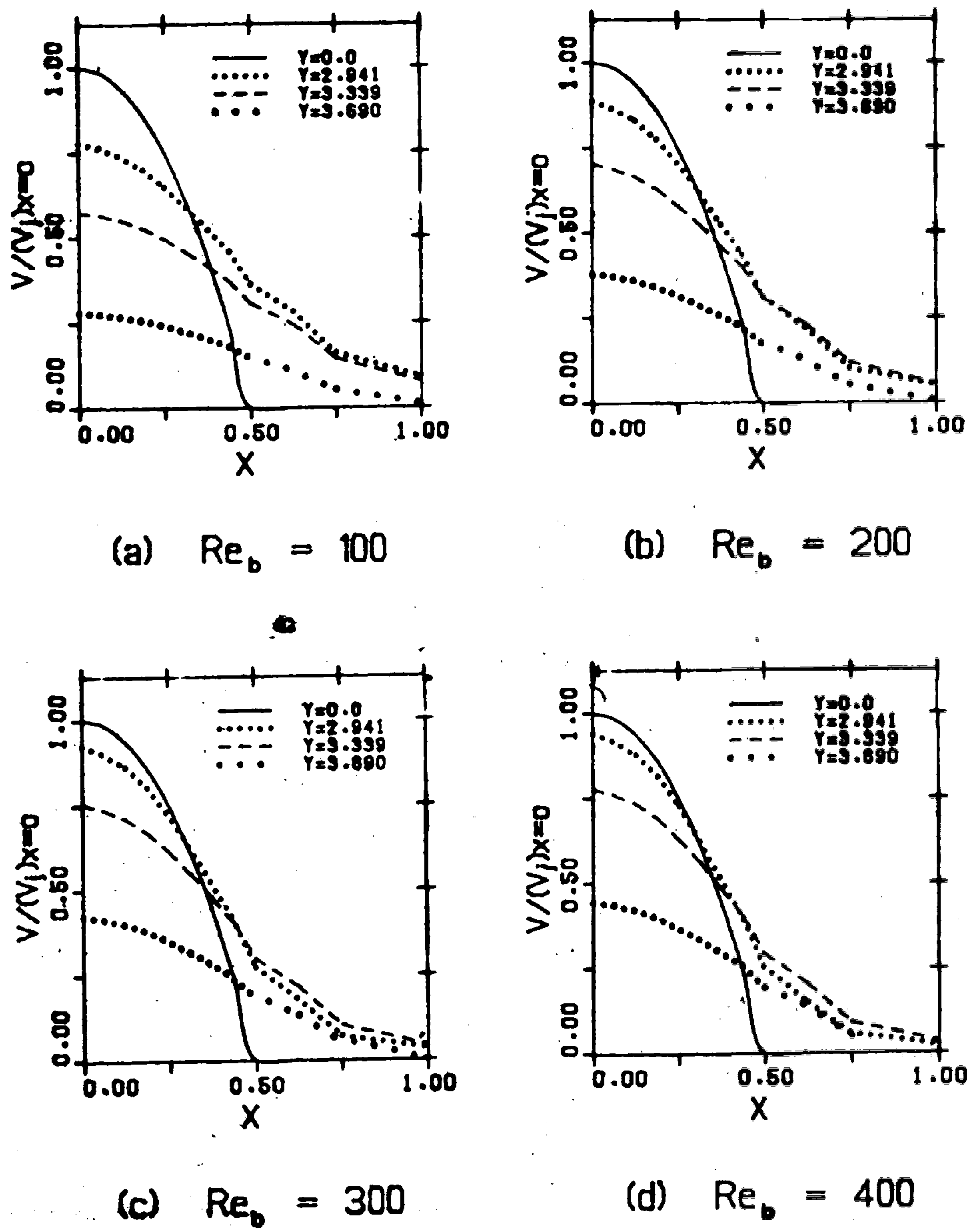

FIGURE 10.12 : AXIAL VELOCITY PROFILES FOR L=4 WITH AN INITIAL PARABOLIC VELOCITY PROFILE

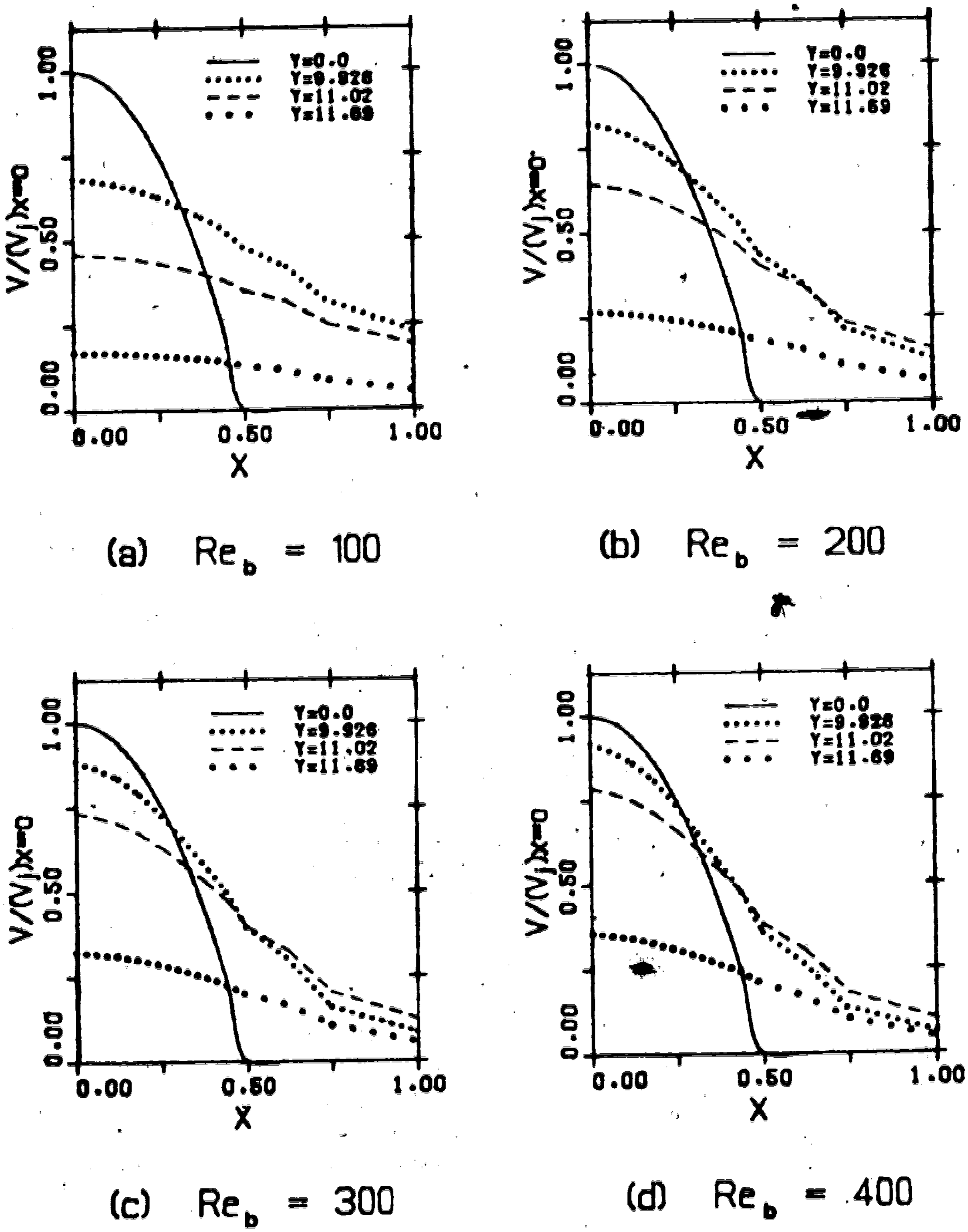

FIGURE 10.13 : AXIAL VELOCITY PROFILES FOR L=12 WITH AN INITIAL PARABOLIC VELOCITY PROFILE

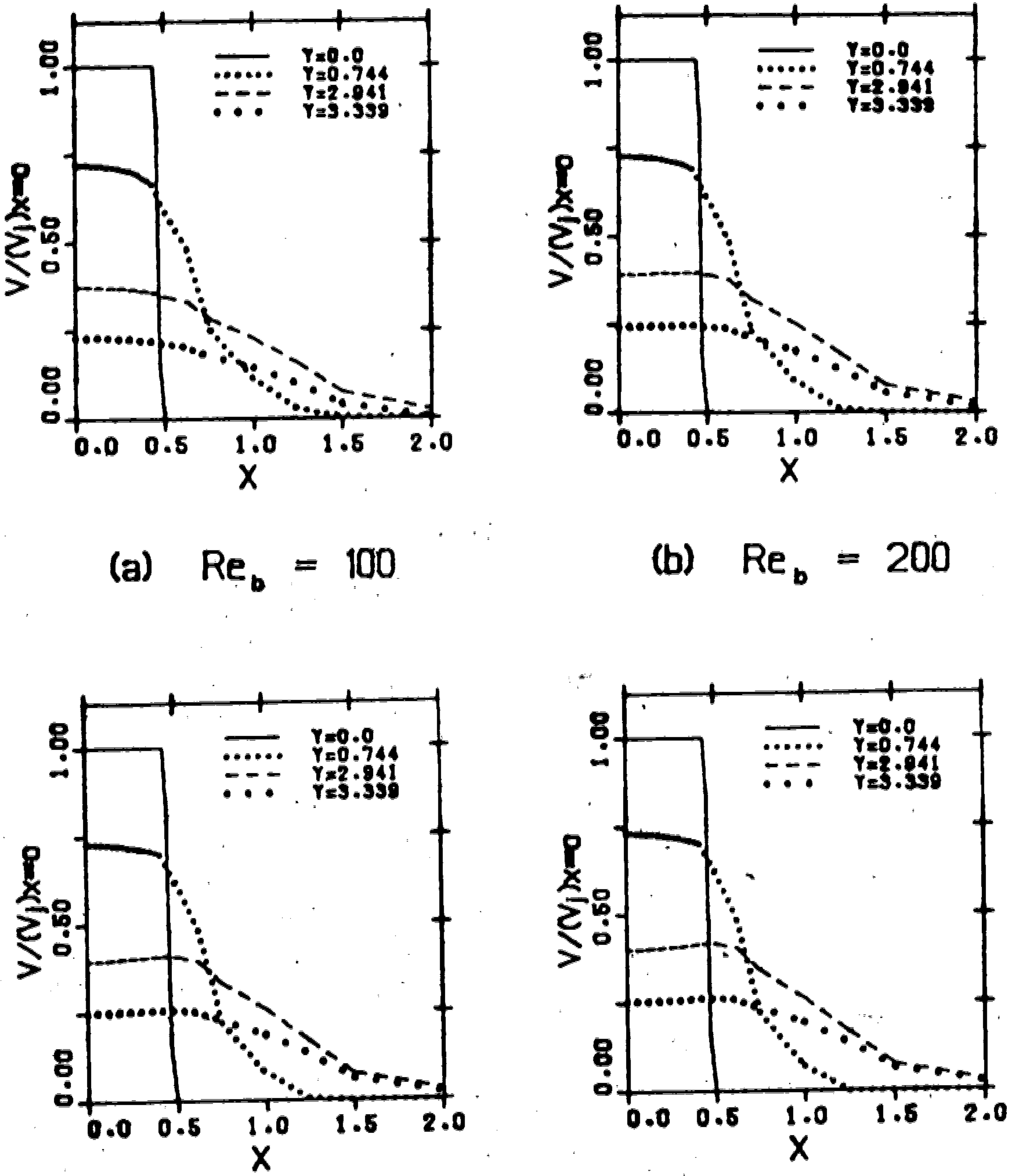

(a) Re_b = 100

(b) Re_b = 200

(c) Re_b = 300

(d) Re_b = 400

FIGURE 10.14 : AXIAL VELOCITY PROFILES FOR L=4 WITH AN INITIAL FLAT VELOCITY PROFILE

The decay of the centerline axial velocity, $V|_{x=0}$, originating from a parabolic velocity profile at nozzle exit for different jet Reynolds numbers is shown in Figures 10.15, 10.16 and 10.17 for L=2, 4 and 12, respectively. The centerline axial velocity increases slightly with axial distance from the nozzle exit due to the contraction of the jet, and then decreases slightly due to the spreading of the jet. Not until the jet flow is about one slot width away from the impingement plate, does the centerline axial velocity decrease rapidly to zero at the stagnation point. In other words, the centerline axial velocity is affected by the presence of the impingement plate at a distance only one slot width from the plate.

The effect of Reynolds number on the decay of the centerline axial velocity for different jet-to-plate spacings can also be studied from Figures 10.15, 10.16 and 10.17. For all cases, the centerline axial velocity decays less rapidly at higher Reynolds numbers. This is mostly due to the more penetration of the jet with higher Reynolds number into the surrounding fluid.

In the stagnation flow region, the centerline axial velocity is linearly proportional to the axial distance away from the stagnation point, (L-Y), as can be noted from Figures 10.15, 10.16 and 10.17. A similar observation has been made by Schlichting (78) for unconfined submerged jet. Introducing the dimensionless variables in Equation 6.6 into Equation 2.5, yields

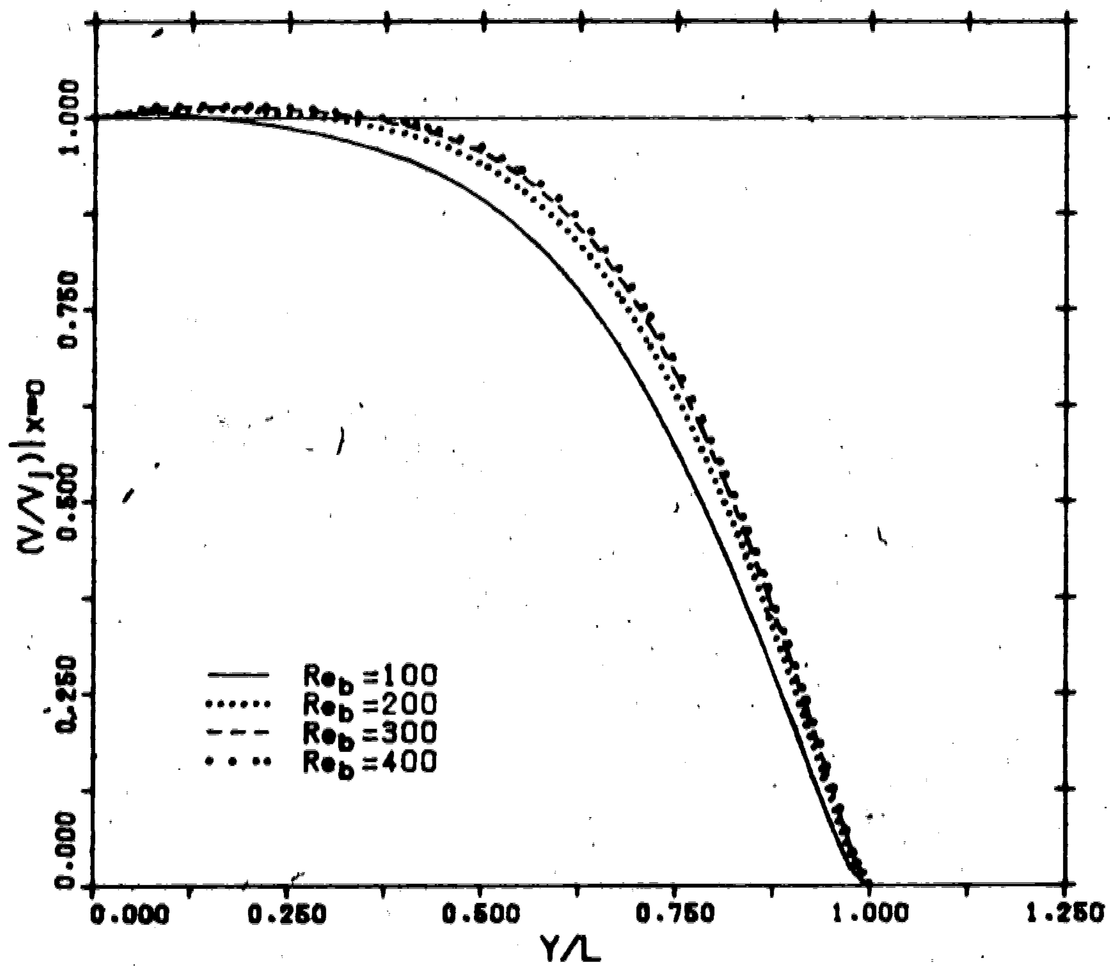

FIGURE 10.15 : DECAY OF CENTERLINE AXIAL VELOCITY FOR L=2 WITH AN INITIAL PARABOLIC VELOCITY PROFILE

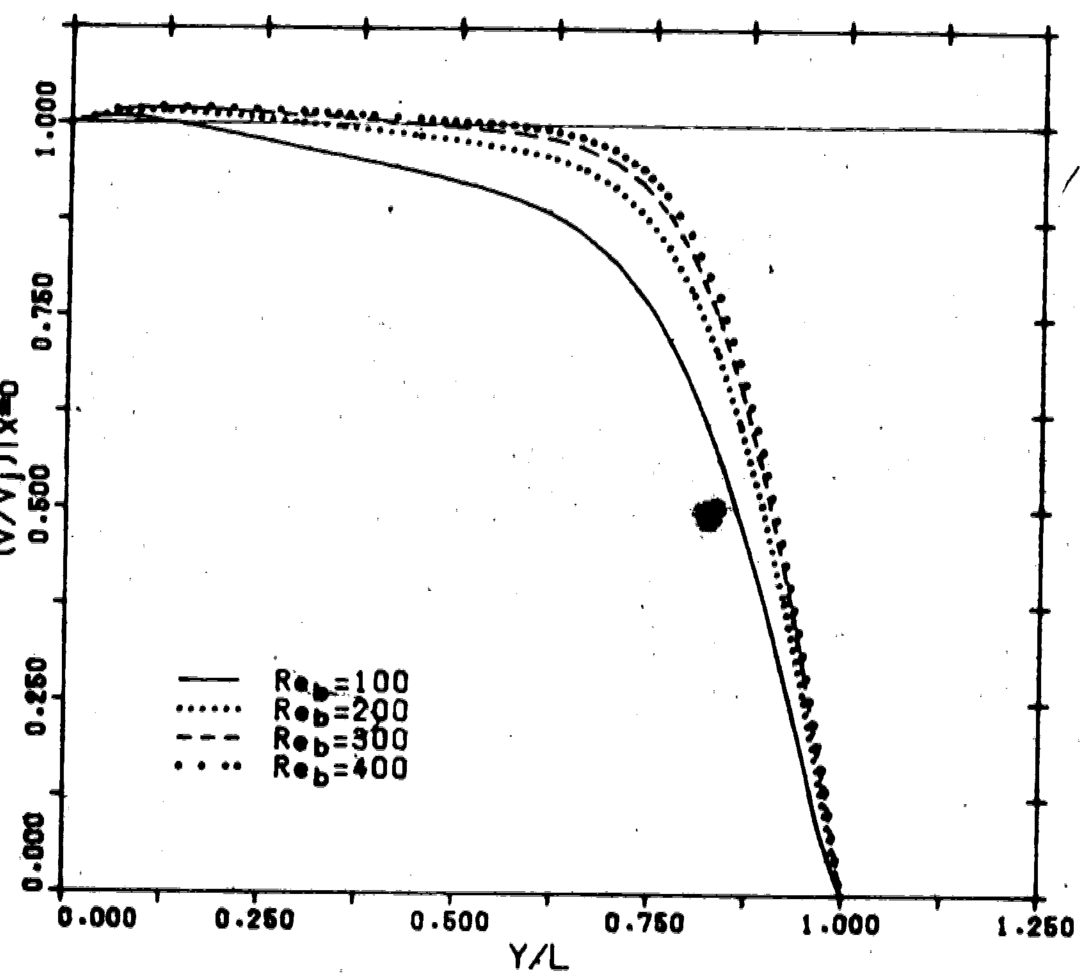

FIGURE 10.16 : DECAY OF CENTERLINE AXIAL VELOCITY FOR L=4 WITH AN INITIAL PARABOLIC VELOCITY PROFILE

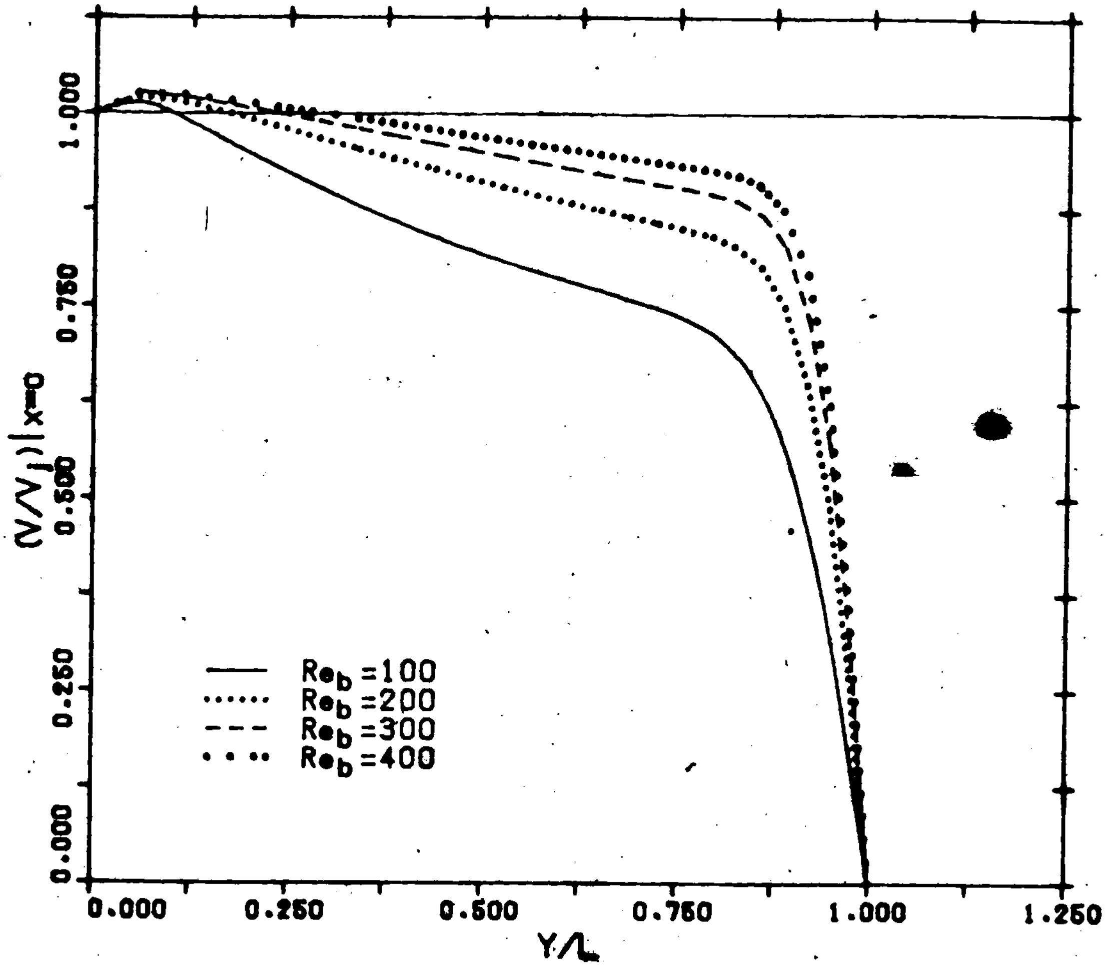

FIGURE 10.17 : DECAY OF CENTERLINE AXIAL VELOCITY FOR L=12 WITH AN INITIAL PARABOLIC VELOCITY PROFILE

$$(V/V_j)|_{x=0} = a_1 \, [L \, / \, (V_j)|_{x=0}] \, [1 - (Y/L)] \quad (10.1)$$

The values of a_1 can be easily evaluated from the slopes of all the curves of Figures 10.15, 10.16 and 10.17 for different Reynolds numbers and jet-to-plate spacings. The values of a_1 are shown in Table 10.1. A plot of a_1 versus L is shown in Figure 10.18. The least square fitted curves for different Reynolds numbers are:

$$a_1 = 2.56 \, L^{-0.512} \quad \text{for } Re_b=100$$
$$a_1 = 2.65 \, L^{-0.391} \quad \text{for } Re_b=200$$
$$a_1 = 2.65 \, L^{-0.330} \quad \text{for } Re_b=300$$
$$a_1 = 2.67 \, L^{-0.316} \quad \text{for } Re_b=400 \quad (10.2)$$

Equation 10.2 shows that the decay of centerline axial velocity in the stagnation flow region for a confined jet with initial parabolic profile depends not only on the Reynolds number but also on the jet-to-plate spacing.

The decay of the centerline axial velocity originating from a flat velocity profile at nozzle exit for different Reynolds numbers is shown in Figure 10.19 for L=4. The centerline axial velocity decreases rapidly near the nozzle exit. This is due to the large spreading effects in this region. The decrease of centerline axial velocity becomes more gentle when the jet flow is further away from the nozzle exit. Not until the presence of the impingement plate is sensed, the centerline axial velocity does decrease

TABLE 10.1 : VALUES OF a_1 EVALUATED FROM EQUATION 10.1

L	Re_b	a_1
2	100	1.75
	200	1.98
	300	2.06
	400	2.12
4	100	1.31
	200	1.59
	300	1.70
	400	1.76
12	100	0.71
	200	0.99
	300	1.13
	400	1.21

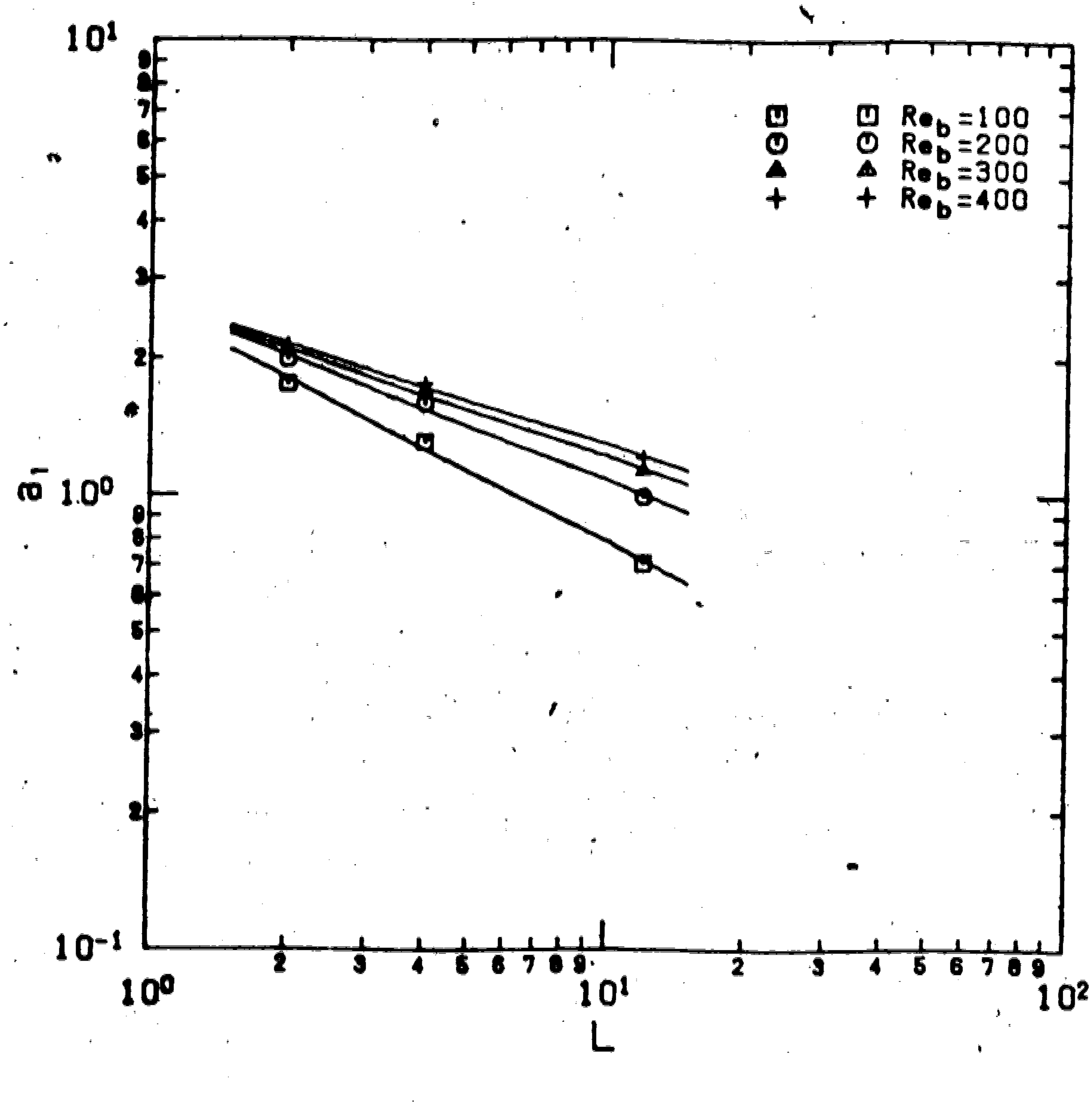

FIGURE 10.18 : a_1 VERSUS JET-TO-PLATE SPACING FOR THE CASE OF PARABOLIC VELOCITY PROFILE

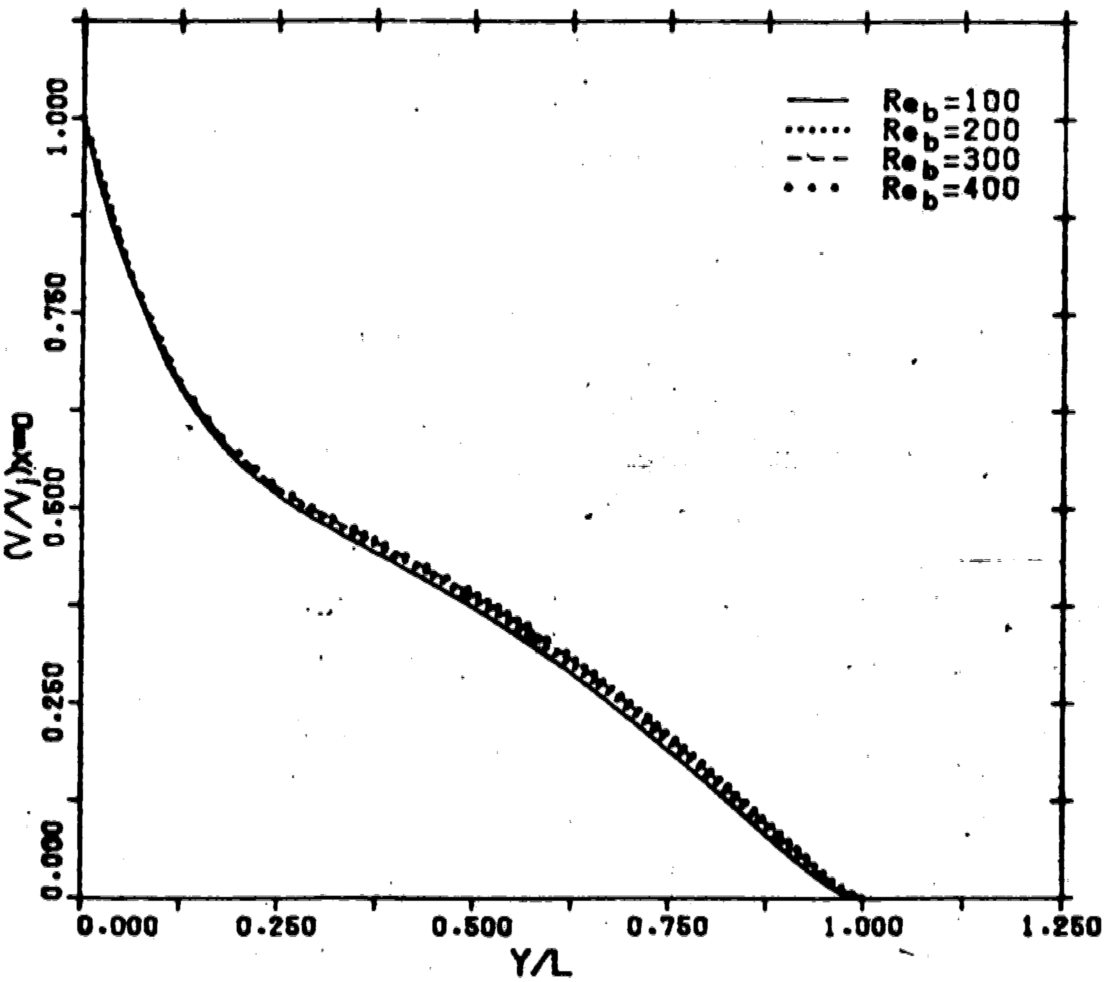

FIGURE 10.19 : DECAY OF CENTERLINE AXIAL VELOCITY FOR L=4 WITH AN INITIAL FLAT VELOCITY PROFILE

rapidly to zero at the stagnation point. The decay of the centerline axial velocity for this case is nearly independent of the Reynolds number.

In the stagnation flow region, the centerline axial velocity is linearly proportional to the axial distance from the stagnation point, (L-Y), as can be noted from Figure 10.19. The values of a, evaluated from the slopes of all curves of Figure 10.19 are approximately equal to 0.38 for all Reynolds numbers.

10.1.3 STREAMWISE VELOCITY PROFILE

The developments of typical streamwise velocity profiles with streamwise distance, X, for different Reynolds numbers and jet-to-plate spacings from a confined jet with initial parabolic velocity profile are shown in Figures 10.20-10.31. Those from a confined jet with initial flat velocity profile are shown in Figures 10.32-10.35. The dotted line in the plots represents the fully developed velocity profile for the particular case. The confinement plate is located at (L-Y)/L=1 and the impingement plate is located at (L-Y)/L=0.

For an individual streamwise velocity profile at a given streamwise distance, the streamwise velocity, U, increases from zero at the impingement plate to a maximum, U_{max}, within a thin layer. Such layer is refered to as the viscous boundary layer in the stagnation flow region. Outside the viscous boundary layer, the streamwise velocity

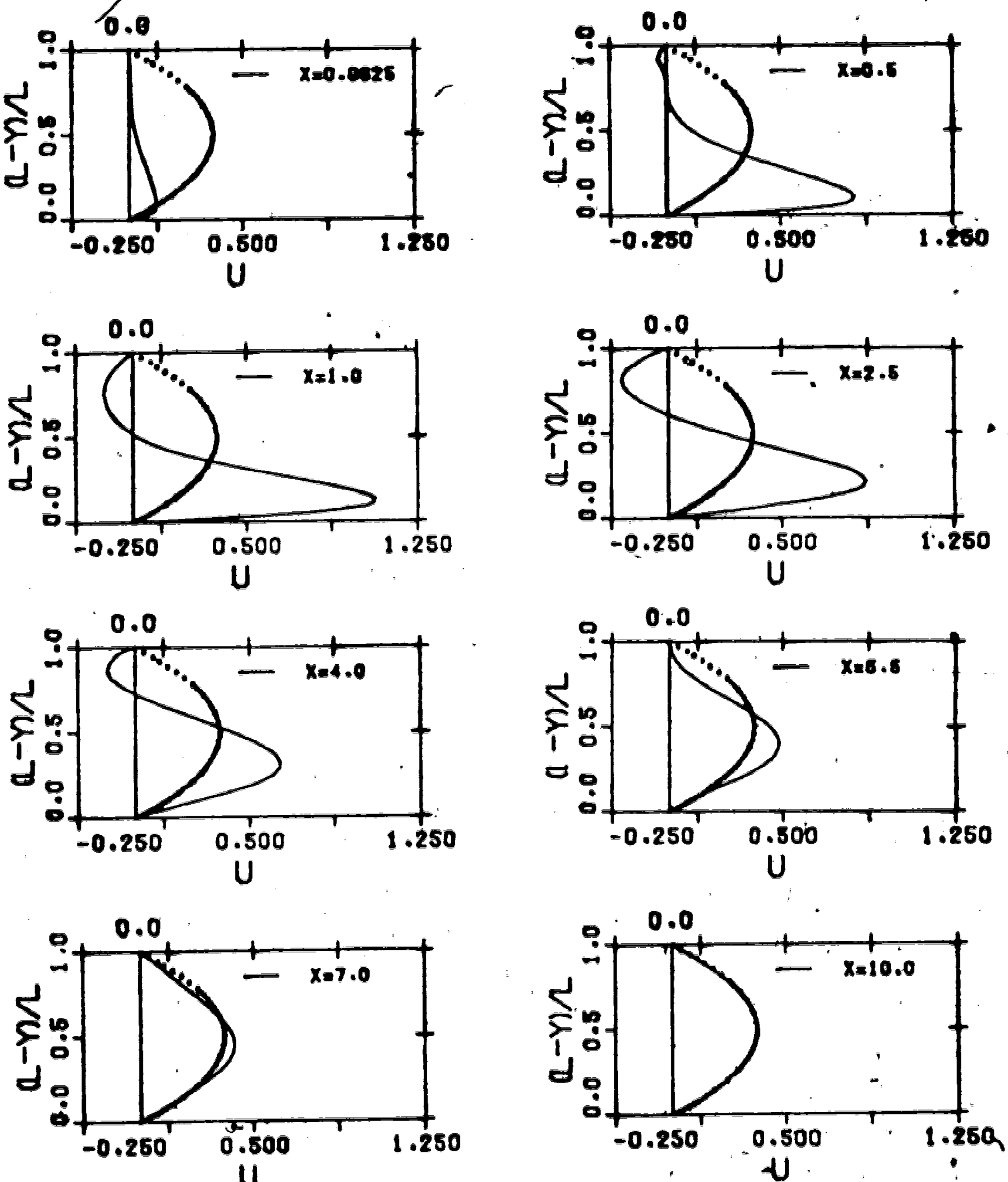

FIGURE 10.20 : STREAMWISE VELOCITY PROFILES FOR L=2 Re_b=100 WITH AN INITIAL PARABOLIC VELOCITY PROFILE

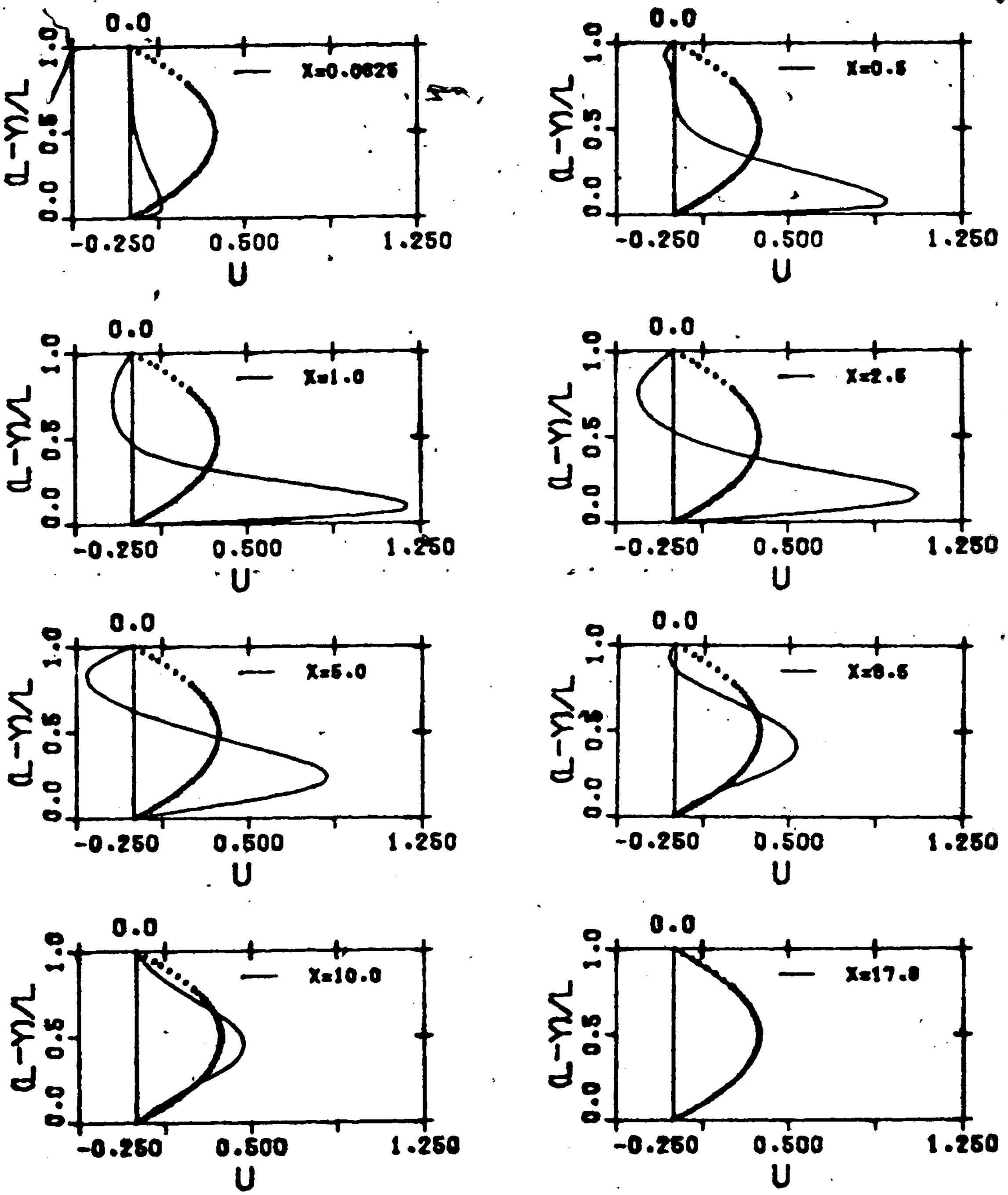

FIGURE 10.21 : STREAMWISE VELOCITY PROFILES FOR L=2 Re_b=200 WITH AN INITIAL PARABOLIC VELOCITY PROFILE

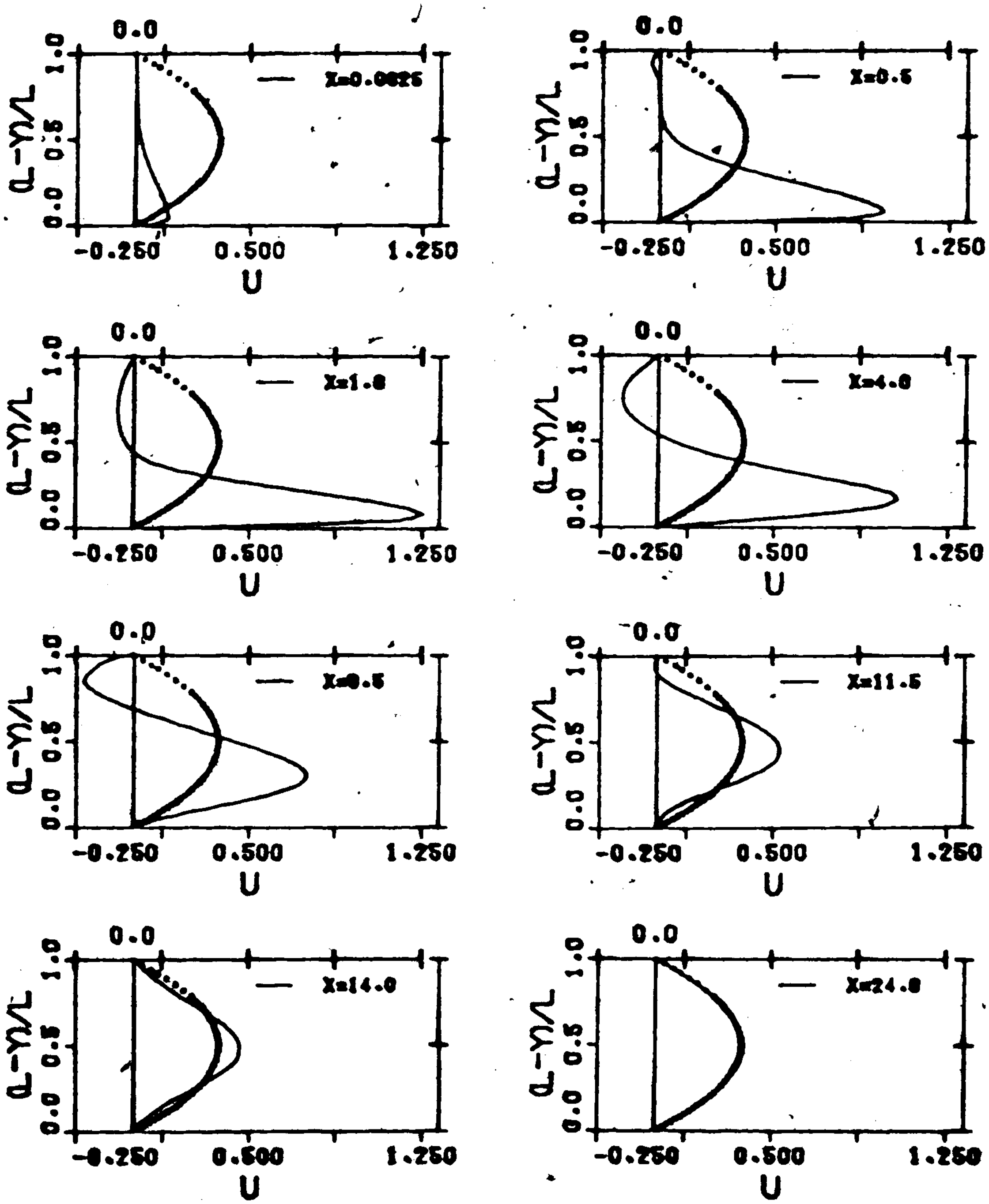

FIGURE 10.22 : STREAMWISE VELOCITY PROFILES FOR L=2 Re_b=300 WITH AN INITIAL PARABOLIC VELOCITY PROFILE

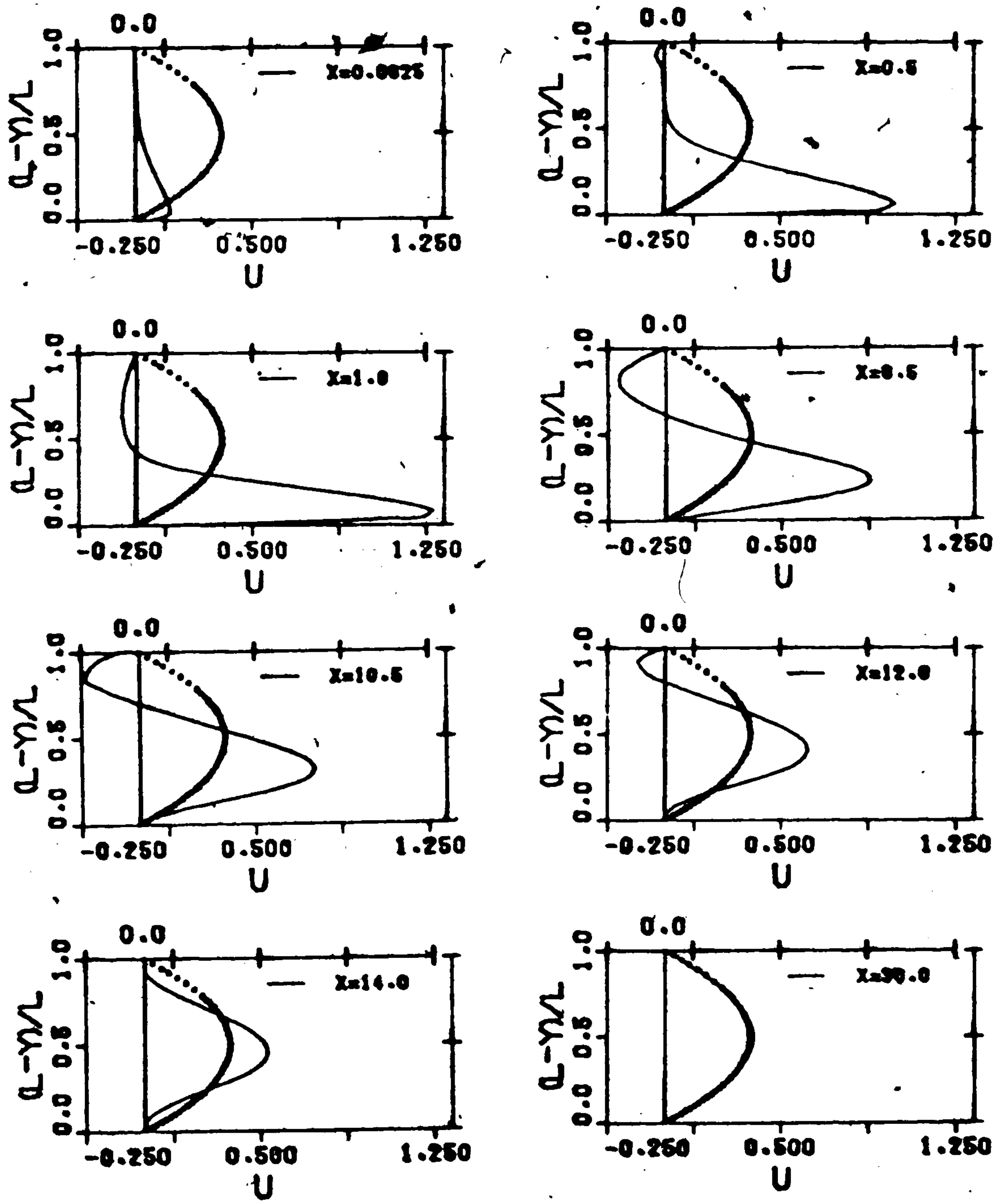

FIGURE 10.23 : STREAMWISE VELOCITY PROFILES FOR L=2 Re_b=400 WITH AN INITIAL PARABOLIC VELOCITY PROFILE

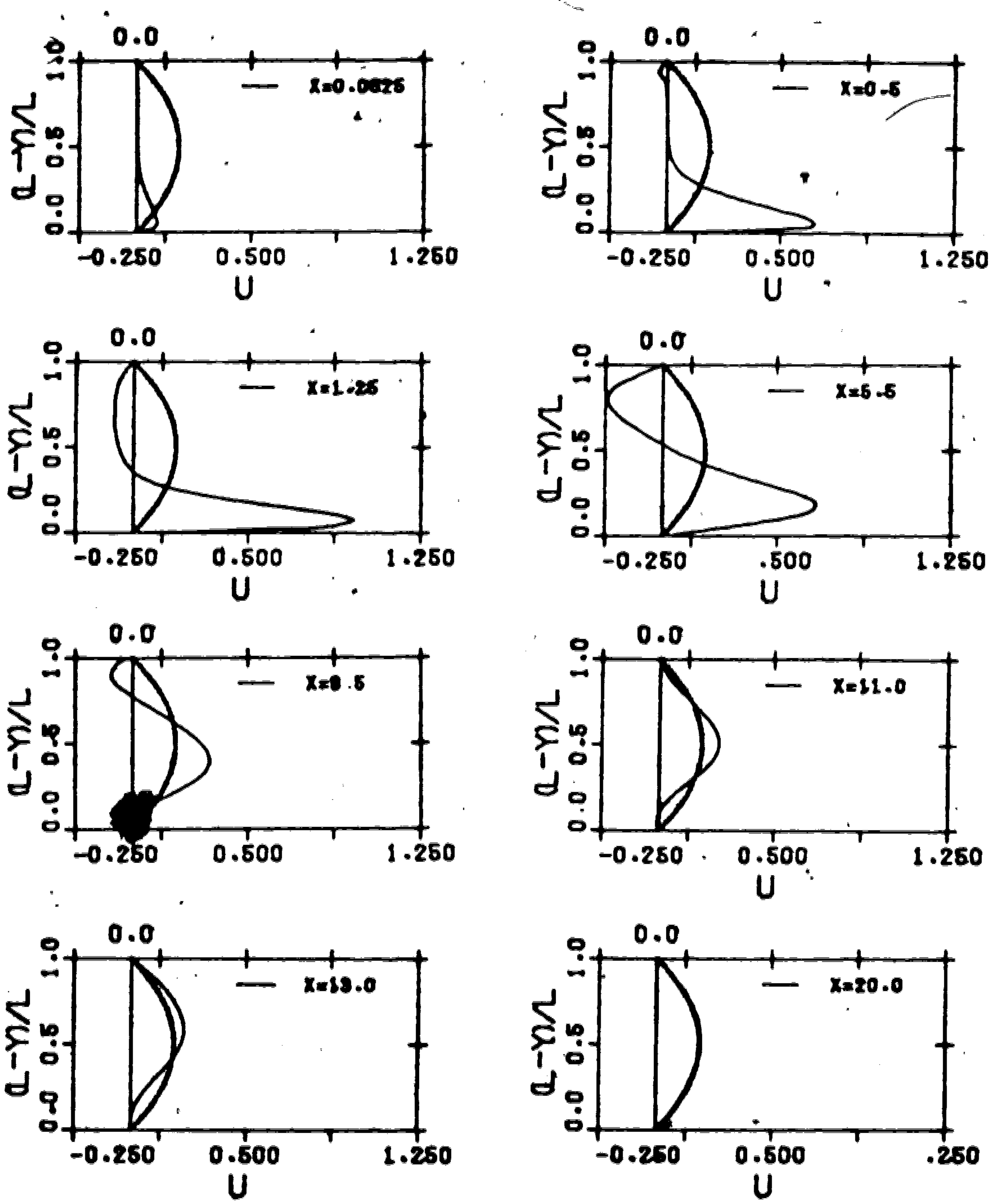

FIGURE 10.24 : STREAMWISE VELOCITY PROFILES FOR L=4 Re_b=100 WITH AN INITIAL PARABOLIC VELOCITY PROFILE

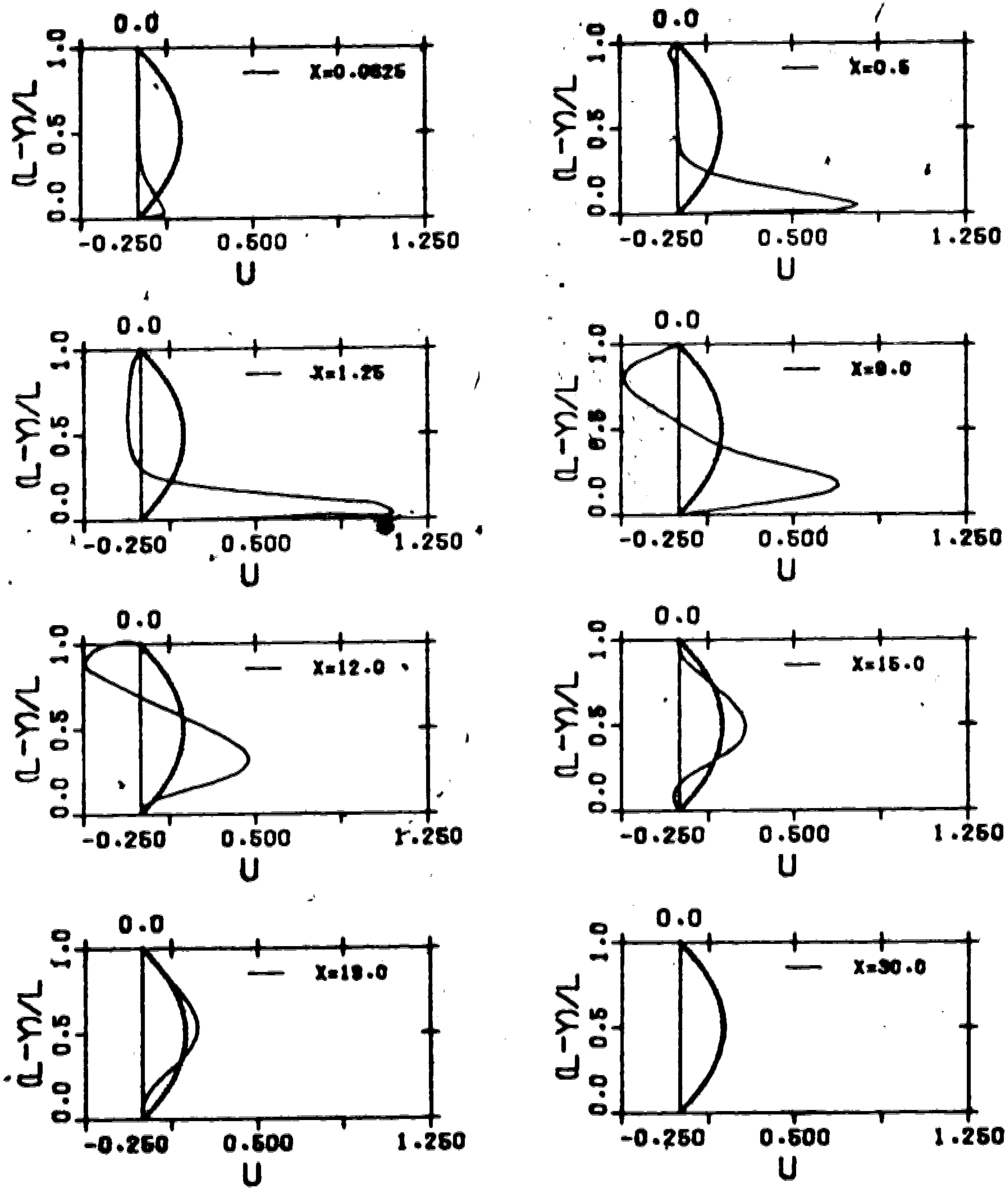

FIGURE 10.25 : STREAMWISE VELOCITY PROFILES FOR L=4 Re_b=200 WITH AN INITIAL PARABOLIC VELOCITY PROFILE

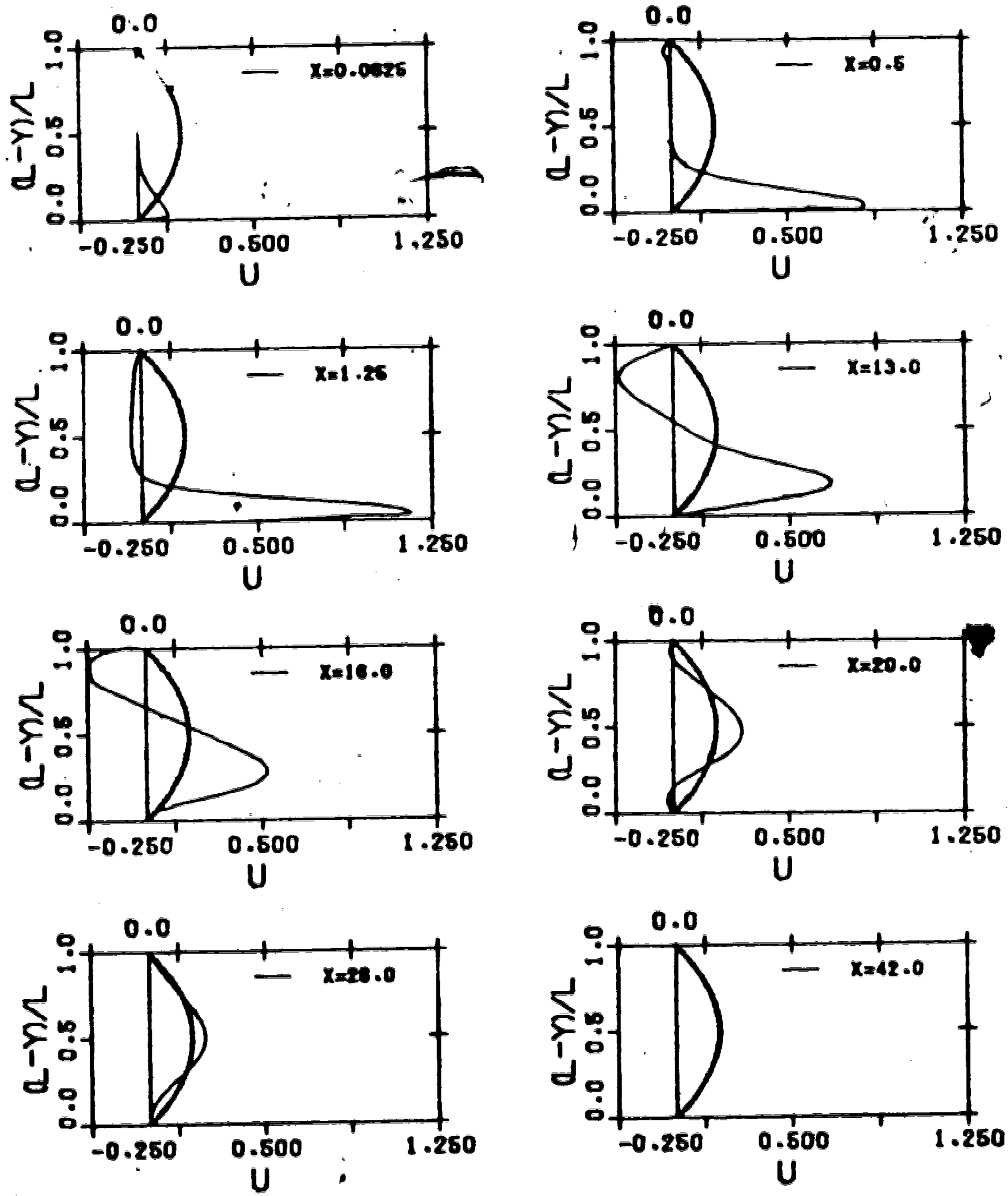

FIGURE 10.26 : STREAMWISE VELOCITY PROFILES FOR L=4 Re_b=300 WITH AN INITIAL PARABOLIC VELOCITY PROFILE

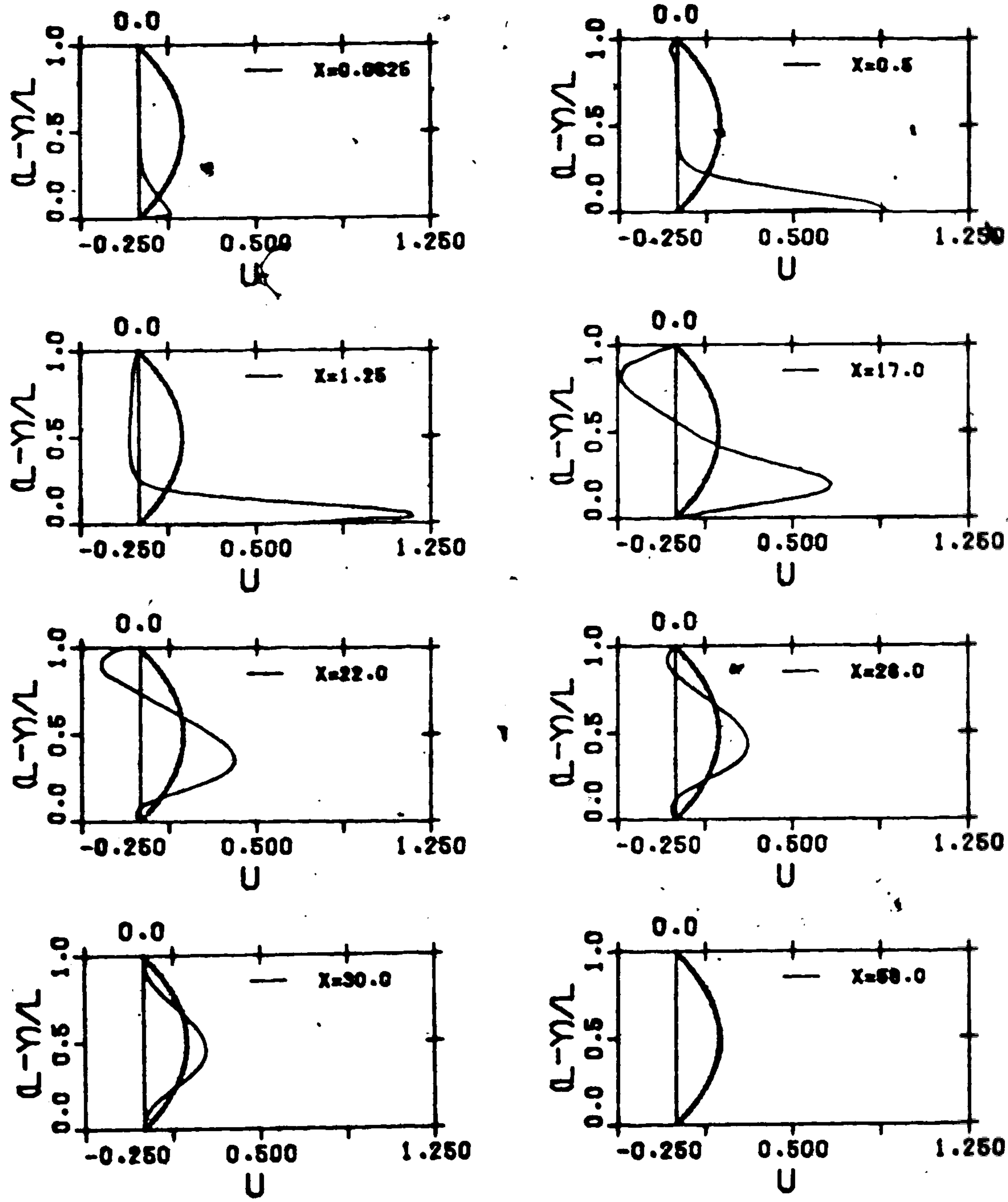

FIGURE 10.27 : STREAMWISE VELOCITY PROFILES FOR L=4 Re_b=400 WITH AN INITIAL PARABOLIC VELOCITY PROFILE

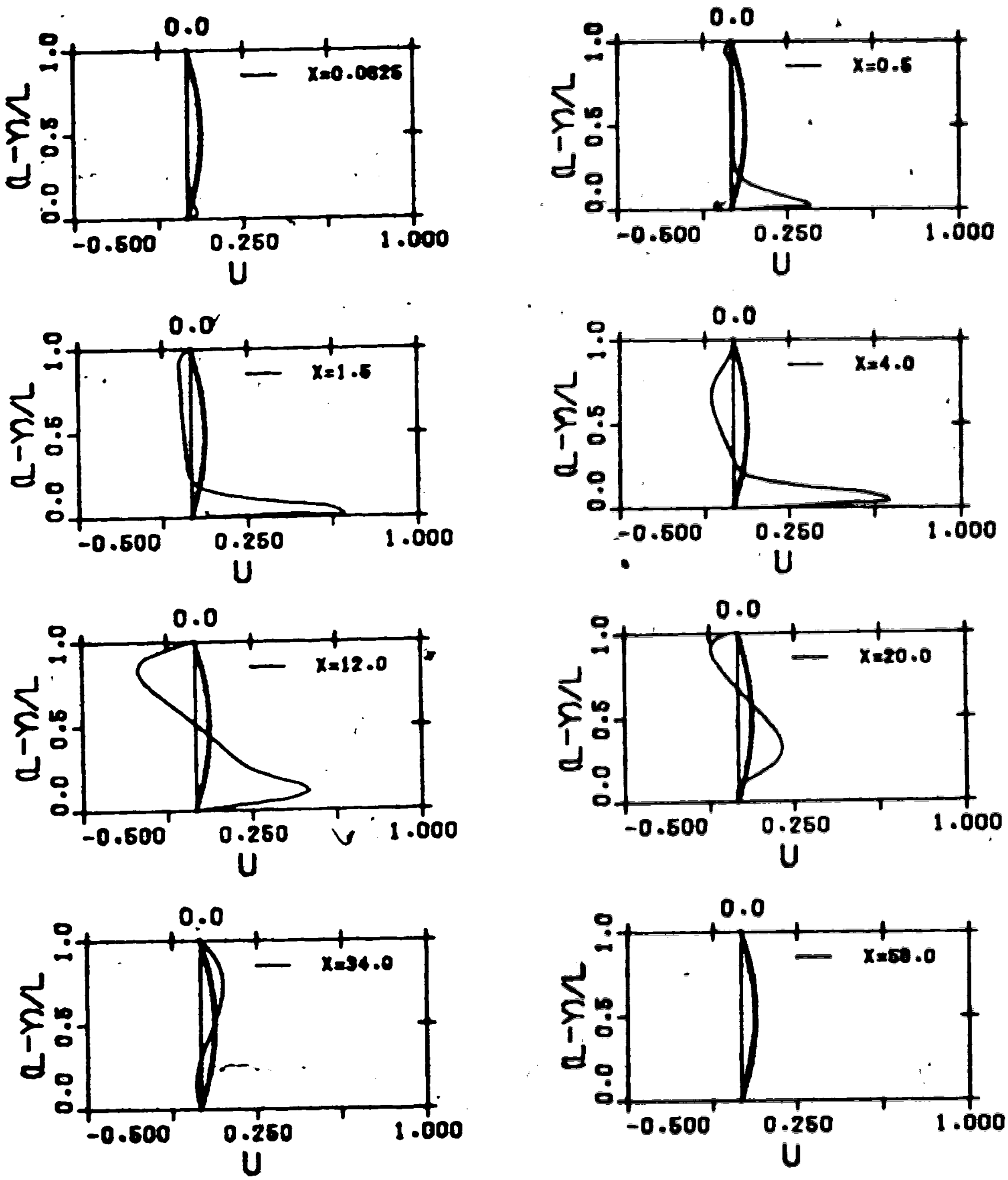

FIGURE 10.28 : STREAMWISE VELOCITY PROFILES FOR L=12 Re_b=100 WITH AN INITIAL PARABOLIC VELOCITY PROFILE

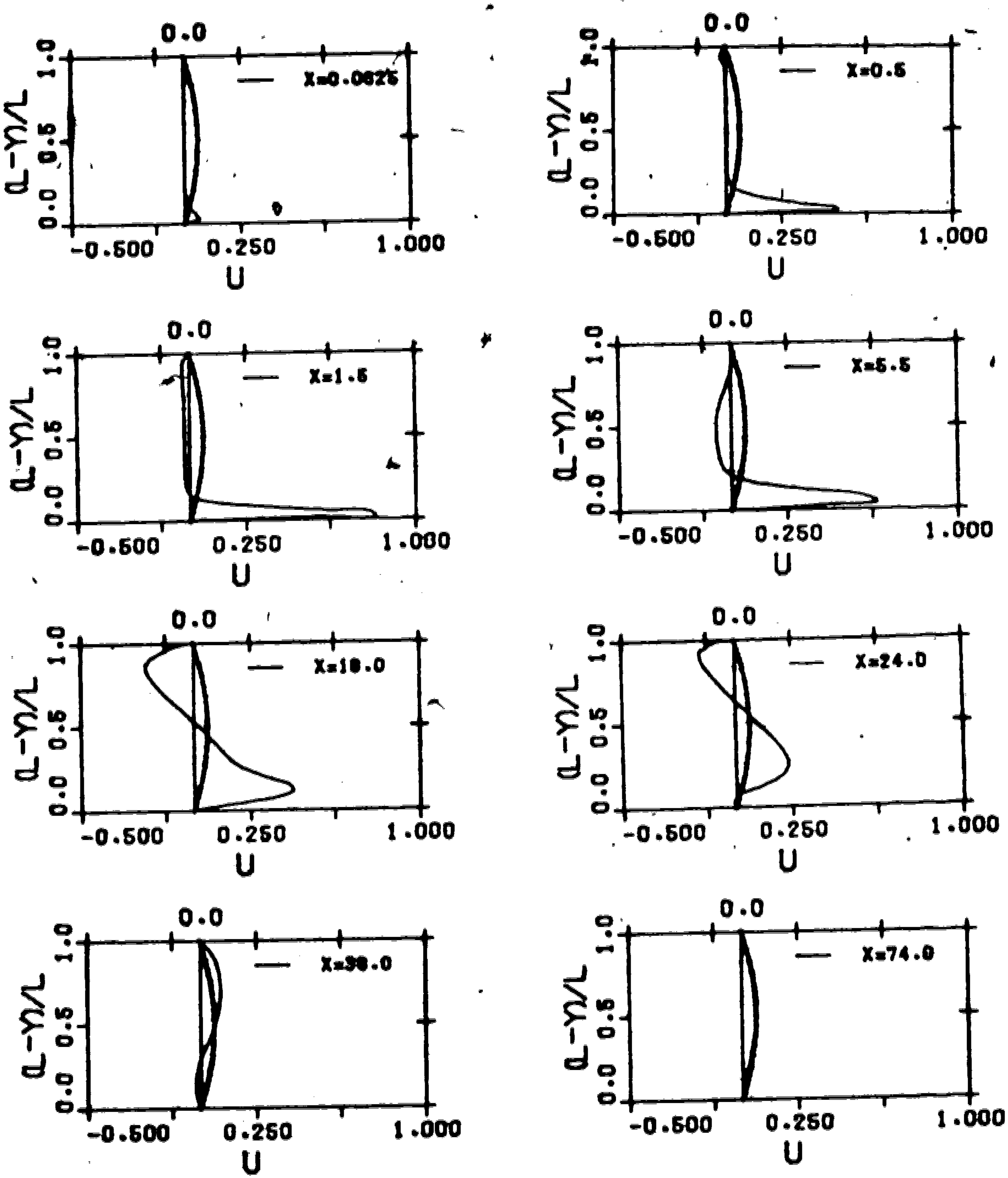

FIGURE 10.29 : STREAMWISE VELOCITY PROFILES FOR L=12 Re_b=200 WITH AN INITIAL PARABOLIC VELOCITY PROFILE

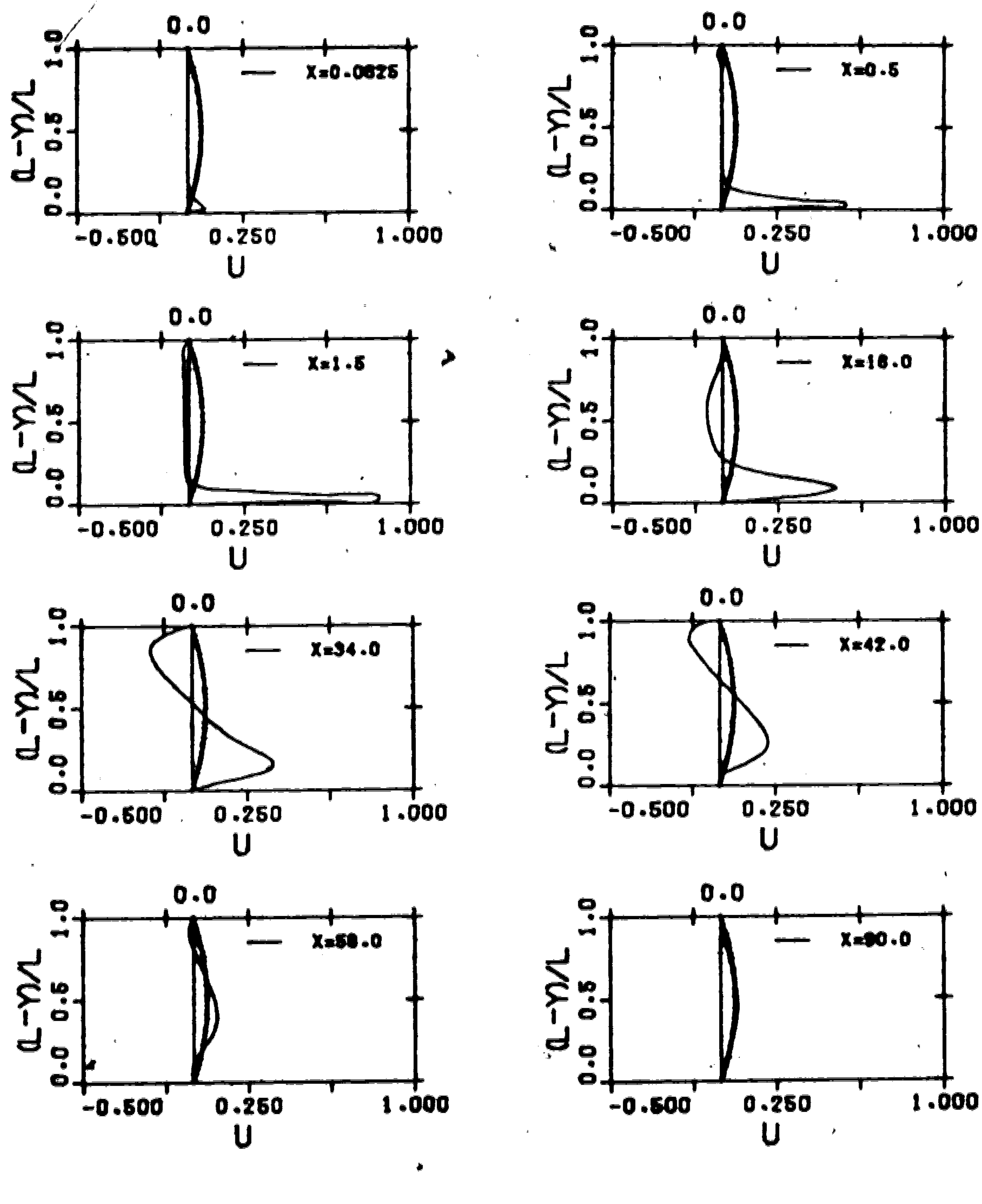

FIGURE 10.30 : STREAMWISE VELOCITY PROFILES FOR L=12 Re_b=300 WITH AN INITIAL PARABOLIC VELOCITY PROFILE

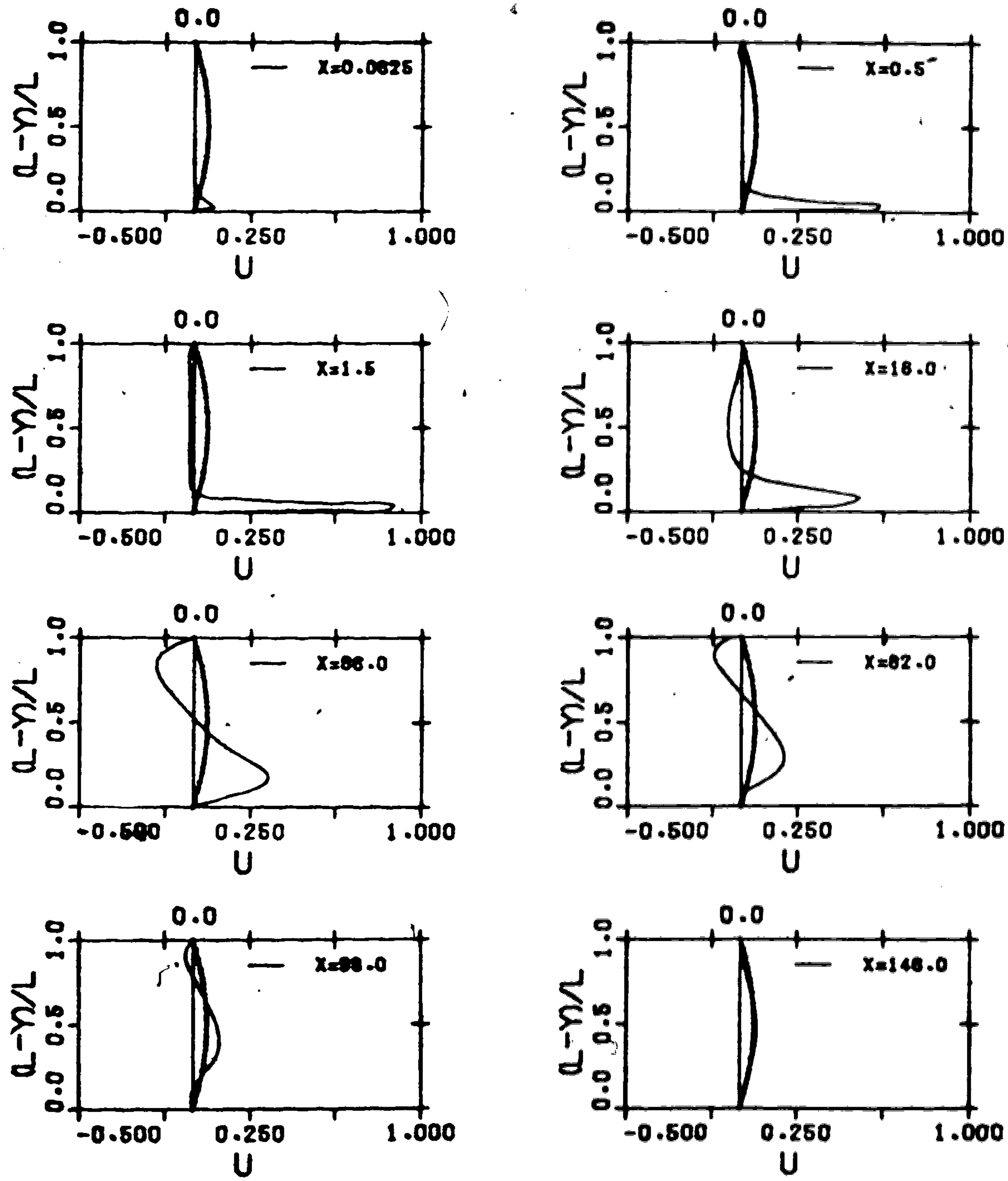

FIGURE 10.31 : STREAMWISE VELOCITY PROFILES FOR L=12 Re_b=400 WITH AN INITIAL PARABOLIC VELOCITY PROFILE

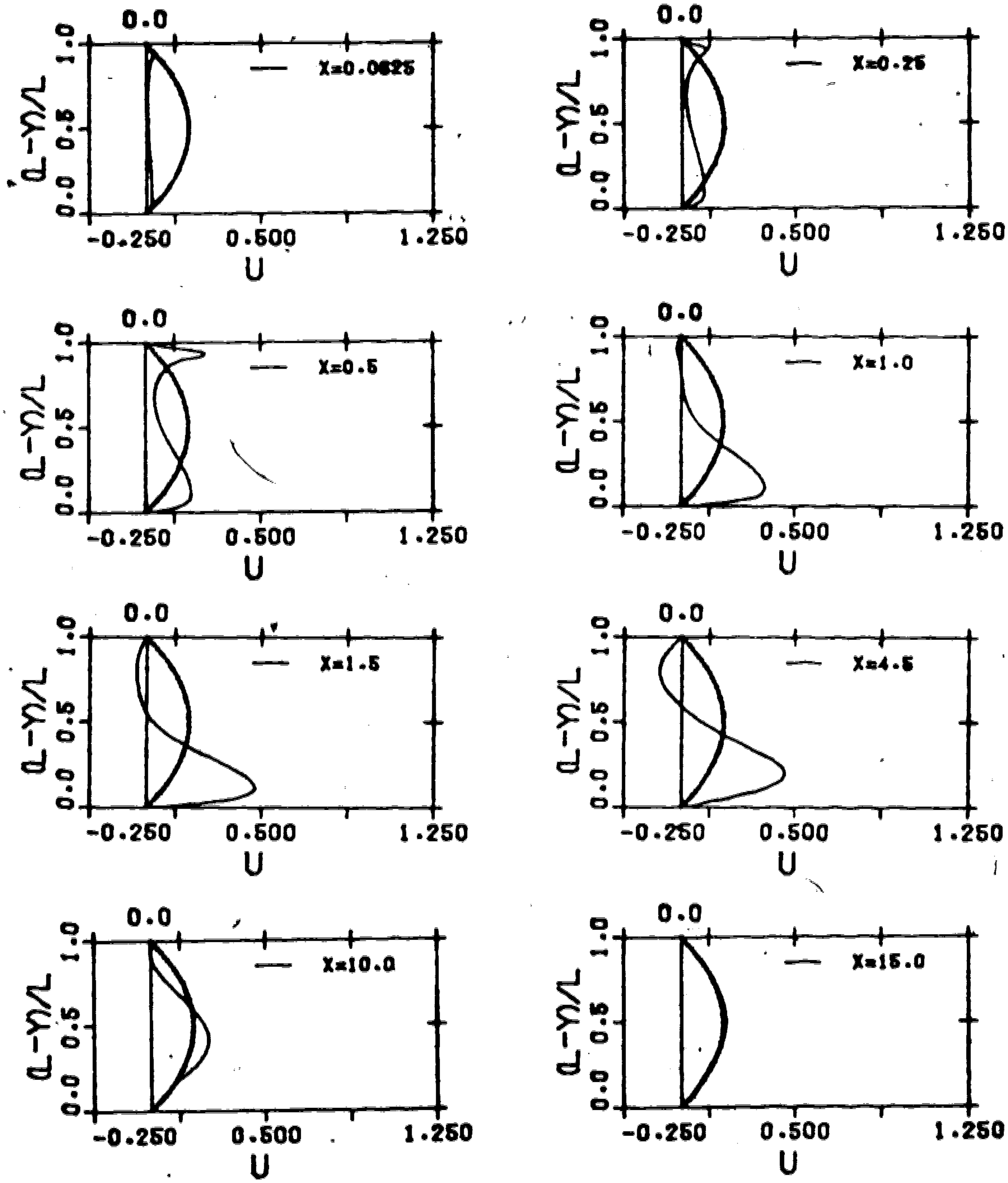

FIGURE 10.32 : STREAMWISE VELOCITY PROFILES FOR L=4 Re_b=100 WITH AN INITIAL FLAT VELOCITY PROFILE

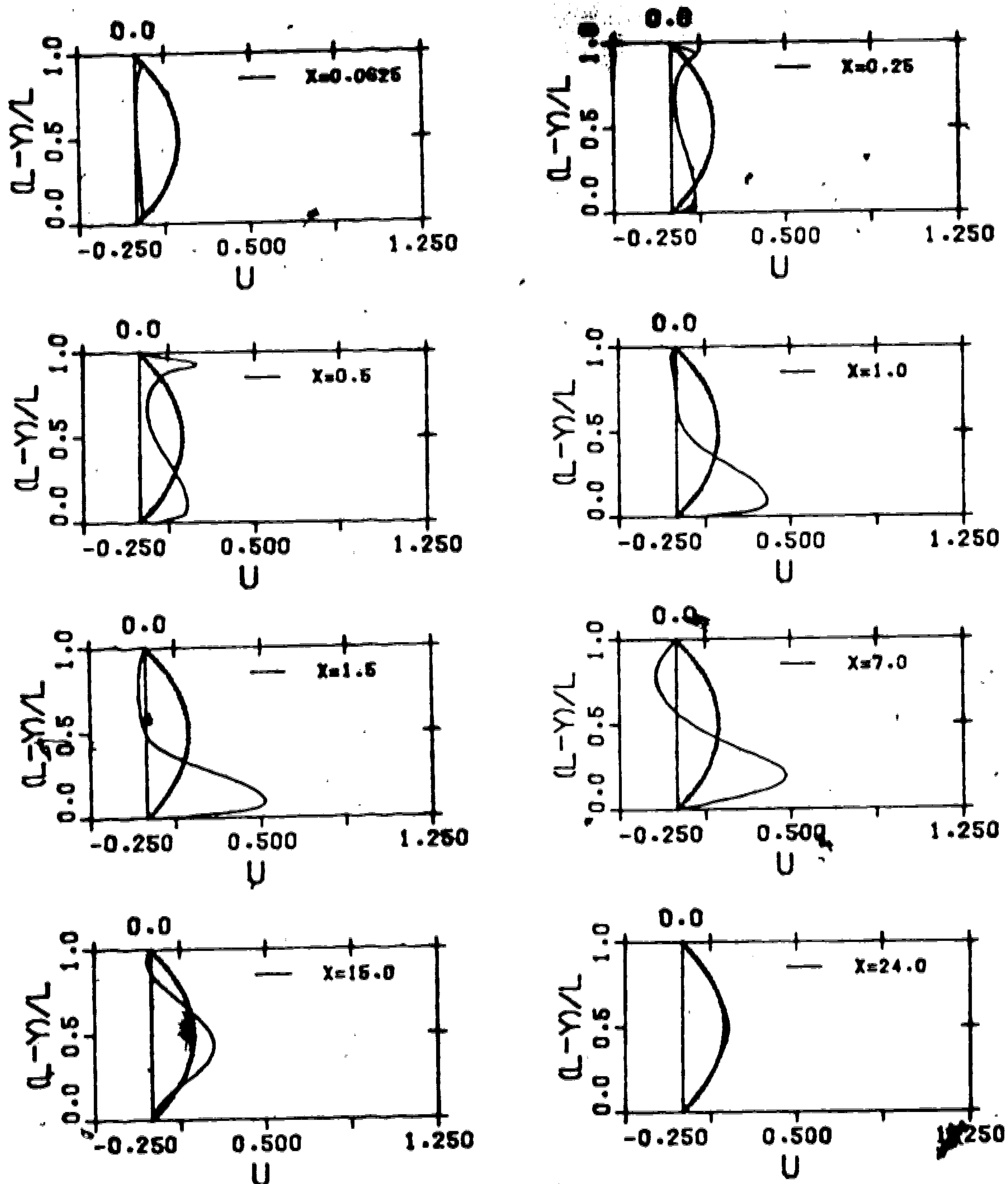

FIGURE 10.33 : STREAMWISE VELOCITY PROFILES FOR L=4 Re_b=200 WITH AN INITIAL FLAT VELOCITY PROFILE

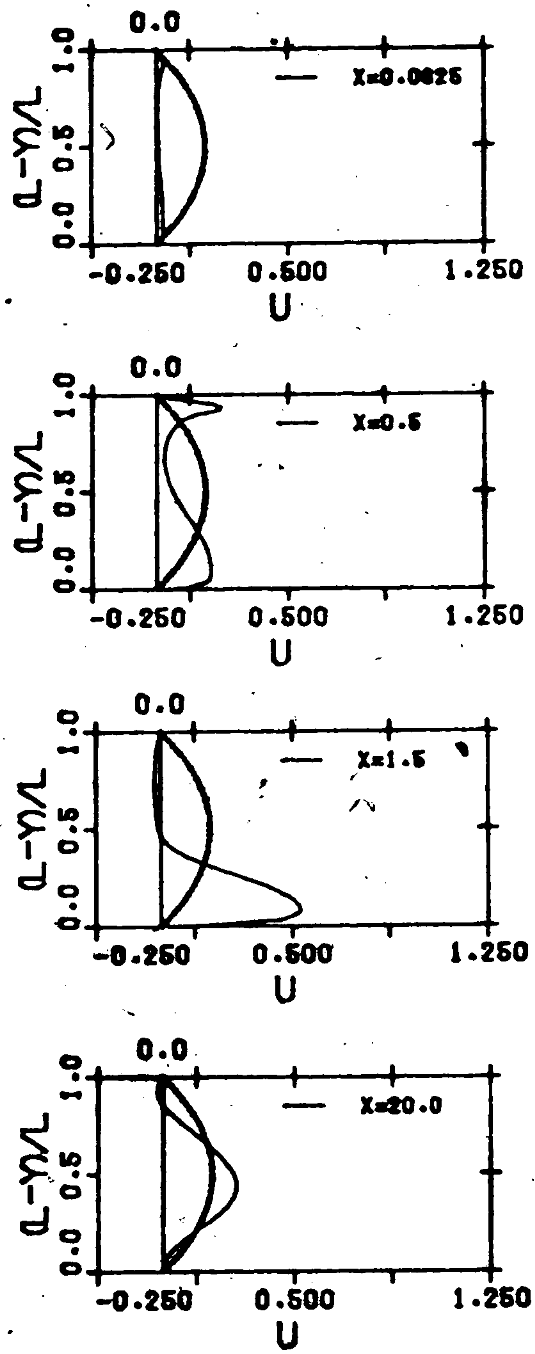

FIGURE 10.34 : STREAMWISE VELOCITY PROFILES FOR L=4 Re_b=300 WITH AN INITIAL FLAT VELOCITY PROFILE

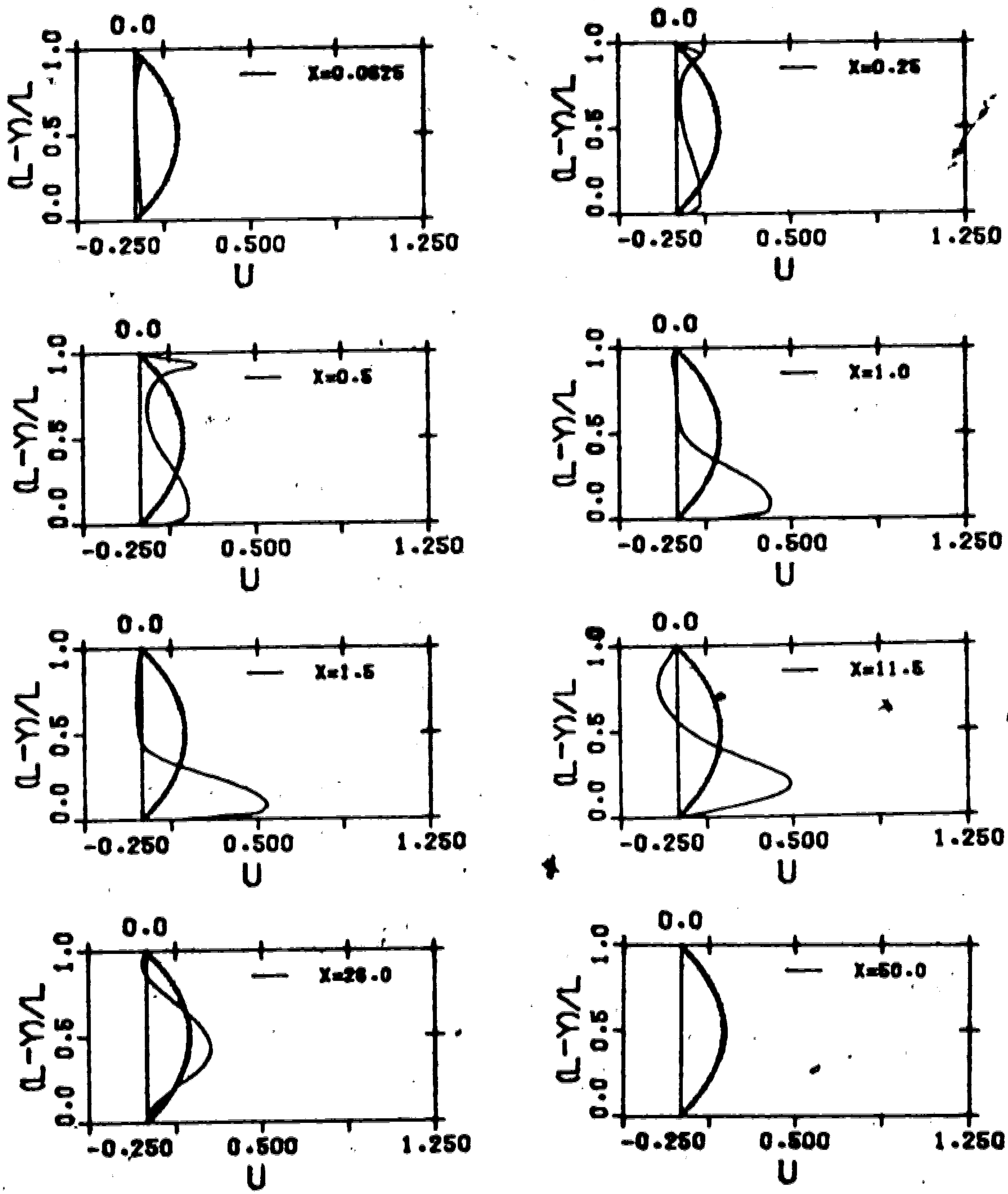

FIGURE 10.35 : STREAMWISE VELOCITY PROFILES FOR L=4 Re_b=400 WITH AN INITIAL FLAT VELOCITY PROFILE

decreases as the axial distance from the impingement plate increases. In some streamwise locations, the streamwise velocity becomes negative near the confingment plate. These negative velocities are caused by the inflow of the primary vortex induced by the confinement plate.

The thickness of the viscous boundary layer in stagnation flow region, σ_*, is defined as the distance from the impingement plate where the streamwise velocity reaches 99% of U_{max} and can be determined from the streamwise velocity profile. The values of σ_* for L=2 and 4 are given in Table 10.2. It is found that for a given Reynolds number and jet-to-plate spacing, the value of σ_* remains quite constant in the stagnation flow region. The values of σ_* for L=12 cannot be accurately determined due to the coarser grid arrangement used near the impingement plate for this case.

The variation of the maximum value of the streamwise velocity at individual streamwise location, U_{max}, with streamwise distance, X, in the region of $X \leq 5$ is shown in Figures 10.36-10.38 for the case of parabolic profile and in Figure 10.39 for the case of flat profile. In the stagnation flow region, U_{max} is linearly proportional to the distance from the stagnation point due to the transformation of the axial momentum into the streamwise momentum. A similar observation has been made by Schlichting (78) for unconfined submerged jet. Introducing the dimensionless variables in Equation 6.6 into Equation 2.6 and choosing U_{max} instead of U, yields

TABLE 10.2 : THICKNESS OF VISCOUS BOUNDARY LAYER IN STAGNATION FLOW REGION

PARABOLIC PROFILE

L	Re_b	σ_e/b
2	100	0.185
	200	0.125
	300	0.105
	400	0.085
4	100	0.215
	200	0.140
	300	0.105
	400	0.099

FLAT PROFILE

L	Re_b	σ_e/b
4	100	0.376
	200	0.287
	300	0.254
	400	0.202

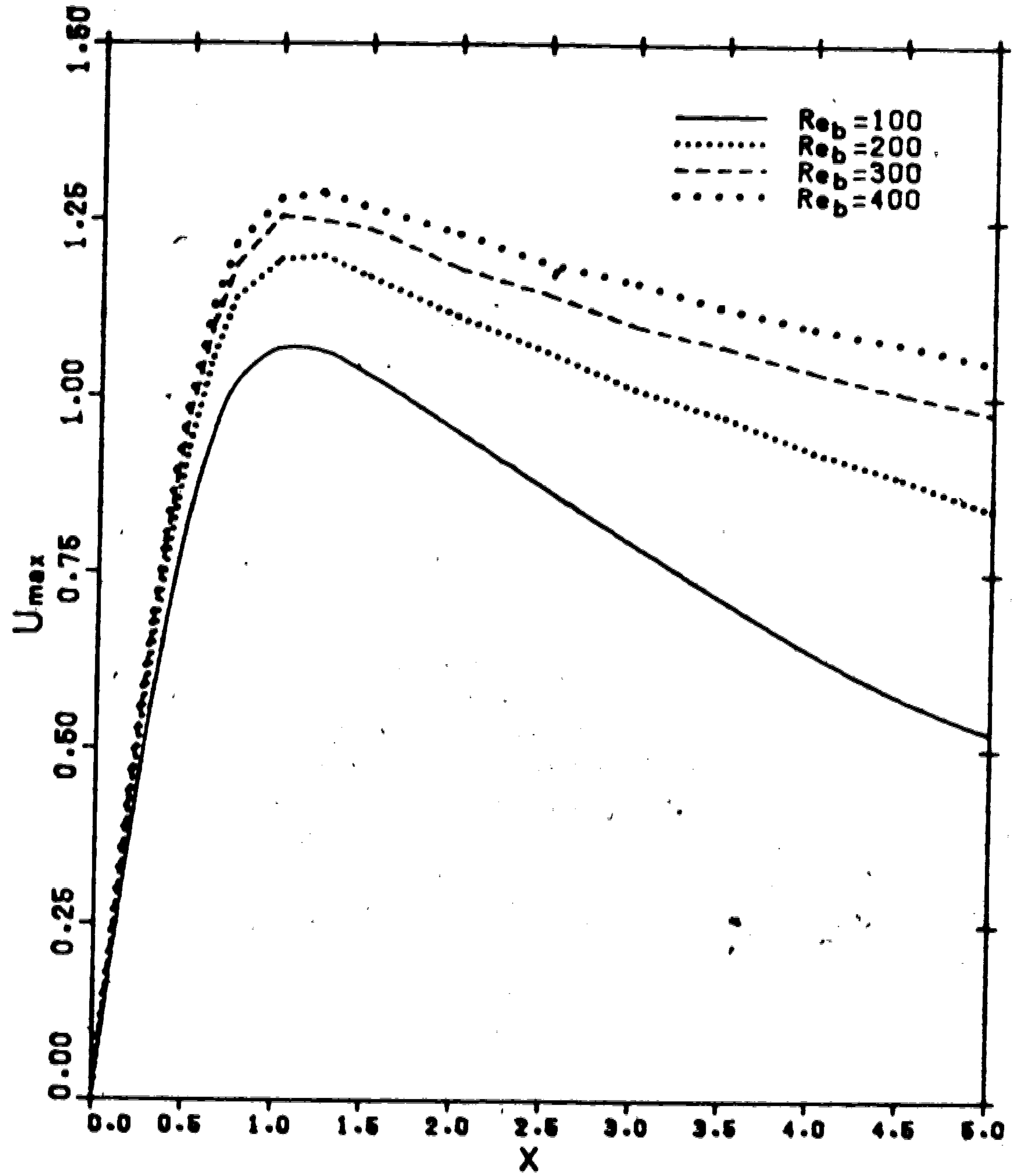

FIGURE 10.36 : VARIATION OF Umax WITH STREAMWISE DISTANCE FOR L=2 WITH AN INITIAL PARABOLIC VELOCITY PROFILE

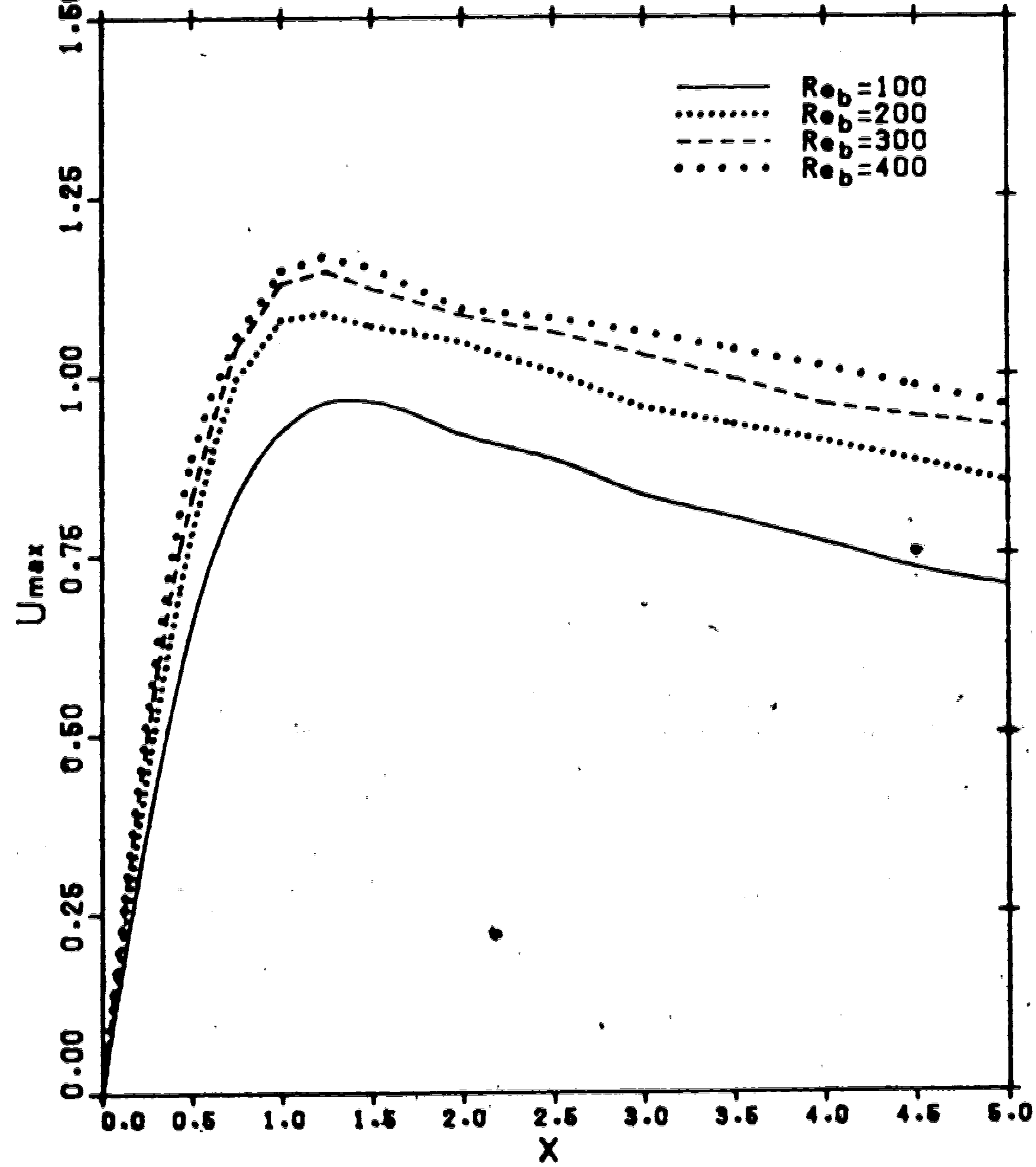

FIGURE 10.37 : VARIATION OF Umax WITH STREAMWISE DISTANCE FOR L=4 WITH AN INITIAL PARABOLIC VELOCITY PROFILE

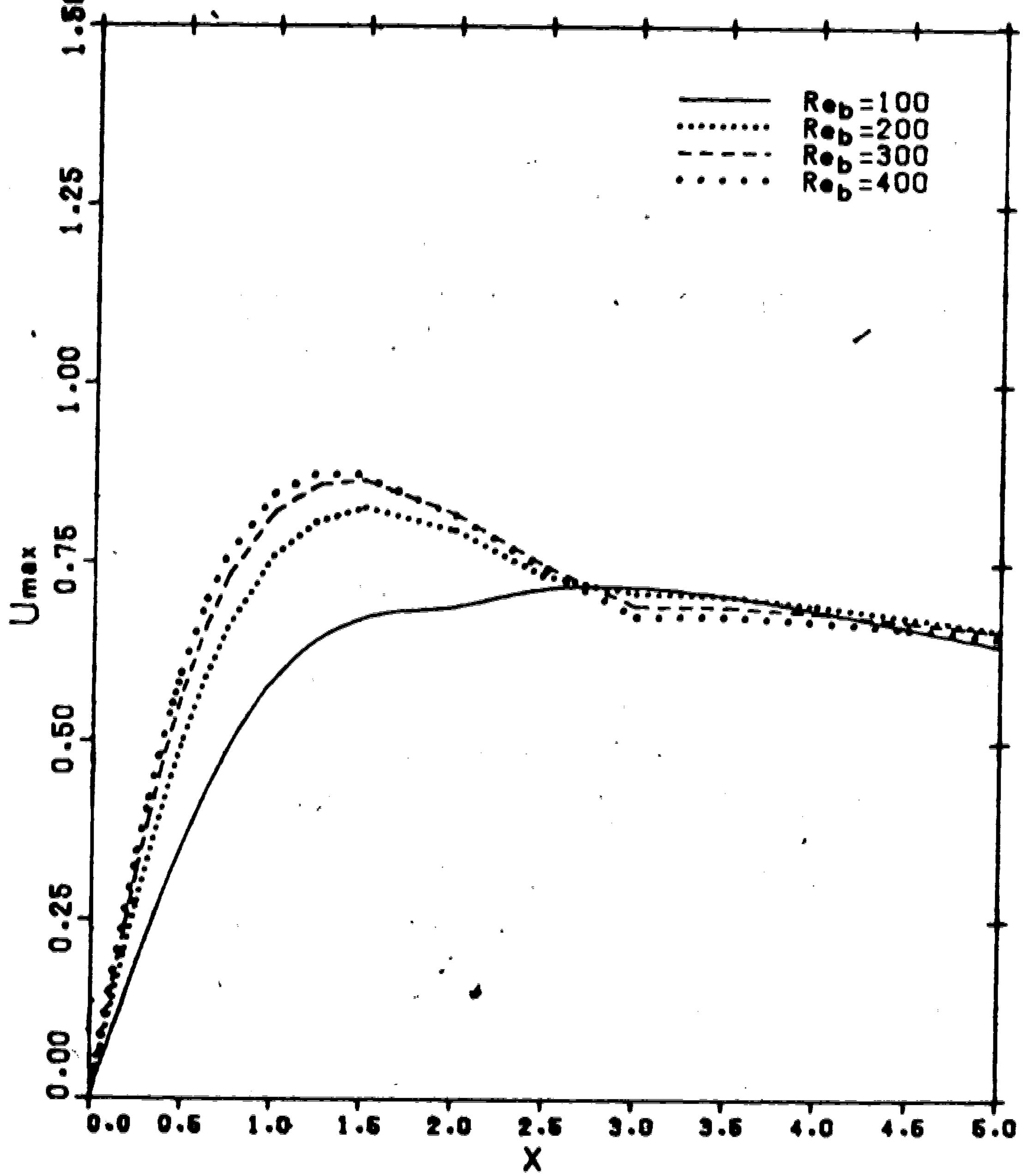

FIGURE 10.38 : VARIATION OF Umax WITH STREAMWISE DISTANCE FOR L=12 WITH AN INITIAL PARABOLIC VELOCITY PROFILE

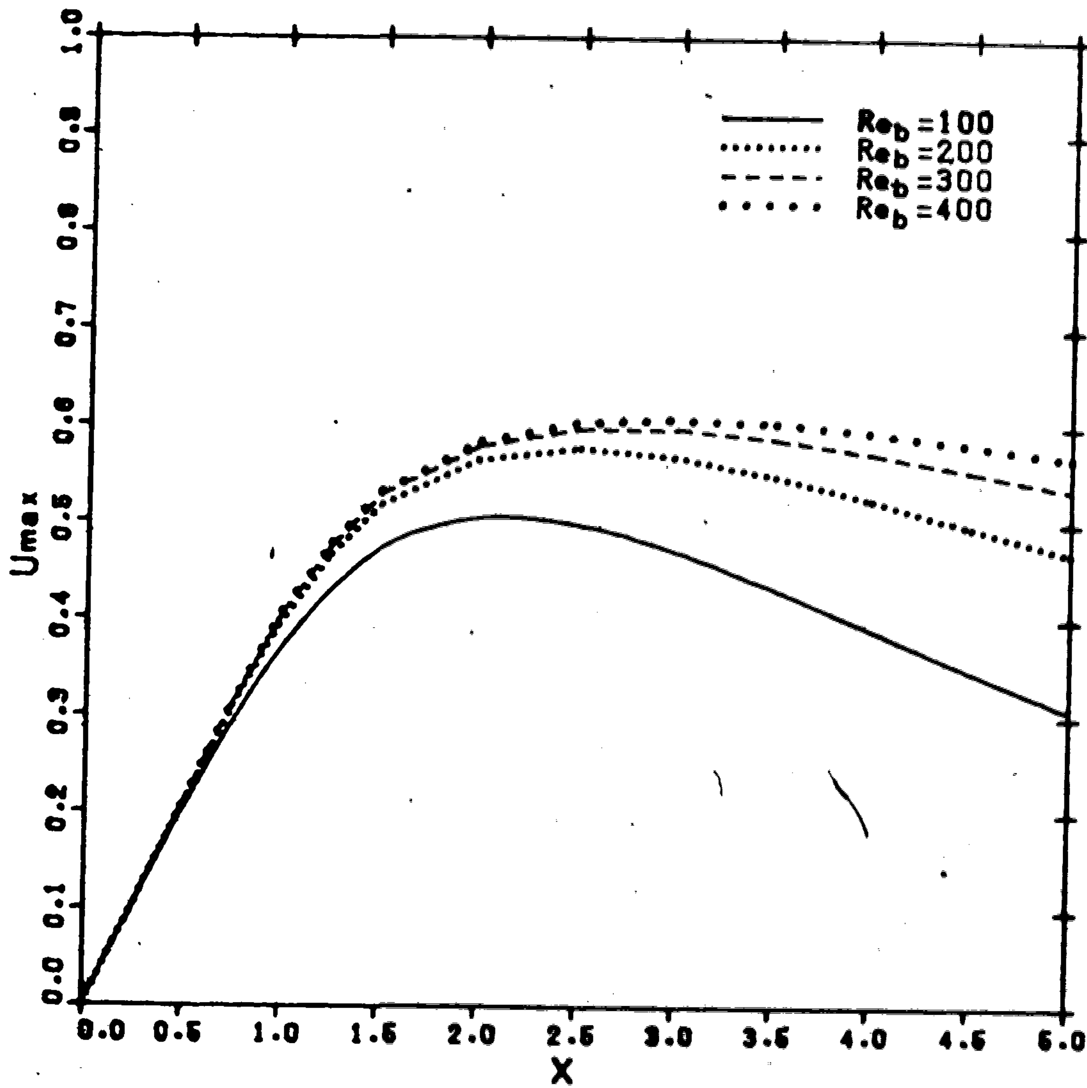

FIGURE 10.39 : VARIATION OF Umax WITH STREAMWISE DISTANCE FOR L=4 WITH AN INITIAL FLAT VELOCITY PROFILE

$$U_{max} = a_1 X \quad (10.3)$$

The values of a_1 can be easily evaluated from the slopes of all the curves of Figures 10.36-10.39 for different Reynolds numbers and jet-to-plate spacings. The values of a_1 for the case of parabolic profile are given in Table 10.3. Comparing the values of a_1 in Table 10.3 to those in Table 10.1, agreement within 2.5% is obtained. The values of a_1 for the case of flat profile are approximately equal to 0.4 for all Reynolds numbers. This value is within 5% agreement with that evaluated in Section 10.1.2.

The thickness of the viscous boundary layer in the stagnation flow region, σ_*, can also be evaluated from a_1 using Equation 2.9,

$$\sigma_*/b = 2.38 \;/\; (a_1 \, Re_b)^{0.5} \quad (10.4)$$

The values of σ_*/b evaluated from Equation 10.4 are compared to those in Table 10.2 in Figure 10.40. The data points fall fairly closely on the zero error straight line with a slope of unity. It is noted that Equation 10.4 was obtained by Schlichting (78) in his study of unconfined submerged jet. Such a good agreement of the data points indicates that the presence of confinement plate has little effect on the flow in the stagnation flow region.

Due to the exchange of momentum with the circulating fluid in the primary vortex, U_{max} which increases with X in

TABLE 10.3 : VALUES OF a_1 EVALUATED FROM EQUATION 10.3

L/d	Re_b	a_1
2	100	1.74
	200	2.01
	300	2.11
	400	2.15
4	100	1.34
	200	1.63
	300	1.72
	400	1.77
12	100	0.71
	200	1.01
	300	1.15
	400	1.22

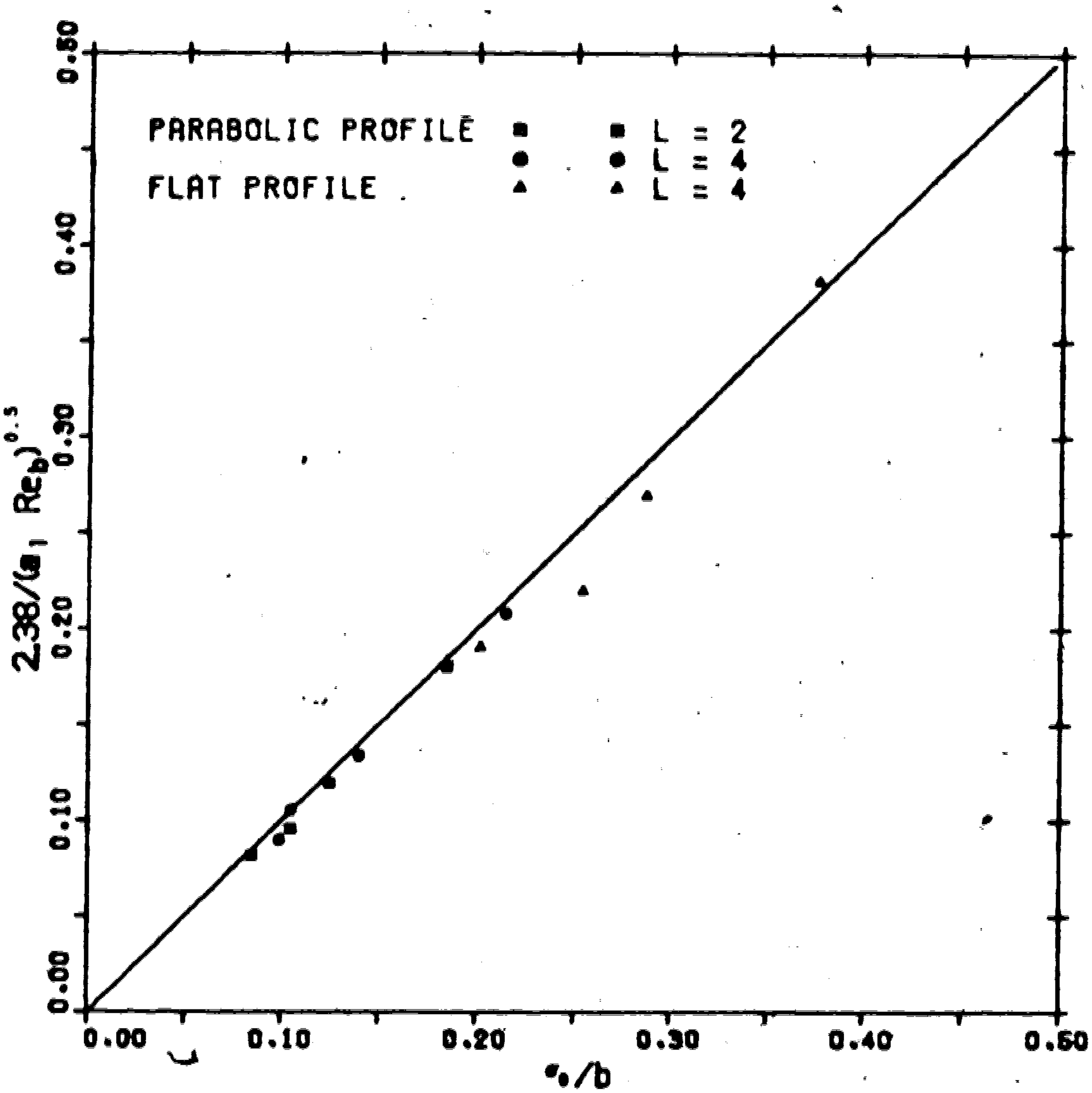

FIGURE 10.40 : TEST OF GOODNESS FIT FOR EQUATION 10.4

the stagnation flow region must eventually reaches a maximum and decreases in the wall jet region. The location of the maximum of U_{max} is a function of Reynolds number and jet-to-plate spacing as can be noted in Figures 10.36-10.39. In the wall jet region, flow separation is observed along the impingement plate for the case of parabolic profile with the exception of the cases of low Reynolds numbers for L=2. The locations where the flow starts to separate from the impingement plate are given in Table 10.4. For the case of flat profile, no flow separation along the impingement plate is observed.

The decay of U_{max} for different Reynolds numbers in the wall jet region are plotted as $\log(U_{max})$ versus $\log(X)$ in Figures 10.41-10.43 for a jet with an initial parabolic profile, and in Figure 10.44 for a jet with an initial flat profile. Obviously, the prediction by Glauert (25) using Equation 2.11 in his study of the decay of maximum streamwise velocity in the wall jet region originating from an unconfined submerged jet cannot be applied here. For a confined air jet, the flow which leaves the stagnation flow region is strongly influenced by the presence of the primary vortex as shown in Figures 10.1-10.4. U_{max} decreases more gently after it reaches its maximum value. As soon as the fluid flows pass the centre of the primary vortex, the flow expands and U_{max} decreases rapidly. Eventually, U_{max} approaches the value of that of the fully developed profile between two parallel plates. The lower the Reynolds number

TABLE 10.4 : LOCATIONS OF FLOW SEPARATION ALONG THE IMPINGEMENT PLATE

L	Re_b	X
2	400	12.0
4	100	9.5
	200	12.0
	300	17.0
	400	20.0
12	100	20.0
	200	24.0
	300	42.0
	400	82.0

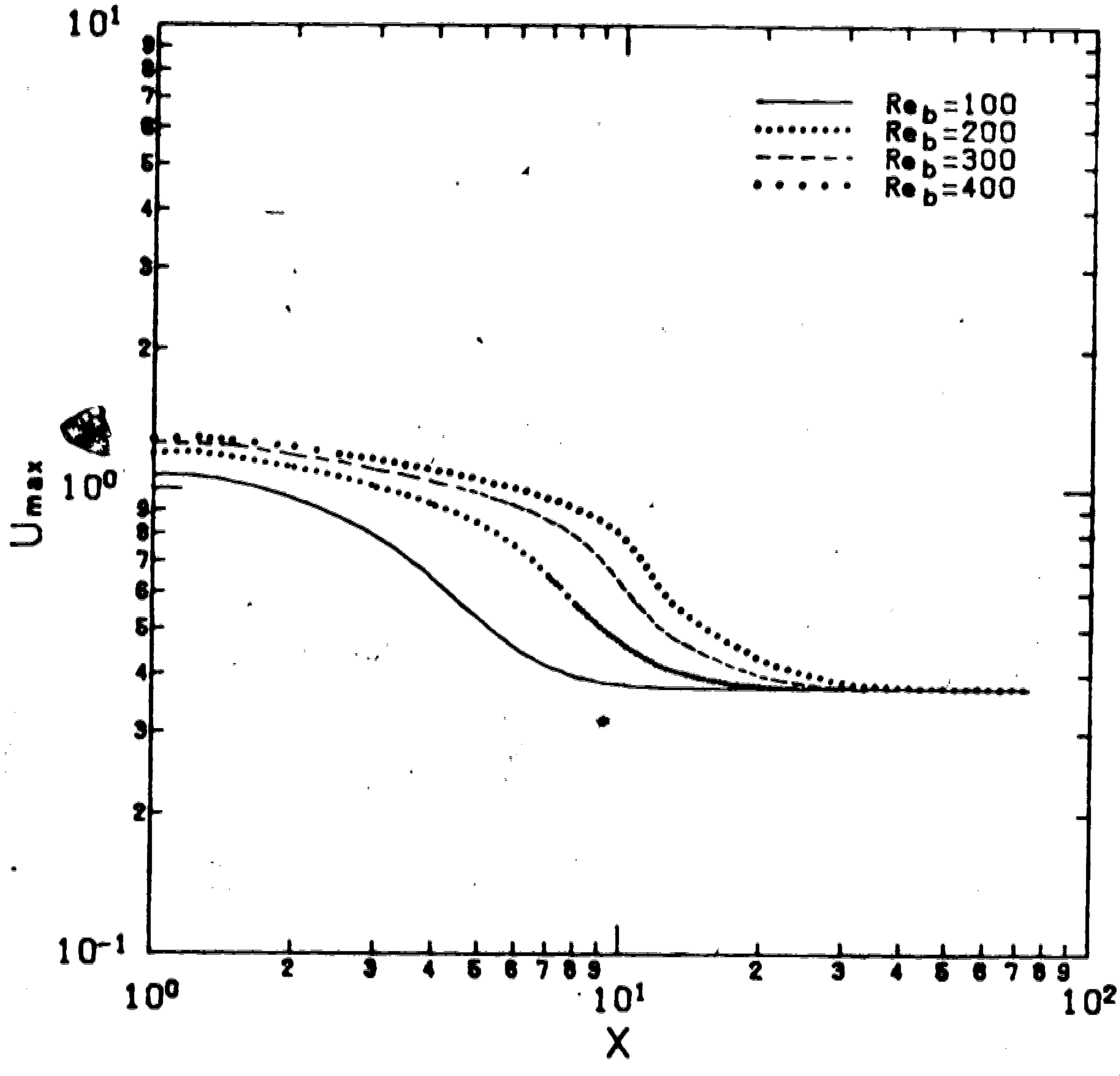

FIGURE 10.41 : DECAY OF MAXIMUM STREAMWISE VELOCITY FOR L=2 WITH AN INITIAL PARABOLIC VELOCITY PROFILE

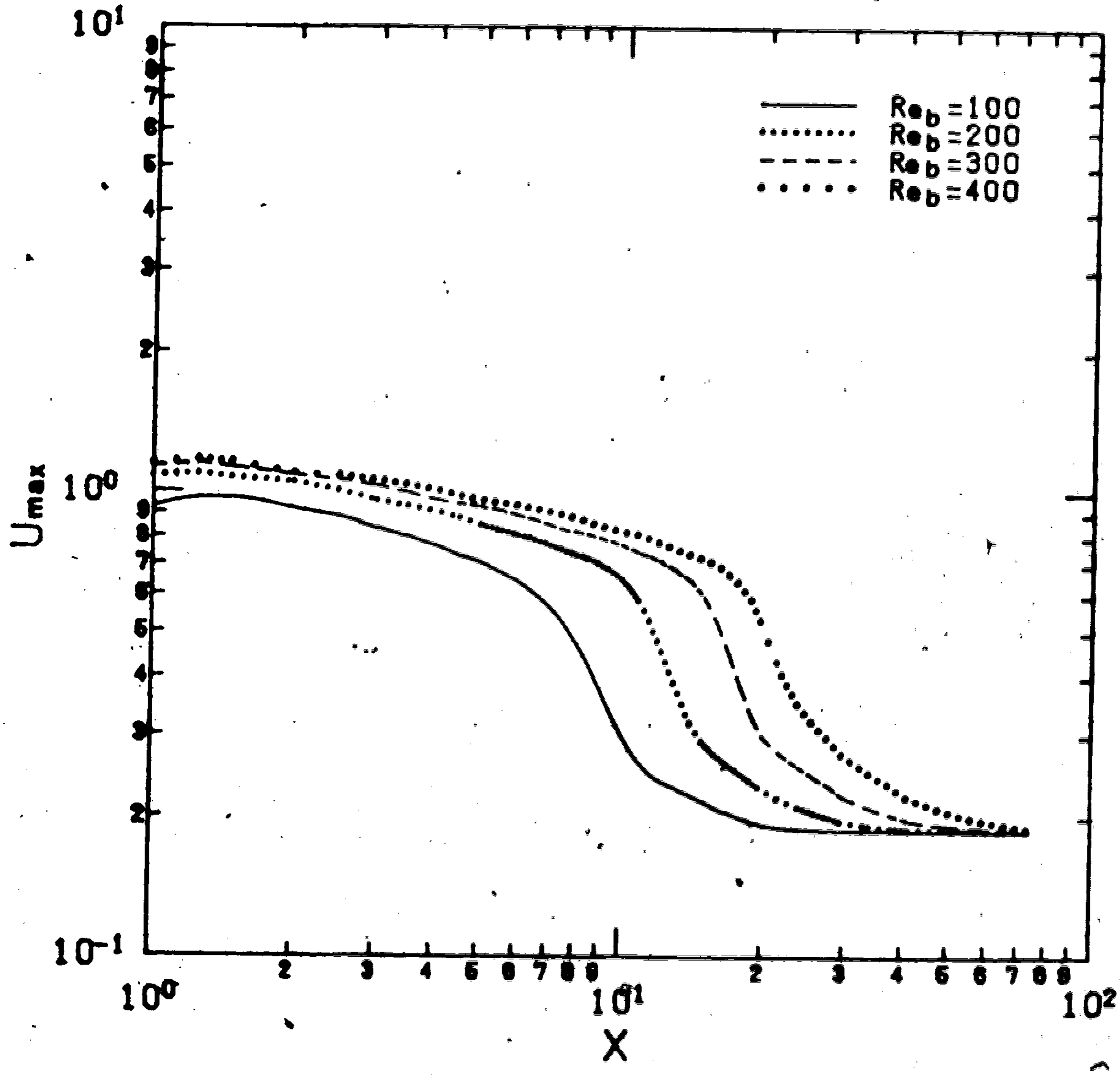

FIGURE 10.42 : DECAY OF MAXIMUM STREAMWISE VELOCITY FOR L=4 WITH AN INITIAL PARABOLIC VELOCITY PROFILE

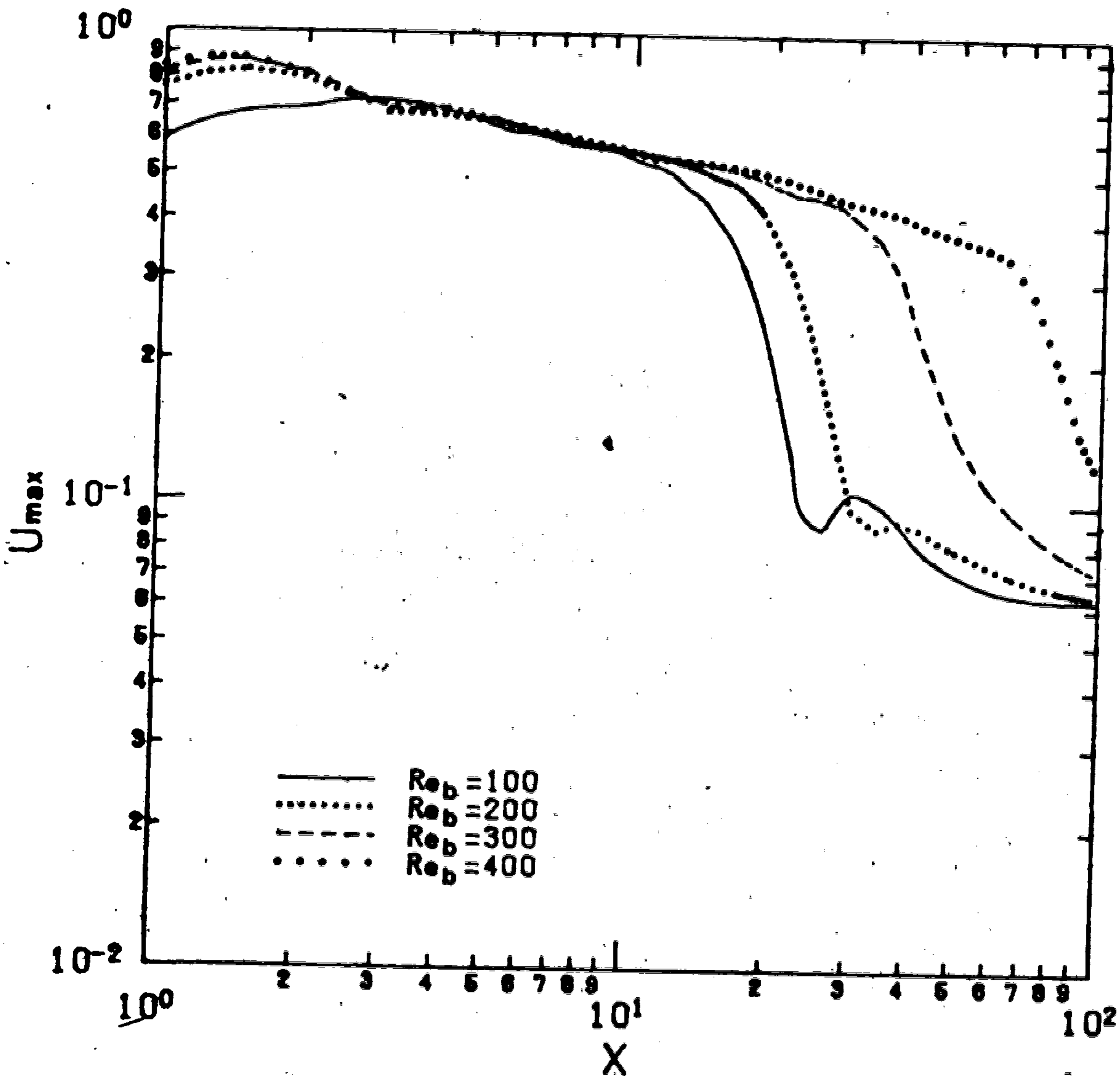

FIGURE 10.43 : DECAY OF MAXIMUM STREAMWISE VELOCITY FOR L=12 WITH AN INITIAL PARABOLIC VELOCITY PROFILE

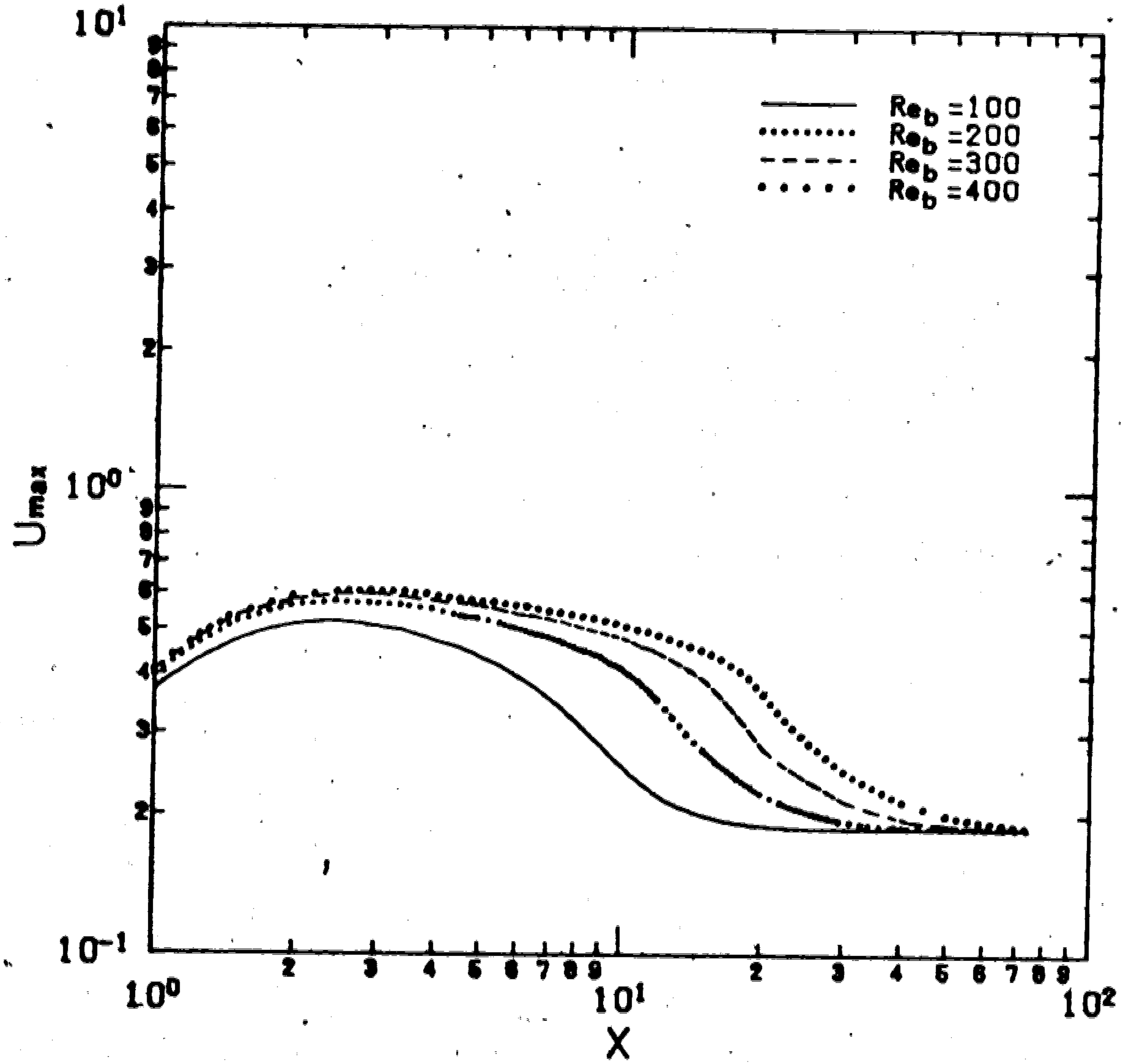

FIGURE 10.44 : DECAY OF MAXIMUM STREAMWISE VELOCITY FOR L=4 WITH AN INITIAL FLAT VELOCITY PROFILE

and the smaller the jet-to-plate spacing, the shorter the streamwise distance needed to approach fully developed flow.

10.1.4 IMPINGEMENT PLATE SKIN-FRICTION FACTOR

The study of local skin-friction factor along the impingement plate provides information of the local shear stress on the plate. The local skin-friction factor is defined by Equation 8.3. For fully developed flow between two parallel plates, the skin-friction factor can be evaluated by setting Y=L in Equation 6.28 and substituting into Equation 8.5 to give

$$(C_f)_{fd} = 6 / (Re_b\ L^2) \qquad (10.5)$$

A plot of $C_f Re_b$ versus X for a given jet-to-plate spacing leads to the collapse of all curves for different Reynolds numbers to a single curve in the region far away from the stagnation flow region where the influence of the impinging flow is not sensed. Individual curves for different jet-to-plate spacings approach the value of $6/L^2$ which is equal to 1.5, 0.375 and 0.0417 for L=2, 4 and 12 respectively. Variations of $C_f Re_b$ versus X are shown in Figures 10.45-10.47 for a jet with an initial parabolic velocity profile and for a jet with an initial flat velocity profile in Figure 10.48. The general variation pattern of the local skin-friction factor is that it increases sharply from zero at the stagnation point to a maximum value in a

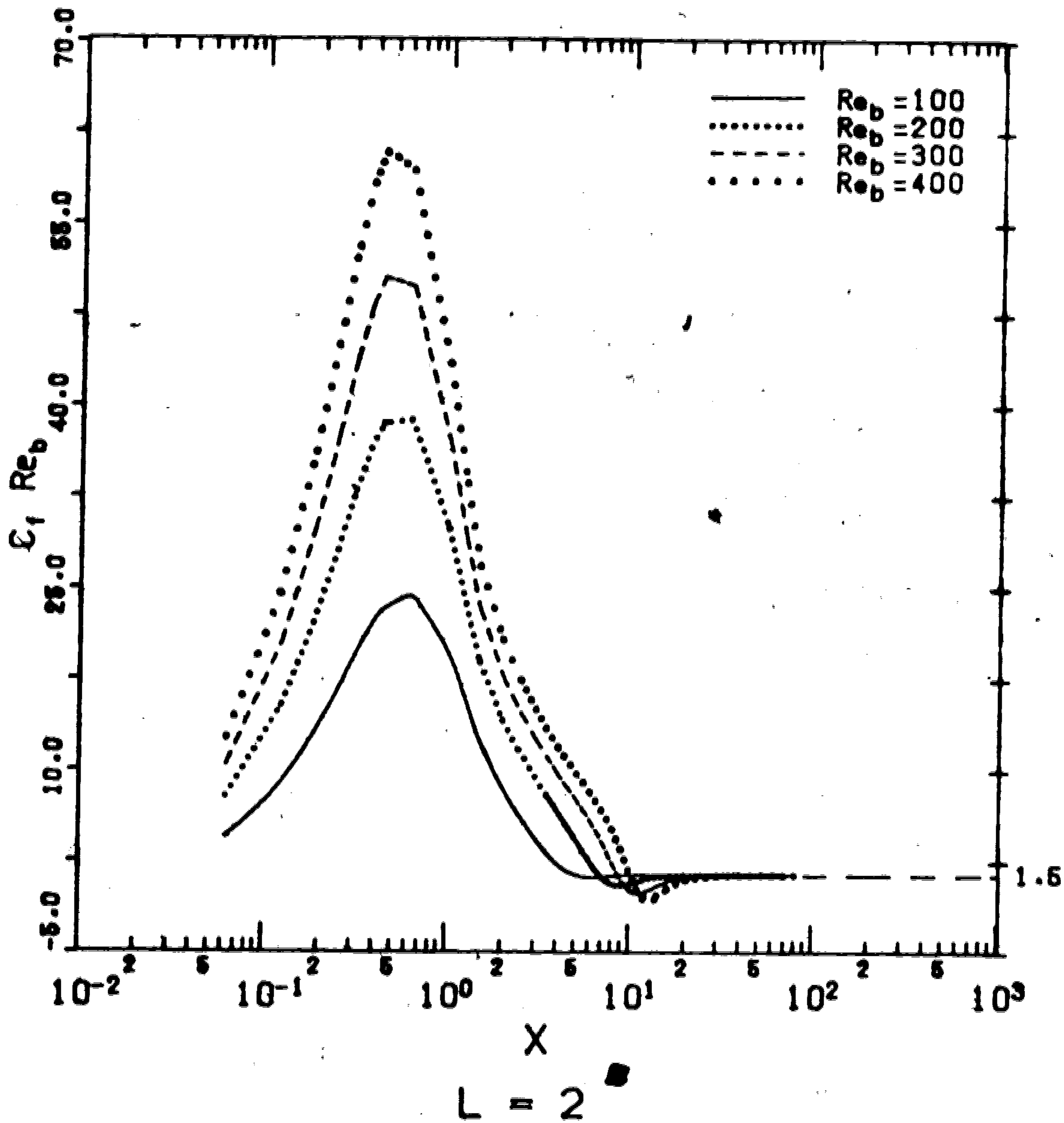

FIGURE 10.45 : VARIATION OF LOCAL SKIN-FRICTION FACTORS FOR L=2 WITH AN INITIAL PARABOLIC VELOCITY PROFILE

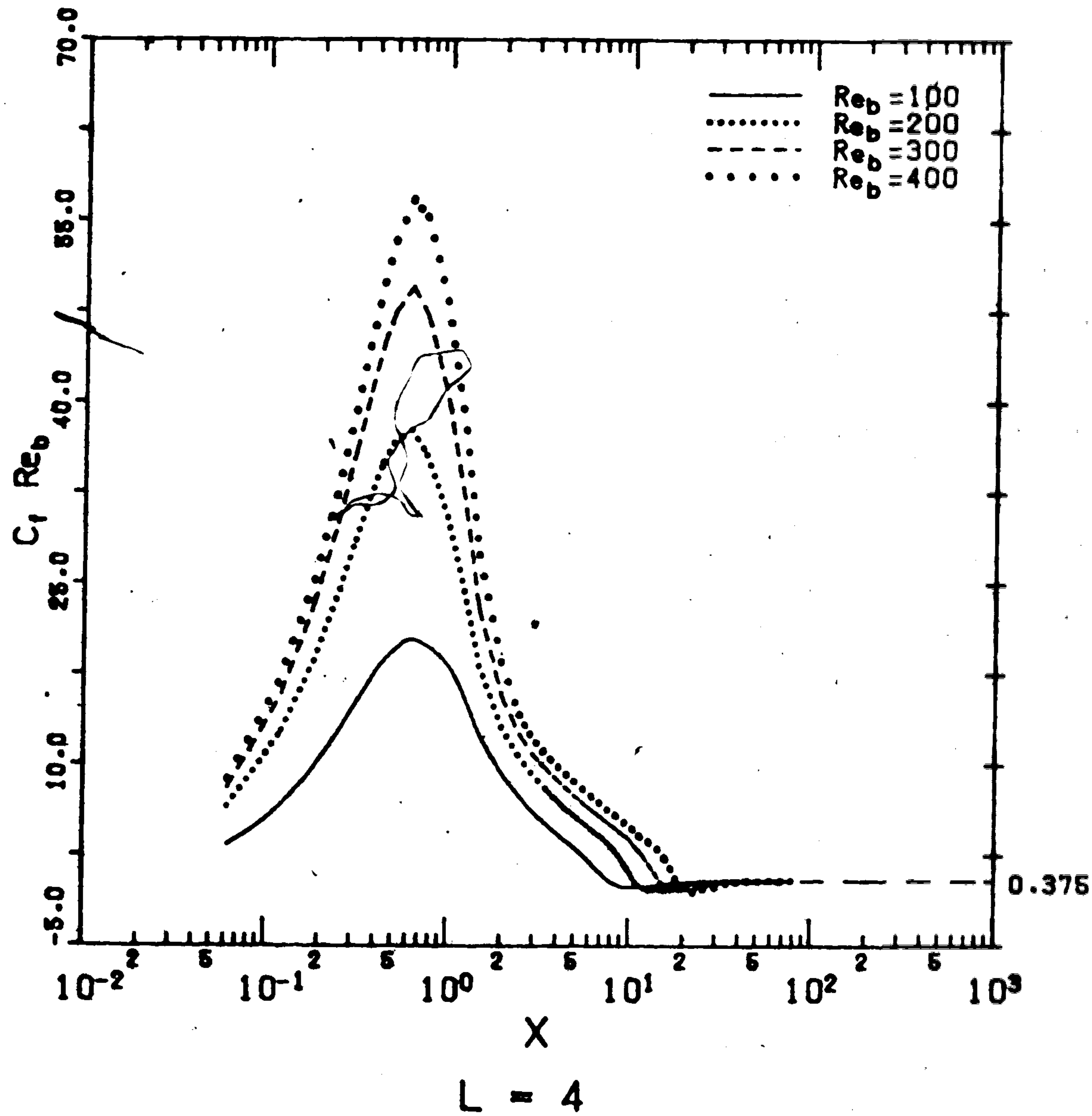

FIGURE 10.46 : VARIATION OF LOCAL SKIN-FRICTION FACTORS FOR L=4 WITH AN INITIAL PARABOLIC VELOCITY PROFILE

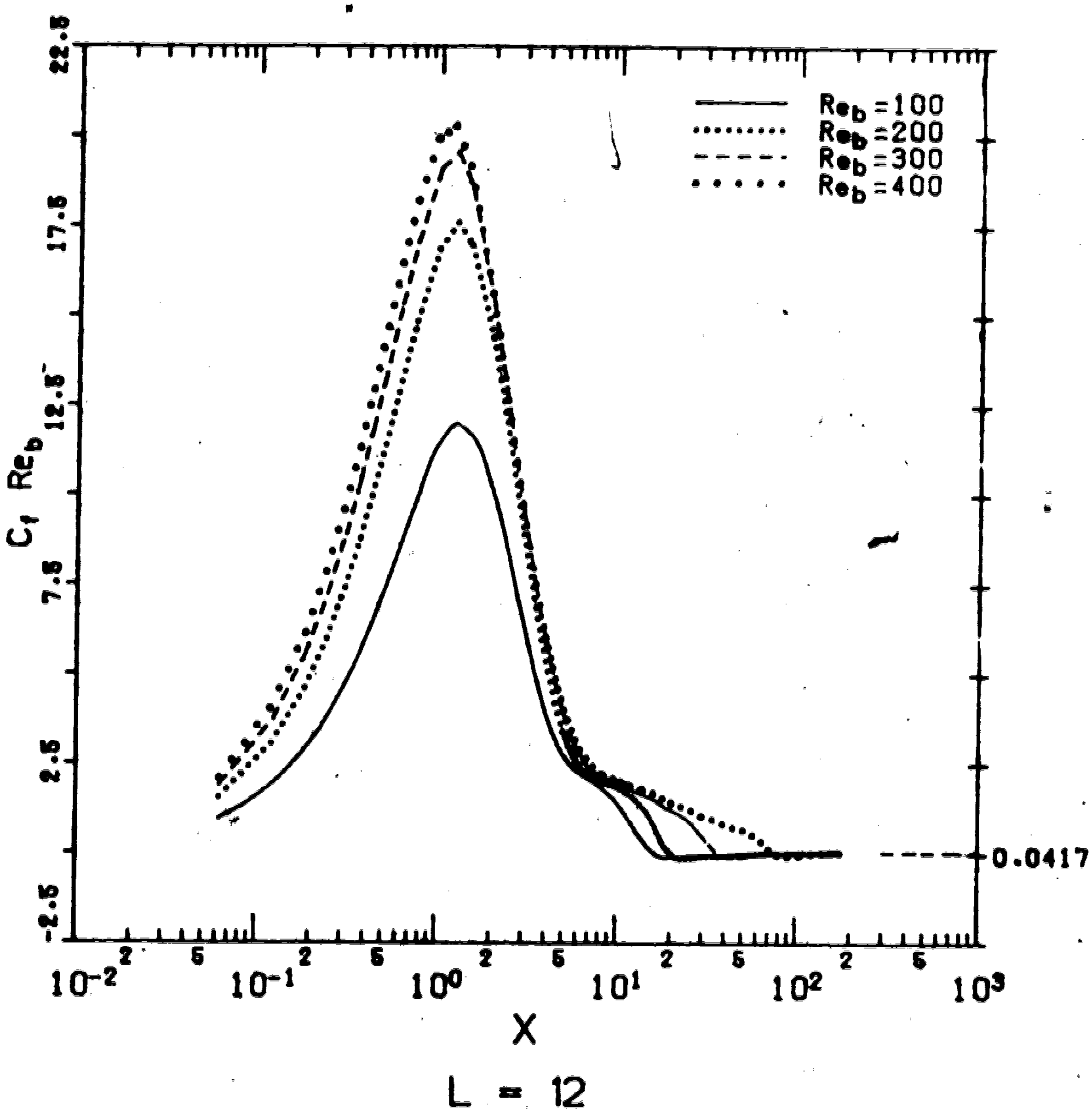

FIGURE 10.47 : VARIATION OF LOCAL SKIN-FRICTION FACTORS FOR L=12 WITH AN INITIAL PARABOLIC VELOCITY PROFILE

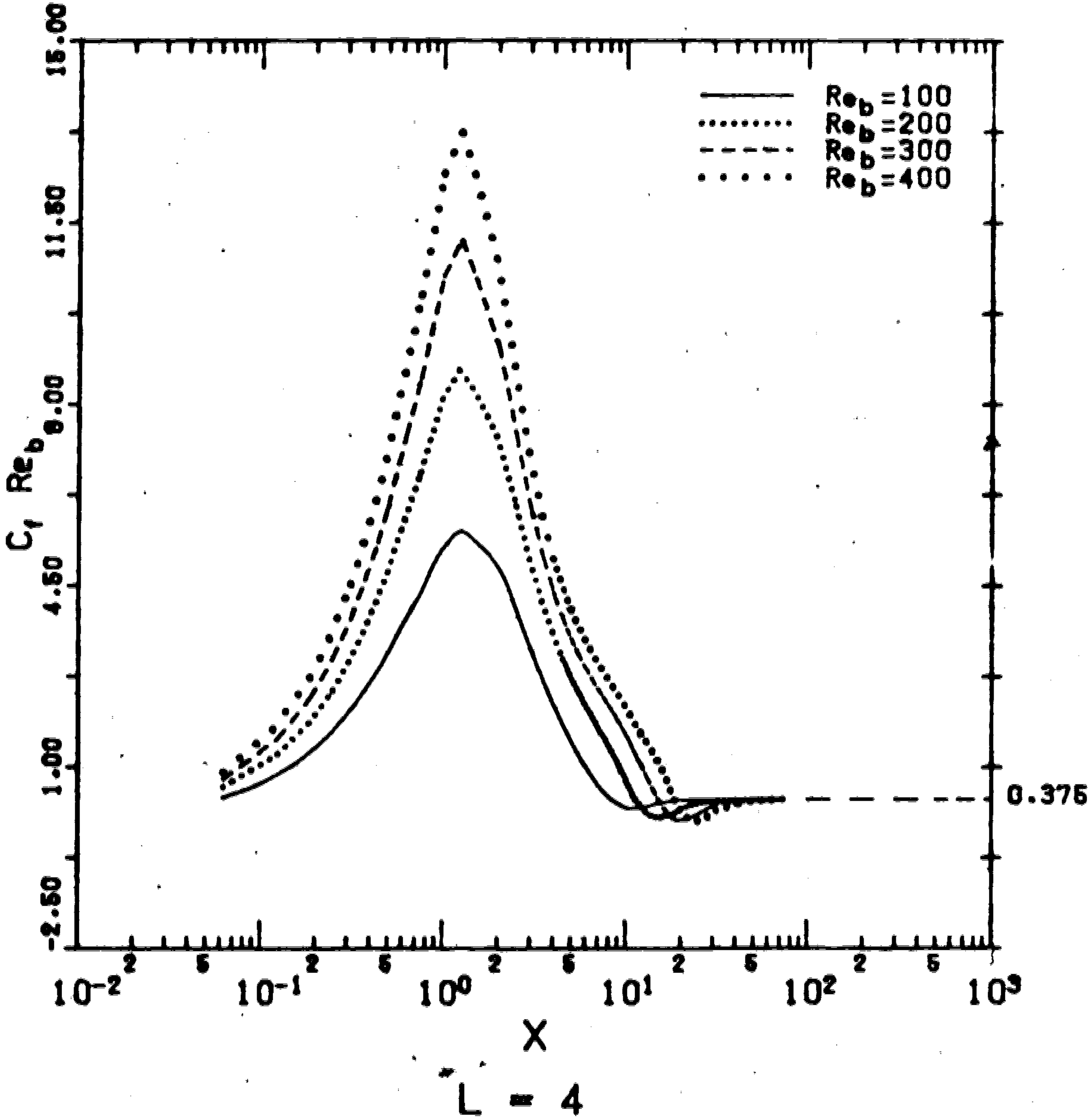

FIGURE 10.48 : VARIATION OF LOCAL SKIN-FRICTION FACTORS FOR L=4 WITH AN INITIAL FLAT VELOCITY PROFILE

short distance and then decreases with the streamwise distance, X. The location of the maximum value is found at X=0.625 for both L=2 and 4, and at X=1.25 for L=12 for a jet with an initial parabolic velocity profile. For a jet with an initial flat velocity profile, the maximum value of $C_f Re_b$ is located approximately at X=1.25 for L=4.

For impinging flow, the skin-friction factor is proportional to the Reynolds number to the power of -0.5. A plot of $0.5C_f Re_b^{0.5}$ versus X for different Reynolds numbers is made so that all the curves will collapse into one general curve in the stagnation flow region. Such plots are shown in Figures 10.49-10.51 for the case of parabolic profile and in Figure 10.52 for the case of flat profile.

For the case of parabolic velocity profile, a general curve cannot be obtained in the range of Reynolds numbers studied. But there is a trend for L=2 and 4 that a general curve may be obtained if the Reynolds number becomes higher. For L=12, the value of $0.5C_f Re_b^{0.5}$ decreases as Reynolds number increases indicating that the normalization of the local skin-friction factor with $Re_b^{0.5}$ may be over-corrected the effect of Reynolds number. This is also probably due to the grid effects as mentioned in Chapter 9 for the case of L=12, resulting in the inaccuracy of the numerical results in the stagnation flow region. The numerical results computed by Van Heiningen et. al. (96) for a semi-confined two-dimensional jet are also included in Figure 10.50. Their results are at Re_b=100 and 450 for L=4. There is good

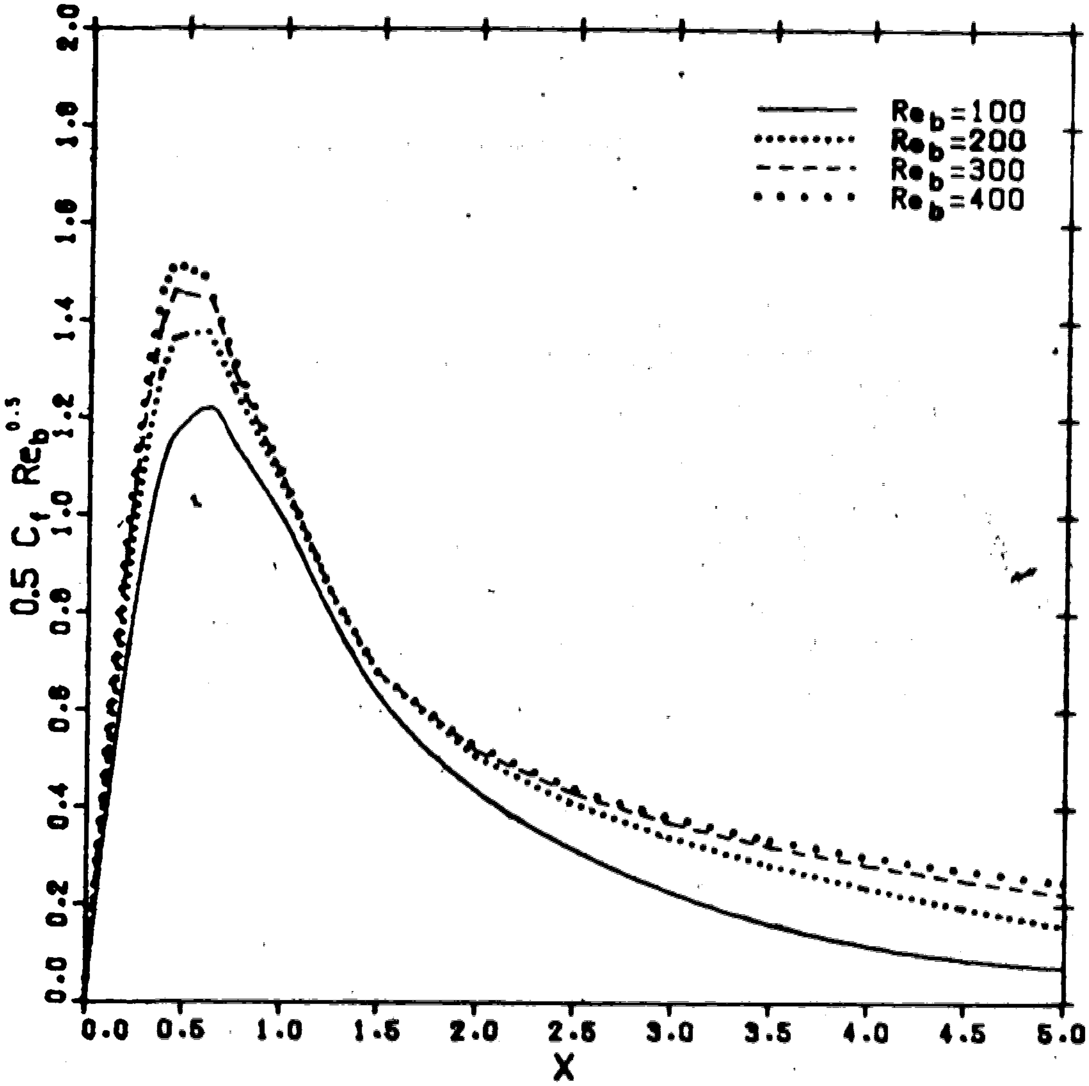

L = 2

FIGURE 10.49 : VARIATION OF LOCAL SKIN-FRICTION FACTORS NEAR THE STAGNATION FLOW REGION FOR L=2 WITH AN INITIAL PARABOLIC VELOCITY PROFILE

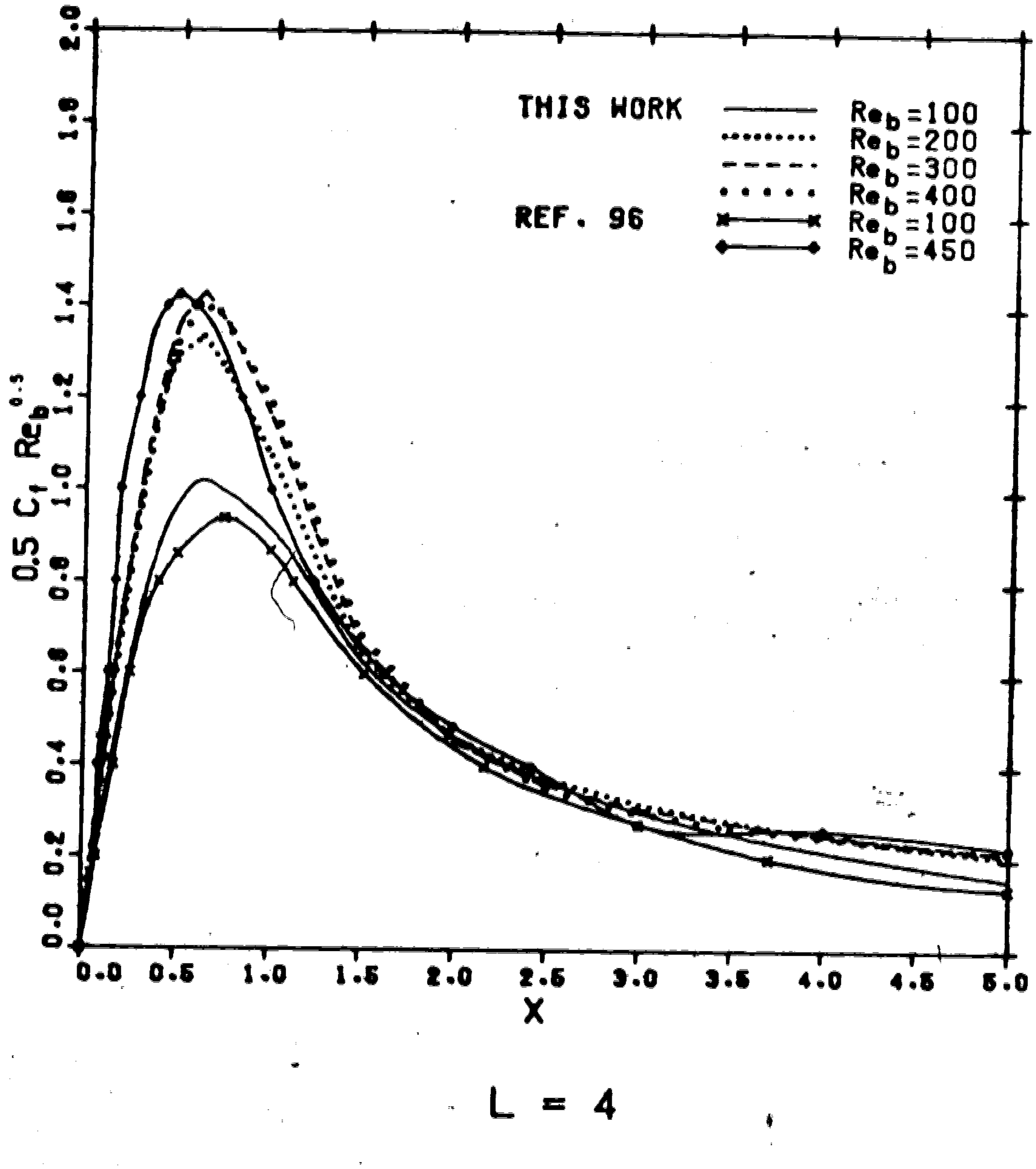

FIGURE 10.50 : VARIATION OF LOCAL SKIN-FRICTION FACTORS NEAR THE STAGNATION FLOW REGION FOR L=4 WITH AN INITIAL PARABOLIC VELOCITY PROFILE

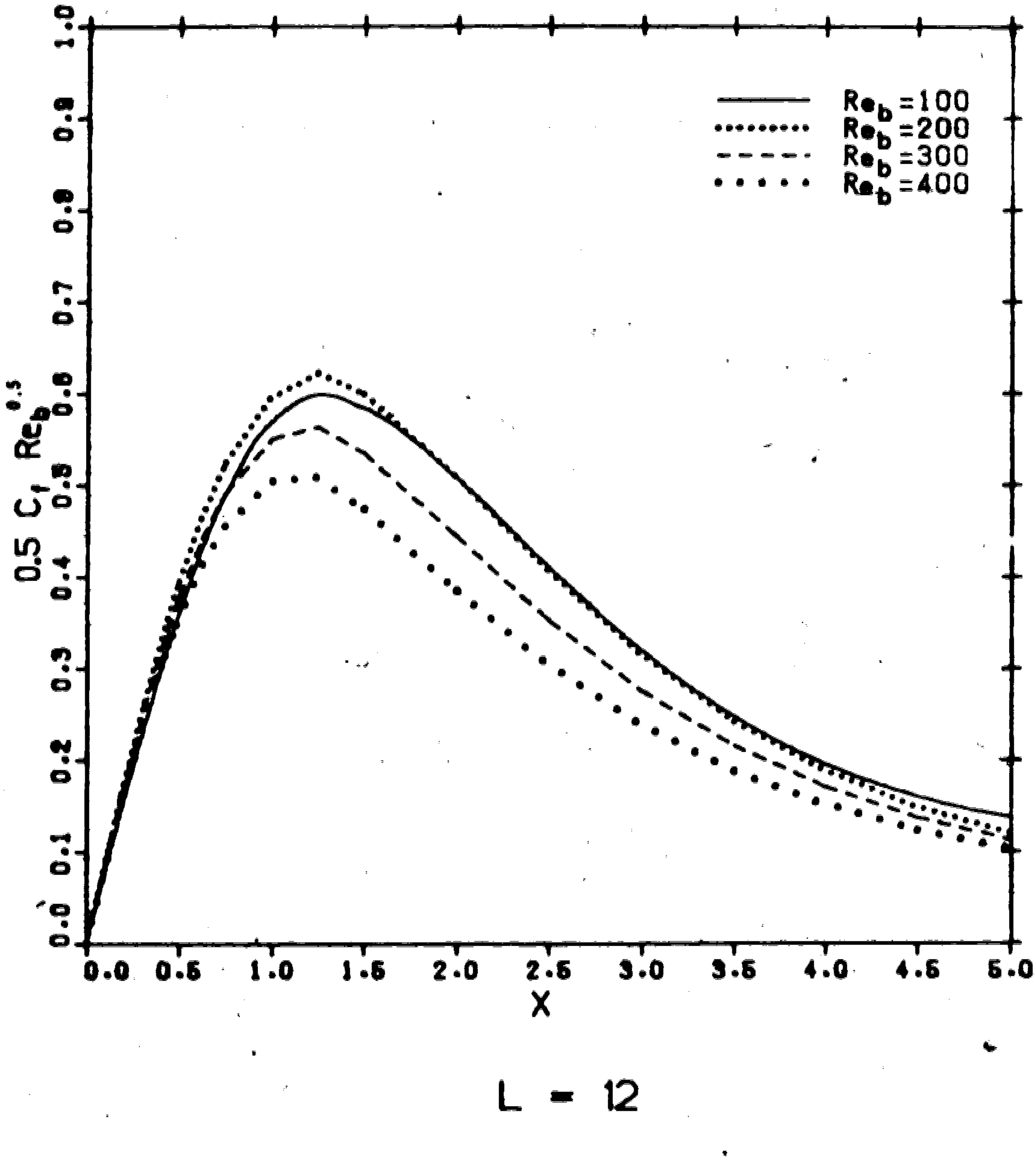

FIGURE 10.51 : VARIATION OF LOCAL SKIN-FRICTION FACTORS NEAR THE STAGNATION FLOW REGION FOR L=12 WITH AN INITIAL PARABOLIC VELOCITY PROFILE

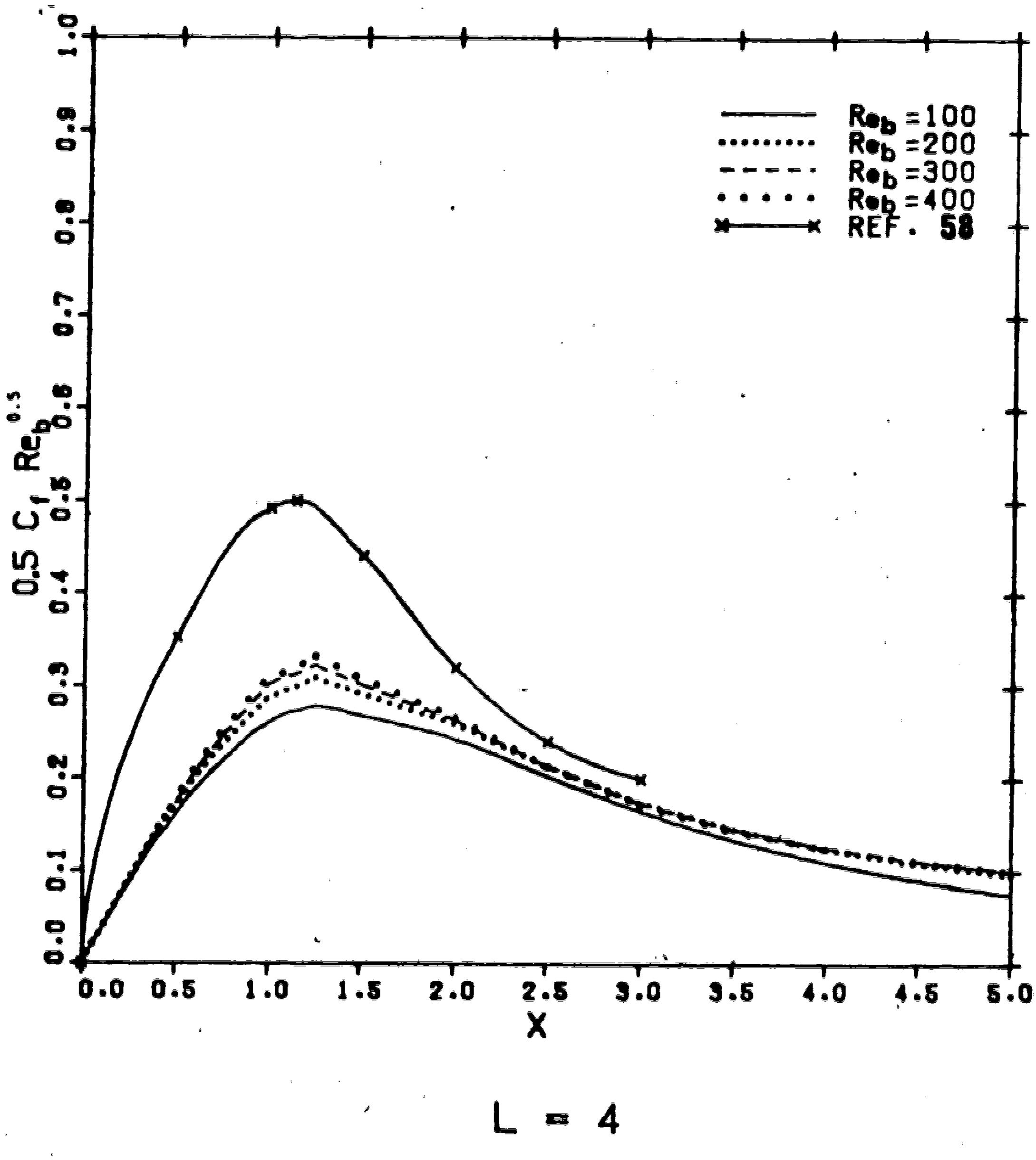

FIGURE 10.52 : VARIATION OF LOCAL SKIN-FRICTION FACTORS NEAR THE STAGNATION FLOW REGION FOR L=4 WITH AN INITIAL FLAT VELOCITY PROFILE

agreement between their results and those of this work.

For the case of flat velocity profile, the collapse of the curves for different Reynolds numbers to nearly a single curve in the stagnation flow region can be noted in Figure 10.52. The curve for Re_b=100 deviates the most from the general curve probably because the Reynolds number in this case is simply not high enough as mentioned above. For Re_b=100, relatively significant retardation of the submerged jet is found on the way from the nozzle exit to the impingement plate. Also included in Figure 10.52 are the theoretical results of Miyazaki and Silberman (58) for an unconfined two-dimensional jet. Their results which are totally independent of Reynolds number and jet-to-plate spacing ($L \geq 1.5$), are consistently higher than those of this work. The disagreement is mainly due to the error introduced by their assumption of potential flow outside the viscous boundary layer.

10.2 MASS TRANSFER CHARACTERISTICS

A measure of local mass transfer is represented by the evaluation of local Sherwood number along the impingement plate. Local Sherwood numbers along the impingement plate are evaluated both experimentally and numerically. Experimental and numerical results of local Sherwood number are first discussed separately, and finally a comparison of these results is made.

10.2.1 EXPERIMENTAL RESULTS

For a confined two-dimensional jet, experimental runs for various experimental variables such as the Reynolds number, jet-to-plate spacing and duration of the mass transfer experiment are made. The range of these experimental variables are listed below

1. Jet-to-plate spacing: L=2, 4, 12
2. Reyolds number: Re_b=100, 200, 306, 400
3. Duration of mass transfer experiment: T=120, 180, 240, 360, 480s
4. Type of velocity profile at nozzle exit: parabolic

A listing of the experimental runs together with the experimental variables and operating conditions are given in Appendix E.

The "frozen fringe" pattern for run no. J021-3B for L=2, Re_b=100 and T=180s is shown in Plate 10.1a. The "frozen fringe" pattern for run no. J021-6A for L=2, Re_b=100 and T=360s is shown in Plate 10.1b. These fringes are interpreted as contours of equal mass transfer rate. The local mass transfer rate can be observed in Plate 10.1 to decrease monotonically from the stagnation flow region. It will be shown later that only for this case of L=2 and Re_b=100, a local minimum and a local maximum in local mass transfer rate is not observed.

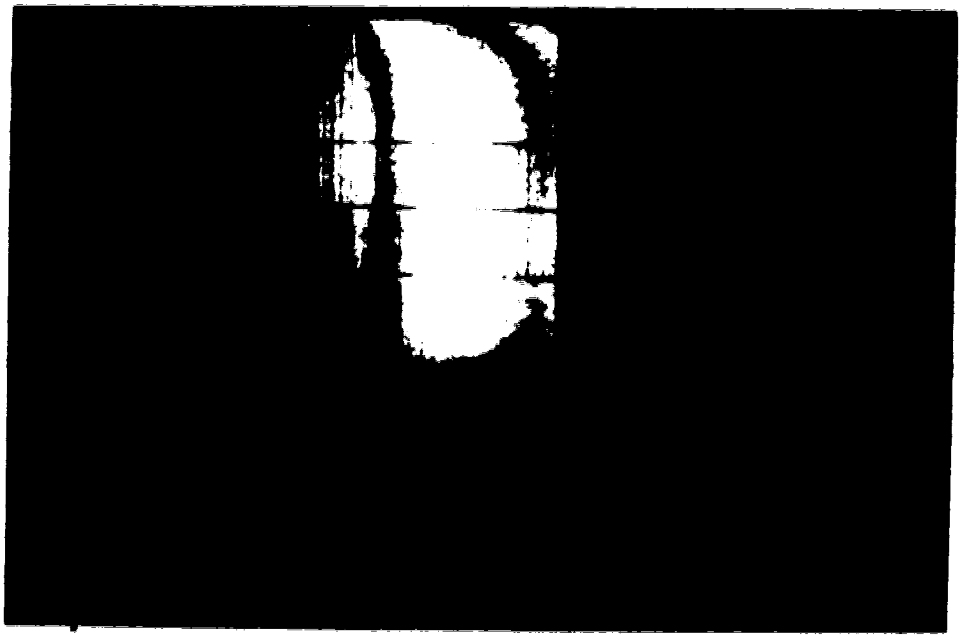

(a) T = 180s

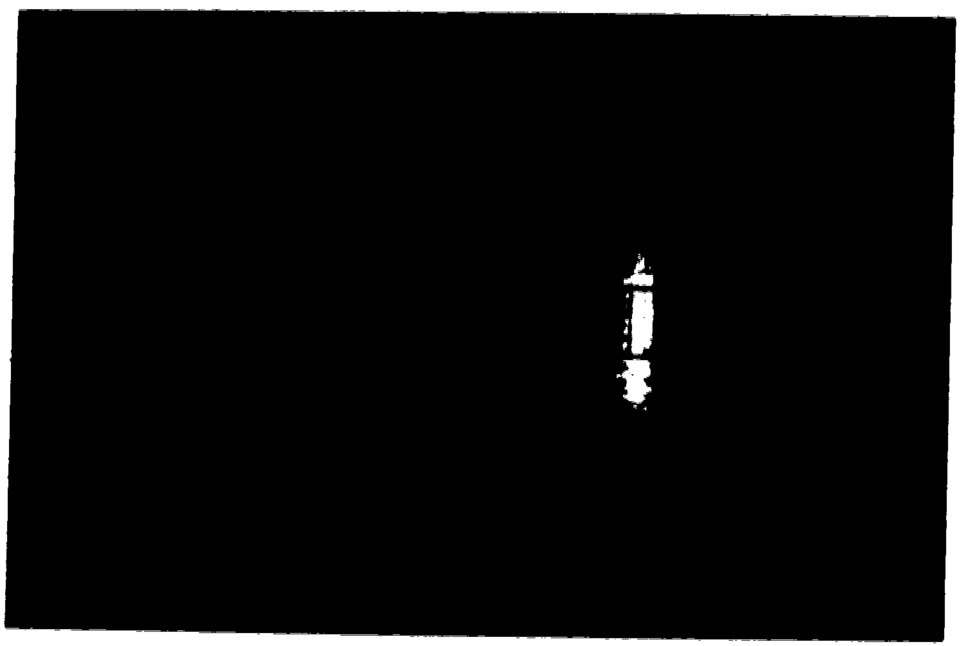

(b) T = 360s

PLATE 10.1 : CONTOURS OF EQUAL MASS TRANSFER RATE FOR A CONFINED TWO-DIMENSIONAL JET (Re_b=100, L=2)

The "frozen fringe" pattern for run no. J023-2B for L=2, Re_b=306 and T=120s is shown in Plate 10.2a. The "frozen fringe" pattern for run no. J023-4B for L=2, Re_b=306 and T=240s is shown in Plate 10.2b. By observing the contours of equal mass transfer rate, the presence of a local minimum and a local maximum in the mass transfer rate can easily be observed in the outer region. The presence of local extrema in the mass transfer rate is observed for all the experimental runs in this work except for the case of Re_b=100 and L=2 mentioned above.

In Plate 10.2, it is of interest to note that the fringes exhibit spanwise fluctuations at the two ends and the outer region. The intensity of these fluctuations increases with Reynolds number and the fluctuation patterns are very much the same for Re_b=306 and 400. This phenomenon was explained by Masliyah and Nguyen (53). The fluctuations are attributed to the presence of very slight roughness at the edge of the aluminum slot tube.

For L=12, a typical "frozen fringe" pattern is shown in Plate 10.3 for run no. J123-2B with Re_b=306 and T=120s. The presence of local extrema in the mass transfer rate is again observed. But in this case the fringes are too wide for analysis. In other words, the local mass transfer rates in this outer region are too small to measure. Therefore, no quantitative study in the outer region for all the experimental runs of L=12 is made.

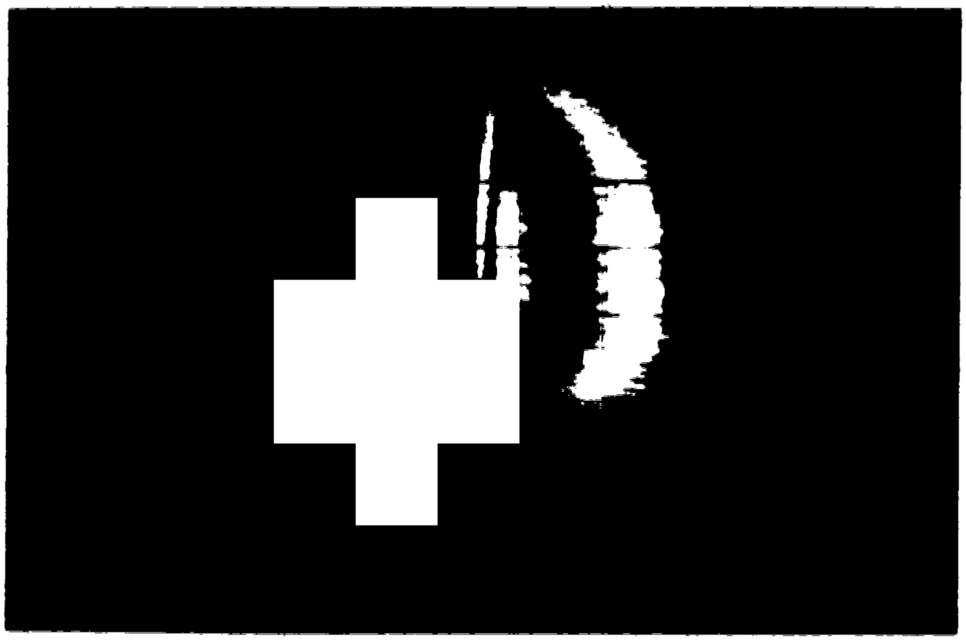

(a) T = 120s

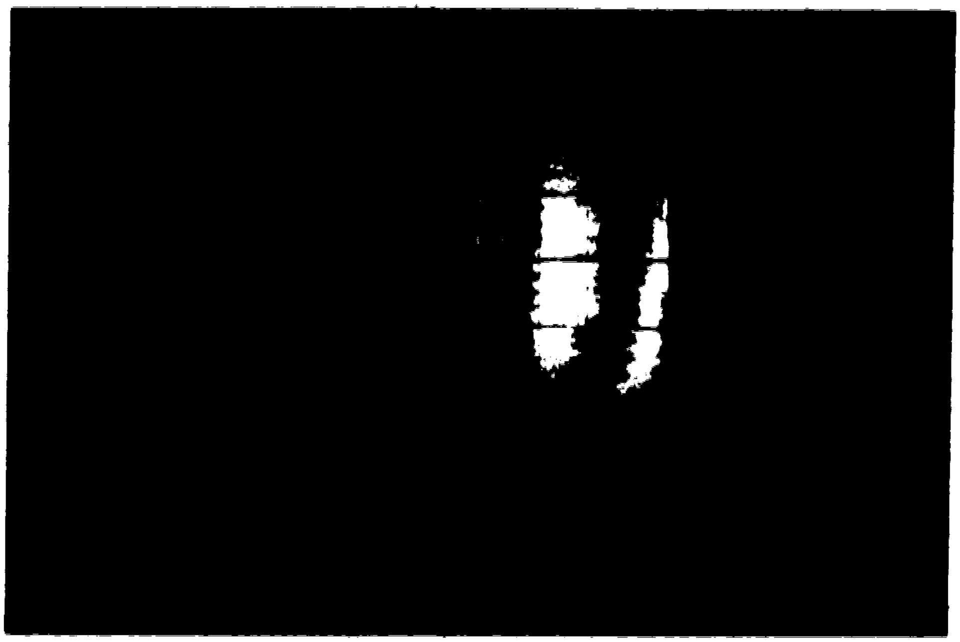

(b) T = 240s

PLATE 10.2 : CONTOURS OF EQUAL MASS TRANSFER RATE FOR A CONFINED TWO-DIMENSIONAL JET (Re_b=306, L=2)

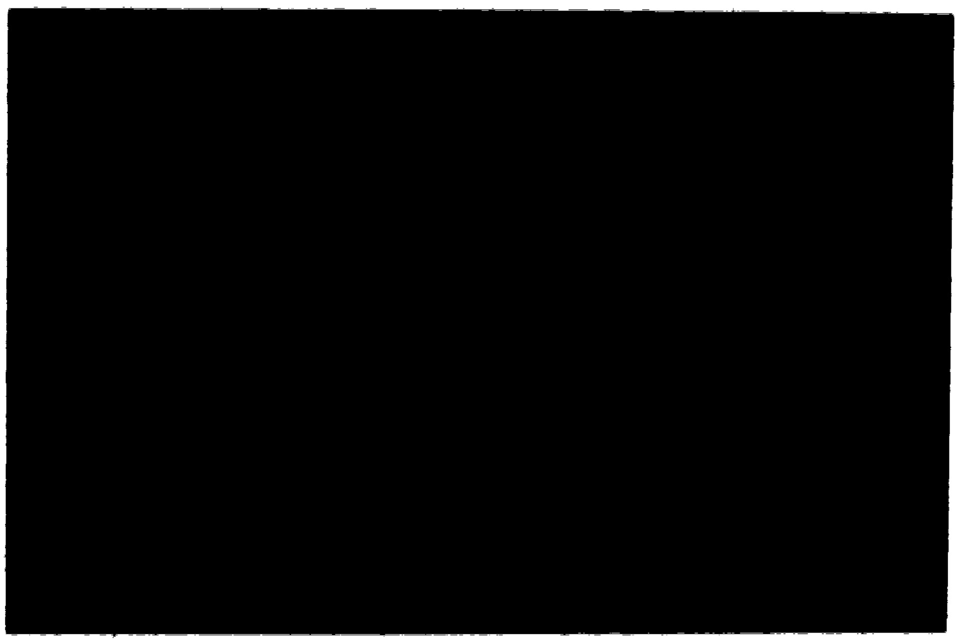

PLATE 10.3 : CONTOURS OF EQUAL MASS TRANSFER RATE FOR A CONFINED TWO-DIMENSIONAL JET (Re_b=306, L=12)

Due to the presence of local extrema in mass transfer rate, more complicated "frozen fringe" pattern for a confined two-dimensional jet is observed. In such a case, in order to determine the local fringe order, the method of zero fringe identification used by Masliyah and Nguyen (51) is no longer applicable. Therefore, real time holographic interferometry is used. In order to determine the fringe order of the "frozen fringe" pattern, a duplicate experimental run is made using real time holography interometric technique.

As soon as the local fringe order is known, local Sherwood number, Sh_b, defined by Equation 5.1 can be easily determined by using Equation 5.9. In this work, only the local Sherwood numbers on the centerline along the streamwise direction are measured. For each experimental run, the variation of local Sherwood number, Sh_b, with dimensionless streamwise distance, x/b or X, are determined. Experimental results of local Sherwood number, Sh_b, and dimensionless streamwise distance, x/b, are given in Appendix E.

Variation of local Sherwood number with X are shown in Figures 10.53-10.55 for L=2, 4 and 12. In general, the variation pattern of the local Sherwood number can be divided into two regions. The first region is where $\log(Sh_b)$ versus $\log(X)$ is linear. The range of such a region is depended on the Reynolds number as can be observed in Figures 10.53-10.55. Regression analysis is made to obtain a

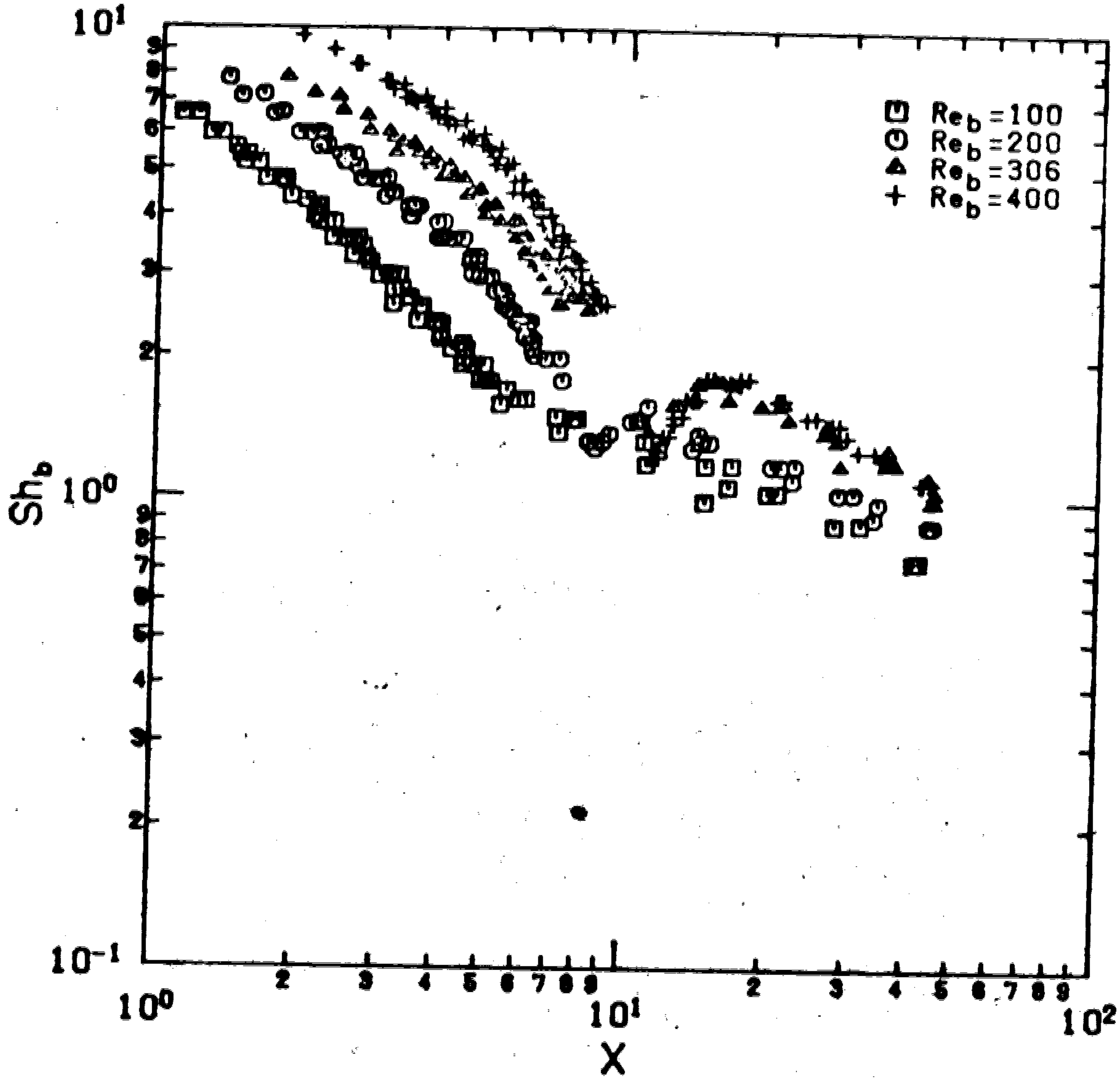

FIGURE 10.53 : VARIATION OF LOCAL SHERWOOD NUMBER WITH DIMENSIONLESS STREAMWISE DISTANCE FOR L = 2

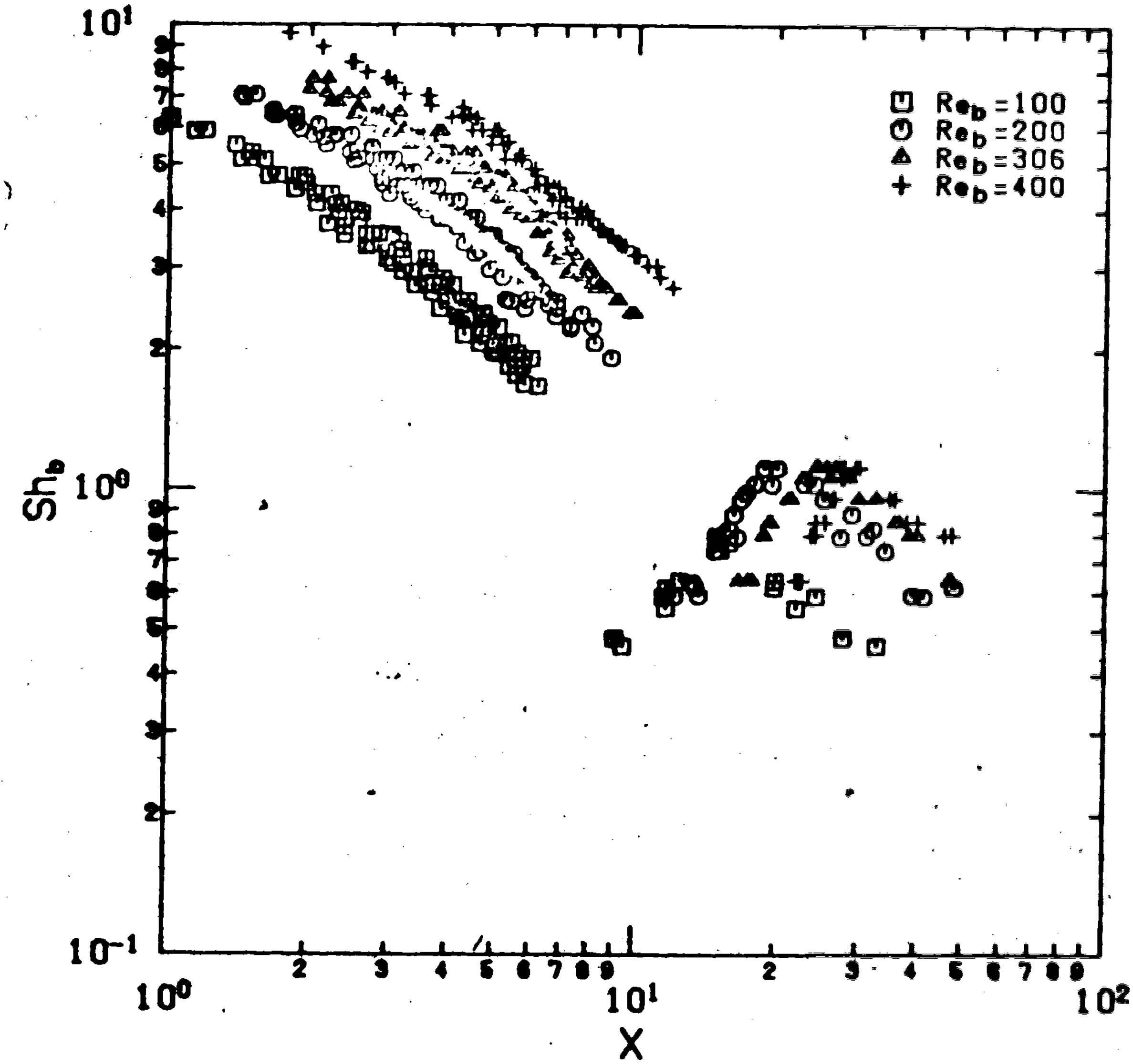

FIGURE 10.54 : VARIATION OF LOCAL SHERWOOD NUMBER WITH DIMENSIONLESS STREAMWISE DISTANCE FOR L = 4

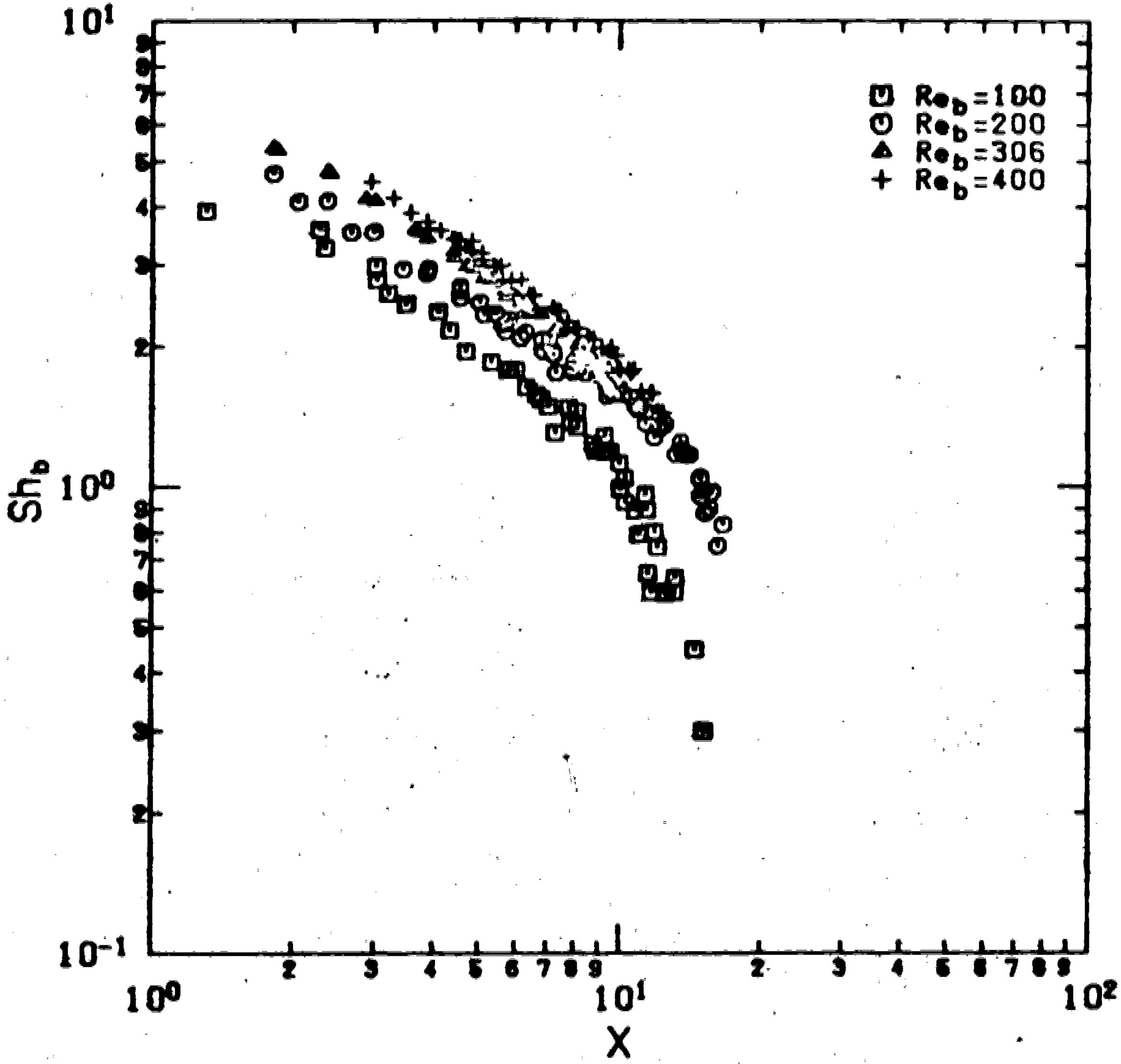

FIGURE 10.55 : VARIATION OF LOCAL SHERWOOD NUMBER WITH DIMENSIONLESS STREAMWISE DISTANCE OF L = 12

correlation for local Sherwood number with the Reynolds number and streamwise distance in this region. The second region is where the local extrema in Sherwood number occured. For L=12, no local Sherwood numbers are measured in this region because the local mass transfer rates are too small to measure. For L=2 and 4, although local Sherwood numbers are measured in this region, no regression analysis is attempted due to the unusual behavior of the local Sherwood number with the Reynolds number and streamwise distance in this region. While the location of the local maximum in Sherwood number shifts further away from the stagnation point when the Reynolds number increases, the value of the local maximum Sherwood number also increases with the Reynolds number.

Two regression equations are obtained from the experimental data for L=2 and 4 and for L=12. The range of data points used is within the region where $\log(Sh_b)$ versus $\log(X)$ is linear and is shown in Table 10.5. The regression analysis is made in such a way that each data point has approximately the same weighting.

The regression equation for L=2 and 4 is given by:

$$Sh_b = 0.34\, Re_b^{0.44}\, X^{-0.70} \qquad (10.6)$$

for $100 \le Re_b \le 400$, with an average error of 6.8%. A total of 685 data points are used. A plot to test the applicability of Equation 10.6 is shown in Figure 10.56. For a perfect fit

TABLE 10.5 : RANGE OF DATA POINTS USED FOR REGRESSIONS EQUATIONS

	Re_b	RANGE	NO. OF DATA POINTS
L=2	100	X≤6	63
	200	X≤8	79
	306	X≤9	66
	400	X≤10	86
L=4	100	X≤7	91
	200	X≤9	111
	306	X≤11	110
	400	X≤12	79
L=12	100	X≤10	32
	200	X≤11	47
	306	X≤12	52
	400	X≤13	60

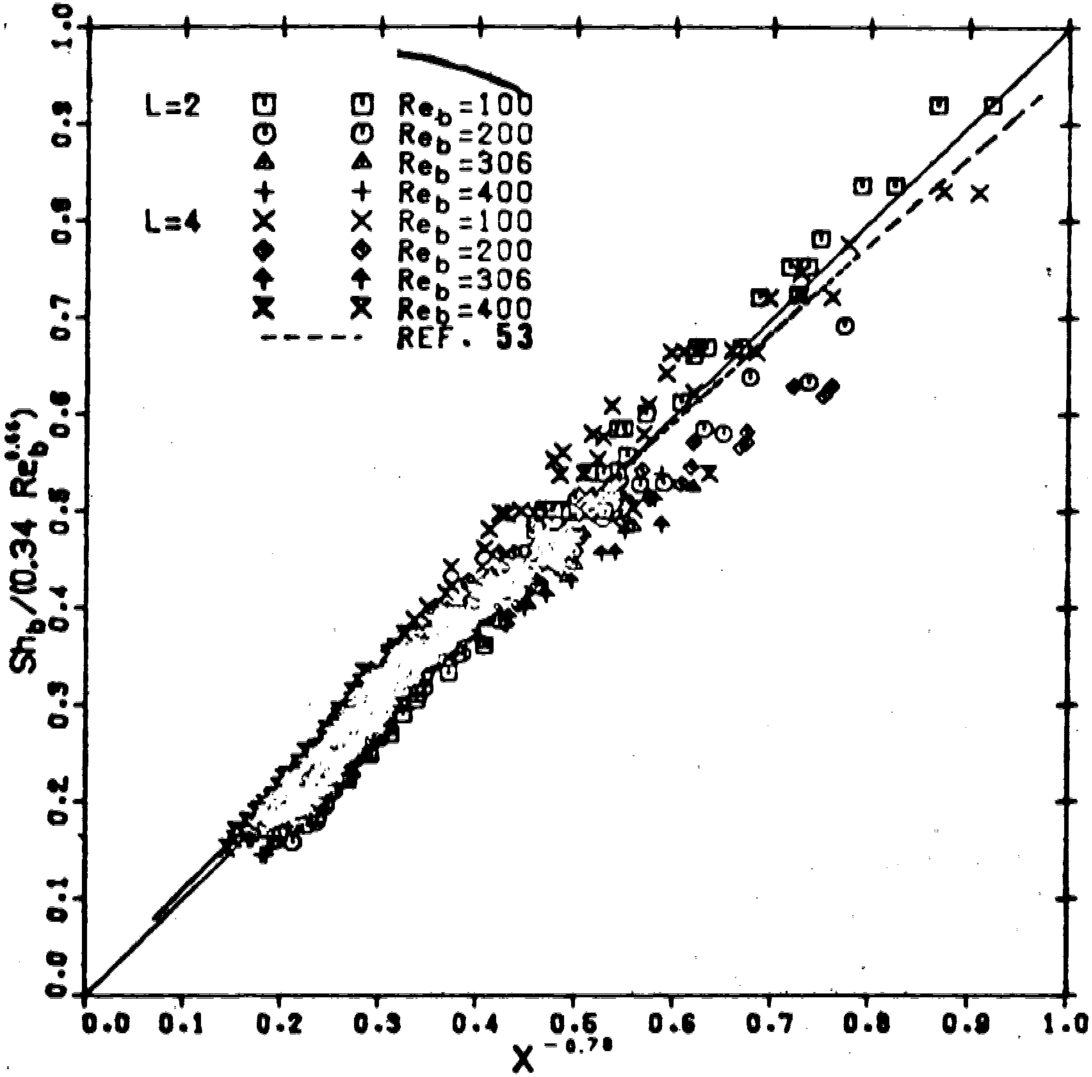

FIGURE 10.56 : TEST OF GOODNESS FIT FOR L = 2 AND 4

with zero experimental error, all data points should lie on a straight line having a slope of unity. In addition, the results obtained by Masliyah and Nguyen (53) presented by Equation 5.14 for unconfined two-dimensional jets with L=4 and 8 are also plotted on Figure 10.56, as a dashed line. Their data are well within the range of the experimental accuracy of this work, indicating that there is little effect of a confinement plate in the wall jet region. However, the effect of confinement plate is obvious in the outer region where the local extrema of the local Sherwood number occur.

The exponent of X, -0.78, in Equation 10.6 is in fair agreement with the experimental findings by Masliyah and Nguyen (53) of -0.73, and the analytical solutions by Schwarz and Caswell (82) of -0.75. Although the exponent of Reynolds number, 0.66, in Equation 10.6 does not agree with either study, it is within the range of their values of 0.55 and 0.75.

The regression equation for L=12 is given by:

$$Sh_b = 1.34\ Re_b^{0.33}\ X^{-0.72} \qquad (10.7)$$

for $100 \le Re_b \le 400$, with an average error of 3.8%. A total of 195 data points are used. A plot to test the applicability of Equation 10.7 is shown in Figure 10.57. The exponent of X, -0.72, in Equation 10.7 is approximately the same as that of L=2 and 4. However, the exponent of Reynolds number,

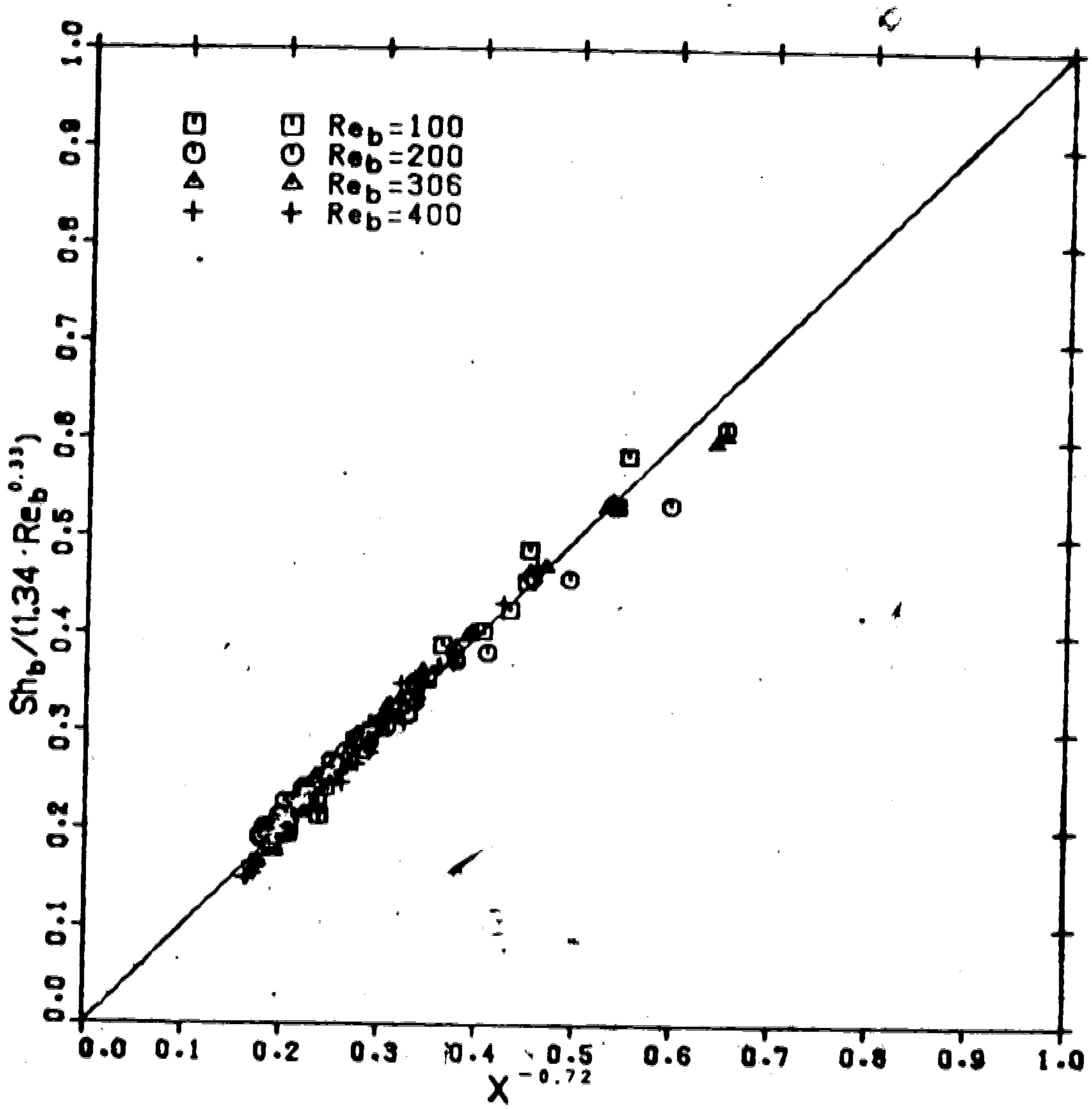

FIGURE 10.57 : TEST OF GOODNESS FIT FOR L = 12

0.33, is less than that for L=2 and 4. This indicates that for L=12, local Sherwood number is a weaker function of Reynolds number than that for L=2 and 4.

10.2.2 NUMERICAL RESULTS

Local Sherwood number, Sh_b', along the impingement plate defined by Equation 5.2 are computed numerically using Equation 8.12 for various Reynolds number, jet-to-plate spacing and type of velocity profile at the nozzle exit. The listings of all the numerical runs for L=2, 4 and 12 are given in Appendix G. In this section, only the numerical results using the upstream-weighted differencing scheme (U.W.D.S.) are presented.

Thermal entrance solutions with a fully developed laminar velocity profile for flow between parallel plates were obtained by McCuen (46,62) for arbitrarily prescribed wall temperature or heat flux. Due to the analogy between heat and mass transfer, entrance solutions of mass transfer with fully developed laminar flow between parallel plates can be obtained. The boundary conditions used in this work are similar to those of the fundamental solution of the third kind. The solution of the third kind corresponding to the coordinate system used in this work is listed in Table 10.6.

Therefore, a plot of 2L Sh_b' versus $(X/2L)/(Re_b Sc)$ for a given jet-to-plate spacing leads to a collapse of curves for the different Reynolds numbers to a general curve in the

TABLE 10.6 : ENTRANCE SOLUTION OF THE THIRD KIND FOR MASS TRANSFER WITH FULLY DEVELOPED LAMINAR FLOW BETWEEN PARALLEL PLATES

$(X/2L)/(Re_b Sc)$	$2L\ Sh_b'$
0.0025	9.250
0.01	6.259
0.015	5.705
0.025	5.206
0.05	4.902
0.075	4.866
0.1	4.861
0.15	4.861
0.25	4.861
INFINITY	4.861

outflow region. The general curve approachs the fully developed value of 2L Sh_b' =4.861 in a manner similar to the solution curve obtained from Table 10.6. Such plots are shown in Figures 10.58-10.60 for a jet with an initial parabolic profile and in Figure 10.61 for a jet with an initial flat profile.

It is noted that in Figures 10.58-10.61, the group $(X/2L)/(Re_b Sc)$ fails to correlate the local Sherwood number for the different Reynolds numbers in the region influenced by the impinging jet. It is only good in the outflow region where the flow behavior is similar to those between two parallel plates. Furthermore, from Figures 10.58-10.61, the values of 2L Sh_b' approach 4.861 in a similar manner regardless of the jet Reynolds number, jet-to-plate spacing and the initial velocity profile at the nozzle exit.

The effect of Reynolds number on the local Sherwood number for different jet-to-plate spacings are shown in Figures 10.62-10.64 for the case of parabolic profile and in Figure 10.65 for the case of flat profile. The maximum local Sherwood number is found to occur at the stagnation point for all cases. The local Sherwood number remains quite constant in the stagnation flow region directly below the jet nozzle ($X \leq 0.5$), and it then decreases with distance away from the stagnation point.

For all cases with an initial parabolic profile, except the case of L=2 and Re_b=100, the local Sherwood number is found to exhibit a local minimum and a local maximum in the

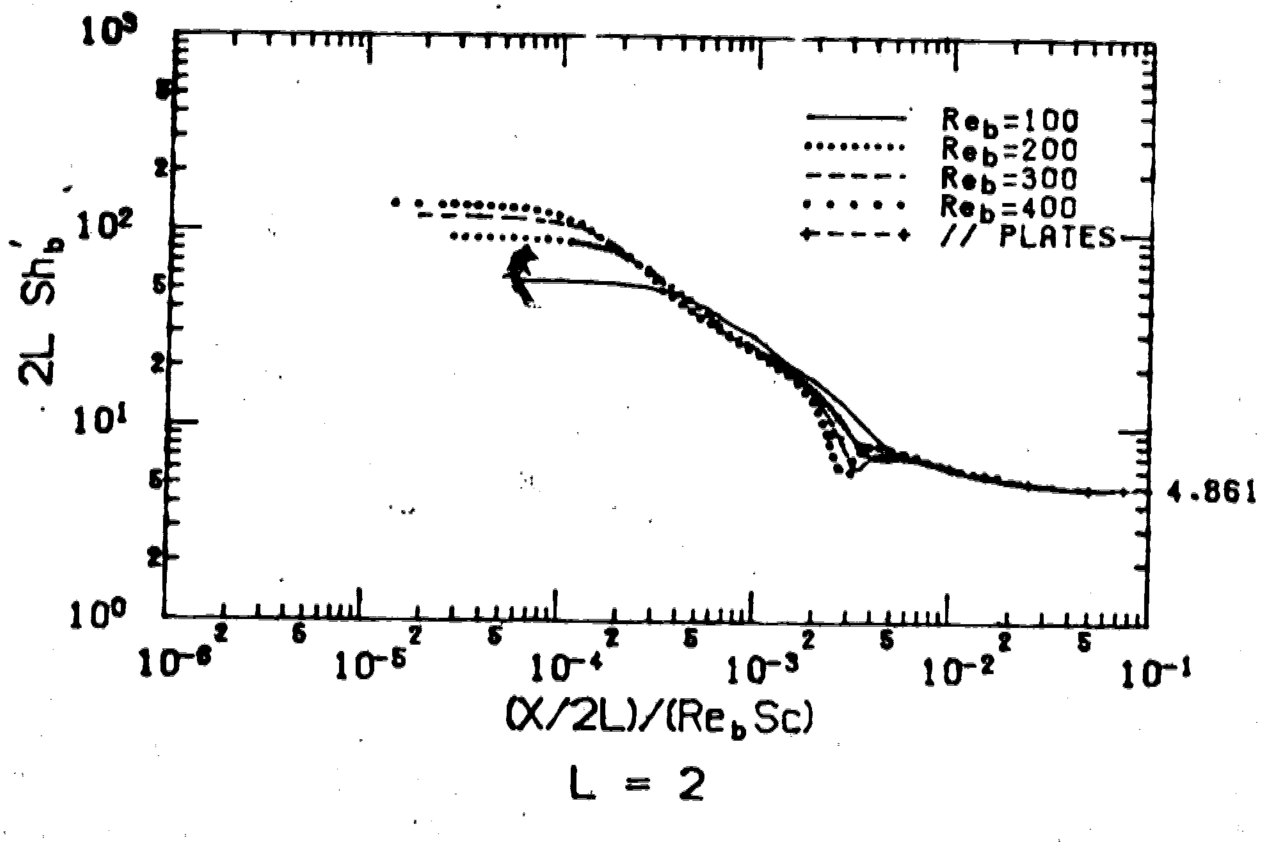

FIGURE 10.58 : PLOTS OF (2L Sh_b') VERSUS (X/2L)/(Re_bSc) FOR L=2 WITH AN INITIAL PARABOLIC PROFILE

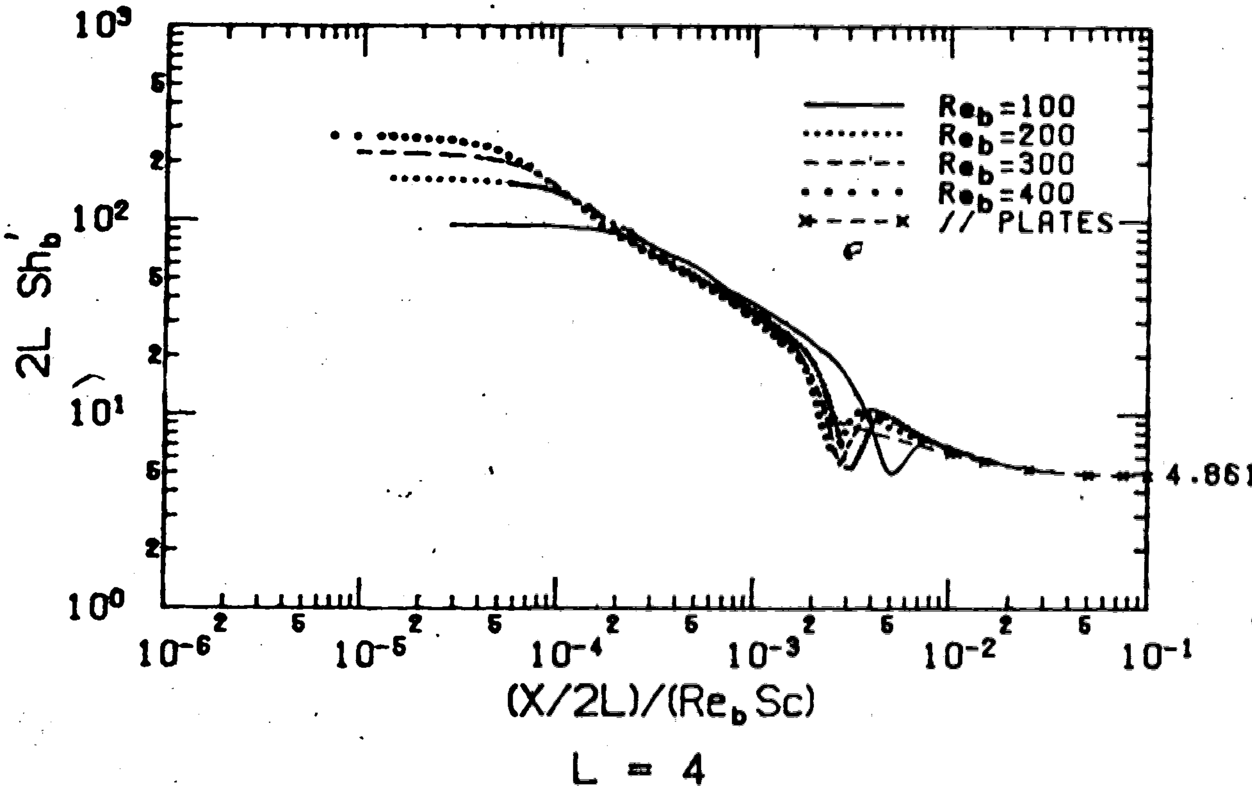

FIGURE 10.59 : PLOTS OF (2L Sh_b') VERSUS (X/2L)/(Re_bSc) FOR L=4 WITH AN INITIAL PARABOLIC PROFILE

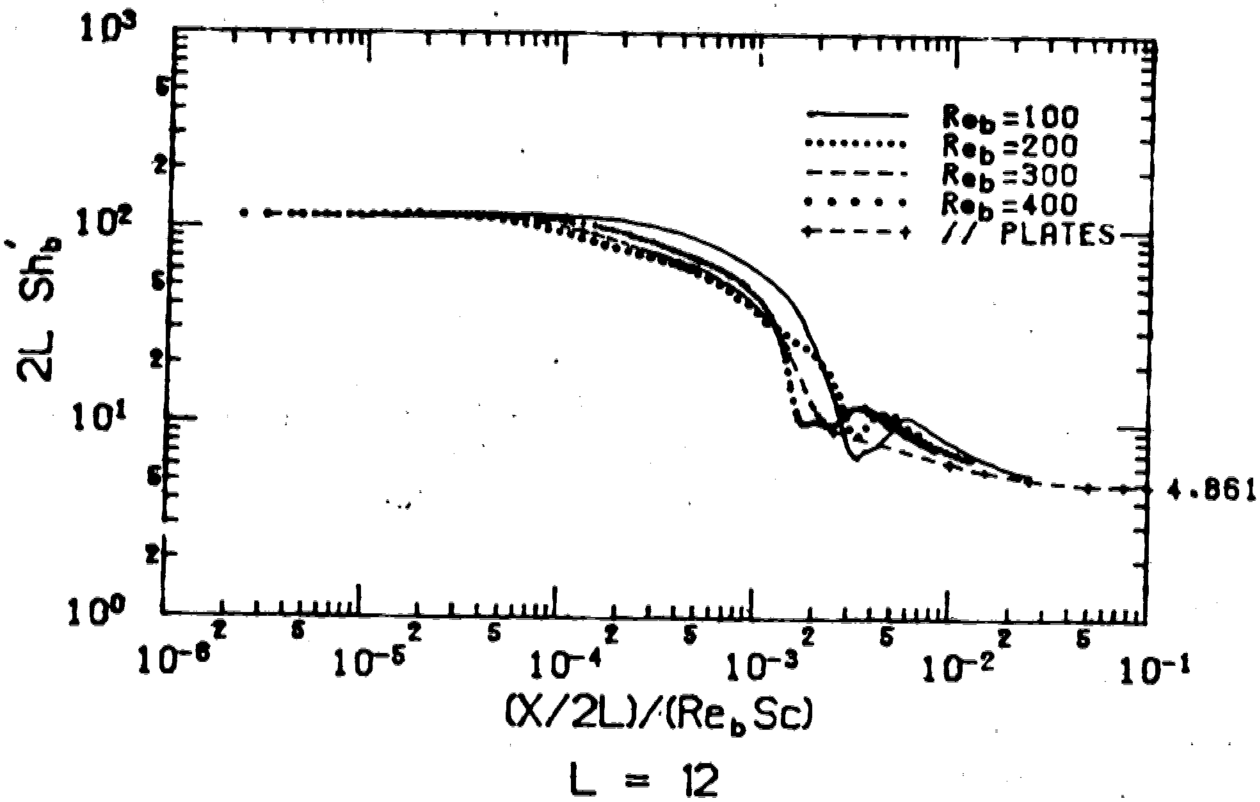

FIGURE 10.60 : PLOTS OF (2L Sh_b') VERSUS (X/2L)/(Re_bSc) FOR L=12 WITH AN INITIAL PARABOLIC PROFILE

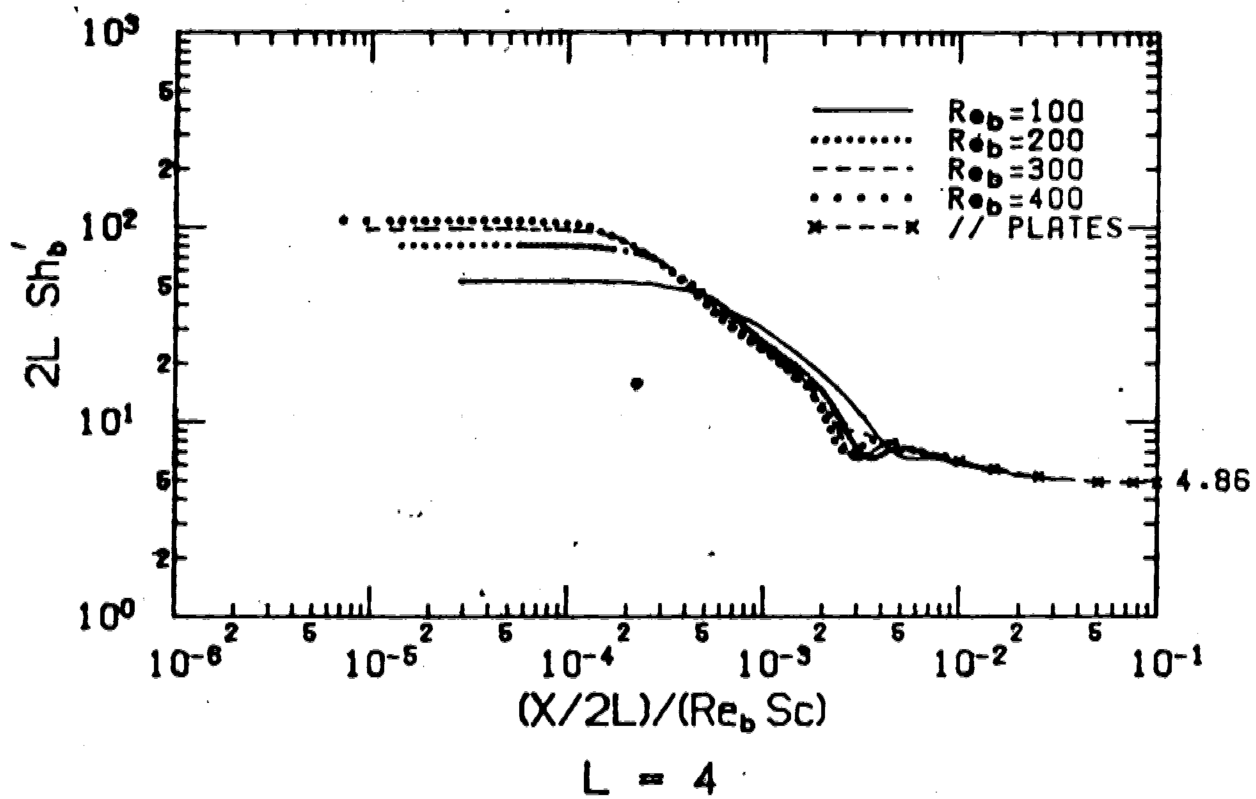

FIGURE 10.61 : PLOTS OF (2L Sh_b') VERSUS (X/2L)/(Re_bSc) FOR L=4 WITH AN INITIAL FLAT PROFILE

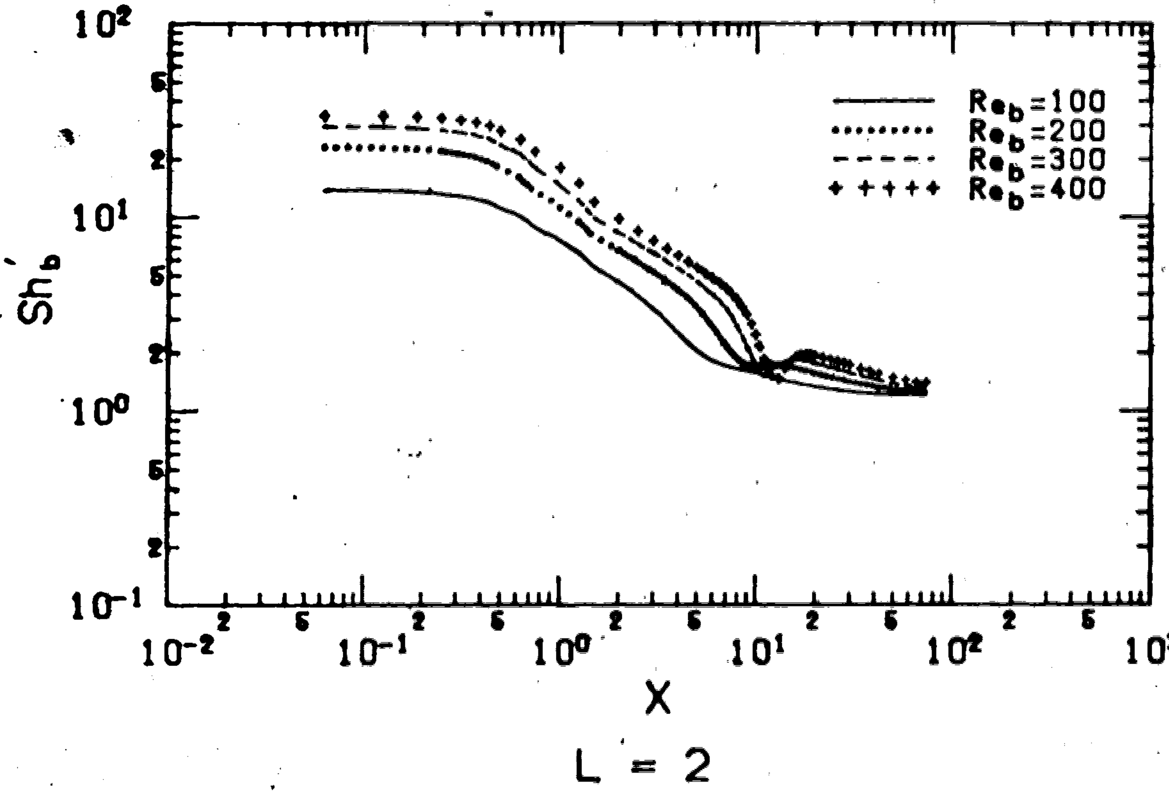

FIGURE 10.62 : VARIATION OF LOCAL SHERWOOD NUMBER FOR L=2 WITH AN INITIAL PARABOLIC PROFILE

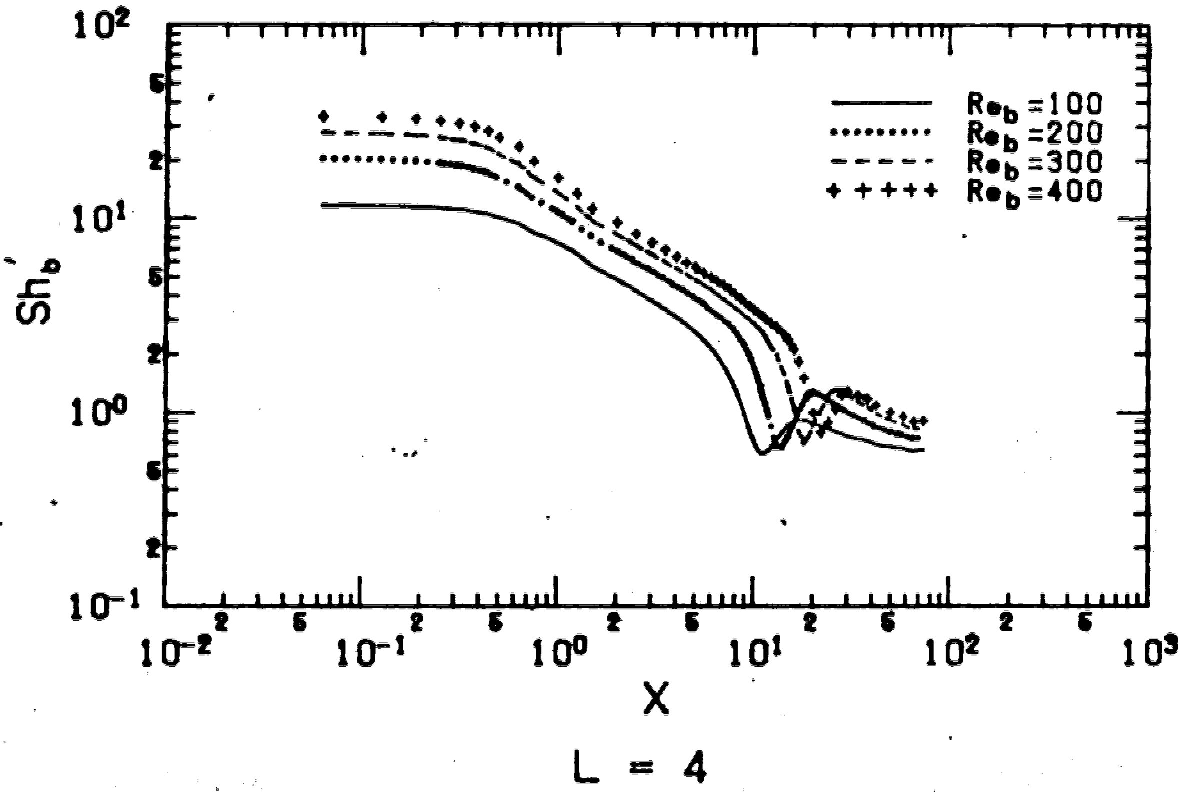

FIGURE 10.63 : VARIATION OF LOCAL SHERWOOD NUMBER FOR L=4 WITH AN INITIAL PARABOLIC PROFILE

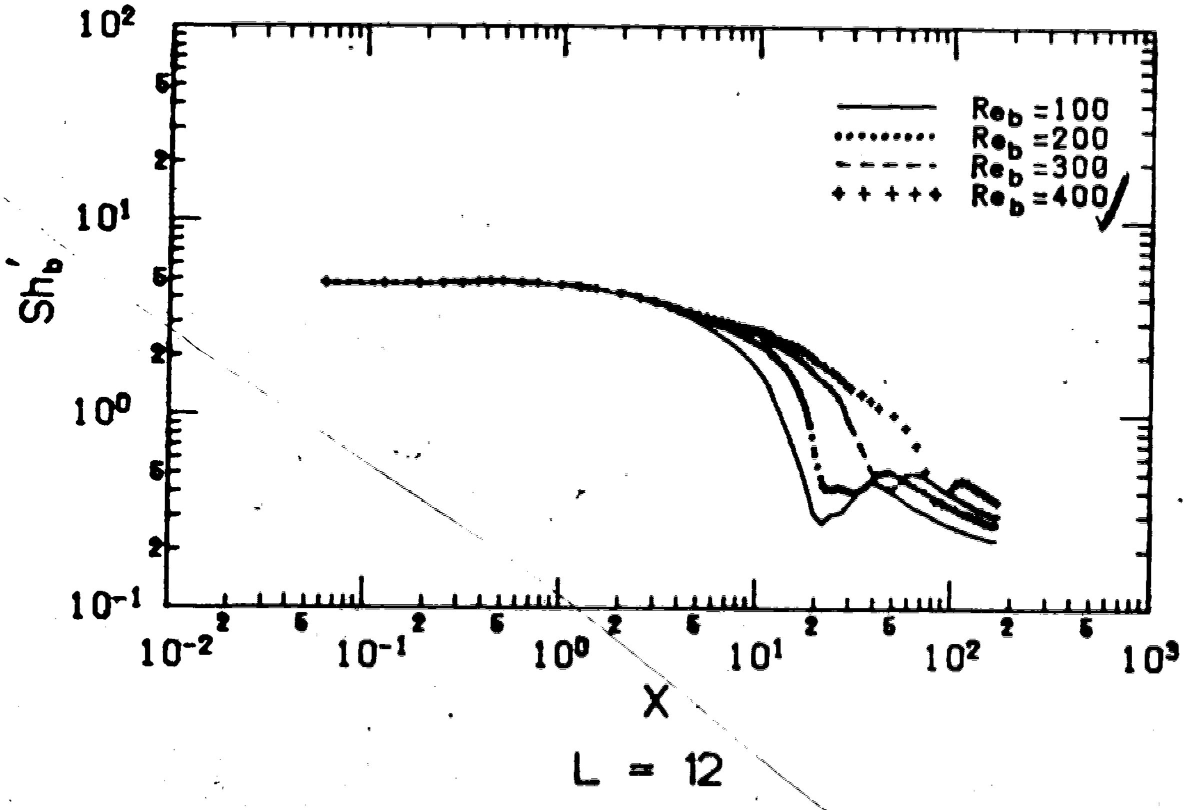

FIGURE 10.64 : VARIATION OF LOCAL SHERWOOD NUMBER FOR L=12 WITH AN INITIAL PARABOLIC PROFILE

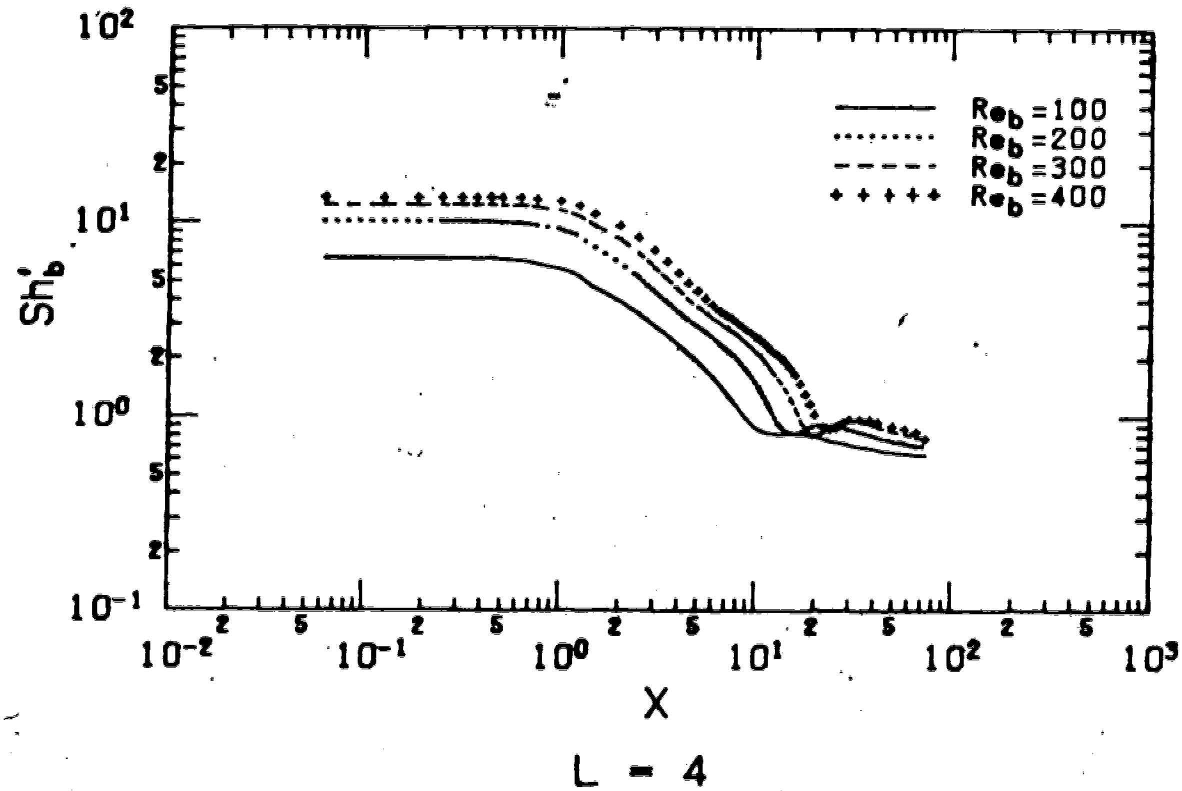

FIGURE 10.65 : VARIATION OF LOCAL SHERWOOD NUMBER FOR L=4 WITH AN INITIAL FLAT PROFILE

region further downstream. The locations of the extrema points are a function of Reynolds number and jet-to-plate spacing. Contours of the stream-function, shown in Figures 10.1-10.3, indicate that the presence of these extrema is attributed to flow recirculation in the region between the confinement plate and the impingement plate. In particular, Figure 10.66 compares the streamwise location of the secondary vortex centre and the streamwise location of the minimum of Sherwood number. The data points fall fairly closely on a straight line with a slope of unity. This indicates that there is a strong correlation between the streamwise location of the secondary vortex and the local minimum of the Sherwood number.

Local extrema in Sherwood number are also found for all cases with an initial flat profile. Only this time, the extrema are not as obvious as those for the case of parabolic profile.

The effect of initial jet velocity profile on local Sherwood number can be studied from Figures 10.63 and 10.65. The local Sherwood number for the case of parabolic profile is consistently higher than that for the case of flat profile at a given Reynolds number except in the region where the local minimum of Sherwood number occurs. Significant difference is found in the stagnation flow region where the stagnation point Sherwood number for the case of parabolic profile is between 1.8 and 2.5 times that for the case of flat profile. Such an effect of initial

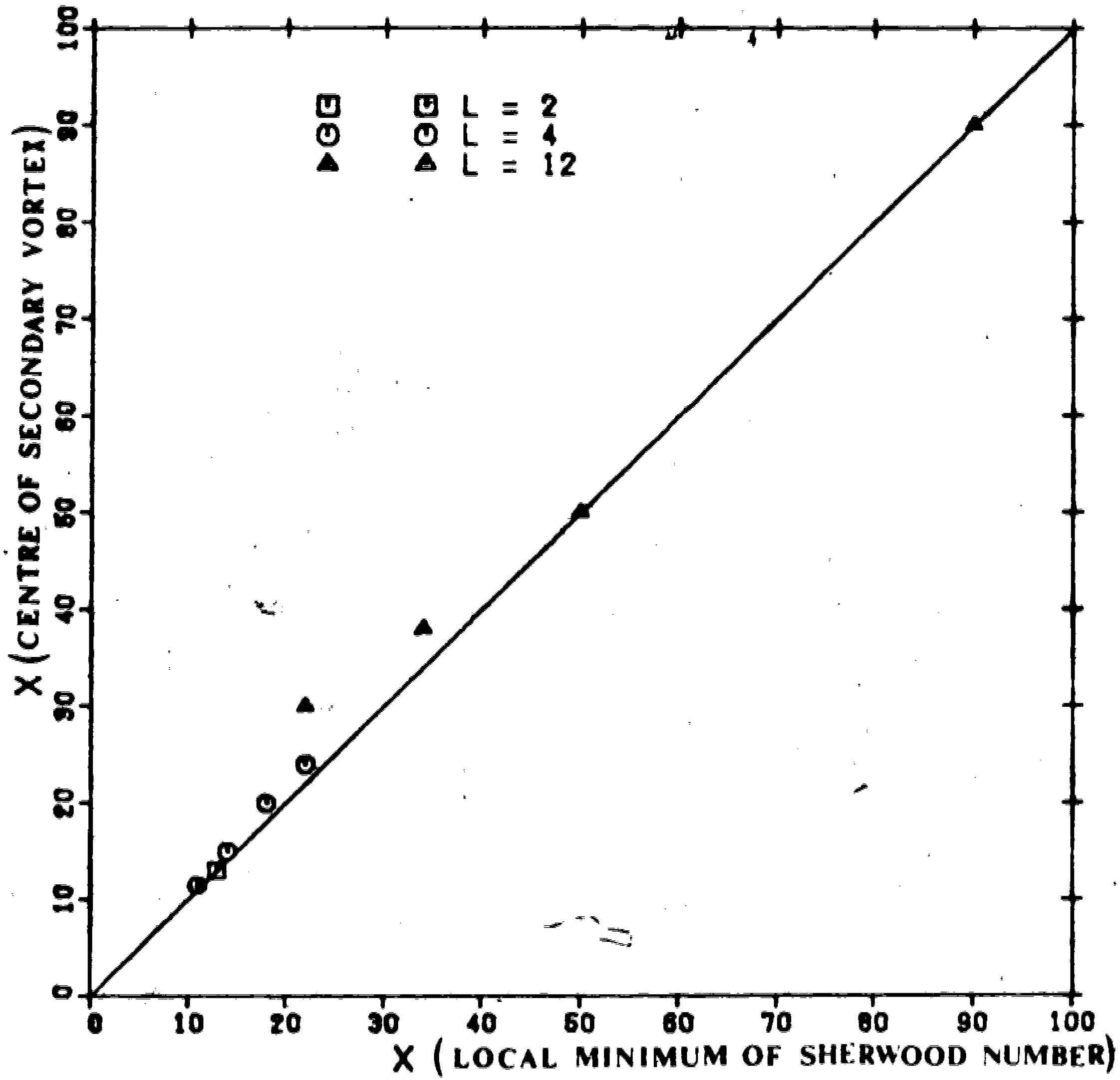

FIGURE 10.66 : STREAMWISE LOCATIONS OF SECONDARY VORTEX CENTRE AND LOCAL MINIMUM SHERWOOD NUMBER

velocity profile was also observed by numerous investigators (77,81,90,96) in their studies of both unconfined and semi-confined jets.

The effect of jet-to-plate spacing on the local Sherwood number for different Reynolds numbers is shown in Figure 10.67 for the case of parabolic profile. Comparing the cases of L=2 and 4, there is no significant difference in the local Sherwood number in the wall jet region before the minimum in Sherwood number occurs. While in the stagnation flow region, only slight difference in Sherwood number is found for the case of low Reynolds numbers. This observation is similar to those by various investigators (19,53,79) studying heat and mass transfer due to an unconfined impinging jet for a small jet-to-plate spacing. But for the case of L=12, local Sherwood numbers in the the stagnation flow and the wall jet regions are consistently lower than those for L=2 and 4. This can be explained in that the impingement plate is no longer located inside the potential core of the submerged jet, therefore the decayed centerline approaching velocity results in a lower mass transfer rate in the stagnation flow region.

10.2.2.1 STAGNATION POINT SHERWOOD NUMBER

Since the stagnation point Sherwood number, Sh_o , is very difficult to measure in the experimental set-up of this work, the stagnation point Sherwood numbers computed numerically are compared with the results in the literature.

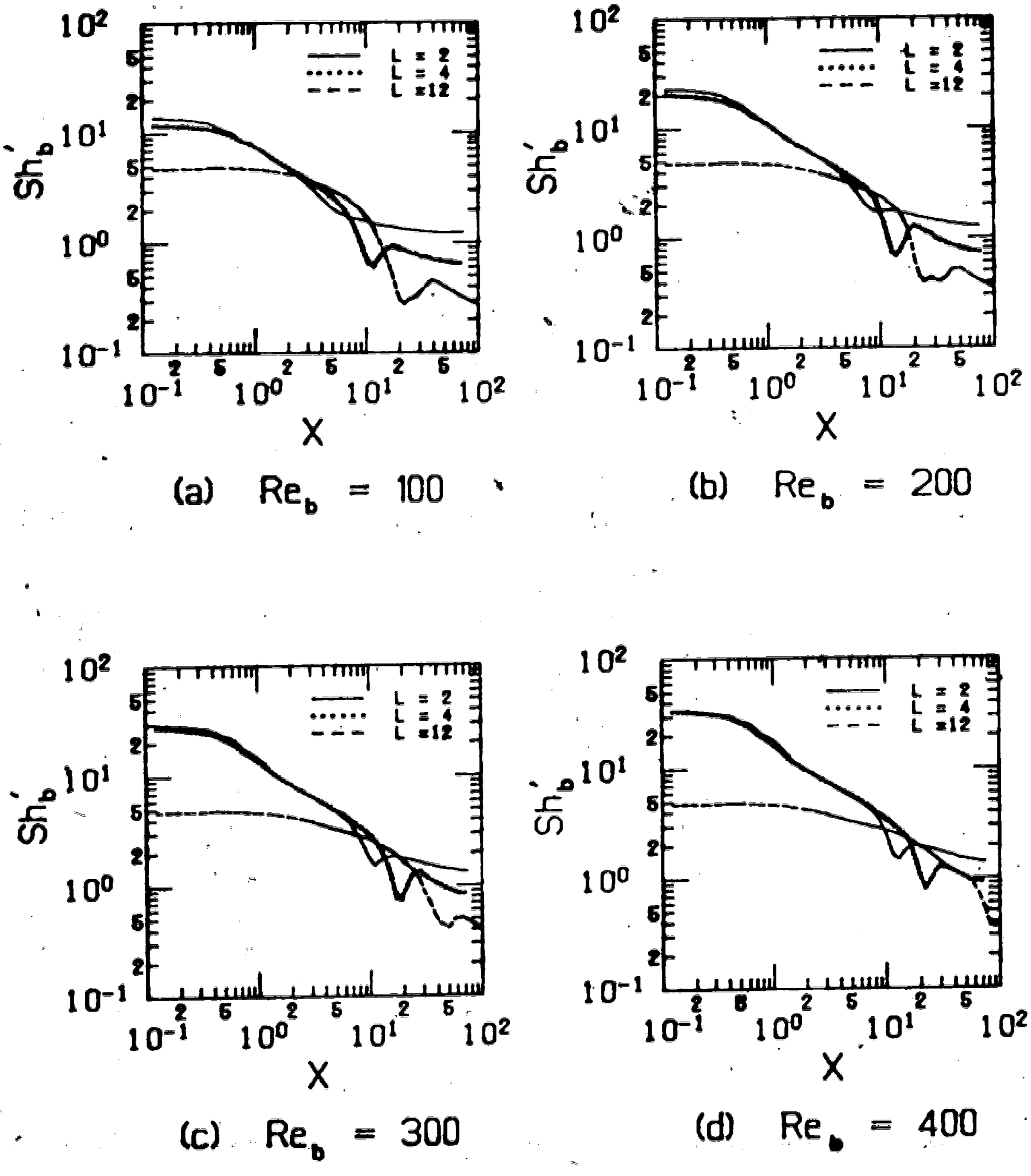

FIGURE 10.67 : EFFECT OF JET-TO-PLATE SPACING ON LOCAL SHERWOOD NUMBER FOR THE CASE OF PARABOLIC VELOCITY PROFILE

Comparison of stagnation point Sherwood numbers evaluated in this work for L=2 and 4 with those in the literature for the case of parabolic profile is shown in Figure 10.68. It is noted that the difference between the stagnation point Sherwood number of this work for two different jet-to-plate spacings of L=2 and 4 is higher at low Reynolds numbers. As Reynolds number increases, this difference diminishs. Also included in Figure 10.68 are the experimental results for an unconfined jet given by Sparrow and Wong (90), the theoretical results for an unconfined jet given by Sparrow and Lee (90) in Equation 2.24 and the numerical results for a semi-confined jet computed by Van Heiningen et. al. (96). Comparing the stagnation point Sherwood number for L=4 of this work with that computed by Van Heiningen et. al., the stagnation point Sherwood number of this work is consistently higher. This is probably due to the assumption of fully developed flow at the outflow region of X=16.4 and 42 for Re_b=100 and 450, respectively by Van Heingingen et. al.. Such streamwise locations of X=16.4 and 42 for Re_b=100 and 450, respectively are very close to the locations where the local extrema in Sherwood number occur as can be noted in Figure 10.63.

Comparison of stagnation point Sherwood numbers evaluated in this work for L=4 with those in the literature for the case of flat profile is shown in Figure 10.69. Included in Figure 10.69 are the theoretical results for an unconfined jet given by Miyazaki and Silberman (58) in

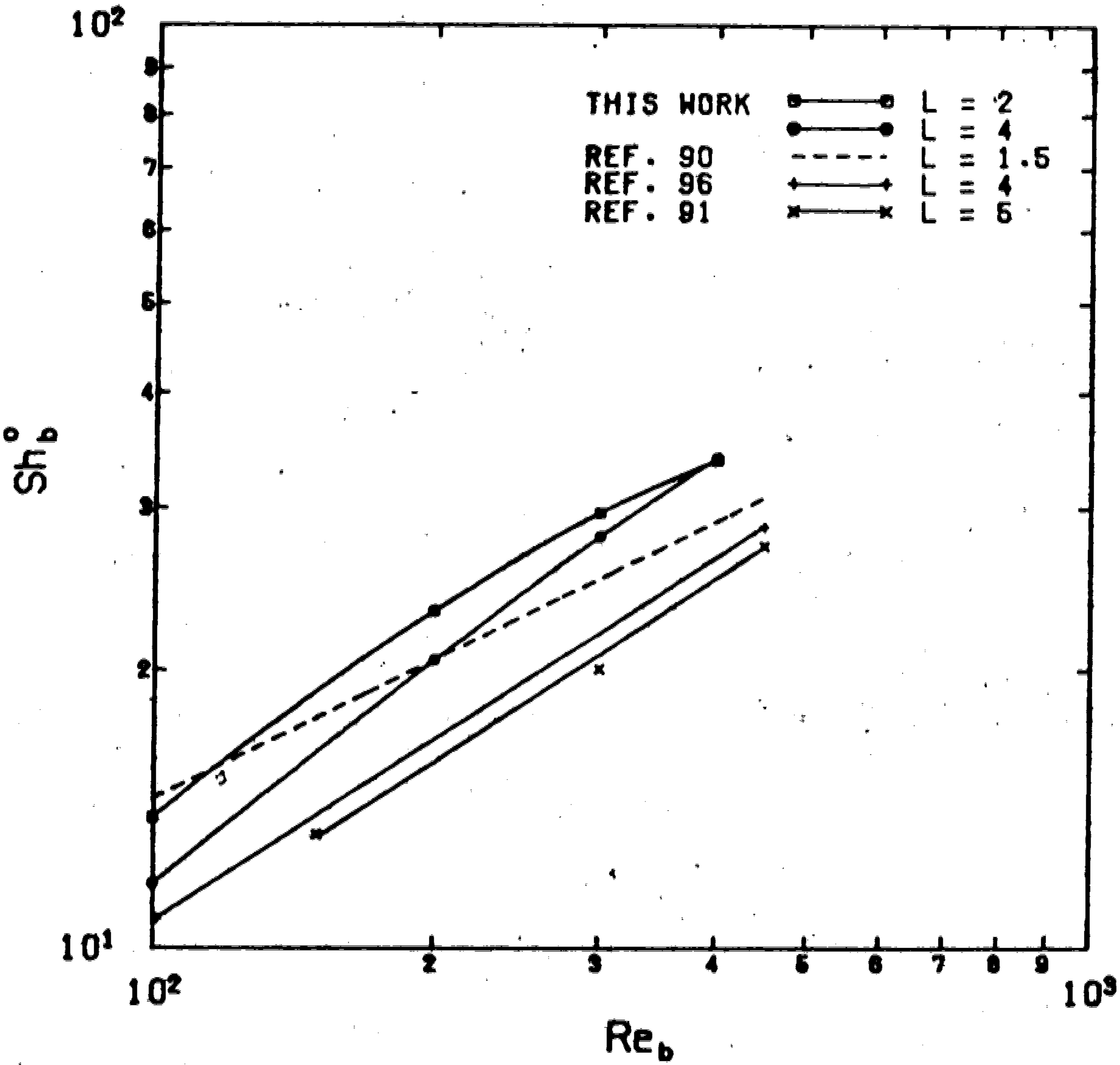

FIGURE 10.68 : COMPARISON OF STAGNATION POINT SHERWOOD NUMBER WITH LITERATURE FOR THE CASE OF PARABOLIC VELOCITY PROFILE (Sc=2.74)

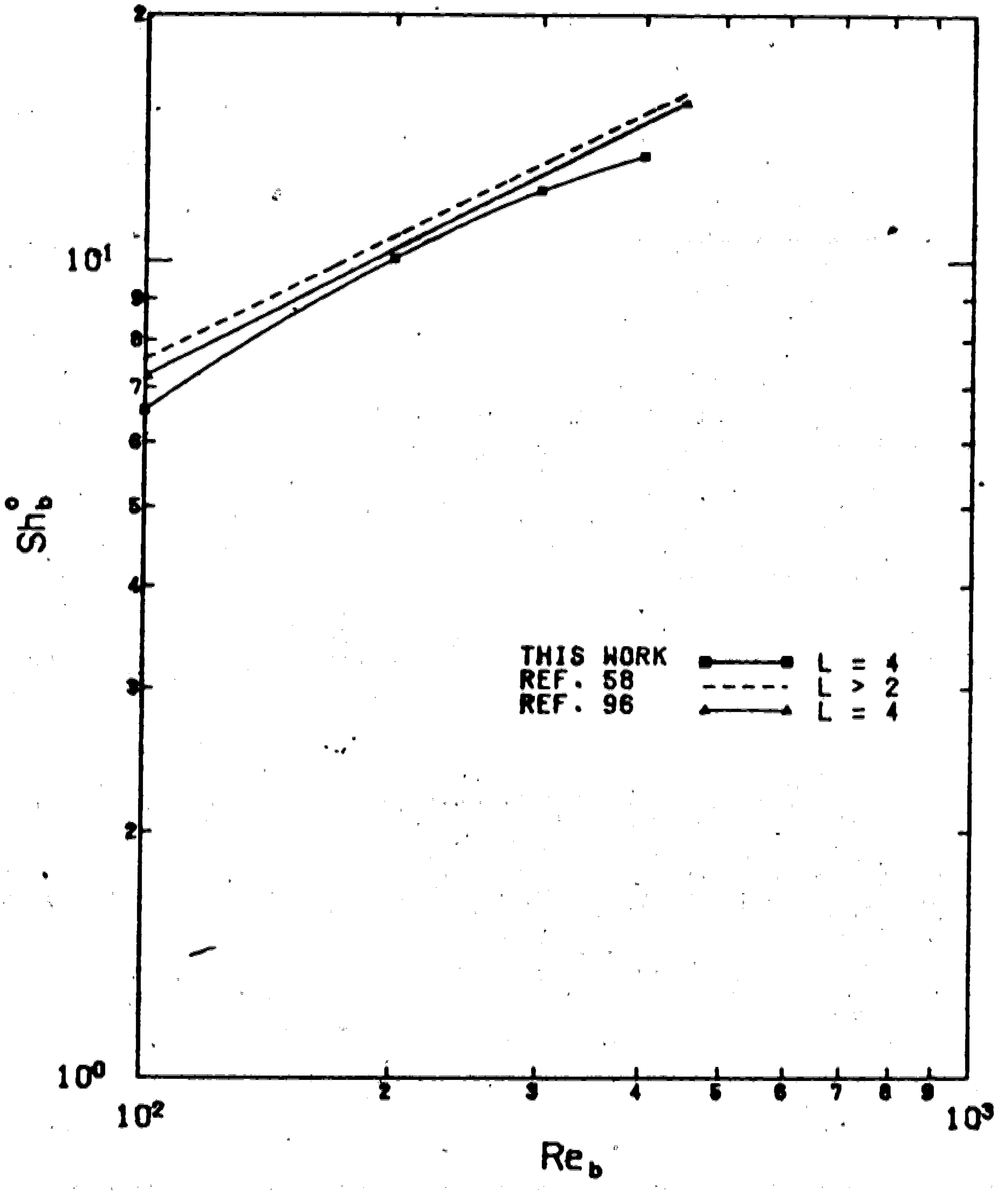

FIGURE 10.69 : COMPARISON OF STAGNATION POINT SHERWOOD NUMBER WITH LITERATURE FOR THE CASE OF FLAT VELOCITY PROFILE (Sc=2.74)

Equation 2.23 and the numerical result for a semi-confined jet computed by Van Heiningen et. al. (96). The stagnation point Sherwood number predicted by Miyazaki and Silberman is consistently higher than that of this work. The disagreement is mainly due to the error introduced by their assumption of potential flow outside the viscous boundary layer. On the other hand, the disagreement between the results computed by Van Heiningen et. al. and that of this work is less obvious.

10.2.3 COMPARISON OF EXPERIMENTAL AND NUMERICAL RESULTS

Comparison of experimental and numerical results can only be made in the region where $X>1$. As mentioned above, local mass transfer within the stagnation flow region ($X\leq 1$) is difficult to measure in the experimental set-up of this work. Comparison of experimental and numerical results are shown in Figures 10.70-10.81 for L=2, 4 and 12 with local Sherwood number defined by Equation 5.1.

For L=2 and 4, excellent agreement is obtained between the experimental and numerical results. Furthermore, the numerical results confirm the presence of local extrema in the Sherwood number. The numerical results from the upstream-weighted differencing scheme (U.W.D.S.) gave a better prediction as would be expected (69).

For L=12, disagreements between experimental and numerical results are found in the stagnation flow and the wall jet regions for the cases of $Re_b\geq 300$. This is probably due to the inaccuracy of the numerical results for L=12 in

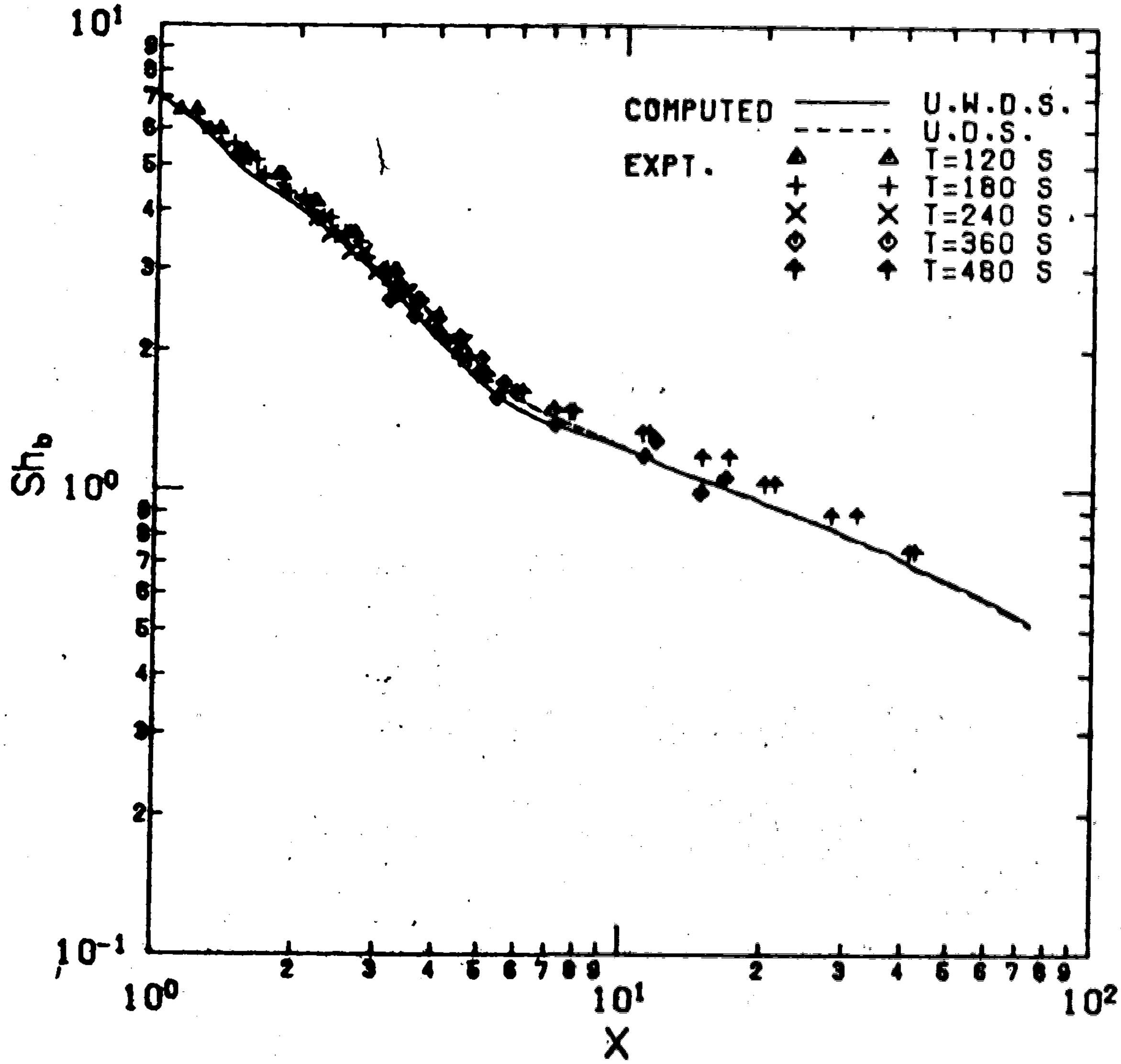

FIGURE 10.70 : COMPARISON OF EXPERIMENTAL AND NUMERICAL RESULTS OF SHERWOOD NUMBER FOR L=2 AND Re_b=100

7

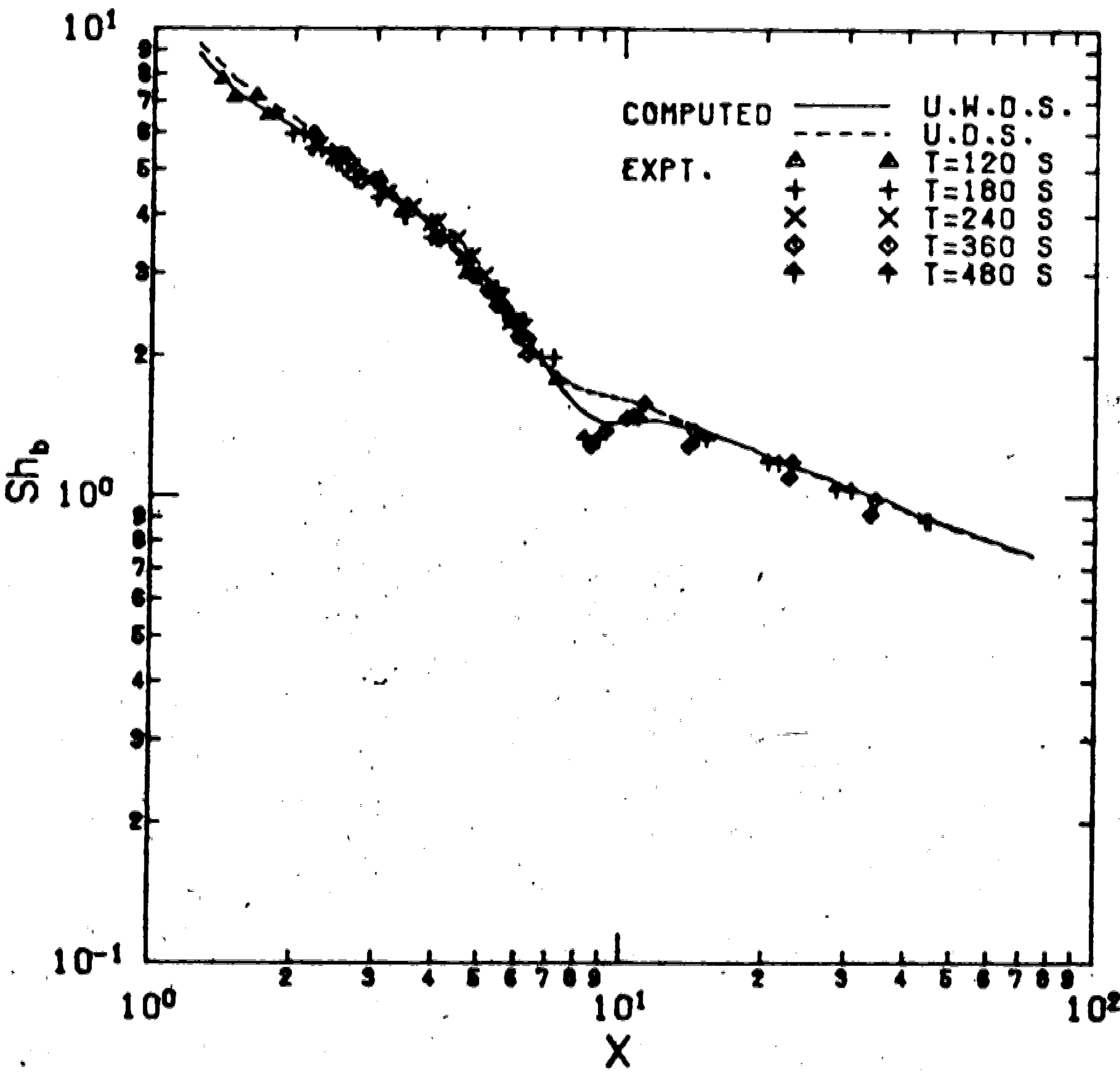

FIGURE 10.71 : COMPARISON OF EXPERIMENTAL AND NUMERICAL RESULTS OF SHERWOOD NUMBER FOR L=2 AND Re_b=200

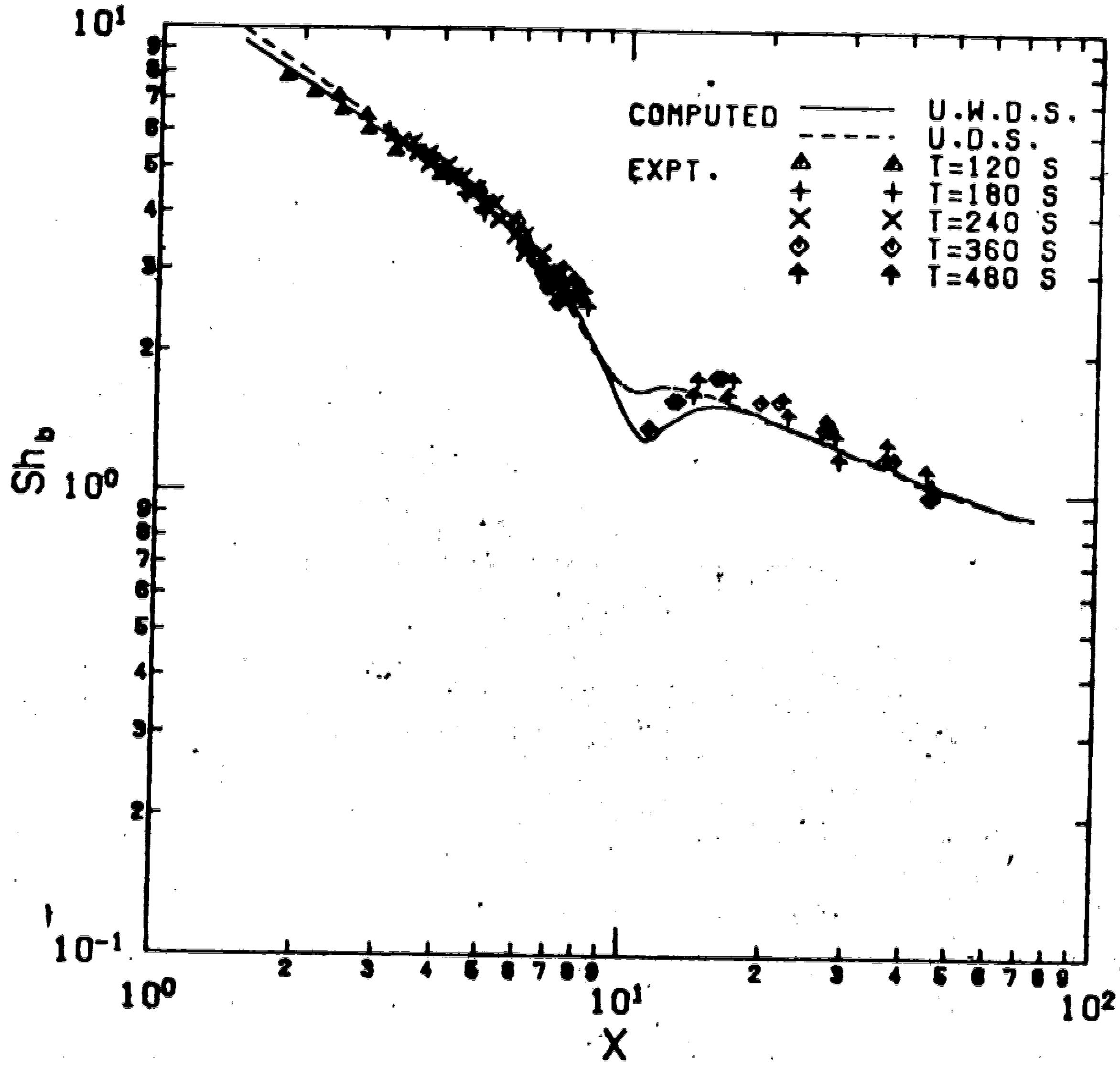

FIGURE 10.72 : COMPARISON OF EXPERIMENTAL AND NUMERICAL RESULTS OF SHERWOOD NUMBER FOR L=2 AND Re_b=300

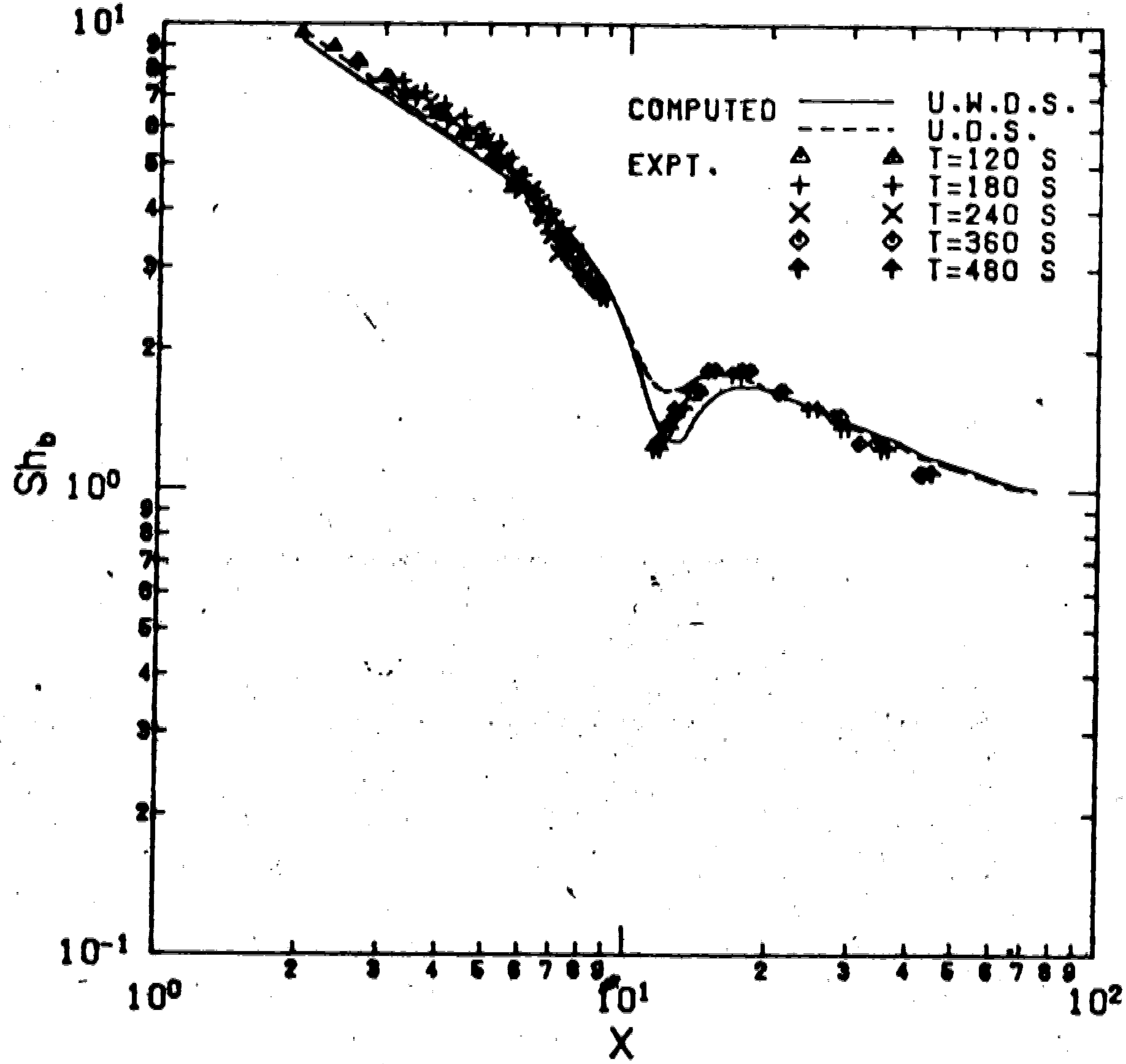

FIGURE 10.73 : COMPARISON OF EXPERIMENTAL AND NUMERICAL RESULTS OF SHERWOOD NUMBER FOR L=2 AND Re_b=400

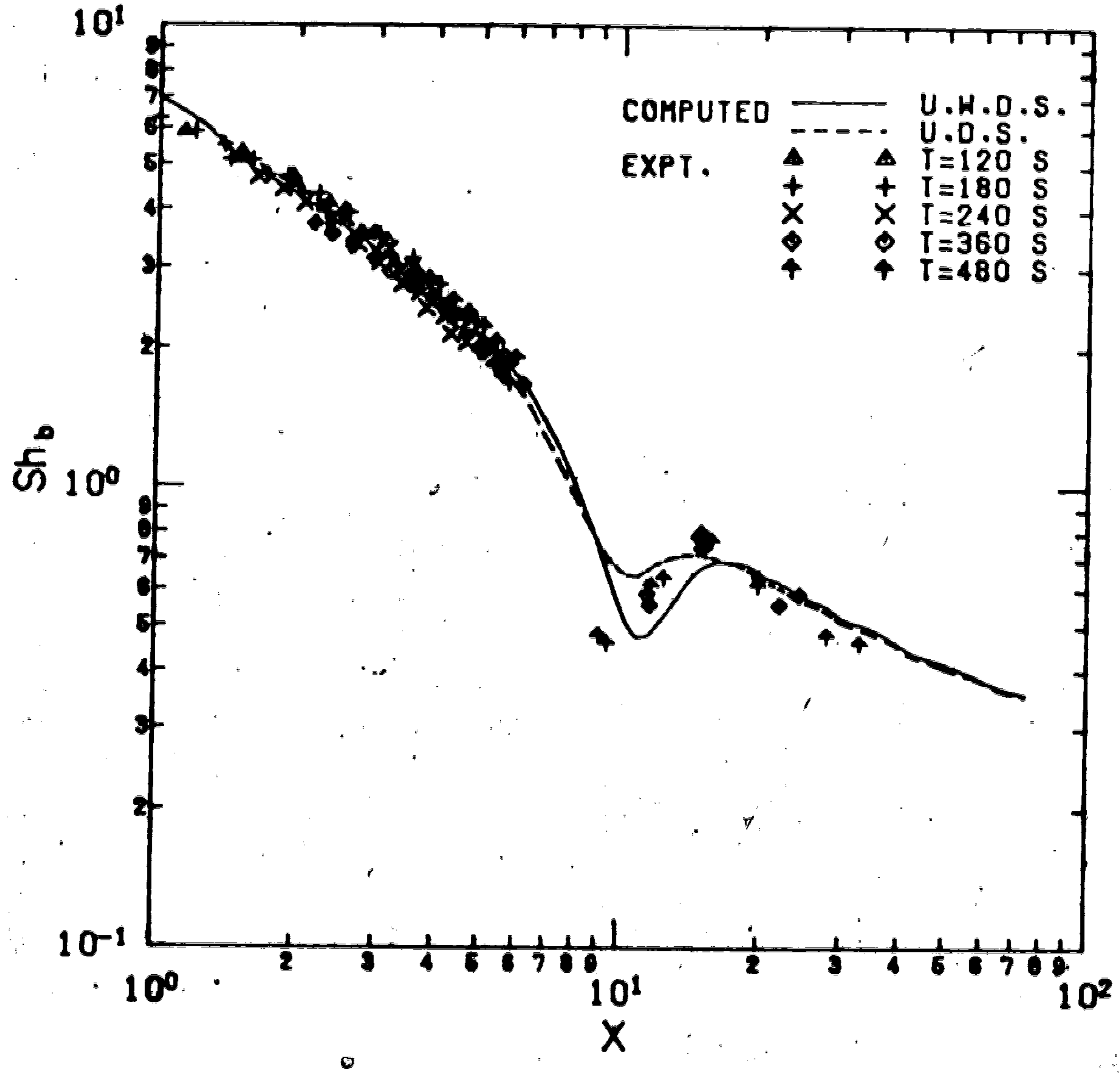

FIGURE 10.74 : COMPARISON OF EXPERIMENTAL AND NUMERICAL RESULTS OF SHERWOOD NUMBER FOR L=4 AND Re_b=100

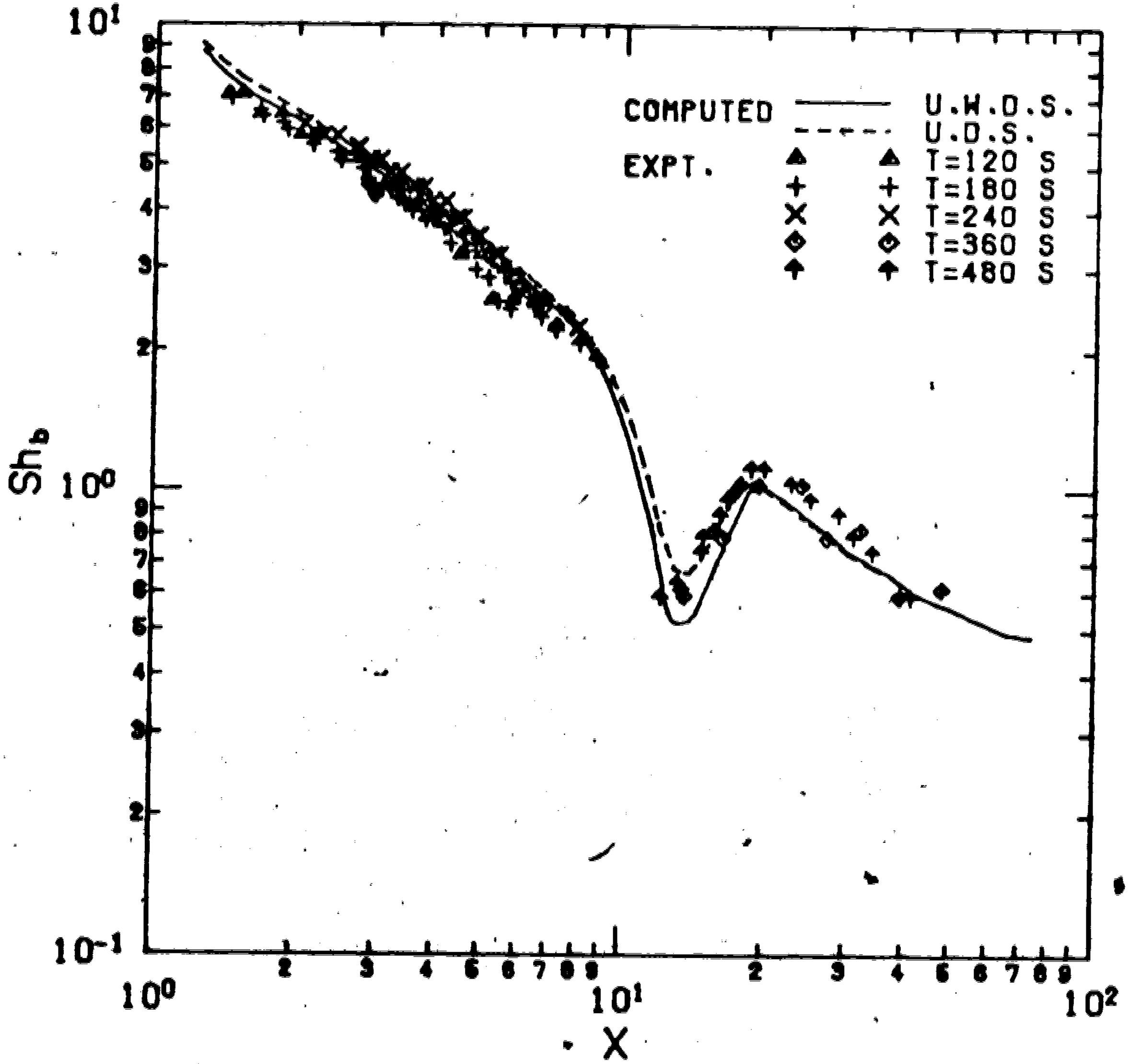

FIGURE 10.75 : COMPARISON OF EXPERIMENTAL AND NUMERICAL RESULTS OF SHERWOOD NUMBER FOR L=4 AND Re_b=200

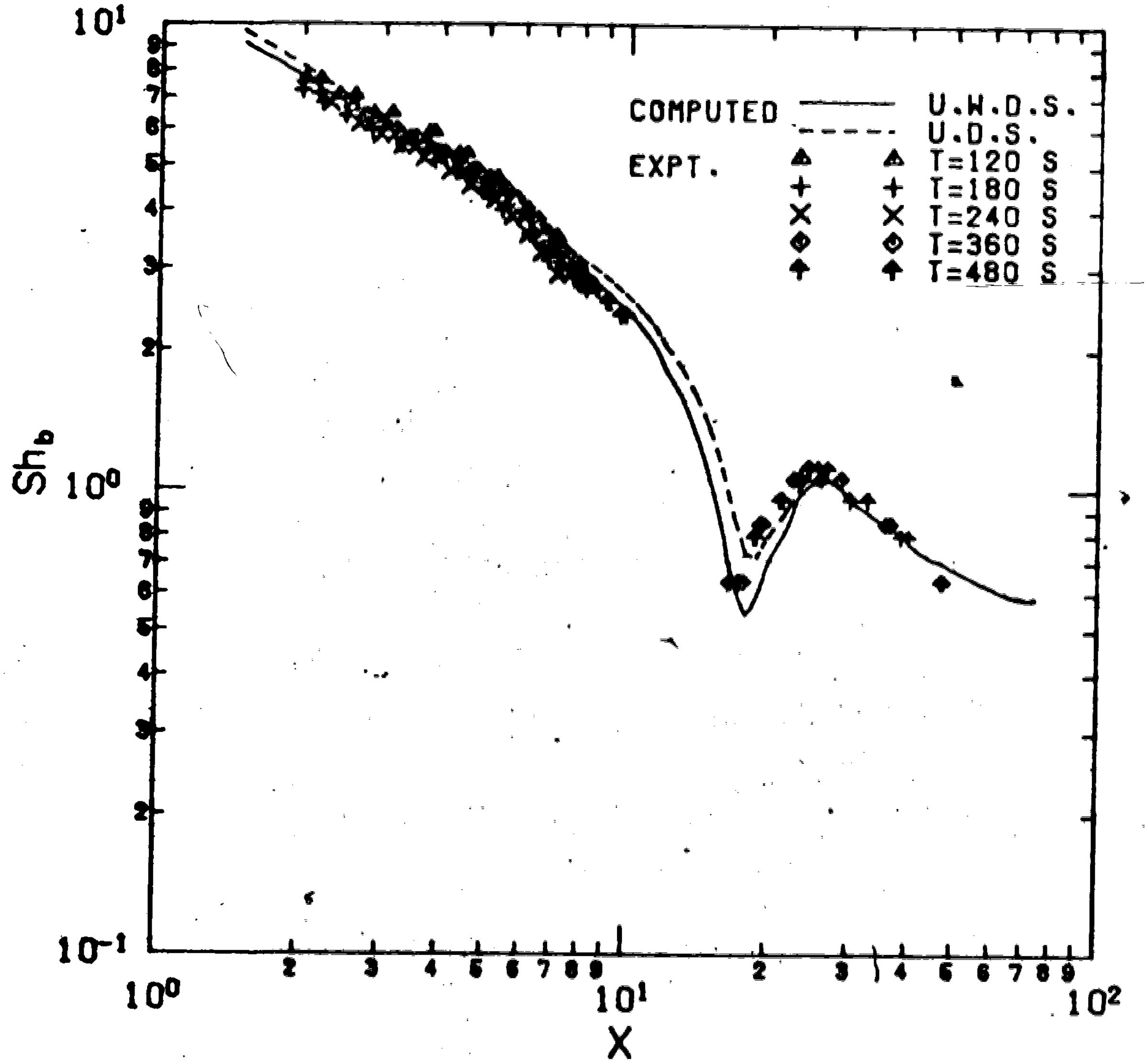

FIGURE 10.76 : COMPARISON OF EXPERIMENTAL AND NUMERICAL RESULTS OF SHERWOOD NUMBER FOR L=4 AND Re_b=300

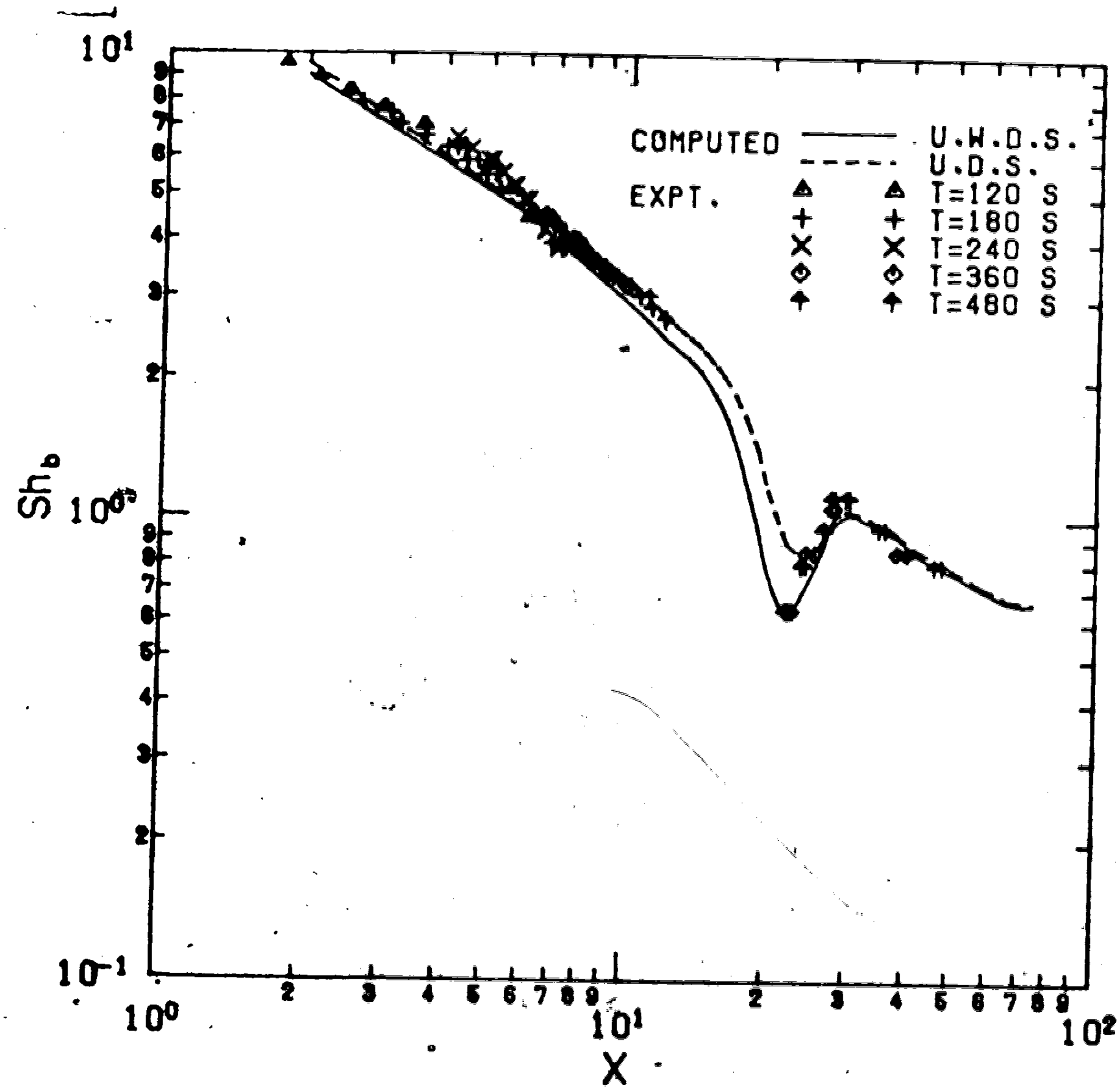

FIGURE 10.77 : COMPARISON OF EXPERIMENTAL AND NUMERICAL RESULTS OF SHERWOOD NUMBER FOR L=4 AND Re_b=400

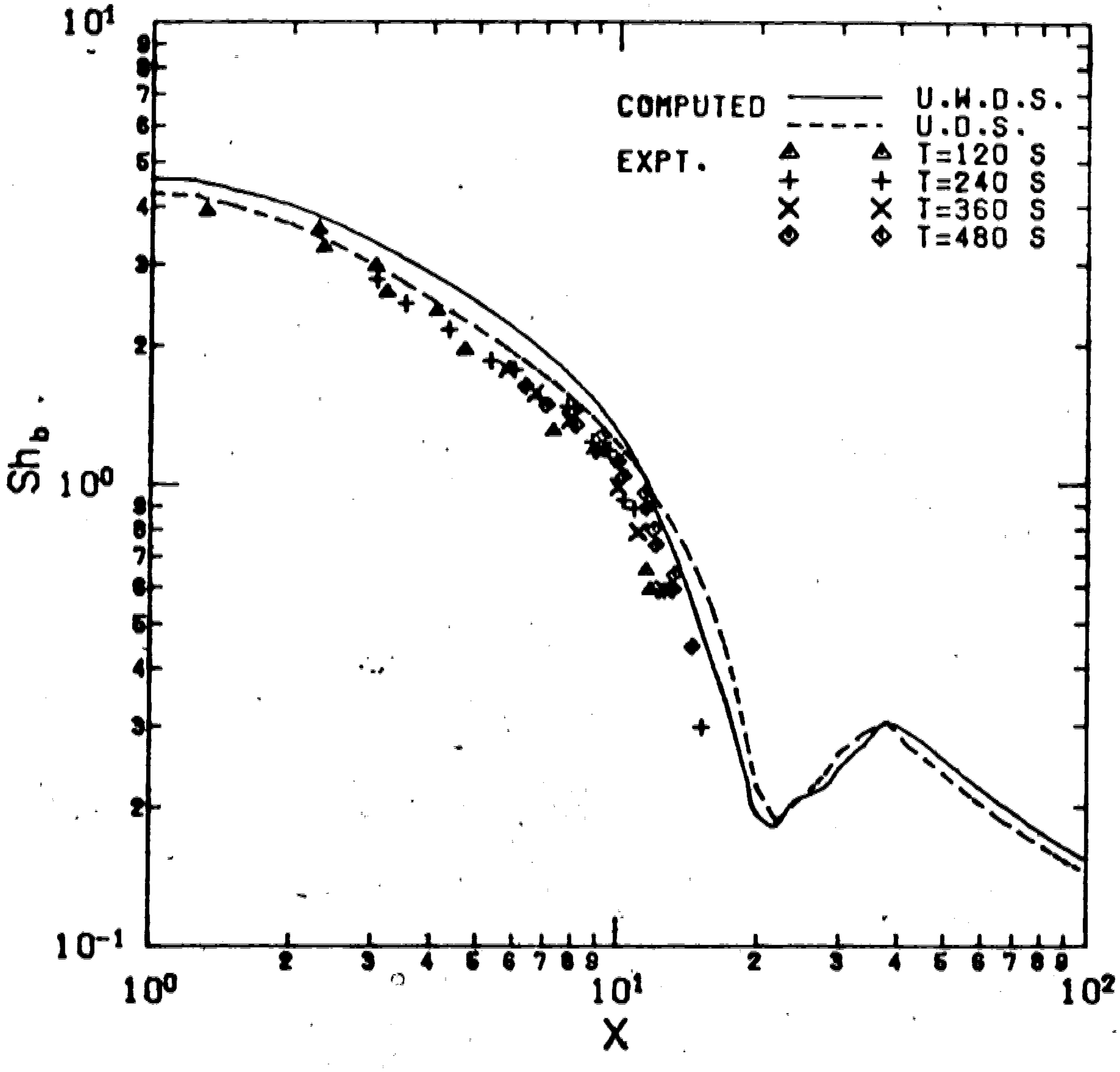

FIGURE 10.78 : COMPARISON OF EXPERIMENTAL AND NUMERICAL RESULTS OF SHERWOOD NUMBER FOR L=12 AND Re_b=100

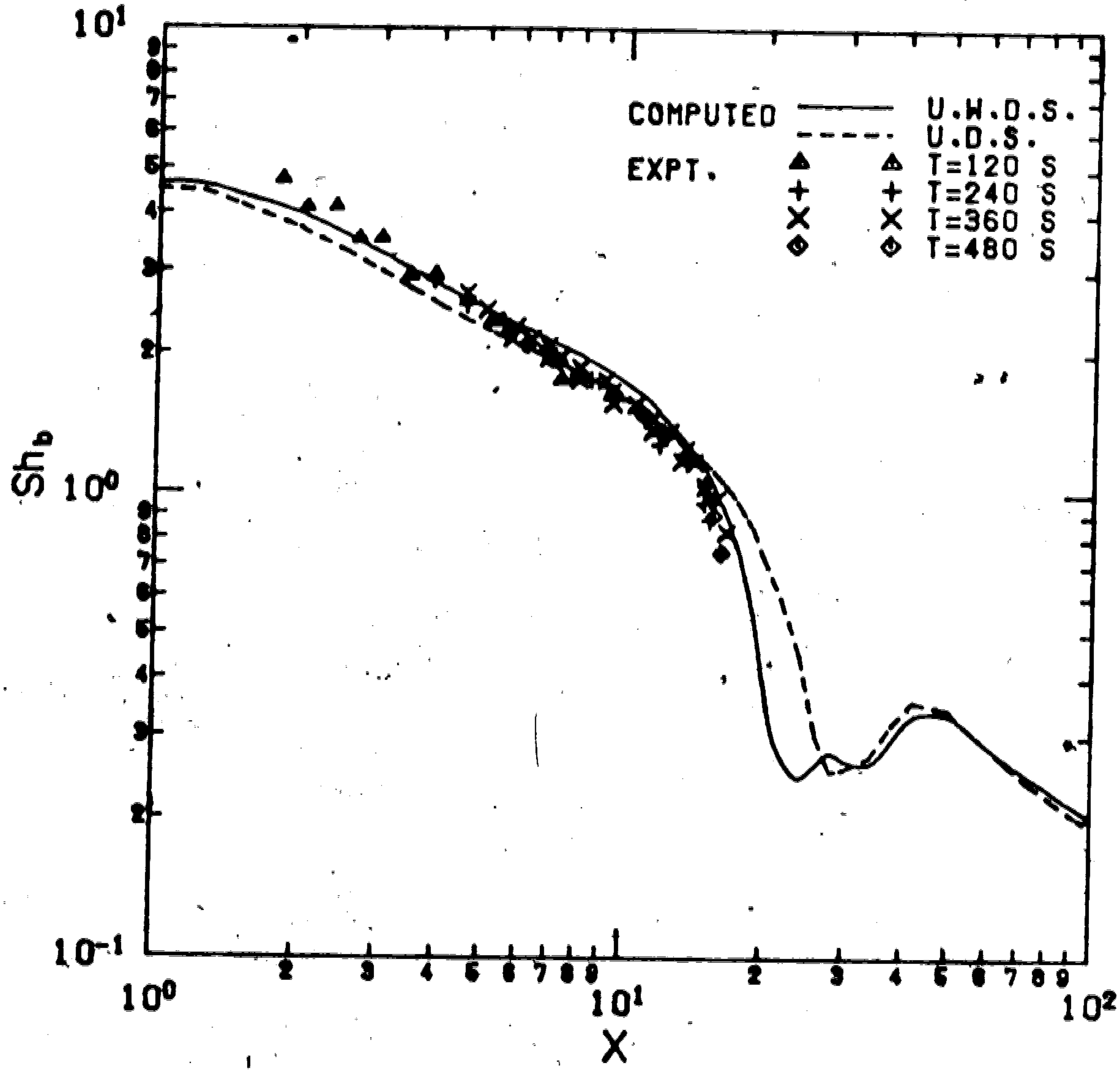

FIGURE 10.79 : COMPARISON OF EXPERIMENTAL AND NUMERICAL RESULTS OF SHERWOOD NUMBER FOR L=12 AND Re_b=200

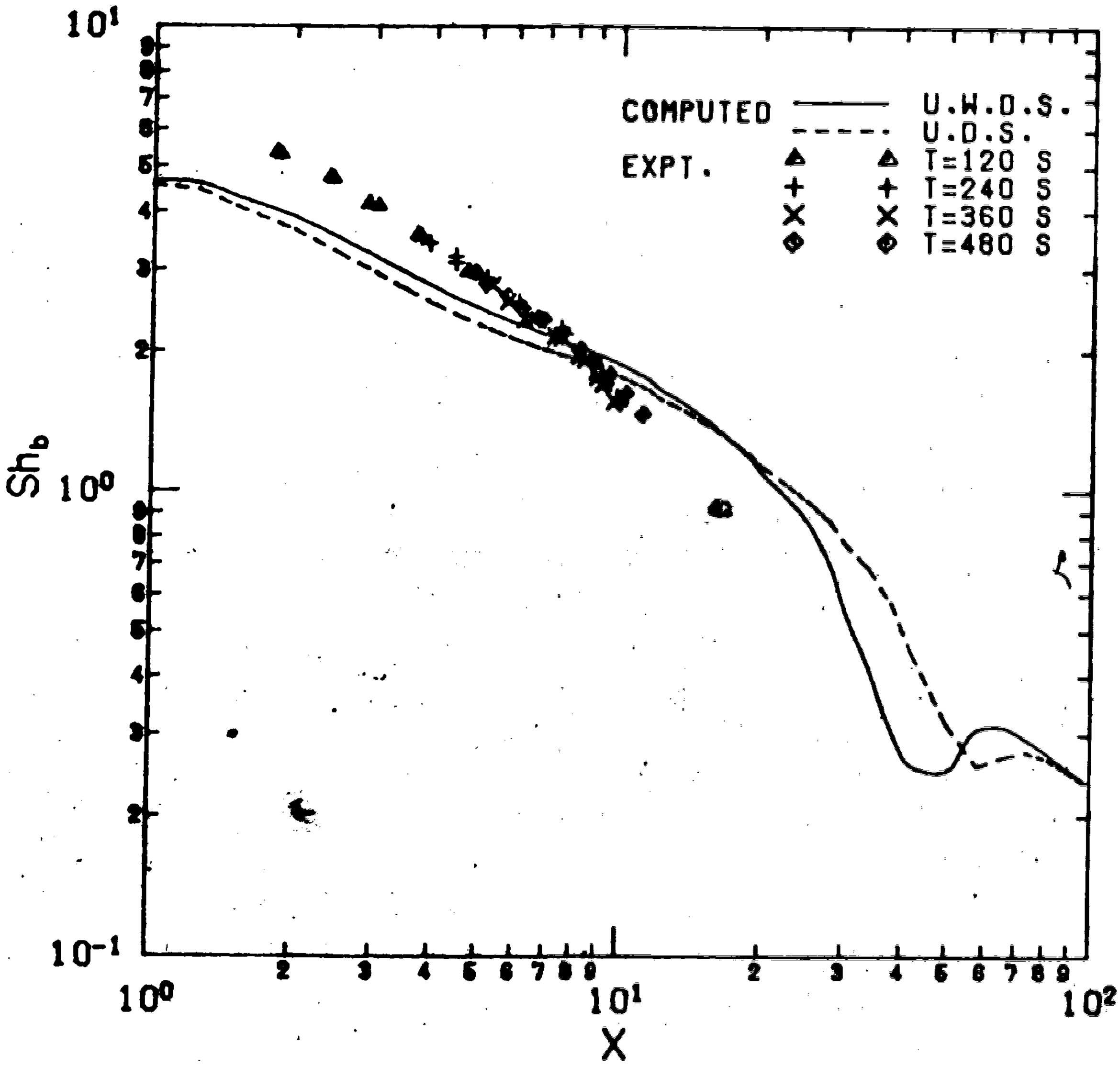

FIGURE 10.80 : COMPARISON OF EXPERIMENTAL AND NUMERICAL RESULTS OF SHERWOOD NUMBER FOR L=12 AND Re_b=300

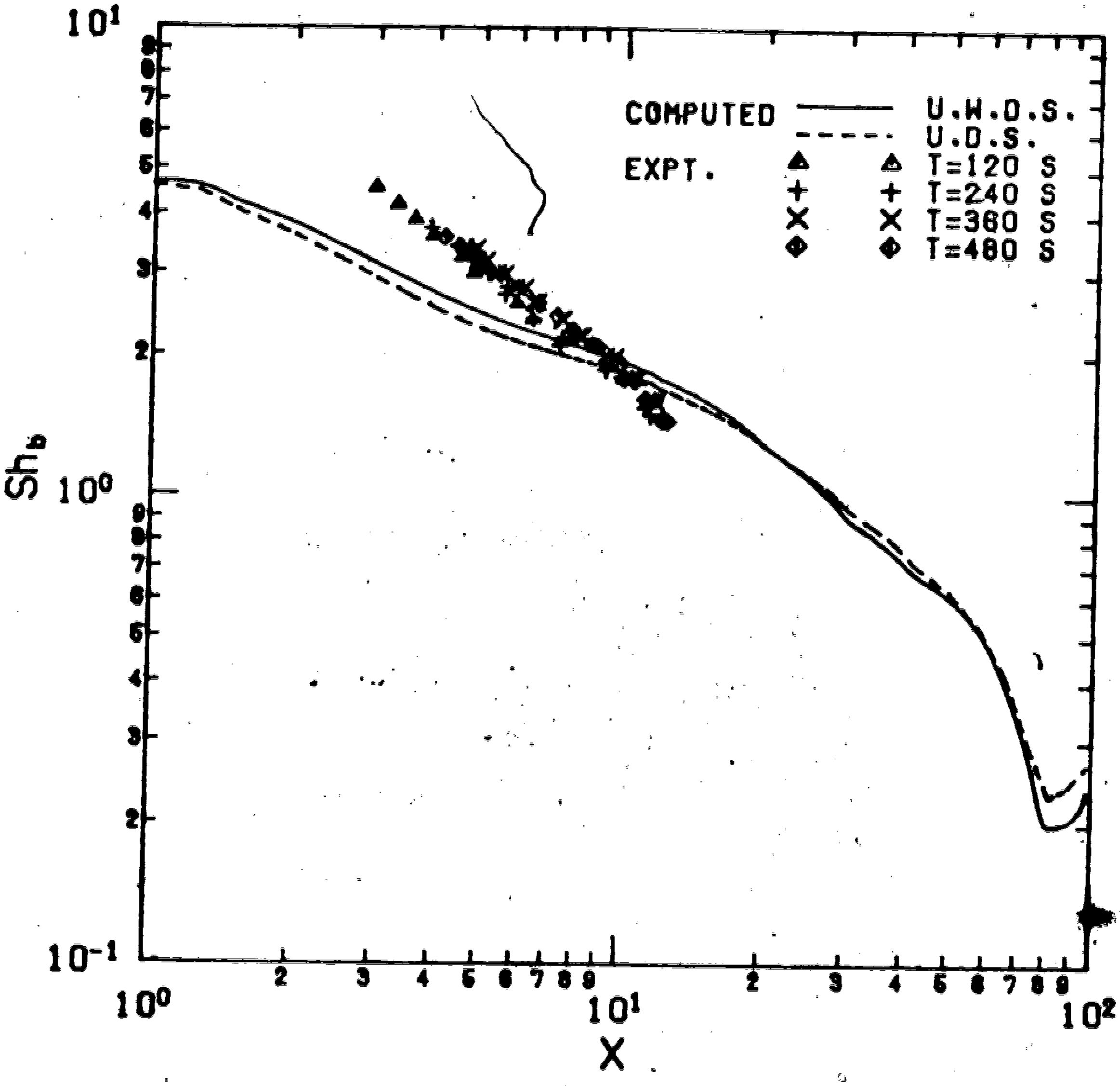

FIGURE 10.81 : COMPARISON OF EXPERIMENTAL AND NUMERICAL RESULTS OF SHERWOOD NUMBER FOR L=12 AND Re_b=400

the stagnation flow region as mentioned in Chapter 9. On the other hand, this may be also due to the large jet-to-plate spacing of the experimental set-up in this case. Since the aspect ratio of the channel is 0.1295 for L=12 comparing to those of 0.0216 and 0.043 for L=2 and 4, respectively, the end effect is important and the geometry of the experimental set-up is no longer two-dimensional. The higher the Reynolds number, the more severe the end effect. This could also be the reason why the two-dimensional model fails to predict the experimental results for L=12 at high Reynolds numbers which are measured along the centerline of a three-dimensional channel. To clarify the failure of the two-dimensional numerical model in this case, a three-dimensional numerical model is recommended to study the mass transfer characteristic due to a confined impinging two-dimensional jet when the jet-to-plate spacing is large. Although no experimental data for L=12 are obtained in the region where the local extrema in Sherwood number occur, the presence of such extrema is confirmed by the qualitative study of the contours of equal mass transfer rate shown in Plate 10.3.

11. CONCLUSIONS

1. Local Sherwood number along the impingement plate is found to exhibit a local minimum and a local maximum in the region far away from the stagnation flow region. The locations of these extrema are a function of Reynolds number and jet-to-plate spacing.
2. Regression equations correlating local Sherwood number in terms of Reynolds number and streamwise distance for different jet-to-plate spacings are presented in the wall jet region up to the region where the local extremum of Sherwood number occurs.
3. In the wall jet region, for the cases of L=2 and 4, no effects of jet-to-plate spacing are found.
4. Effect of initial nozzle exit velocity profile on the stagnation point mass transfer rate is important. The stagnation point mass transfer rate for an initial parabolic velocity profile is between 1.8 and 2.5 times the value for an initial flat velocity profile.
5. Mass transfer due to a confined laminar impinging two-dimensional jet can be successfully predicted by using a two-dimensional numerical model with upstream-weighted differencing scheme (U.W.D.S.).

12. RECOMMENDATIONS

1. A more advanced interferometric technique can be used instead of the holographic interferometry employed in the present experimental study. A technique, so called "speckle interferometry", can be employed by replacing the hologram in the holographic interferometry by an electronic system. This technique deals with ordinary images rather than holographic reconstructions, therefore the intermediate production, processing and reconstruction of a hologram is avoided. An image of the object illuminated by a coherent light, is formed by conventional optical methods at a photo-sensitive surface of a vidicon tube and can be stored and handled electronically. In this way, the development of fringes can then be studied quantitatively in real time in front of the video monitor.
2. A three-dimensional numerical model should be developed for the study of mass transfer due to a confined impinging two-dimensional jet with large jet-to-plate spacing. This model can then be used to predict the experimental results for L=12.
3. The two-dimensional numerical model, developed in this work, can be improved by using a high order differencing scheme derived from local solutions of the differential equation. This numerical technique, so called "single

cell high order differencing scheme" (SCHOS) is understudy by Manohar and Masliyah at the University of Alberta.

13. NOMENCLATURE

a	dimensionless parameter defined in Equation 7.1
a_1, a_2	proportional constants in Equations 2.5 and 2.7
A	calibration constant, kg/m³
b	slot width, m
b_1	arbitrary stretch constant used to adjust the grid transformation in Y-direction
B	geometric constant of optical set-up
c	concentration of swelling agent, kmole/m³
c_1, c_2, c_3, c_4	coefficients in Equations 2.15, 2.16, 2.21 and 2.22
C	dimensionless concentration of swelling agent, $(c-c_j)/(c_s-c_j)$
C_f	skin-friction factor, $\tau_s/(0.5\,\rho\,\bar{v}_j^2)$
d	nozzle diameter, m
d_1, d_2	proportional constants in Equations 2.1 and 2.3
D	diffusion coefficient, m/s²
e_1, e_2	proportional constants in Equation 2.2 and 2.4
E_i	eigenconstants in Equation 6.29
f	coefficient in Equation 7.50
f_1, f_2	proportional constants in Equations 2.11 and

	2.13
F_r	exterior flux of momentum flux, m^3/s^2
g	coefficient in Equation 7.50
g_1, g_2	proportional constants in Equations 2.12 and 2.14
$-g'(0)$	dimensionless gradient of concentration at impingement plate
G	constant value defined in Equation 5.9, m
h	jet-to-plate spacing, m
k	local mass transfer coefficient defined in Equation 5.1, m/s
k'	local mass transfer coefficient defined in Equation 5.2, m/s
k_1	constant value equals to $\cos\beta_1$
K	parameter in Equation 7.50
L	dimensionless jet-to-plate spacing, h/b
m_1, m_2, m_3, m_4, m_5	coefficients defined in Equation 7.16
Mw	molecular weight of swelling agent, kg/kmole
n	fringe order
n_1, n_2, n_3, n_4, n_5	coefficients defined in Equation 7.21
n_p	refractive index of glass prism
n_s	refractive index of swollen polymer coating
nj	number of nodes in X-direction which covers half of the slot width
nx	total number of nodes in X-direction
ny	total number of nodes in Y-direction
N	mass flux, kg/m^2s

Nu_b	Nussult number for two-dimensional jet
p_B	partial vapor pressure of swelling agent in bulk flow, kPa
p_j	partial vapor pressure of swelling at jet nozzle exit, kPa
p_s	partial vapor pressure of swelling at polymer surface, kPa
P	total pressure, kPa
P^*	vapor pressure of swelling agent, kPa
Pr	Prandlt number
Q	volumetric flow rate of air, m^3/s
r	radial distance measured from the jet centre, m
r'	displacement or recession of polymer coating, m
R	molar rate of production of swelling agent per unit volume, $kmole/m^3s$
Re_b	Reynolds number for two-dimensional jet, $\bar{v}_j b/\nu$
Re_d	Reynolds number for axisymmetric jet, $\bar{v}_j d/\nu$
Rs	local Reynolds number based on the local velocity and distance between adjacent nodes in Y-direction defined in Equation 7.46
Rw	local Reynolds number based on the local velocity and distance between adjacent nodes in X-direction defined in Equation 7.44
S	parameter in Equation 8.2

Sc	Schmidt number, D/ν
Sh_b	Sherwood number, kb/D
Sh_d	Sherwood number, kd/D
Sh'_b	Sherwood number, k'b/D
Sh°_b	stagnation point Sherwood number
t	temperature, °C or K
T	duration of mass transfer experiment, s
u	streamwise velocity in X-direction, m/s
u_{max}	maximum value of streamwise velocity in X-direction for an individual streamwise velocity profile, m/s
$\tilde{u}_o$	mean velocity in X-direction in outflow region, m/s
U	dimensionless streamwise velocity in X-direction, $u/\bar{v}_j$
U_{max}	maximum value of dimensionless streamwise velocity in X-direction for an individual streamwise velocity profile, $u_{max}/\bar{v}_j$
v	axial velocity in Y-direction, m/s
$\bar{v}_j$	mean velocity of jet at nozzle exit, m/s
V	dimensionless axial velocity in Y-direction, $v/\bar{v}_j$
w	constant relaxation factor
x	streamwise distance measured from the jet centre, m
X	dimensionless streamwise coordinate, x/b
y	axial distance measured from the jet nozzle

	exit, m
Y	dimensionless axial coordinate, y/b
Y_i	eigenfunctions in Equation 6.29
Z_1, Z_2	coefficients defined in Equations 7.38 and 7.40

GREEK SYMBOLS

α	weighting factor for convective term in X-direction
α_i	eigenvalues in Equation 6.25
β	weighting factor for convective term in Y-direction
β_1	incident angle of light path travelling from glass prism to polymer coating
β_2	refractive angle of light path travelling from glass prism to polymer coating
γ	weighting factor for diffusion term in X-direction
δ	weighting factor for diffusion term in Y-direction
ΔX	grid increment in X-direction measured between adjacent boundaries of control volume
ΔY	grid increment in Y-direction measured between adjacent boundaries of control volume

$\bar{\Delta}X$	grid increment in X-direction measured between adjacent nodes
$\bar{\Delta}Y$	grid increment in Y-direction measured between adjacent nodes
ϵ	maximum absolute different of parameter S between two consecutive iterations defined in Equation 8.13
ζ	spread of jet, m
η	coefficient defined in Equation 7.17
λ	wavelength of light, m
λ_i	eigenvalues in Equation 6.29
μ	viscosity of air, kg/m s
ν	kinematic viscosity of air, m^2/s
ξ	coefficient defined in Equation 7.17
ρ	density of air, kg/m^3
ρ_s	density of swollen polymer coating, kg/m^3
ρ^*	molar density of gas mixture, $kmole/m^3$
σ	viscous boundary layer thickness in wall jet region, m
σ_0	viscous boundary layer thickness in stagnation flow region, m
τ_s	shear stress at impingement plate, N/m^2
Φ	dimensionless variable in Equation 7.1
ψ	stream-function, m^2/s
Ψ	dimensionless stream-function, $\psi/(b\ \bar{v}_j)$
ω	vorticity, s^{-1}
Ω	dimensionless vorticity, $\omega(b/\ \bar{v}_j)$

SUBSCRIPTS

b	slot width as characteristic length
B	bulk flow
d	nozzle diameter as characteristic length
e,w,n,s	east, west, north and south side boundaries of control volume
fd	fully developed flow
i	element number
j	at jet nozzle exit
max	maximum value
o	in outflow region
s	at coating surface or impingement plate

14. BIBLIOGRAPHY

1. **Abramson N.**, "The 'Interferoscope' A New Type of Interferometer with Variable Fringe Separation", *Optik*, 30, 56-71(1969).

2. **Abramson N.**, "The Holo-Diagram: A Practical Device for Making and Evaluating Holograms", *Appl. Opt.*, 8, #6, 1235-1240(1969).

3. **Abramson N.**, "The Holo-Diagram. II : A Practical Device for Information Retrieval in Hologram Interferometry", *Appl. Opt.*, 9, #1, 97-101(1970).

4. **Abramson N.**, "The Holo-Diagram. III : A Practical Device for Predicting Fringe Patterns in Hologram Interferometry", *Appl. Opt.*, 9, #10, 2311-2319(1970).

5. **Ames M. F.**, "Numerical Methods for Partial Differential Equations", *Academic Press*, 2nd Ed. (1977).

6. **Baines W. D. and Keffer J. F.**, "Shear Stress and Heat Transfer at a Stagnation Point", *Int. J.*

Heat Mass Transfer, 19, 21-26(1976).

7. Bakke P., "An Experimental Investigation of a Wall Jet", *J. Fluid Mech.*, 2, 467-472(1957).

8. Bouchez J. P. and Goldstein R. J., "Impingement Cooling from a Circular Jet in a Cross Flow", *Int. J. Heat Mass Transfer*, 18, 719-730(1975).

9. Cadek F. F. and Zerkle R. D., "Local Heat Transfer Characteristics of Two-Dimensional Impinging Air Jets - Theory and Experiment", *5th Int. Heat Transfer Conference, Tokyo*, 2, Paper # FC1.4, 15-19(1974).

10. Cartwright W. G. and Russell P. J., "Characteristics of a Turbulent Slot Jet Impinging on a Plane Surface", *Proc. Instn. Mech. Engrs.*, 182, 309-319(1968).

11. Chaudhury Z. H., "Heat Transfer in a Radial Liquid Jet", *J. Fluid Mech.*, 20, 501-511(1964).

12. Chia C. J., Giralt F. and Trass O., "Mass Transfer in Axisymmetric Turbulent Impinging Jets", *Ind. Eng. Chem., Fundam.*, 16, #1, 28-35(1977).

13. Collier R. J., Burckhardt C. B. and Lin L. H., "Optical Holography", *Academic Press*, (1971).

14. Dawson D. A. and Trass O., "Mass Transfer in a Turbulent Radial Wall Jet", *Can. J. Chem. Eng.*, 44, 121-129(1966).

15. Donaldson C. Dup. and Snedeker R. S., "A Study of Free Jet Impingement. Part 1. Mean Properties of Free and Impinging Jets", *J. Fluid Mech.*, 45, 281-319(1971).

16. Donaldson C. Dup., Snedeker R. S. and Margolis D. P., "A Study of Free Jet Impingement. Part 2. Free Jet Turbulent Structure and Impingement Heat Transfer", *J. Fluid Mech.*, 45, 477-512(1971).

17. Dyban E. P., Mazur A. I. and Golovanov V. P., "Heat Transfer and Hydrodynamics of an Array of Round Impinging Jets with One-Sided Exhaust of the Spent Air", *Int. J. Heat Mass Transfer*, 23, 667-676(1980).

18. Gardon R. and Akfirat J. C., "The Role of Turbulence in Determining the Heat-Transfer Characteristics of Impinging Jets", *Int. J. Heat Mass Transfer*,

8, 1261-1272(1965).

19. Gardon R. and Akfirat J. C., "Heat Transfer Characteristics of Impinging Two-Dimensional Air Jets", *J. of Heat Transfer, Trans. ASME*, 88, Series C, 101-108(1966).

20. Gardon R. and Cobonpue J., "Heat Transfer Between a Flat Plate and Jets of Air Impinging on It", *Int. Developments in Heat Transfer*, Part II, 454-460(1962).

21. Gauntner J. W., Livingood J. N. B. and Hrycak P., "Survey of Literature on Flow Characteristics of a Single Turbulent Jet Impinging on a Flat Plate", *NASA*, Paper # TN-D-5652, Feb., 45-89(1970).

22. Giralt F., Chia C. J. and Trass O., "Characterization of the Impingement Region in an Axisymmetric Turbulent Jet", *Ind. Eng. Chem., Fundam.*, 16, #1, 21-28(1977).

23. Giralt F. and Trass O., "Mass Transfer from Crystalline Surfaces in a Turbulent Impinging Jet. Part 1 : Transfer by Erosion", *Can. J. Chem. Eng.*, 53, 505-511(1975).

24. Giralt F. and Trass O., "Mass Transfer from Crystalline Surfaces in a Turbulent Impinging Jet. Part 2 : Erosion and Diffusional Transfer", *Can. J. Chem. Eng.*, 54, 148-153(1976).

25. Glauert M. B., "The Wall Jet", *J. Fluid Mech.*, 1, 625-643(1956).

26. Goldstein R. J., "Some Measurement Techniques in Heat Transfer", *6th Int. Heat Transfer Conference, Toronto*, 6, Paper # KS-36, 494-508(1978).

27. Gosman A. D., Pun W. M., Runchal A. K., Spalding D. B. and Wolfshtein M., "Heat and Mass Transfer in Recirculation Flows", *Academic Press*, (1969).

28. Harlow F. H. and Welch J. D., "Numerical Calculation of Time-Dependent Viscous Incompressible Flow of Fluid with Free Surface", *The Physics of Fluids*, 8, #12, 2182-2189(1965).

29. Hauf W. and Grigull, "Optical Methods in Heat Transfer", *Advances in Heat Transfer*, 6, 133-366(1970).

30. Hirt C. W., Nichols B. D. and Romero N. C., "SOLA -

A Numerical Solutuion Algorithm for Transient Fluid Flow", *Los Alamos Scientific Laboratory of University of California, Los Alamos, New Mexico*, LA-5852, UC-34 and UC-79d, (1975).

31. Hoogendoorn C. J., "The Effect of Turbulence on Heat Transfer at a Stagnation Point", *Int. J. Heat Mass Transfer*, 20, 1333-1338(1977).

32. Hrycak P., Lee D. T., Gaunter J. W. and Livingood J. N. B., "Experimental Flow Characteristics of a Single Turbulent Jet Impinging on a Flate Plate", *NASA*, Paper # TN-D-5690, (1970).

33. Huang G. C., "Investigations of Heat-Transfer Coefficients for Air Flow Through Round Jets Impinging Normal to a Heat-Transfer Surface", *J. of Heat Transfer, Trans. ASME*, 85, Series C, 237-245(1963).

34. Huang B., Douglas W. J. M. and Mujumdar A. S., "Heat Transfer under a Laminar Swirling Impinging Jet-A Numerical Study", *6th Int. Heat Transfer Conference, Toronto*, 5, Paper # FC(b)-23, 311-316(1978).

35. Joseph B., Smith E. P. and Adler R. J., "Numerical

Treatment of Laminar Flow in Helically Coiled Tubes of Square Cross Section. Part 1. Stationary Helically Coiled Tubes", *A. I. Ch. E. J.*, 2[illegible] 965-974(1975).

36. **Kapur D. N. and Macleod N.**, "Determination of Local Mass-Transfer Coefficients by Holography", *Nature Phys. Sci.*, 237, 57-59(1972).

37. **Kapur D. N. and Macleod N.**, "The Determination of Local Mass-Transfer Coefficients by Holographic Interferometry - I", *Int. J. Heat Mass Transfer*, 17, 1151-1162(1974).

38. **Kapur D. N. and Macleod N.**, "Holographic Determination of Local Mass Transfer Coefficients at a Solid-Liquid Boundary", *A. I. Ch. E. J.*, 21, 184-187(1975).

39. **Kataoka K. and Mizushina T.**, "Local Enhancement of the Rate of Heat-Transfer in an Impinging Round Jet by Free-Stream Turbulence", *5th Int. Heat Transfer Conference, Tokyo*, 2, Paper # FC8.3, 305-309(1974).

40. **Kercher D. M. and Tabakoff W.**, "Heat Transfer by a Square Array of Round Air Jets Impinging

Perpendicular to a Flat Surface Including the Effect of Spent Air", *J. Engng. Power, Trans ASME*, 92, Series A, 73-82(1970).

41. Koopman R. N. and Sparrow E. M., "Local and Average Transfer Coefficients due to an Impinging Row of Jets", *Int. J. Heat Mass Transfer*, 19, 673-683(1976).

42. Korger M. and Krizek F., "Mass Transfer Coefficient in Impingement Flow from Slotted Nozzles", *Int. J. Heat Mass Transfer*, 9, 337-344(1966).

43. Lehman M., "Holography", *The Focal Press*, (1970).

44. Leith E. M. and Upatnicks J., "Photography by Laser", *Scientific American*, 212, 24-35(1965).

45. Li Y.-K., "Heat and Mass Transfer under a Laminar Impinging Jet", M. Eng. Thesis, McGill University, (1977).

46. Lundberg R. E., McCuen P. A. and Reynolds W. C., "Heat Transfer in Annular Passages. Hydrodynamically Developed Laminar Flow with Arbitrarily Prescribed Wall Temperatures or Heat Fluxes", *Int. J. Heat Mass Transfer*, 6,

495-529(1963).

47. **Macleod N. and Todd R. B.**, "The Experimental Determination of Wall-Fluid Mass Transfer Coefficients Using Plasticized Polymer Surface Coatings", *Int. J. Heat Mass Transfer*, 16, 485-504(1973).

48. **Martin H.**, "Heat and Mass Transfer between Impinging Gas Jets and Solid Surfaces", *Advances in Heat Transfer*, 13, 1-60(1977).

49. **Masliyah J. H. and Nandakumar K.**, "Fluid Flow and Heat Transfer in Internally Finned Helical Coils", *Can. J. Chem. Eng.*, 55, 27-36(1977).

50. **Masliyah J. H. and Nguyen T. T.**, "Qualitative Study in Mass Transfer by Laser Holography", *Can. J. Chem. Eng.*, 52, 664-665(1974).

51. **Masliyah J. H. and Nguyen T. T.**, "Holographic Determination of Mass Transfer due to Impinging Square Jet", *Can. J. Chem. Eng.*, 54, 299-304(1976).

52. **Masliyah J. H. and Nguyen T. T.**, "Experimental Study of Mass Transfer due to an Impinging Rectangular

Jet", *Can. J. Chem. Eng.*, 55, 156-160(1977).

53. Masliyah J. H. and Nguyen T. T., "Mass Transfer due to an Impinging Slot Jet", *Int. J. Heat Mass Transfer*, 22, 237-244(1979).

54. Mayinger F. and Pankin W., "Holography in Heat and Mass Transfer", *5th Int. Heat Transfer Conference, Tokyo*, 6, Paper # IL3, 28-43(1974).

55. Metzger D. E., Cummings K. N. and Ruby W. A., "Effects of Prandtl Number on Heat Transfer Characteristics of Impinging Liquid Jets", *5th Int. Heat Transfer Conference, Tokyo*, 2, Paper # FC1.5, 20-24(1974).

56. Metzger D. E., Florschuetz L. W., Takeuchi D. I., Behee R. D. and Berry R. A., "Heat Transfer Characteristics for Inline and Staggered Arrays of Circular Jets with Crossflow of Spent Air", *J. of Heat Transfer, Trans. ASME*, 101, Series C, #3, 526-531(1979).

57. Metzger D. E. and Korstad R. J., "Effects of Crossflow on Impingement Heat Transfer", *J. Engng. Power, Trans. ASME*, 94, Series A, 35-41(1972).

58. Miyazaki H. and Silberman E., "Flow and Heat Transfer on a Flat Plate Normal to a Two-Dimensional Laminar Jet Issuing from a Nozzle of Finite Height", *Int. J. Heat Mass Transfer*, 15, 2097-2107(1972).

59. Murray B. G. and Patten T. D., "Heat Transfer Under an Array of Impinging Jets", *6th Int. Heat Transfer Conference, Toronto*, 4, Paper # HX-14, 207-212(1978).

60. Myers G. E., Schauer J. J. and Eustis R. H., "Heat Transfer to Plane Turbulent Wall Jets", *J. of Heat Transfer, Trans. ASME*, 85, Series C, 209-214(1963).

61. Myers G. E., Schauer J. J. and Eustis R. H., "Plane Turbulent Wall Jet Flow Development and Friction Factor", *J. of Basic Engineering, Trans. ASME*, 85, Series D, 47-54(1963).

62. McCuen P. A., "Heat Transfer with Laminar and Turbulent Flow between Parallel Planes with Constant and Variables Wall Temperature and Heat Flux", Ph. D. Dissertation, Stanford University, (1961).

63. **McMurray D. C., Myers P. S. and Uyehara O. A.**, "Influence of Impinging Jet Variables on Local Heat Transfer Coefficients along a Flat Surface with Constant Heat Flux", *3rd Int. Heat Transfer Conference, Chicago*, 2, 292-299(1966).

64. **Nakatogawa T., Nishiwaki N., Hirata M. and Torii K.**, "Heat Transfer of Round Turbulent Jet Impinging Normally on Flat Plate", *4th Int. Heat Transfer Conference, Versailles*, 2, Paper # FC-5-2, 1-11(1970).

65. **Nakayama P. I. and Romero N. C.**, "Numerical Method for Almost Three-Dimensional Incompressible Fluid Flow and a Simple Internal Obstacle Treatment", *J. of Computational Physics*, 8, 230-240(1971).

66. **Pamadi B. N. and Belov I. A.**, "Heat Transfer Characteristics of the Axially Symmetrical Impinging Jet", *Indian J. of Technology*, 16, 404-408(1978).

67. **Pamadi B. N. and Belov I. A.**, "A Note on the Heat Transfer Characteristics of Circular Impinging Jet", *Int. J. Heat Mass Transfer*, 23, 783-787(1980).

68. **Perry K. P.,** "Heat Transfer by Convection from a Hot Gas Jet to a Plane Surface", *Proc. Instn. Mech. Engrs.*, 168, 755-780(1954).

69. **Raithby G. D. and Torrance K. E.,** "Upstream-Weighted Differencing Schemes and Their Application to Elliptic Problems Involving Fluid Flow", *Computers and Fluids*, 2, 191-206(1974).

70. **Rao V. V. and Trass O.,** "Mass Transfer from a Flat Surface to an Impinging Turbulent Jet", *Can. J. of Chem Eng.*, 42, 95-99(1964).

71. **Riley N.,** "Effects of Compressibility on a Laminar Wall Jet", *J. Fluid Mech.*, 4, 615-628(1958).

72. **Roache P. J.,** "Computational Fluid Dynamics", *Hermosa Publishers*, (1972).

73. **Robertson E. R. and Harvey J. M.,** "The Engineering Uses of Holography", *Cambridge Press*, (1970).

74. **Runchal A. K.,** "Convergence and Accuracy of Three Finite Difference Schemes for a Two-Dimensional Conduction and Convection Problem", *Int. J. for Numerical Methods in Engineering*, 4, 541-550(1972).

75. Runchal A. K., Spalding D. B. and Wolfshtein M., "The Numerical Solution of Elliptic Equations for the Transport of Vorticity, Heat and Matter in Two-Dimensional Flows", *Suppl. Physics Fluids*, 12, 21-27(1969).

76. Runchal A. K. and Wolfshtein M., "A Finite Difference Procedure for the Integration of the Navier-Stokes Equations", *J. Mech. Engng. Sci*, 11, 445-453(1969).

77. Saad N. R., Douglas W. J. M. and Mujumdar A. S., "Prediction of Heat Transfer under an Axisymmetric Laminar Impinging Jet", *Ind. Eng. Chem., Fundam.*, 16, #1, 148-154(1977).

78. Schlichting H., "Boundary Layer Theory", *McGraw-Hill Book Company*, 6th Ed. (1968).

79. Scholtz M. T. and Trass O., "Mass Transfer in the Laminar Radial Wall Jet", *A. I. Ch. E. J.*, 9, 548-554(1963).

80. Scholtz M. T. and Trass O., "Mass Transfer in a Nonuniform Impinging Jet. Part I. Stagnation Flow - Velocity and Pressure Distribution", *A. I. Ch. E. J.*, 16, 82-90(1970).

81. Scholtz M. T. and Trass O., "Mass Transfer in a Nonuniform Impinging Jet. Part II. Boundary Layer Flow - Mass Transfer", *A. I. Ch. E. J.*, 16, 90-96(1970).

82. Schwarz W. H. and Caswell B., "Some Heat Transfer Characteristics of the Two-Dimensional Laminar Incompressible Wall Jet", *Chem. Eng. Sci.*, 16, 338-351(1961).

83. Schwarz W. H. and Cosart W. P., "The Two-Dimensional Turbulent Wall-Jet", *J. Fluid Mech.*, 10, 481-495(1961).

84. Seban R. A. and Back L. H., "Velocity and Temperature Profiles in a Wall Jet", *Int. J. Heat Mass Transfer*, 3, 255-265(1961).

85. Shah R. K. and London A. L., "Advances in Heat Transfer, Laminar Flow Forced Convection in Ducts", *Academic Press*, (1978).

86. Sitharamayya S. and Subba Raju K., "Heat Transfer between an Axisymmetric Jet and a Plate Held Normal to the Flow", *Can. J. Chem. Eng.*, 47, 365-368(1969).

87. **Smirnov V. A., Verevochkin G. E. and Brdlick P.M.**, "Heat Transfer between a Jet and a Held Plate Normal to Flow", *Int. J. Heat Mass Transfer*, 2, 1-7(1961).

88. **Spalding D. B.**, "A Novel Finite Difference Formulation for Differential Expressions Involving both First and Second Derivatives", *Int. J. for Numerical Method in Engineering*, 4, 551-559(1972).

89. **Sparrow E. M., Goldstein R. J. and Rouf M. A.**, "Effect of Nozzle-Surface Separation Distance on Impingement Heat Transfer for a Jet in a Crossflow", *J. of Heat Transfer, Trans. ASME*, 97, Series C, 528-533(1975).

90. **Sparrow E. M. and Lee L.**, "Analysis of Flow Field and Impingement Heat/Mass Transfer due to a Nonuniform Slot Jet", *J. of Heat Transfer, Trans. ASME*, 97, Series C, 191-197(1975).

91. **Sparrow E. M. and Wong T. C.**, "Impingement Transfer Coefficients due to Initially Laminar Slot Jets", *Int. J. Heat Mass Transfer*, 18, 597-605(1975).

92. Sparrow E. M., Lin S. H. and Lundgren T. S., "Flow Development in the Hydrodynamic Entrance Region of Tubes and Ducts", *Physics of Fluid*, 7, #3, 338-347(1964).

93. Stephani L. M. and Butler T. D., "A Numerical Method for Studying the Circulation Patterns of a Fluid in a Cavity", *Los Alamos Scientific Laboratior of University of California, Los Alamos, New Mexico*, LA-6014, UC-34, (1975).

94. Torrance K. E. and Rockett J. A., "Numerical Study of Natural Convection in an Enclosure with Localized Heating from Below", *J. Fluid Mech.*, 36, 33-54(1969).

95. Vallis E. A., Patrick M. A. and Wragg A. A., "Radial Distribution of Convective Heat Transfer Coefficient between an Axisymmetric Turbulent Jet and a Flat Plate Held Normal to the Flow", *6th Int. Heat Transfer Conference, Toronto*, 5, Paper # FC(b)-21, 297-303(1978).

96. van Heiningen A. R. P., Mujumdar A. S. and Douglas W. J. M., "Numerical Prediction of the Flow Field and Impingement Heat Transfer due to a Laminar Slot Jet", *J. of Heat Transfer, Trans.*

ASME, 98, Series C, 654-658(1976).

97. **Vickers J. M. F.**, "An Unusual Flow Pattern May Explain the Behavior of Heat Transfer Coefficients between Fluid Jets and Normal Surfaces", *Ind. Eng. Chem.*, 51, 967-972(1959).

98. **Watson E. J.**, "The Radial Spread of a Liquid Jet over a Horizontal Plane", *J. Fluid Mech.*, 20, 481-499(1964).

99. **Welch J. E., Harlow F. H., Shannon J. P. and Daly B. J.**, "The MAC Method, A Computing Technique for Solving Viscous, Incompressible, Transient Fluid-Flow Problems Involving Free Surfaces", *Los Alamos Scientific Laboratory of the University of California, Los Alamos, New Mexico*, LA-3425, UC-32, (1969).

100. **Wilkes M. V.**, "A Short Introduction to Numerical Analysis", *Cambridge University Press*, (1966).

101. **Yokobori S., Kasagi N., and Hirata M.**, "Characteristic Behavior of Turbulence in the Stagnation Region of a Two-Dimensional Submerged Jet Impinging Normally on a Flat-Plate", *1st Int. Symposium on Turbulent Shear Flows*,

University Park, Pennsylvania, 3.17-3.25(1977).

102. **Yokobori S., Kasagi N., Hirata M. and Nishiwaki N.**, "Role of Large-Scale Eddy Structure on Enhancement of Heat Transfer in Stagnation Region of Two-Dimensional, Submerged, Impinging Jet", *6th Int. Heat Transfer Conference, Toronto*, 5, Paper # FC(b)-22, 305-310(1978).

15. APPENDIX A : PHYSICAL PROPERTIES

The physical properties used in this work in determination of local Sherwood number are given by Masliyah and Nguyen (51,52,53). The physical data which are independent of the operating conditions are given as follows:

density of swollen polymer, $\rho_s = 1.01\times10^{3}$ kg/m^{3}
molecular weight of ethylsalicylate, $M_w = 166.17$ kg/kmol
wave length of laser light, $\lambda = 632.8\times10^{-9}$ m

Other physical properties such as vapor pressure of ethylsalicylate, viscosity of air, molar density of the gas mixture and diffusion coefficient for ethylsalicylate and air are functions of the operating conditions. The correlations for evaluating these properties at given operating temperature and pressure are given as follows:

1. The vapor pressure of ethylsalicylate, P^*, is a strong function of operating temperature, t, and can be evaluated from the following equation (36),

$$\log_{10} P^* = 7.897 - (2931.6 / t) \qquad (15.1)$$

where t is in K.

i.e. P^* (at 21°C and 93.9kPa) = 0.00843 kPa

2. The molar density of gas mixture, ρ^*, can be approximated by using the molar density of air at the operating conditions. Applying ideal gas law, the molar density of gas mixture can be evaluated from the following equation,

$$\rho^* = P / (8.31\ t) \qquad (15.2)$$

where P and t are operating pressure and temperature, respectively.

i.e. ρ^* (at 21°C and 93.9kPa) = 0.0385 kmol/m^3

3. The viscosity of air, μ, is used in the evaluation of the Reynolds number for an air jet. This property is almost independent of pressure at low pressure, but increases with increasing temperature (51).

i.e. μ (at 21°C and 93.9kPa) = 1.817×10^{-5} kg/m s

4. The diffusion coefficient, D, is evaluated by using the Lennard-Jones expression for gas pairs of non-polar molecules.

i.e. D (at 21°C and 93.9kPa) = 5.95×10^{-6} m^2/s

16. APPENDIX B : CALIBRATION OF FLOWMETERS

Two rotameters are used in this work. Rotameter A, a Fischer & Porter Rotameter (Tube no. FP-0.25-09-G-6.75/61) is used for volumetric air flow rate less than $1.1798 \times 10^{-4} m^3/s$. Rotameter B, a Brook Rotameter, is used for volumetric air flow rate greater than $1.1798 \times 10^{-4} m^3/s$ up to $8.6 \times 10^{-4} m^3/s$.

Rotameter A was calibrated at 22.2°C and 93.45kPa. The calibration curve of volumetric air flow rate is shown in Figure 16.1 with rotameter reading at the top of the float. The calibration curve of volumetric air flow rate of Rotameter B was supplied by Masliyah and Nguyen (51) with calibration conditions at 22°C and 95,73kPa. This curve is shown in Figure 16.2. The rotameter reading is at the bottom of the float.

The value of volumetric flow rate from the calibration curve, Q', must be corrected for the actual experimental operating conditions using the following expression

$$Q = Q' \, (t/t')^{0.5} \, (P'/P)^{0.5} \qquad (16.1)$$

where Q is actual experimental volumetric flow rate, Q' is volumetric flow rate from calibration curve, t is operating temperature, t' is calibration temperature, P is operating pressure and P' is calibration pressure. All temperatures

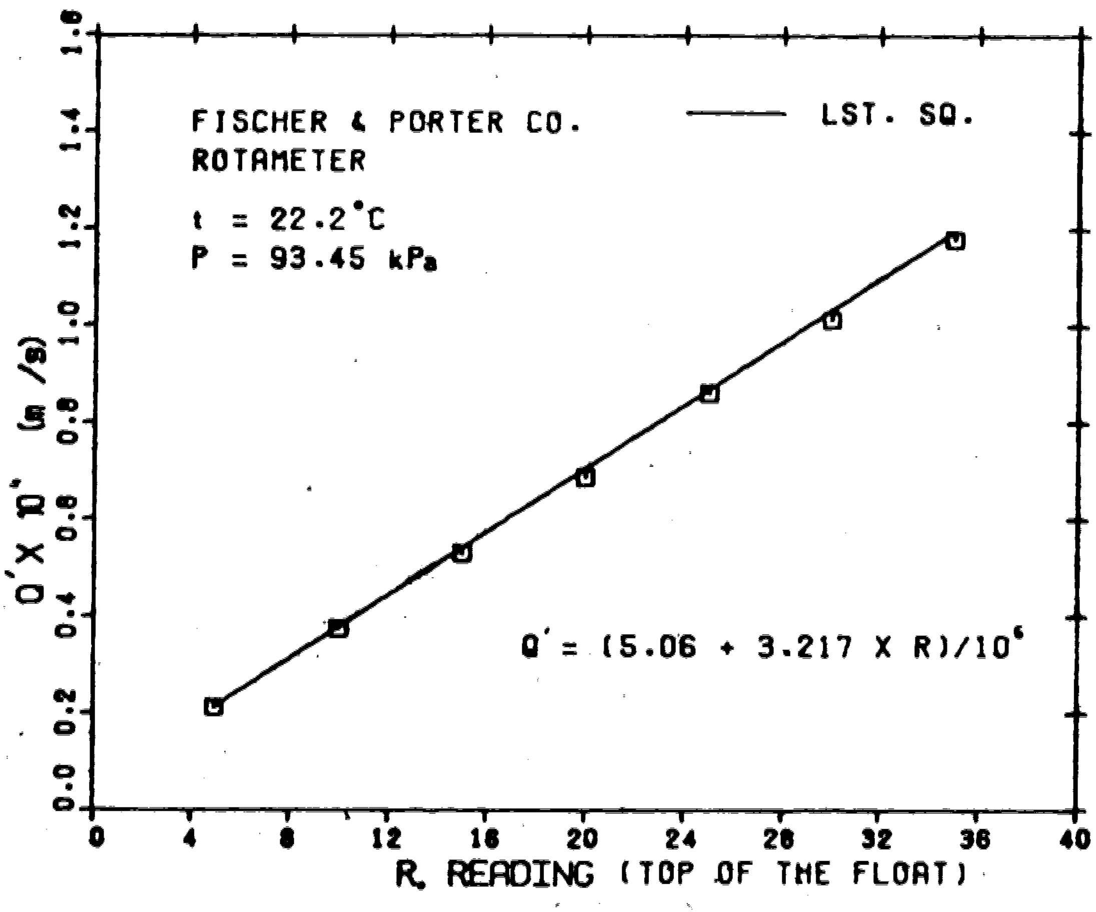

FIGURE 16.1 : CALIBRATION LINE FOR ROTAMETER A

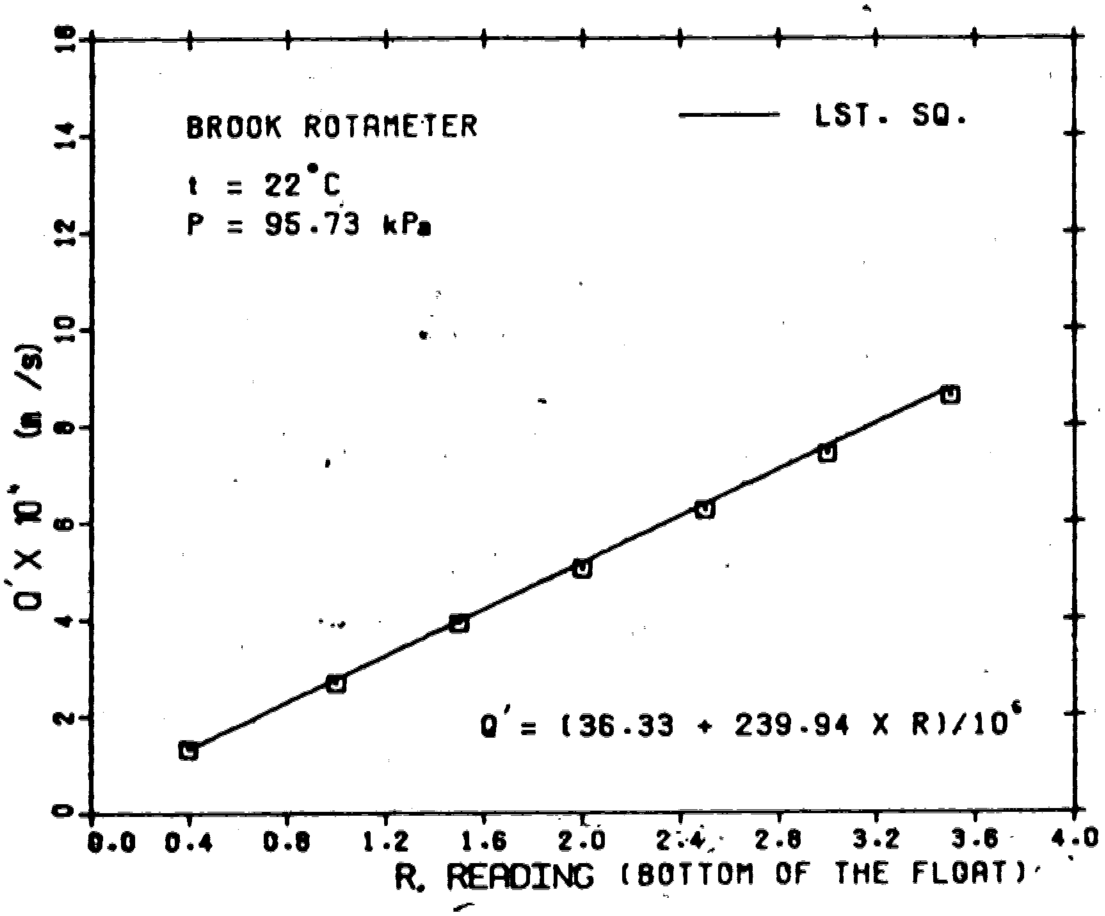

FIGURE 16.2 : CALIBRATION LINE FOR ROTAMETER B

and pressures in Equation 16.1 are in K and kPa, respectively.

The Reynolds number for an air jet issuing from a circle tube with diameter d or a slot tube with width b can then be evaluated from the volumetric flow rate, Q, as follows:

$$Re_b = \bar{v}_j d / \nu = 4 Q / M \nu \qquad (16.2)$$

or

$$Re_b = \bar{v}_j b / \nu = 2 Q / M \nu \qquad (16.3)$$

where M is the wetted perimeter of the tube.

17. APPENDIX C : LISTINGS OF EXPERIMENTAL RESULTS FOR UNCONFINED AXISYMMETRIC JET

A listing of the experimental runs together with the mass transfer duration, operating pressure and operating temperature for unconfined axisymmetric jet are given in Table 17.1. Local fringe orders of different experimental runs are given in Table 17.2.

TABLE 17.1 : EXPERIMENTAL RUNS FOR UNCONFINED AXISYMMETRIC JET

Re_d	RUN NO.	T (s)	t (°C)	P (kPa)
1210	CJ12-1.5A	90	21.0	93.4
	CJ12-3C	180	20.0	93.2
	CJ12-6A	360	21.0	93.2
1470	CJ14-1.5B	90	21.0	94.4
	CJ14-3A	180	20.0	94.5
	CJ14-6A	360	21.0	94.5

TABLE 17.2 : EXPERIMENTAL RESULTS FOR UNCONFINED AXISYMMETRIC JET

RUN NO.	r/d	n	RUN NO.	r/d	n
CJ12-1.5A	6.00	3	CJ14-1.5B	6.79	3
	4.95	4		5.57	4
	3.96	5		4.53	5
	3.43	6		4.07	6
	3.00	7		3.50	7
	2.68	8		3.11	8
CJ12-3C	11.70	3	CJ14-3A	11.93	3
	9.22	4		9.97	4
	7.63	5		7.79	5
	6.58	6		6.83	6
	5.71	7		5.97	7
	5.07	8		5.43	8
	4.64	9		4.89	9
	4.21	10		4.50	10
	3.89	11		4.18	11
	3.64	12		3.84	12
	3.39	13		3.67	13
	3.14	14			
CJ12-6A	18.93	3	CJ14-6A	20.71	3
	15.61	4		17.50	4
	12.93	5		13.64	5
	11.11	6		11.93	6
	9.78	7		10.64	7
	8.83	8		9.50	8
	7.90	9		8.50	9
	7.29	10		7.93	10
	6.74	11		7.39	11
	6.25	12		6.90	12
	5.83	13		6.46	13
	5.54	14		6.12	14
	5.23	15		5.79	15

18. APPENDIX D : LISTINGS OF EXPERIMENTAL RESULTS FOR UNCONFINED TWO-DIMENSIONAL JET

A listing of the experimental runs together with the mass transfer duration, operating pressure and operating temperature for unconfined two-dimensional jet are given in Table 18.1. Local Sherwood numbers of different experimental runs are given in Table 18.2.

TABLE 18.1 : EXPERIMENTAL RUNS FOR UNCONFINED TWO-DIMENSIONAL JET

Re_b	RUN NO.	T (s)	t (°C)	P (kPa)
94	SJ1-2A	120	21.0	94.6
	SJ1-4F	240	21.0	94.3
	SJ1-8E	480	21.0	93.9
204	SJ2-2C	120	20.0	93.6
	SJ2-4A	240	20.0	94.2
	SJ2-8D	480	21.0	93.3

TABLE 18.2 : EXPERIMENTAL RESULTS FOR UNCONFINED TWO-DIMENSIONAL JET

RUN NO.	x/b	Sh_b	RUN NO.	x/b	Sh_b
SJ1-2A	7.13	1.789			
	4.68	2.385			
	3.42	2.846			
	2.59	3.578			
	2.10	4.174			
	1.69	4.773			
SJ1-4F	22.07	0.892	SJ2-4A	29.33	0.962
	13.07	1.189		19.33	1.283
	9.66	1.486		14.00	1.604
	7.33	1.783		10.57	1.925
	5.85	2.080		8.67	2.245
	4.95	2.377		7.07	2.566
	4.14	2.674		5.89	2.887
	3.58	2.971		5.07	3.208
	3.05	3.268		4.36	3.528
				3.82	3.849
				3.53	4.170
SJ1-8E	18.74	0.887	SJ2-8D	23.33	1.030
	14.96	1.035		19.71	1.177
	12.06	1.183		16.66	1.324
	10.17	1.331		14.66	1.971
	8.64	1.478		13.00	1.618
	7.80	1.626		11.66	1.765
	6.76	1.774		10.33	1.912
	5.94	1.922		9.31	2.059
	5.31	2.070		8.57	2.206
	4.80	2.217		7.71	2.353
				7.13	2.500
				6.57	2.647
				5.97	2.795
				5.57	2.942

19. APPENDIX E : LISTINGS OF EXPERIMENTAL RESULTS FOR CONFINED TWO-DIMENSIONAL JET

Listings of the experimental runs together with the mass transfer duration, operating pressure and operating temperature for confined two-dimensional jet are given in Tables 19.1, 19.2 and 19.3. Local Sherwood numbers for different experimental runs are given in Tables 19.4, 19.5 and 19.6 for L=2, 4 and 12, respectively.

TABLE 19.1 : EXPERIMENTAL RUNS FOR CONFINED TWO-DIMENSIONAL JET (L=2).

Re_b	RUN NO.	T (s)	t (°C)	P (kPa)
100	J021-2B	120	21.0	94.3
	J021-2C	120	21.0	94.4
	J021-3A	180	21.0	94.3
	J021-3B	180	20.0	94.2
	J021-4A	240	21.0	94.1
	J021-4B	240	21.0	93.6
	J021-6A	360	21.0	94.1
	J021-6B	360	20.0	94.0
	J021-8A	480	21.0	93.7
	J021-8B	480	21.0	93.9
200	J022-2A	120	21.0	94.0
	J022-2B	120	21.0	94.8
	J022-3A	180	21.0	94.3
	J022-3B	180	21.0	94.2
	J022-4A	240	21.0	93.8
	J022-4B	240	21.0	94.0
	J022-6A	360	21.0	93.7
	J022-6B	360	22.0	94.3
	J022-8A	480	21.0	93.4
	J022-8B	480	21.0	93.7

TABLE 19.1 (CONTINUED)

Re_b	RUN NO.	T (s)	t (°C)	P (kPa)
306	J023-2A	120	21.0	95.2
	J023-2B	120	20.0	94.9
	J023-3A	180	21.0	95.0
	J023-4A	240	21.0	94.9
	J023-4B	240	21.0	94.6
	J023-6A	360	21.0	94.0
	J023-6B	360	21.0	94.2
	J023-8A	480	21.0	93.9
	J023-8B	480	20.0	94.1
400	J024-2A	120	20.0	93.7
	J024-2B	120	20.0	94.2
	J024-3A	180	21.0	94.2
	J024-3B	180	22.0	94.1
	J024-4A	240	21.0	93.4
	J024-4B	240	21.0	93.6
	J024-6A	360	22.0	93.3
	J024-6B	360	22.0	93.5
	J024-8A	480	22.0	93.6
	J024-8B	480	22.0	93.8

TABLE 19.2 : EXPERIMENT RUNS FOR CONFINED TWO-DIMENSIONAL JET (L=4)

Re_b	RUN NO.	T (s)	t (°C)	P (kPa)
100	J041-2A	120	21.5	94.2
	J041-2B	120	21.0	93.6
	J041-3A	180	21.0	93.8
	J041-3B	180	21.0	93.7
	J041-4A	240	22.0	94.1
	J041-4B	240	20.5	93.7
	J041-4C	240	21.0	93.5
	J041-6A	360	21.0	93.4
	J041-6B	360	21.5	93.3
	J041-8A	480	20.0	93.9
	J041-8B	480	20.5	93.9
200	J042-2A	120	20.0	94.2
	J042-2B	120	20.0	94.2
	J042-3A	180	20.5	93.6
	J042-3C	180	20.0	93.6
	J042-4A	240	20.0	94.4
	J042-4B	240	20.0	94.4
	J042-6A	360	20.5	94.1
	J042-6B	360	21.0	94.0
	J042-8A	480	20.0	93.6
	J042-8B	480	21.0	93.7

TABLE 19.2 (CONTINUED)

Re_b	RUN NO.	T (s)	t (°C)	P (kPa)
306	J043-2A	120	21.0	93.4
	J043-2B	120	21.0	93.3
	J043-3A	180	19.5	93.9
	J043-3B	180	20.0	93.9
	J043-4A	240	20.0	95.2
	J043-4B	240	20.0	95.2
	J043-6A	360	20.0	93.9
	J043-6B	360	20.0	93.9
	J043-8A	480	20.0	93.9
	J043-8B	480	20.0	93.9
400	J044-2A	120	20.0	93.9
	J044-2B	120	20.0	93.9
	J044-3A	180	21.0	93.9
	J044-3B	180	21.0	93.9
	J044-4A	240	19.0	93.9
	J044-4B	240	19.0	93.9
	J044-6A	360	20.0	93.9
	J044-6B	360	20.0	93.9
	J044-8A	480	20.0	93.9
	J044-8B	480	20.0	93.9

TABLE 19.3 : EXPERIMENTAL RUNS FOR CONFINED TWO-DIMENSIONAL JET (L=12)

Re_b	RUN NO.	T (s)	t (°C)	P (kPa)
100	J121-2A	120	20.0	95.7
	J121-2B	120	21.0	94.5
	J121-4A	240	20.5	94.5
	J121-4B	240	21.0	94.1
	J121-6A	360	21.0	94.6
	J121-6B	360	21.0	94.0
	J121-8A	480	21.0	94.5
	J121-8B	480	20.0	94.4
200	J122-2A	120	21.0	93.1
	J122-2B	120	21.0	93.3
	J122-4A	240	20.0	93.7
	J122-4B	240	21.0	93.1
	J122-6A	360	20.5	95.0
	J122-6B	360	21.0	93.2
	J122-6D	360	21.0	92.7
	J122-8A	480	21.0	94.9
	J122-8C	480	21.0	94.1

TABLE 19.3 (CONTINUED)

Re_b	RUN NO.	T (s)	t (°C)	P (kPa)
306	J123-2A	120	21.0	94.2
	J123-2B	120	21.0	93.1
	J123-4A	240	20.5	95.1
	J123-4B	240	20.0	94.2
	J123-6A	360	21.0	93.3
	J123-6B	360	20.0	94.3
	J123-8A	480	20.5	95.0
	J123-8B	480	20.0	95.6
400	J124-2A	120	21.0	94.6
	J124-2B	120	20.0	95.0
	J124-4A	240	20.5	94.5
	J124-4B	240	21.0	94.8
	J124-6A	360	21.0	94.6
	J124-6B	360	21.0	94.7
	J124-8A	480	20.0	95.0
	J124-8B	480	20.0	94.1

TABLE 19.4 : EXPERIMENTAL RESULTS FOR CONFINED TWO-DIMENSIONAL JET (L=2)

RUN NO.	x/b	Sh_b	RUN NO.	x/b	Sh_b
J021-2B	3.22	2.971	J021-2C	3.25	2.971
	2.58	3.566		2.65	3.566
	2.16	4.160		2.19	4.160
	1.80	4.754		1.84	4.754
	1.48	5.348		1.53	5.348
	1.28	5.942		1.35	5.942
	1.11	6.537		1.20	6.537
J021-3A	3.16	2.773	J021-3B	4.45	2.135
	2.82	3.169		3.60	2.562
	2.52	3.566		3.10	2.989
	2.14	3.962		2.72	3.416
	1.90	4.358		2.35	3.843
	1.68	4.754		2.05	4.270
	1.51	5.150		1.85	4.696
				1.62	5.123
				1.45	5.550
J021-4A	4.48	2.076	J021-4B	4.54	2.066
	3.90	2.373		3.90	2.361
	3.40	2.670		3.45	2.656
	2.95	2.966		3.14	2.951
	2.59	3.263		2.77	3.247
	2.34	3.560		2.48	3.542
	2.19	3.856		2.27	3.837
J021-6A	14.72	0.989	J021-6B	16.50	1.066
	11.08	1.187		11.75	1.279
	7.19	1.384		7.10	1.492
	5.38	1.582		5.55	1.705
	5.01	1.780		4.95	1.918
	4.50	1.978		4.45	2.131
	4.01	2.175		4.01	2.344
	3.57	2.373		3.65	2.557
	3.16	2.571		3.30	2.771

TABLE 19.4 (CONTINUED)

RUN NO.	x/b	Sh_b	RUN NO.	x/b	Sh_b
J021-8A	41.14	0.738	J021-8B	42.19	0.739
	27.95	0.886		31.65	0.887
	20.04	1.033		21.10	1.035
	14.77	1.181		16.82	1.183
	10.97	1.328		11.37	1.331
	7.70	1.476		7.86	1.478
	5.91	1.623		6.10	1.626
	5.12	1.771		4.87	1.774
	4.69	1.919		4.45	1.922
				4.22	2.070
				3.99	2.217
J022-2A	7.28	1.777	J022-2B	4.64	2.986
	6.12	2.369		4.01	3.584
	4.96	2.961		3.64	4.181
	4.11	3.554		3.04	4.778
	3.50	4.146		2.50	5.375
	2.95	4.738		2.18	5.973
	2.58	5.330		1.81	6.570
	2.22	5.923		1.65	7.167
	1.74	6.515		1.39	7.764
	1.48	7.107			
J022-3A	7.17	1.981	J022-3B	6.71	1.978
	6.20	2.377		5.92	2.373
	5.40	2.773		5.32	2.769
	4.76	3.169		4.58	3.164
	4.00	3.566		3.90	3.560
	3.40	3.962		3.45	3.955
	3.02	4.358		3.01	4.351
	2.68	4.754		2.71	4.756
	2.50	5.150		2.45	5.142
	2.17	5.547		2.27	5.537
	1.97	5.942		2.08	5.932

TABLE 19.4 (CONTINUED)

RUN NO.	x/b	Sh_b	RUN NO.	x/b	Sh_b
J022-4A	6.27	2.070	J022-4B	4.77	3.257
	5.78	2.365		4.43	3.554
	5.49	2.661		4.02	3.850
	5.08	2.956		3.57	4.156
	4.59	3.252		3.12	4.442
	4.22	3.548		2.87	4.738
	3.90	3.843		2.64	5.034
	3.38	4.139		2.46	5.330
	3.16	4.434		2.26	5.626
	2.85	4.730			
	2.62	5.026			
	2.41	5.321			
	2.22	5.617			
J022-6A	6.31	2.164	J022-6B	6.33	2.012
	6.08	2.361		6.01	2.195
	5.40	2.558		5.76	2.378
	5.16	2.754		5.51	2.561
	4.81	2.951		5.22	2.744
	9.21	1.377		8.60	1.280
	11.12	1.574		10.21	1.463
	14.26	1.377		13.84	1.280
	22.90	1.181		22.63	1.098
	34.49	0.984		33.76	0.915
J022-8A	6.20	2.206	J022-8B	6.04	2.214
	5.91	2.353		5.84	2.361
	5.68	2.500		5.55	2.509
	8.92	1.324		8.33	1.328
	10.80	1.471		10.55	1.476
	15.09	1.324		14.45	1.328
	21.48	1.177		20.36	1.181
	30.59	1.030		28.48	1.033
	45.04	0.883		44.30	0.885
J023-2A	6.01	3.602	J023-2B	6.33	3.229
	5.12	4.202		5.80	3.875
	3.95	4.806		4.78	4.521
	3.16	5.403		3.88	5.167
	2.77	6.003		3.12	5.813
	2.43	6.604		2.74	6.459
	2.11	7.204		2.38	7.104
	1.85	7.804			

TABLE 19.4 (CONTINUED)

RUN NO.	x/b	Sh_b	RUN NO.	x/b	Sh_b
J023-3A	6.92	2.797			
	6.52	3.196			
	5.85	3.596			
	4.92	3.995			
	4.48	4.395			
	4.14	4.794			
	3.69	5.194			
	3.48	5.594			
	3.06	5.993			
J023-4A	7.59	2.692	J023-4B	7.22	2.683
	6.96	2.992		6.71	2.981
	6.59	3.290		6.01	3.280
	6.03	3.590		5.73	3.578
	5.65	3.889		5.27	3.876
	5.17	4.188		4.91	4.174
	4.75	4.487		4.60	4.472
	4.24	4.786		4.42	4.770
	3.74	5.085		4.11	5.068
	3.53	5.385		3.74	5.366
	3.27	5.684		3.46	5.664
J023-6A	7.17	2.567	J023-6B	7.11	2.571
	6.96	2.764		6.78	2.769
	6.65	2.961		6.57	2.966
	6.33	3.159		6.31	3.164
	6.12	3.356		5.98	3.362
	5.91	3.554		11.18	1.384
	5.67	3.751		12.55	1.582
	12.90	1.580		15.51	1.780
	15.93	1.777		21.10	1.582
	19.30	1.580		27.22	1.384
	26.37	1.382		37.45	1.187
	35.60	1.185		44.62	0.989
	45.36	0.987			

TABLE 19.4 (CONTINUED)

RUN NO.	x/b	Sh_b	RUN NO.	x/b	Sh_b
J023-8A	8.23	2.513	J023-8B	8.02	2.717
	7.86	2.661		7.70	2.877
	7.32	2.809		7.30	3.037
	6.96	2.957		14.19	1.758
	6.49	3.104		16.80	1.758
	13.90	1.626		21.60	1.599
	16.48	1.626		26.79	1.439
	22.15	1.478		36.20	1.279
	27.95	1.331		44.12	1.119
	28.50	1.183			
	45.36	1.035			
J024-2A	7.49	3.186	J024-2B	7.82	3.202
	6.50	3.823		6.77	3.843
	5.59	4.460		5.88	4.483
	5.11	5.098		5.15	5.123
	4.55	5.735		4.37	5.764
	4.01	6.372		3.86	6.404
	3.43	7.009		3.30	7.045
	3.06	7.646		2.99	7.685
	2.64	8.284		2.59	8.325
	2.32	8.921			
	1.98	9.558			
J024-3A	6.77	3.566	J024-3B	7.56	3.281
	6.52	3.962		7.20	3.646
	6.13	4.358		6.78	4.010
	5.90	4.754		6.33	4.375
	5.59	5.150		5.95	4.739
	5.27	5.546		5.45	5.104
	4.85	5.942		4.99	5.468
	4.43	6.339		4.49	5.833
	4.01	6.735		4.06	6.198
	3.64	7.131		3.75	6.562
	3.27	7.527		3.48	6.927

TABLE 19.4 (CONTINUED)

RUN NO.	x/b	Sh_b	RUN NO.	x/b	Sh_b
J024-4A	7.10	3.236	J024-4B	7.70	3.247
	6.86	3.530		7.38	3.542
	6.54	3.824		6.90	3.837
	6.38	4.118		6.50	4.132
	5.89	4.412		6.22	4.427
	5.65	4.706		5.85	4.722
	5.38	5.001		5.44	5.017
	5.22	5.295		5.06	5.312
	4.93	5.589		4.80	5.608
	4.60	5.883			
	4.20	6.177			
	4.00	6.471			
	3.74	6.765			
	3.38	7.060			
	3.11	7.354			
J024-6A	8.40	2.712	J024-6B	8.58	2.716
	7.91	2.892		8.29	2.897
	7.58	3.073		7.90	3.078
	7.31	3.254		7.58	3.259
	7.17	3.435		7.19	3.440
	6.85	3.616		11.60	1.268
	6.65	3.796		12.66	1.449
	6.46	3.977		14.24	1.630
	6.22	4.158		15.30	1.811
	11.60	1.266		17.41	1.811
	12.55	1.4[illegible]6		21.10	1.630
	13.82	1.627		28.48	1.449
	14.77	1.808		33.76	1.268
	18.14	1.808		42.19	1.087
	20.83	1.627			
	27.43	1.446			
	31.12	1.266			
	42.72	1.085			

TABLE 19.4 (CONTINUED)

RUN NO.	x/b	Sh_b	RUN NO.	x/b	Sh_b
J024-8A	8.97	2.585	J024-8B	8.70	2.589
	8.49	2.721		8.38	2.725
	7.92	2.857		7.88	2.862
	11.33	1.224		11.71	1.227
	12.00	1.360		12.34	1.363
	12.55	1.497		13.19	1.499
	13.40	1.633		14.03	1.635
	17.41	1.769		16.61	1.772
	21.62	1.633		21.10	1.635
	24.26	1.497		25.32	1.499
	28.48	1.360		29.54	1.363
	34.81	1.224		35.86	1.227
	44.30	1.088		44.83	1.090

TABLE 19.5 : EXPERIMENTAL RESULTS FOR CONFINED TWO-DIMENSIONAL JET (L=4)

RUN NO.	x/b	Sh_b	RUN NO.	x/b	Sh_b
J041-2A	4.81	2.279	J041-2B	5.54	1.768
	3.85	2.854		4.46	2.355
	3.11	3.423		3.60	2.949
	2.52	3.991		2.95	3.536
	1.96	4.566		2.33	4.123
	1.50	5.134		1.94	4.717
				1.50	5.304
				1.13	5.890
J041-3A	4.95	1.973	J041-3B	5.54	1.969
	4.22	2.363		4.69	2.359
	3.57	2.760		4.05	2.756
	3.18	3.150		3.54	3.145
	2.72	3.548		3.01	3.542
	2.30	3.938		2.58	3.931
	2.04	4.335		2.22	4.328
	1.71	4.732		1.89	4.725
	1.42	5.123		1.59	5.114
				1.38	5.510
				1.19	5.900
				1.00	6.295
J041-4A	5.47	1.916	J041-4C	4.64	2.065
	4.80	2.185		4.16	2.355
	4.27	2.461		3.67	2.652
	3.83	2.737		3.32	2.949
	3.53	3.006		2.95	3.239
	3.16	3.281		2.64	3.536
	2.83	3.557		2.38	3.833
	2.54	3.826		2.06	4.123
	2.27	4.101		1.85	4.420
				1.63	4.717
J041-4B	4.28	2.147			
	3.80	2.448			
	3.36	2.757			
	3.01	3.066			
	2.70	3.367			
	2.37	3.676			

TABLE 19.5 (CONTINUED)

RUN NO.	x/b	Sh_b	RUN NO.	x/b	Sh_b
J041-6A	5.54	1.765	J041-6B	6.17	1.669
	5.06	1.963		5.70	1.856
	4.65	2.160		5.08	2.043
	4.32	2.351		4.69	2.223
	3.96	2.549		4.24	2.410
	3.55	2.746		3.92	2.597
	3.16	2.942		3.69	2.784
	2.92	3.138		11.66	0.557
	2.64	3.334		15.12	0.742
	2.37	3.530		22.05	0.557
	2.18	3.726			
	11.52	0.589			
	14.89	0.785			
	24.37	0.589			
J041-8A	5.96	1.915	J041-8B	5.75	1.689
	5.38	2.076		5.33	1.844
	5.06	2.237		4.92	1.999
	4.69	2.397		4.66	2.154
	4.35	2.551		4.37	2.309
	9.06	0.479		4.15	2.457
	12.50	0.638		3.90	2.612
	15.04	0.798		3.66	2.766
	19.94	0.638		9.34	0.461
	27.90	0.479		11.71	0.615
				15.82	0.769
				19.83	0.615
				32.91	0.461
J042-2A	5.83	2.564	J042-2B	5.25	2.564
	4.95	3.210		4.49	3.210
	4.14	3.849		3.80	3.849
	3.36	4.488		3.07	4.488
	2.72	5.135		2.53	5.135
	2.24	5.773		2.03	5.773
	1.85	6.412		1.66	6.412
	1.52	7.059		1.42	7.059

TABLE 19.5 (CONTINUED)

RUN NO.	x/b	Sh_b	RUN NO.	x/b	Sh_b
J042-3A	5.76	2.448	J042-3C	5.38	2.542
	5.16	2.860		4.84	2.970
	4.60	3.264		4.27	3.389
	4.17	3.676		3.77	3.817
	3.69	4.080		3.28	4.237
	3.16	4.492		2.84	4.664
	2.77	4.904		2.48	5.092
	2.43	5.308		2.16	5.511
	2.13	5.718		1.90	5.939
	1.86	6.128		1.68	6.359
	1.66	6.535			
	1.44	6.945			
J042-4A	6.49	2.564	J042-4B	8.01	2.248
	5.76	2.887		6.51	2.564
	5.27	3.210		5.80	2.887
	4.85	3.526		5.34	3.210
	4.40	3.849		4.94	3.526
	3.90	4.172		4.53	3.849
	3.59	4.488		4.16	4.172
	3.16	4.811		3.74	4.488
	2.89	5.135		3.33	4.811
	2.72	5.450		3.02	5.135
	2.27	5.773		2.69	5.450
	2.07	6.097		2.44	5.773
J042-6A	7.23	2.261	J042-6B	6.54	2.566
	6.75	2.461		6.08	2.765
	6.27	2.668		5.65	2.964
	5.89	2.875		5.33	3.156
	5.44	3.081		4.96	3.355
	5.16	3.218		4.64	3.554
	4.66	3.488		4.24	3.753
	4.35	3.695		4.00	3.952
	3.90	3.902		3.64	4.145
	3.48	4.108		3.26	4.340
	2.95	4.310		2.85	4.540
	13.44	0.616		13.66	0.592
	15.77	0.821		16.43	0.790
	19.54	1.026		17.20	0.987
	24.10	1.026		27.43	0.790
	32.20	0.821		39.24	0.592
	48.05	0.616			

TABLE 19.5 (CONTINUED)

RUN NO.	x/b	Sh_b	RUN NO.	x/b	Sh_b
J042-8A	7.59	2.389	J042-8B	8.80	1.919
	6.75	2.542		8.08	2.066
	6.00	2.702		7.20	2.217
	5.80	2.863		6.70	2.359
	5.38	3.023		6.43	2.508
	5.15	3.183		6.01	2.656
	4.82	3.345		5.74	2.805
	4.55	3.495		5.54	2.954
	4.12	3.655		5.26	3.103
	3.92	3.815		5.04	3.244
	3.53	3.975		4.81	3.393
	13.19	0.634		4.55	3.542
	14.94	0.794		4.23	3.690
	16.77	0.954		4.01	3.839
	18.79	1.115		3.71	3.988
	20.04	1.115		3.39	4.130
	25.21	0.954		12.13	0.590
	31.12	0.794		14.80	0.738
				16.21	0.886
				17.91	1.033
				22.90	1.033
				29.01	0.886
				34.20	0.738
				41.35	0.590
J043-2A	7.05	3.530	J043-2B	5.55	4.116
	5.80	4.116		5.02	4.709
	5.21	4.709		4.30	5.295
	4.48	5.295		3.72	5.881
	3.82	5.881		2.83	6.474
	3.09	6.474		2.38	7.060
	2.58	7.060		2.01	7.625
	2.17	7.625			

TABLE 19.5 (CONTINUED)

RUN NO.	x/b	Sh_b	RUN NO.	x/b	Sh_b
J043-3A	6.76	3.115	J043-3B	7.16	2.980
	6.12	3.556		6.59	3.401
	5.33	4.004		5.81	3.830
	4.81	4.444		5.01	4.251
	4.25	4.893		4.48	4.680
	3.85	5.341		3.82	5.109
	3.28	5.782		3.25	5.530
	2.80	6.230		2.80	5.959
	2.52	6.671		2.46	6.380
	2.15	7.119		2.20	6.809
				1.98	7.230
J043-4A	7.53	2.911	J043-4B	7.06	2.911
	6.86	3.238		6.49	3.238
	6.44	3.556		6.08	3.556
	5.96	3.882		5.60	3.882
	5.49	4.208		5.12	4.208
	4.94	4.526		4.54	4.526
	4.38	4.852		4.11	4.852
	3.89	5.178		3.62	5.178
	3.49	5.497		3.24	5.497
	3.13	5.823		2.93	5.823
	2.79	6.149		2.63	6.149
	2.53	6.467			
	2.28	6.793			

TABLE 19.5 (CONTINUED)

RUN NO.	x/b	Sh_b	RUN NO.	x/b	Sh_b
J043-6A	8.31	2.765	J043-6B	7.94	2.765
	7.70	2.980		7.33	2.980
	7.38	3.194		7.03	3.194
	7.01	3.401		6.70	3.401
	6.66	3.615		6.53	3.615
	6.39	3.830		6.20	3.830
	6.04	4.044		5.91	4.044
	5.75	4.259		5.65	4.259
	5.42	4.465		5.26	4.465
	5.05	4.680		4.96	4.680
	4.69	4.894		4.63	4.894
	4.32	5.109		4.28	5.109
	4.01	5.315		3.91	5.315
	3.69	5.530		3.66	5.530
	3.48	5.744		3.39	5.744
	3.16	5.959		3.16	5.959
	2.95	6.173		2.92	6.173
	2.74	6.383		2.70	6.383
	2.54	6.595		2.53	6.595
	16.56	0.638		17.76	0.638
	19.23	0.851		19.51	0.851
	22.63	1.064		23.42	1.064
	28.59	1.064		25.94	1.064
	35.76	0.851		36.60	0.851
	47.33	0.638			
J043-8A	9.62	2.394	J043-8B	9.85	2.394
	8.97	2.553		9.12	2.553
	8.12	2.711		8.55	2.711
	7.61	2.872		8.12	2.872
	7.23	3.033		7.82	3.033
	6.91	3.194		17.38	0.638
	6.64	3.355		18.65	0.798
	17.30	0.638		21.10	0.957
	18.86	0.798		24.46	1.117
	21.50	0.957		25.51	1.117
	24.23	1.117		29.96	0.957
	26.79	1.117		38.50	0.798
	32.70	0.957		46.84	0.638
	40.02	0.798			

TABLE 19.5 (CONTINUED)

RUN NO.	x/b	Sh_b	RUN NO.	x/b	Sh_b
J044-2A	6.00	4.468	J044-2B	6.14	4.468
	5.45	5.106		5.61	5.106
	4.87	5.744		5.07	5.744
	4.24	6.383		4.35	6.383
	3.53	7.021		3.59	7.021
	2.90	7.659		2.93	7.659
	2.48	8.297		2.43	8.297
	2.11	8.936			
	1.79	9.574			
J044-3A	6.76	3.942	J044-3B	5.19	5.124
	6.43	4.336		4.85	5.518
	6.07	4.730		4.41	5.913
	5.64	5.124		3.99	6.307
	5.12	5.518		3.59	6.701
	4.64	5.913			
	4.20	6.307			
	3.61	6.701			
	3.16	7.095			
	3.02	7.489			
	2.62	7.883			
	2.43	8.278			
J044-4A	7.01	3.837	J044-4B	7.38	3.837
	6.56	4.186		6.96	4.186
	6.33	4.535		6.38	4.535
	5.88	4.884		6.02	4.884
	5.54	5.232		5.64	5.232
	5.25	5.581		5.27	5.581
	4.91	5.930		5.01	5.930
	4.49	6.279			
	4.20	6.628			

TABLE 19.5 (CONTINUED)

RUN NO.	x/b	Sh_b	RUN NO.	x/b	Sh_b
J044-6A	9.92	3.191	J044-6B	9.81	3.191
	9.07	3.404		9.02	3.404
	8.23	3.617		8.40	3.617
	7.59	3.830		7.91	3.830
	7.23	4.042		7.54	4.402
	6.80	4.255		7.01	4.255
	6.59	4.468		6.75	4.468
	22.15	0.638		22.68	0.638
	24.26	0.851		25.32	0.851
	27.95	1.064		27.43	1.064
	37.97	0.851		40.08	0.851
J044-8A	10.97	3.032	J044-8B	11.89	2.713
	10.02	3.191		11.15	2.872
	9.39	3.351		10.50	3.032
	8.81	3.511		10.02	3.191
	8.23	3.670		9.18	3.351
	7.97	3.830		8.60	3.511
	7.75	3.989		8.20	3.670
	21.94	0.638		7.81	3.830
	23.73	0.798		7.50	3.989
	26.37	0.957		22.47	0.638
	27.43	1.117		24.26	0.798
	29.54	1.117		26.69	0.957
	34.81	0.957		27.95	1.117
	47.47	0.798		30.06	1.117
				35.86	0.957
				45.89	0.798

TABLE 19.6 : EXPERIMENTAL RESULTS FOR CONFINED TWO-DIMENSIONAL JET (L=12)

RUN NO.	x/b	Sh_b	RUN NO.	x/b	Sh_b
J121-2A	11.54	0.652	J121-2B	11.71	0.593
	7.29	1.306		8.89	1.193
	4.70	1.954		5.85	1.786
	3.21	2.603		4.10	2.379
	2.35	3.260		3.03	2.979
	1.31	3.908		2.29	3.572
J121-4A	10.31	0.927	J121-4B	15.15	0.299
	8.81	1.238		12.55	0.590
	6.83	1.542		10.82	0.889
	5.33	1.854		9.55	1.187
	4.35	2.165		7.79	1.478
	3.52	2.469		6.02	1.777
	3.05	2.780			
J121-6A	12.55	0.595	J121-6B	12.68	0.592
	11.13	0.793		11.00	0.789
	10.04	0.993		10.03	0.988
	9.20	1.193		9.30	1.187
	7.90	1.386		7.90	1.379
				6.67	1.578
				5.78	1.777
J121-8A	14.50	0.447	J121-8B	13.20	0.639
	13.16	0.593		11.90	0.801
	12.08	0.743		11.39	0.962
	11.49	0.893		10.00	1.124
	10.28	1.043		9.27	1.286
	9.33	1.193		8.07	1.447
	8.14	1.343			
	7.05	1.486			
	6.34	1.636			
J122-2A	7.34	1.759	J122-2B	7.34	1.765
	5.15	2.343		5.41	2.353
	3.46	2.934		3.91	2.944
	2.68	3.518		2.99	3.530
	2.06	4.102		2.38	4.116
				1.82	4.709

TABLE 19.6 (CONTINUED)

RUN NO.	x/b	Sh_b	RUN NO.	x/b	Sh_b
J122-4A	14.84	0.956	J122-4B	15.21	0.880
	11.87	1.277		13.81	1.175
	9.59	1.591		10.98	1.464
	7.26	1.912		8.45	1.759
	5.71	2.233		6.85	2.055
	4.57	2.546		5.48	2.343
	3.88	2.867		4.57	2.639
J122-6A	16.62	0.829	J122-6B	15.09	0.980
	14.89	1.038		13.20	1.177
	13.52	1.247		11.42	1.367
	11.42	1.448		9.41	1.565
	9.36	1.657		7.99	1.762
	8.01	1.866		6.85	1.959
	6.85	2.075		5.71	2.157
	5.84	2.284			
	5.04	2.486			
	4.57	2.695			
J122-6D	15.75	0.975			
	14.08	1.171			
	12.50	1.361			
	10.53	1.557			
	9.08	1.753			
	7.24	1.950			
	6.32	2.146			
J122-8A	16.23	0.747	J122-8C	13.60	1.189
	15.57	0.898		12.24	1.339
	14.89	1.048		10.96	1.481
	13.60	1.199		9.47	1.630
	12.06	1.350		8.11	1.780
	10.97	1.494		7.19	1.929
	9.43	1.644		6.16	2.079
	7.89	1.795		5.59	2.228
	6.93	1.946			
	6.16	2.097			
	5.73	2.247			

TABLE 19.6 (CONTINUED)

RUN NO.	x/b	Sh_b	RUN NO.	x/b	Sh_b
J123-2A	8.88	1.783	J123-2B	9.03	1.762
	6.61	2.375		6.75	2.347
	4.70	2.974		4.88	2.939
	3.67	3.566		3.73	3.524
	2.88	4.157		3.02	4.109
	2.38	4.756		2.42	4.701
	1.82	5.348		1.86	5.286
J123-4A	9.90	1.553	J123-4B	9.77	1.599
	8.73	1.866		8.73	1.921
	7.61	2.180		7.47	2.244
	6.18	2.486		6.05	2.559
	5.14	2.799		5.15	2.882
	4.43	3.113		4.43	3.205
	3.89	3.419		3.73	3.520
J123-6A	9.71	1.565	J123-6B	9.16	1.709
	8.90	1.762		8.37	1.925
	8.15	1.959		7.47	2.140
	7.24	2.157		6.44	2.356
	6.21	2.347		5.72	2.564
				5.29	2.779
J123-8A	10.00	1.553	J123-8B	11.08	1.467
	9.31	1.710		10.22	1.623
	8.83	1.866		9.44	1.787
	8.14	2.023			
	7.44	2.180			
	6.84	2.337			
	6.14	2.486			
	5.69	2.643			
	5.12	2.799			
	4.86	2.956			
J124-2A	10.01	1.789	J124-2B	9.38	1.893
	6.41	2.385		5.94	2.581
	4.78	2.981		4.52	3.232
	3.92	3.578		3.59	3.875
	3.29	4.174		2.96	4.519

TABLE 19.6 (CONTINUED)

RUN NO.	x/b	Sh_b	RUN NO.	x/b	Sh_b
J124-4A	[illegible].16	1.545	J124-4B	11.44	1.491
	9.16	1.857		9.90	1.792
	7.40	2.169		7.32	2.093
	6.47	2.473		6.42	2.387
	5.64	2.785		5.58	2.688
	4.91	3.097		5.12	2.989
	4.41	3.402		4.69	3.283
	3.89	3.713			
J124-6A	11.79	1.589	J124-6B	11.70	1.591
	10.76	1.789		10.44	1.792
	9.59	1.989		9.16	1.993
	8.01	2.190		8.18	2.193
	7.44	2.383		7.38	2.387
	6.41	2.583		6.57	2.588
	6.17	2.783		5.89	2.788
	5.58	2.984		5.38	2.989
	5.09	3.177		4.86	3.182
	4.85	3.377		4.58	3.383
J124-8A	12.10	1.457	J124-8B	12.39	1.443
	11.14	1.612		11.66	1.596
	10.03	1.775		10.59	1.757
	9.44	1.938		9.84	1.918
	8.58	2.101		8.80	2.079
	7.78	2.263			
	7.21	2.426			
	6.58	2.581			
	5.87	2.744			
	5.46	2.957			
	5.09	3.069			
	4.81	3.232			
	4.46	3.395			
	4.15	3.550			

20. APPENDIX F : COMPUTER PROGRAM

The main program, PROGRAM, together with four subroutines, ITER1, CALC1, ITER2 and CALC2 are listed in this appendix.

A typical output for numerical run no. 2B100 for L=2 and Re_b=100 with an initial parabolic velocity profile are also listed. The differencing scheme used in this numerical run is the upstream-weighted differencing scheme (U.W.D.S.).

```
C     NOTATIONS:
C
C     C   : DIMENSIONLESS MOLAR CONCENTRATION
C     L   : JET-TO-PLATE SPACING
C     RE  : REYNOLDS NUMBER BASED ON JET WIDTH
C     S   : DIMENSIONLESS STREAM FUNCTION
C     SC  : SCHMIDT NUMBER
C     SH  : SHERWOOD NUMBER BASED ON JET WIDTH
C     W   : DIMENSIONLESS VORTICITY
C     UC  : DIMENSIONLESS VELOCITY IN X-DIRECTION
C     VC  : DIMENSIONLESS VELOCITY IN Y-DIRECTION
C     X   : DIMENSIONLESS HORIZONTAL COORDINATE
C     Y   : DIMENSIONLESS VERTICAL COORDINATE
C
      REAL L
      COMMON RE,L,A,B,SC,ISCH
      COMMON N1,N2,N3,N4,N5,N6,N7,N8,N9,N10
      COMMON N11,N12,N13,N14,N15,N16,N17,N18
      COMMON NY,NT,NJ1,NJ,DX128
      COMMON DX1,DX2,DX4,DX8,DX16,DX32,DX64
      COMMON ISTOR,DYP
      COMMON X(70),XC(70),Y(35),YP(35),YC(35)
      COMMON DXB(70),DXC(70),DYB(35),DYC(35)
      COMMON S(70,35),W(70,35),C(70,35)
      COMMON U(70,35),V(70,35)
C
C     ****************************
C     *  READ INITIAL INPUT DATA  *
C     ****************************
C
      WRITE (6,100)
  100 FORMAT (/)
      WRITE (6,110)
  110 FORMAT (1X,'(1) ENTER THE PARAMETERS OF THE PROBLEM:')
      WRITE (6,100)
      WRITE (6,111)
  111 FORMAT (1X,'REYNOLDS NUMBER, RE:')
      READ (5,112) RE
  112 FORMAT (F10.4)
      WRITE (6,113)
  113 FORMAT (1X,'JET-TO-PLATE SPACING, L:')
      READ (5,112) L
C
      WRITE (6,100)
      WRITE (6,120)
  120 FORMAT (1X,'(2) ENTER DATA FOR CALCULATING GRID SIZE:')
      WRITE (6,100)
      WRITE (6,121)
  121 FORMAT (1X,'NO. OF INTERVALS IN Y-DIRECTION:')
      READ (5,122) NY
  122 FORMAT (I5)
      WRITE (6,123)
  123 FORMAT (1X,'VALUE OF STRETCH CONSTANT, A:')
      READ (5,112) A
      WRITE (6,124)
  124 FORMAT (1X,'NO. OF INTERVALS IN X-DIRECTION:')
      READ (5,122) NT
C
      WRITE (6,100)
      WRITE (6,150)
```

```
  190 FORMAT (1X,'(3) CHOICE OF DIFFERENCING SCHEMES:')
      WRITE (6,191)
  191 FORMAT (1X,'(1=C.D.S.,2=U.D.S.,3=U.V.D.S.)')
      READ (5,122) ISCH
C
C     ************************
C     *  CALCULATE GRID SIZE  *
C     ************************
C
      NJ=16
      N1=NJ/2+1
      N2=N1+1
      N3=N2+1
      N4=N3+1
      N5=N4+2
      N6=N5+1
      N7=N6+20
      N8=N7+1
      N9=N8+7
      N10=N9+1
      N11=N10+4
      N12=N11+1
      N13=N12+3
      N14=N13+1
      N15=NY+1
      N16=NY+1
      N17=NY-1
      N18=NY-1
      NJ1=N1-1
C
      DX1=1./NJ
      DX2=DX1*2.
      DX4=DX1*4.
      DX8=DX1*8.
      DX16=DX1*16.
      DX32=DX1*32.
      DX64=DX1*64.
      DX128=DX1*128.
C
      DO 200 J=1,N1
      X(J)=DX1*(J-1)
  200 CONTINUE
C
      DO 210 J=N2,N15
C
      IF (J.GE.N2.AND.J.LE.N3) GO TO 2002
      IF (J.GE.N4.AND.J.LE.N5) GO TO 2004
      IF (J.GE.N6.AND.J.LE.N7) GO TO 2008
      IF (J.GE.N8.AND.J.LE.N9) GO TO 2016
      IF (J.GE.N10.AND.J.LE.N11) GO TO 2032
      IF (J.GE.N12.AND.J.LE.N13) GO TO 2064
      IF (J.GE.N14.AND.J.LE.N15) GO TO 2128
C
 2002 DX=DX2
      GO TO 2222
 2004 DX=DX4
      GO TO 2222
 2008 DX=DX8
      GO TO 2222
 2016 DX=DX16
```

```
      GO TO 2222
 2032 DX=DX32
      GO TO 2122
 2064 DX=DX64
      GO TO 2212
 2128 DX=DX128
      GO TO 2222
C
 2222 X(J)=DX+X(J-1)
  210 CONTINUE
C
      DO 215 I=1,NT
      XC(I)=X(I)+(X(I+1)-X(I))/2.
      DXB(I)=X(I+1)-X(I)
  215 CONTINUE
C
      DO 217 I=2,NT
      DXC(I)=XC(I)-XC(I-1)
  217 CONTINUE
C
      DYP=L/FLOAT(NY)
      B=L/(1.-EXP(-A*L))
C
      DO 220 K=1,N16
      YP(K)=DYP*(K-1)
      Y(K)=B*(1.-EXP(-A*YP(K)))
  220 CONTINUE
C
      DO 225 J=1,NY
      YC(J)=Y(J)+(Y(J+1)-Y(J))/2.
      DYB(J)=Y(J+1)-Y(J)
  225 CONTINUE
C
      DO 227 J=2,NY
      DYC(J)=YC(J)-YC(J-1)
  227 CONTINUE
C
      SC=2.74
C
      CALL ITER1
C
      IF (ISTOR.EQ.1) GO TO 9090
C
      CALL CALC1
C
      CALL ITER2
C
      IF (ISTOR.EQ.1) GO TO 9090
C
      CALL CALC2
C
 9090 STOP
      END
End of file
```

```
      SUBROUTINE ITER1
      REAL L
      COMMON RE,L,A,B,SC,ISCH
      COMMON N1,N2,N3,N4,N5,N6,N7,N8,N9,N10
      COMMON N11,N12,N13,N14,N15,N16,N17,N18
      COMMON NY,NT,NJ1,NJ,DX128
      COMMON DX1,DX2,DX4,DX8,DX16,DX32,DX64
      COMMON ISTOR,DYP
      COMMON X(70),XC(70),Y(35),YP(35),YC(35)
      COMMON DXB(70),DXC(70),DYB(35),DYC(35)
      COMMON S(70,35),W(70,35),C(70,35)
      COMMON U(70,35),V(70,35)
      DIMENSION SN(70,35),WN(70,35)
      DIMENSION UC(70,35),VC(70,35)
      DIMENSION ALPHA(70,35),BETA(70,35),GAMMA(70,35),DETA(70,35)
      DIMENSION XI(70,35),ETA(70,35)
      DIMENSION A1(70,35),A2(70,35),A3(70,35),A4(70,35),A5(70,35)
      DIMENSION B1(70),B2(70),B3(70,35),B4(35),B5(35)
      DIMENSION SFD(35),WFD(35)
      DIMENSION ERS(70,35),ERW(70,35),RS(70,35),RW(70,35)
C
C     ***************************
C     *  READ INITIAL INPUT DATA  *
C     ***************************
C
      WRITE (6,100)
  100 FORMAT (//)
      WRITE (6,130)
  130 FORMAT (1X,'(1) ENTER INPUT DATA FOR ITERATIONS:')
      WRITE (6,100)
      WRITE (6,131)
  131 FORMAT (1X,'DO YOU WANT TO USE DATA FROM THE FILE?')
      WRITE (6,132)
  132 FORMAT (1X,' (0=YES,1=NO)')
      READ (5,122) IGUES
  122 FORMAT (I5)
C
      IF (IGUES.EQ.0) GO TO 1001
C
      WRITE (6,133)
  133 FORMAT (1X,'INITIAL GUESSES, SS,WW:')
      READ (5,134) SS,WW
  134 FORMAT (2F10.4)
 1001 WRITE (6,135)
  135 FORMAT (1X,'RELAXATION FACTORS, FS,FW:')
      READ (5,134) FS,FW
C
      WRITE (6,136)
  136 FORMAT (1X,'MAXIMUM NO. OF ITERATIONS FOR VORTICITY, IMAX:')
      READ (5,122) IMAX
      WRITE (6,137)
  137 FORMAT (1X,'CONVERGENCE CRITERION:')
      READ (5,112) CONV
  112 FORMAT (F10.4)
C
      WRITE (6,100)
      WRITE (6,140)
  140 FORMAT (1X,'(2) ENTER INPUT DATA FOR PRINT OUT:')
      WRITE (6,100)
```

```
      WRITE (6,141)
  141 FORMAT (1X,'NO. OF ITERATIONS FOR VORTICITY BEFORE ',
     .  'FIRST PRINT OUT:')
      READ (5,122) IMIN
      WRITE (6,142)
  142 FORMAT (1X,'NO. OF ITERATIONS FOR VORTICITY OF EACH ',
     .  'PRINT OUT:')
      READ (5,122) NS
      WRITE (6,143)
  143 FORMAT (1X,'NO. OF ITERATIONS OF STREAM FUNCTION PER EACH ',
     .  'ITERATION OF VORTICITY:')
      READ (5,122) IST
      WRITE (6,144)
  144 FORMAT (1X,'ISTEP,ISTEPY:')
      READ (5,145) ISTEP,ISTEPY
  145 FORMAT (2I5)
C
C
C     ******************************
C     *  COMPUTE PROBLEM CONSTANTS  *
C     ******************************
C
      CONS=4.49341
      BO=EXP(-8.*CONS**2*(X(N1B)-X(NT))/L/RE)
C
      DO 300 J=2,NY
      DO 300 I=2,N1B
      XI(I,J)=DYC(J)/DXB(I-1)/RE
  300 CONTINUE
C
      DO 310 J=2,N1B
      DO 310 I=2,NT
      ETA(I,J)=DXC(I)/DYB(J-1)/RE
  310 CONTINUE
C
      DO 330 I=2,NT
      B1(I)=2./DXB(I-1)/(DXB(I)+DXB(I-1))
      B2(I)=2./DXB(I)/(DXB(I)+DXB(I-1))
  330 CONTINUE
C
      DO 340 J=2,NY
      B4(J)=2./DYB(J-1)/(DYB(J)+DYB(J-1))
      B5(J)=2./DYB(J)/(DYB(J)+DYB(J-1))
  340 CONTINUE
C
      DO 350 J=2,NY
      DO 350 I=2,NT
      B3(I,J)=2.*(1./DXB(I)/DXB(I-1)+1./DYB(J)/DYB(J-1))
  350 CONTINUE
C
      IF (ISCH.EQ.3) GO TO 4000
      IF (ISCH.EQ.2) GO TO 3000
C
C     CENTRAL DIFFERENCING SCHEMES (C.D.S.)
C     (ALPHA=BETA=GAMMA=DETA=0)
C
      DO 360 J=1,N1B
      DO 360 I=1,N1B
      ALPHA(I,J)=0.0
      BETA(I,J)=0.0
```

```
      GAMMA(I,J)=0.0
      DETA(I,J)=0.0
  300 CONTINUE
      GO TO 4000
C
C     UPSTREAM DIFFERENCING SCHEMES (U.D.S.)
C     (ALPHA=BETA=0.5,GAMMA=DETA=0)
C
 3000 DO 370 J=1,N16
      DO 370 I=1,N15
      ALPHA(I,J)=0.5
      BETA(I,J)=0.5
      GAMMA(I,J)=0.0
      DETA(I,J)=0.0
  370 CONTINUE
C
C     ********************
C     *  INITIAL GUESSES  *
C     ********************
C
 4000 IF (IGUES.EQ.0) GO TO 4001
C
      DO 400 J=2,NY
      DO 400 I=2,NT
      S(I,J)=SS
      V(I,J)=VV
  400 CONTINUE
C
      IF (IGUES.EQ.1) GO TO 4002
C
 4001 DO 401 I=1,N15
  401 READ (3,402) (V(I,J),J=1,N16)
  402 FORMAT (8E12.4)
C
      DO 403 I=1,N15
  403 READ (3,402) (S(I,J),J=1,N16)
      GO TO 4003
C
C     *************************
C     *  BOUNDARY CONDITIONS  *
C     *************************
C
C     NOZZLE EXIT
C
 4002 DO 410 I=2,NJ1
      S(I,1)=-1.5*X(I)+2.*X(I)**3
      V(I,1)=12.*X(I)
  410 CONTINUE
C
C     UPPER PLATE
C
      DO 420 I=N1,NT
      S(I,1)=-0.5
      V(I,1)=((S(I,2)-S(I,1))*(DYB(2)+DYB(1))**3-(S(I,3)-S(I,1))
     *DYB(1)**3)*2./DYB(1)**2/DYB(2)/(DYB(1)+DYB(2))**2
  420 CONTINUE
C
C     AXIS OF SYMMETRY
C
      DO 430 J=1,N16
```

```
      S(1,J)=0.0
      W(1,J)=0.0
  430 CONTINUE
C
C     IMPINGEMENT PLATE
C
      DO 440 I=2,NT
      S(I,N16)=0.0
      W(I,N16)=((S(I,NY)-S(I,N16))*(DYB(NY)+DYB(N18))**3-
     1 (S(I,N18)-S(I,N16))*DYB(NY)**3)*2./DYB(NY)**2/DYB(N18)/
     2 (DYB(NY)+DYB(N18))**2
  440 CONTINUE
C
C     OUTFLOW REGION
C
      DO 450 J=1,N16
      SFD(J)=1.5*(Y(J)/L)**2-(Y(J)/L)**3-0.5
      WFD(J)=3.*(1.-2.*(Y(J)/L))/L**2
      S(N15,J)=SFD(J)+(S(NT,J)-SFD(J))*DD
      W(N15,J)=WFD(J)+(W(NT,J)-WFD(J))*DD
  450 CONTINUE
      SFD(1)=-0.5
      SFD(N16)=0.0
      GO TO 4004
C
 4000 DO 460 J=1,N16
      SFD(J)=1.5*(Y(J)/L)**2-(Y(J)/L)**3-0.5
      WFD(J)=3.*(1.-2.*(Y(J)/L))/L**2
  460 CONTINUE
      SFD(1)=-0.5
      SFD(N16)=0.0
C
C     **********************
C     *  START ITERATIONS  *
C     **********************
C
 4004 ITERV=0
      DO 5555 II=1,IMAX
C
      SUMS=0.0
      SUMV=0.0
C
C     SET VALUES AT N-1 LEVEL
C
      DO 500 J=1,N16
      DO 500 I=2,N15
      WI(I,J)=W(I,J)
  500 CONTINUE
C
      DO 505 J=2,NY
      DO 505 I=1,NT
      UC(I,J)=(S(I+1,J+1)+S(I,J+1)-S(I+1,J-1)-S(I,J-1))/4./DYC(J)
  505 CONTINUE
C
      DO 506 J=1,NY
      DO 506 I=2,NT
      VC(I,J)=-(S(I+1,J+1)+S(I+1,J)-S(I-1,J+1)-S(I-1,J))/4./DXC(I)
  506 CONTINUE
C
      IF (ISCH.EQ.1) GO TO 5000
```

```
      IF (ISCH.EQ.2) GO TO 5000
      IF (ITERV.EQ.0) GO TO 5500
      IF (IPSAVE.EQ.0) GO TO 5500
C
 5500 DO 503 J=2,NY
      DO 503 I=2,N15
      RV(I,J)=RE*ABS(UC(I-1,J))*DXB(I-1)
  503 CONTINUE
C
      DO 506 J=2,N16
      DO 506 I=2,NT
      RS(I,J)=RE*ABS(VC(I,J-1))*DYB(J-1)
  506 CONTINUE
C
      DO 509 J=2,NY
      DO 509 I=2,N15
C
      IF (RV(I,J).LE.0.001) GO TO 5091
      IF (RV(I,J).GT.0.001.AND.RV(I,J).LT.20.) GO TO 5093
      IF (RV(I,J).GE.20.) GO TO 5092
C
 5091 ALPHA(I,J)=0.0
      GAMMA(I,J)=0.0
      GO TO 509
C
 5092 ALPHA(I,J)=0.5
      GAMMA(I,J)=1.0
      GO TO 509
C
 5093 ALPHA(I,J)=0.5-(EXP(RV(I,J)*0.5)-1.)/(EXP(RV(I,J))-1.)
      GAMMA(I,J)=1.-RV(I,J)*EXP(RV(I,J)*0.5)/(EXP(RV(I,J))-1.)
  509 CONTINUE
C
      DO 504 J=2,N16
      DO 504 I=2,NT
C
      IF (RS(I,J).LE.0.001) GO TO 5041
      IF (RS(I,J).GT.0.001.AND.RS(I,J).LT.20.) GO TO 5043
      IF (RS(I,J).GE.20.) GO TO 5042
C
 5041 BETA(I,J)=0.0
      DETA(I,J)=0.0
      GO TO 504
C
 5042 BETA(I,J)=0.5
      DETA(I,J)=1.0
      GO TO 504
C
 5043 BETA(I,J)=0.5-(EXP(RS(I,J)*0.5)-1.)/(EXP(RS(I,J))-1.)
      DETA(I,J)=1.-RS(I,J)*EXP(RS(I,J)*0.5)/(EXP(RS(I,J))-1.)
  504 CONTINUE
C
 5000 DO 507 J=2,NY
      DO 507 I=2,NT
      A1(I,J)=(1.-GAMMA(I,J))*XI(I,J)+0.5*(UC(I-1,J)*DYC(J))+
     1  ALPHA(I,J)*ABS(UC(I-1,J)*DYC(J))
      A2(I,J)=(1.-GAMMA(I+1,J))*XI(I+1,J)-0.5*(UC(I,J)*DYC(J))+
     1  ALPHA(I+1,J)*ABS(UC(I,J)*DYC(J))
      A3(I,J)=(ABS(UC(I,J)*DYC(J))*ALPHA(I+1,J)+ABS(UC(I-1,J)*
     1  DYC(J))*ALPHA(I,J)+ABS(VC(I,J)*DXC(I))*BETA(I,J+1)+
```

NOT LEGIBLE
ILLISIBLE

```
     ABS(VC(I,J-1)*DXC(I))*BETA(I,J))+((1.-GAMMA(I+1,J))*
     XI(I+1,J)+(1.-GAMMA(I,J))*XI(I,J)+(1.-DETA(I,J+1))*
     ETA(I,J+1)+(1.-DETA(I,J))*ETA(I,J))
    A4(I,J)=(1.-DETA(I,J))*ETA(I,J)+0.5*(VC(I,J-1)*DXC(I))+
     BETA(I,J)*ABS(VC(I,J-1)*DXC(I))
    A5(I,J)=(1.-DETA(I,J+1))*ETA(I,J+1)-0.5*(VC(I,J)*DXC(I))+
     BETA(I,J+1)*ABS(VC(I,J)*DXC(I))
507 CONTINUE
C
C     CALCULATE THE VALUE OF VORTICITIES ON SUBGRID 1
C
    DO 510 J=2,NY,2
    DO 510 I=3,NI7,2
C
    WTEMP=(A1(I,J)*W(I-1,J)+A2(I,J)*W(I+1,J)+A4(I,J)*W(I,J-1)+
     A5(I,J)*W(I,J+1))/A3(I,J)
    W(I,J)=WN(I,J)+FW*(WTEMP-WN(I,J))
    ERW(I,J)=ABS(W(I,J)-WN(I,J))
510 CONTINUE
C
    DO 515 J=3,N18,2
    DO 515 I=2,NT,2
C
    WTEMP=(A1(I,J)*W(I-1,J)+A2(I,J)*W(I+1,J)+A4(I,J)*W(I,J-1)+
     A5(I,J)*W(I,J+1))/A3(I,J)
    W(I,J)=WN(I,J)+FW*(WTEMP-WN(I,J))
    ERW(I,J)=ABS(W(I,J)-WN(I,J))
515 CONTINUE
C
C     CALCULATE THE VALUE OF VORTICITIES ON SUBGRID 2
C
    DO 520 J=3,N18,2
    DO 520 I=3,NI7,2
C
    WTEMP=(A1(I,J)*W(I-1,J)+A2(I,J)*W(I+1,J)+A4(I,J)*W(I,J-1)+
     A5(I,J)*W(I,J+1))/A3(I,J)
    W(I,J)=WN(I,J)+FW*(WTEMP-WN(I,J))
    ERW(I,J)=ABS(W(I,J)-WN(I,J))
520 CONTINUE
C
    DO 525 J=2,NY,2
    DO 525 I=2,NT,2
C
    WTEMP=(A1(I,J)*W(I-1,J)+A2(I,J)*W(I+1,J)+A4(I,J)*W(I,J-1)+
     A5(I,J)*W(I,J+1))/A3(I,J)
    W(I,J)=WN(I,J)+FW*(WTEMP-WN(I,J))
    ERW(I,J)=ABS(W(I,J)-WN(I,J))
525 CONTINUE
C
C     CALCULATE THE VALUE OF STREAM FUNCTIONS ON SUBGRID 1
C
    ITEPS=0 0
    DO 5556 JJ=1,IST
C
C     SET VALUES AT N-1 LEVEL
C
    DO 550 J=1,N16
    DO 550 I=2,N15
    SN(I,J)=S(I,J)
550 CONTINUE
```

NOT LEGIBLE
ILLISIBLE

```
C
      DO 530 J=2,NY,2
      DO 530 I=3,N17,2
C
      STEMP=(B1(I)*S(I-1,J)+B2(I)*S(I+1,J)+B4(J)*S(I,J-1)+B5(J)*
     S(I,J+1)-W(I,J))/B3(I,J)
      S(I,J)=SN(I,J)+FS*(STEMP-SN(I,J))
      ERS(I,J)=ABS(S(I,J)-SN(I,J))
  530 CONTINUE
C
      DO 535 J=3,N16,2
      DO 535 I=2,NT,2
C
      STEMP=(B1(I)*S(I-1,J)+B2(I)*S(I+1,J)+B4(J)*S(I,J-1)+B5(J)*
     S(I,J+1)-W(I,J))/B3(I,J)
      S(I,J)=SN(I,J)+FS*(STEMP-SN(I,J))
      ERS(I,J)=ABS(S(I,J)-SN(I,J))
  535 CONTINUE
C
C     CALCULATE THE VALUE OF STREAM FUNCTIONS ON SUBGRID 2
C
      DO 540 J=3,N18,2
      DO 540 I=3,N17,2
C
      STEMP=(B1(I)*S(I-1,J)+B2(I)*S(I+1,J)+B4(J)*S(I,J-1)+B5(J)*
     S(I,J+1)-W(I,J))/B3(I,J)
      S(I,J)=SN(I,J)+FS*(STEMP-SN(I,J))
      ERS(I,J)=ABS(S(I,J)-SN(I,J))
  540 CONTINUE
C
      DO 545 J=2,NY,2
      DO 545 I=2,NT,2
C
      STEMP=(B1(I)*S(I-1,J)+B2(I)*S(I+1,J)+B4(J)*S(I,J-1)+B5(J)*
     S(I,J+1)-W(I,J))/B3(I,J)
      S(I,J)=SN(I,J)+FS*(STEMP-SN(I,J))
      ERS(I,J)=ABS(S(I,J)-SN(I,J))
  545 CONTINUE
C
 5566 CONTINUE
C
C     UPDATE THE BOUNDARY CONDITIONS AT OUTFLOW REGION
C
      DO 555 J=1,N16
      W(N15,J)=WFO(J)+(W(NT,J)-WFO(J))*DD
      S(N15,J)=SFO(J)+(S(NT,J)-SFO(J))*DD
      ERW(N15,J)=ABS(W(N15,J)-WN(N15,J))
      ERS(N15,J)=ABS(S(N15,J)-SN(N15,J))
  555 CONTINUE
C
C     UPDATE THE BOUNDARY CONDITIONS AT PLATES
C
      DO 560 I=N1,NT
      W(I,1)=((S(I,2)-S(I,1))*(DYB(2)+DYB(1))**3-(S(I,3)-S(I,1))
     *DYB(1)**3)*2./DYB(1)**2/DYB(2)/(DYB(1)+DYB(2))**2
      ERW(I,1)=ABS(W(I,1)-WN(I,1))
  560 CONTINUE
C
      DO 570 I=2,NT
      W(I,N16)=((S(I,NY)-S(I,N16))*(DYB(NY)+DYB(N18))**3-
```

```
     (S(I,N18)-S(I,N16))*DYB(NY)**3)*2./DYB(NY)**2/DYB(N18)/
     (DYB(NY)+DYB(N18))**2
      ERV(I,N16)=ABS(V(I,N16)-WN(I,N16))
  570 CONTINUE
C
      DO 580 J=2,NY
      DO 580 I=2,N15
      SUMV=SUMV+ABS(V(I,J)-WN(I,J))
      SUMS=SUMS+ABS(S(I,J)-SN(I,J))
  580 CONTINUE
C
      DO 585 I=N2,NT
      SUMV=SUMV+ABS(V(I,1)-WN(I,1))
  585 CONTINUE
C
      DO 590 I=2,NT
      SUMV=SUMV+ABS(V(I,N16)-WN(I,N16))
  590 CONTINUE
C
      ITERV=ITERV+1
      ITERS=ITERV*IST
C
      IPSAVE=0
      KSAVE=ITERV/50
      IDSAVE=ITERV-50*KSAVE
C
      IF (IDSAVE.EQ.0) IPSAVE=1
C
C     CONVERGENCE TEST
C
      IWRITE=0
      ERRV=SUMV/(FLOAT(NT*N18)-FLOAT(NJ/2))
      ERRS=SUMS/FLOAT(NT)/FLOAT(N18)
C
      ERVMAX=0.0
      DO 591 J=2,NY
      DO 591 I=2,N15
      IF (ERV(I,J)-ERVMAX) 591,591,592
  592 ERVMAX=ERV(I,J)
  591 CONTINUE
C
      DO 593 I=N2,NT
      IF (ERV(I,1)-ERVMAX) 593,593,594
  594 ERVMAX=ERV(I,1)
  593 CONTINUE
C
      DO 595 I=2,NT
      IF (ERV(I,N16)-ERVMAX) 595,595,596
  596 ERVMAX=ERV(I,N16)
  595 CONTINUE
C
      ERSMAX=0.0
      DO 597 J=2,NY
      DO 597 I=2,N15
      IF(ERS(I,J)-ERSMAX) 597,597,598
  598 ERSMAX=ERS(I,J)
  597 CONTINUE
C
      IF (ERVMAX.LT.CONV.AND.ERSMAX.LT.CONV) IWRITE=1
C
```

```
      IF (IWRITE.EQ.1) GO TO 6000
C
      IPRINT=0
      KV=ITERV/NS
      IDIV=ITERV-NS*KV
C
      IF (IDIV.EQ.0) IPRINT=1
C
      IF (ITERV.LT.IMIN) IPRINT=0
C
      IF (IPRINT.EQ.0) GO TO 6001
C
C     **********************
C     *  OUTPUT STATEMENTS  *
C     **********************
C
 6000 WRITE (6,100)
      WRITE(6,600)
  600 FORMAT (1X,'****************************************************',
     '****************************************************',
     '**********')
      WRITE (6,100)
      WRITE (6,610) ITERW,ERRW,ERWMAX
  610 FORMAT (1X,'VALUES OF VORTICITY, W, AFTER ',I4,1X,'ITERATIONS ',
     'WITH ERRW=',F12.8,' AND ERWMAX=',F12.8)
      WRITE (6,100)
      WRITE (6,620) (Y(J),J=1,N16,ISTEPY)
  620 FORMAT (6X,'X',11X,'Y=',F6.3,4X,'Y=',F6.3,4X,'Y=',F6.3,4X,
     'Y=',F6.3,4X,'Y=',F6.3,4X,'Y=',F6.3,4X,'Y=',F6.3,4X,'Y=',
     F6.3,4X,'Y=',F6.3)
      WRITE (6,100)
      DO 630 I=1,N15,ISTEP
  630 WRITE (6,640) X(I),(W(I,J),J=1,N16,ISTEPY)
  640 FORMAT (E12.4,4X,9E12.4)
      WRITE (6,100)
      WRITE (6,650) ITERS,ERRS,ERSMAX
  650 FORMAT (1X,'VALUES OF STREAM FUNCTION, S, AFTER ',I4,1X,
     'ITERATIONS WITH ERRS=',F12.8,' AND ERSMAX=',F12.8)
      WRITE (6,100)
      WRITE (6,620) (Y(J),J=1,N16,ISTEPY)
      WRITE (6,100)
      DO 660 I=1,N15,ISTEP
  660 WRITE (6,640) X(I),(S(I,J),J=1,N16,ISTEPY)
C
 6001 IF (IWRITE.EQ.1) GO TO 6003
C
 5555 CONTINUE
C
 6003 WRITE (6,100)
      WRITE (6,700)
  700 FORMAT (1X,'DO YOU WANT TO STORE THE RESULTS IN THE FILE?',
     '(0=YES,1=NO)')
      READ (5,122) ISTOR
C
      IF (ISTOR.EQ.1) GO TO 6002
C
C     STORE RESULTS IN THE FILE
C
      REWIND 4
C
```

```
      DO 710 I=1,N15
  710 WRITE (4,720) (V(I,J),J=1,N16)
  720 FORMAT (9E12.4)
C
      DO 730 I=1,N15
  730 WRITE (4,720) (S(I,J),J=1,N16)
C
      WRITE (6,740)
  740 FORMAT (1X,'**DONE**')
C
      IF (IWRITE.EQ.1) GO TO 6666
C
      WRITE (6,100)
 8002 WRITE (6,750)
  750 FORMAT (1X,'DO YOU WANT TO CONTINUE THIS RUN?',
     -'(0=YES,1=NO)')
      READ (5,122) IEND
C
      IF (IEND.EQ.1) GO TO 6666
C
      WRITE (6,100)
      WRITE (6,136)
      READ (5,122) IMAX
      WRITE (6,137)
      READ (5,112) CONV
      WRITE (6,135)
      READ (5,134) FS,FW
      WRITE (6,141)
      READ (5,122) IMIN
      WRITE (6,142)
      READ (5,122) NS
      WRITE (6,143)
      READ (5,122) IST
      WRITE (6,144)
      READ (5,145) ISTEP,ISTEPY
C
      IF (IEND.EQ.0) GO TO 4000
C
 6666 RETURN
      END
End of file
```

```
      SUBROUTINE CALC1
      REAL L
      COMMON RE,L,A,B,SC,ISCH
      COMMON N1,N2,N3,N4,N5,N6,N7,N8,N9,N10
      COMMON N11,N12,N13,N14,N15,N16,N17,N18
      COMMON NY,NT,NJ1,NJ,DX128
      COMMON DX1,DX2,DX4,DX8,DX16,DX32,DX64
      COMMON ISTOR,DYP
      COMMON X(70),YC(70),Y(35),YP(35),YC(35)
      COMMON DYB(70),DYC(70),DYB(35),DYC(35)
      COMMON S(70,35),W(70,35),C(70,35)
      COMMON U(70,35),V(70,35)
      DIMENSION CY1(35),CYS(35),UFD(35),VFD(35)
      DIMENSION CF(70),CFF(70)
C
C     ******************************
C     *  COMPUTE PROBLEM CONSTANTS  *
C     ******************************
C
      D2Y=2.*DYP
C
      DO 300 J=1,N16
      CY1(J)=(EXP(A*YP(J)))/A/B
      CYS(J)=CY1(J)/D2Y
  300 CONTINUE
C
C     *************************************
C     *  BOUNDARY CONDITIONS FOR VELOCITY  *
C     *************************************
C
C     NOZZLE EXIT
C
      DO 410 I=1,N1
      U(I,1)=0.0
      V(I,1)=1.5*(1.-4.*X(I)**2)
  410 CONTINUE
C
C     UPPER PLATE
C
      DO 420 I=N2,N15
      U(I,1)=0.0
      V(I,1)=0.0
  420 CONTINUE
C
C     AXIS OF SYMMETRY
C
      DO 430 J=2,NY
      U(1,J)=0.0
      V(1,J)=(3.*S(1,J)+S(3,J)-4.*S(2,J))/2./DX1
  430 CONTINUE
C
C     IMPINGEMENT PLATE
C
      DO 440 I=1,N15
      U(I,N16)=0.0
      V(I,N16)=0.0
  440 CONTINUE
C
C     OUTFLOW REGION
```

NOT LEGIBLE
ILLISIBLE

```
C
      DO 450 J=2,NY
      U(N15,J)=(S(N15,J+1)-S(N15,J-1))*CYS(J)
      V(N15,J)=(4.*S(NT,J)-S(N17,J)-3.*S(N15,J))/2./DX128
      UFD(J)=3.*(Y(J)/L**2)*(1.-(Y(J)/L))
      VFD(J)=0.0
  450 CONTINUE
      UFD(1)=0.0
      UFD(N16)=0.0
      VFD(1)=0.0
      VFD(N16)=0.0
C
C     **********************************
C     *  CALCULATE VELOCITY COMPONENTS  *
C     **********************************
C
      DO 510 J=2,NY
      DO 510 I=2,NT
      U(I,J)=CYS(J)*(S(I,J+1)-S(I,J-1))
C
      IF (I.LT.N1) GO TO 5101
      IF (I.EQ.N1) GO TO 5102
      IF (I.GT.N1.AND.I.LT.N3) GO TO 5103
      IF (I.EQ.N3) GO TO 5104
      IF (I.GT.N3.AND.I.LT.N5) GO TO 5105
      IF (I.EQ.N5) GO TO 5106
      IF (I.GT.N5.AND.I.LT.N7) GO TO 5107
      IF (I.EQ.N7) GO TO 5108
      IF (I.GT.N7.AND.I.LT.N9) GO TO 5109
      IF (I.EQ.N9) GO TO 5110
      IF (I.GT.N9.AND.I.LT.N11) GO TO 5111
      IF (I.EQ.N11) GO TO 5112
      IF (I.GT.N11.AND.I.LT.N13) GO TO 5113
      IF (I.EQ.N13) GO TO 5114
      IF (I.GT.N13) GO TO 5115
C
 5101 DX=DX1
      GO TO 5001
 5102 DX=DX1
      GO TO 5002
 5103 DX=DX2
      GO TO 5001
 5104 DX=DX2
      GO TO 5002
 5105 DX=DX4
      GO TO 5001
 5106 DX=DX1
      GO TO 5002
 5107 DX=DX8
      GO TO 5001
 5108 DX=DX8
      GO TO 5002
 5109 DX=DX16
      GO TO 5001
 5110 DX=DX16
      GO TO 5002
 5111 DX=DX32
      GO TO 5001
 5112 DX=DX32
      GO TO 5002
```

```
 9113 DX=DX64
      GO TO 9001
 9114 DX=DX64
      GO TO 9002
 9115 DX=DX128
      GO TO 9001
C
 9001 D2X=DX*2.
      V(I,J)=-(S(I+1,J)-S(I-1,J))/D2X
      GO TO 510
C
 9002 D3X=DX*3.
      V(I,J)=-(S(I+1,J)-S(I-1,J))/D3X
  510 CONTINUE
C
C     ********************************************
C     *  CALCULATE DRAG FORCE AT IMPINGEMENT PLATE  *
C     ********************************************
C
      DO 800 I=1,N15
      CF(I)=-2.*V(I,N16)/RE
      CFF(I)=CF(I)*RE
  800 CONTINUE
C
C     ********************************
C     *  CALCULATE VOLUMETRIC FLOW RATE  *
C     ********************************
C
      SUMV=0.0
      DO 700 I=2,NJ1,2
      SUMV=SUMV+4.*V(I,1)+2.*V(I+1,1)
  700 CONTINUE
      SUMV=SUMV+V(1,1)-V(N1,1)
      SUMV=SUMV*DX1/3.
C
      SUMOF=0.0
      DO 710 J=2,NY,2
      SUMOF=SUMOF+4.*U(N15,J)/CY1(J)+2.*U(N15,J+1)/CY1(J+1)
  710 CONTINUE
      SUMOF=SUMOF+U(N15,1)/CY1(1)-U(N15,N16)/CY1(N16)
      SUMOF=SUMOF*DYP/3.
C
      SUMU=0.0
      DO 720 J=2,NY,2
      SUMU=SUMU+4.*U(NT,J)/CY1(J)+2.*U(NT,J+1)/CY1(J+1)
  720 CONTINUE
      SUMU=SUMU+U(NT,1)/CY1(1)-U(NT,N16)/CY1(N16)
      SUMU=SUMU*DYP/3.
C
      SUMFD=0.0
      DO 730 J=2,NY,2
      SUMFD=SUMFD+4.*UFD(J)/CY1(J)+2.*UFD(J+1)/CY1(J+1)
  730 CONTINUE
      SUMFD=SUMFD+UFD(1)/CY1(1)-UFD(N16)/CY1(N16)
      SUMFD=SUMFD*DYP/3.
C
C     ****************************
C     *  STORE RESULTS IN THE FILE  *
C     ****************************
C
```

NOT LEGIBLE
ILLISIBLE

```
      DO 910 I=1,N15
  910 WRITE (7,402) (U(I,J),J=1,N16)
  402 FORMAT (9E12.4)
C
      DO 920 I=1,N15
  920 WRITE (7,402) (V(I,J),J=1,N16)
C
      DO 930 I=1,N15
  930 WRITE (7,940) X(I),CF(I),CFF(I)
  940 FORMAT (3E12.4)
C
C     **********************
C     *  OUTPUT STATEMENTS  *
C     **********************
C
      ISTEP=2
      IF (NY.EQ.24) ISTEP=3
      WRITE (8,100)
  100 FORMAT (/)
      WRITE (8,600)
  600 FORMAT ('1',1X,'**********************************************',
     *'*********************************************************',
     *'**************')
      WRITE (8,100)
      WRITE (8,610) RE,L,N15,N16
  610 FORMAT (1X,'JET REYNOLDS NUMBER =',F6.1,2X ,'JET-TO-PLATE',
     *' SPACING =',F5.1,45X,'NX = ',I2,2X,'NY = ',I2)
      WRITE (8,611) ISCH
  611 FORMAT (1X,'DIFFERENCING SCHEME (1=C.D.S.,2=U.D.S.,',
     *'3=U.W.D.S.) = ',I1)
      WRITE (8,612)
  612 FORMAT (1X,'INITIAL VELOCITY PROFILE = PARABOLIC')
      WRITE (8,100)
      WRITE (8,620) SUMV
  620 FORMAT (1X,'VOLUMETRIC FLOW RATE AT NOZZLE EXIT =',E12.4)
      WRITE (8,630) SUMU
  630 FORMAT (1X,'VOLUMETRIC FLOW RATE AT I=NX-1 =',E12.4)
      WRITE (8,640) SUMDF
  640 FORMAT (1X,'VOLUMETRIC FLOW RATE AT OUTFLOW REGION =',E12.4)
      WRITE (8,645) SUMFD
  645 FORMAT (1X,'VOLUMETRIC FLOW RATE WHEN FULLY DEVELOPED =',E12.4)
      WRITE (8,100)
      WRITE (8,605)
  605 FORMAT (1X,'**************************************************',
     *'*********************************************************',
     *'**********')
      WRITE (8,100)
      WRITE (8,650)
  650 FORMAT (1X,'VALUES OF VORTICITY, W:')
      WRITE (8,100)
      WRITE (8,655) (Y(J),J=1,N16,ISTEP)
  655 FORMAT (6X,'X',11X,'Y=',F6.3,4X,'Y=',F6.3,4X,'Y=',F6.3,4X,
     *'Y=',F6.3,4X,'Y=',F6.3,4X,'Y=',F6.3,4X,'Y=',F6.3,4X,'Y=',
     *F6.3,4X,'Y=',F6.3)
      WRITE (8,100)
      DO 660 I=1,N15
  660 WRITE (8,670) X(I),(W(I,J),J=1,N16,ISTEP)
  670 FORMAT (E12.4,4X,9E12.4)
      WRITE (8,100)
      WRITE (8,605)
```

```
      WRITE (8,900)
      WRITE (8,100)
      WRITE.(8,610) RE,L,N1S,N16
      WRITE (8,611) ISCH
      WRITE (8,612)
      WRITE (8,100)
      WRITE (8,605)
      WRITE (8,100)
      WRITE (8,675)
  675 FORMAT (1X,'VALUES OF STREAM-FUNCTION, S:')
      WRITE (8,100)
      WRITE (8,655) (Y(J),J=1,N16,ISTEP)
      WRITE (8,100)
      DO 680 I=1,N1S
  680 WRITE (8,670) X(I),(S(I,J),J=1,N16,ISTEP)
      WRITE (8,100)
      WRITE (8,605)
      WRITE (8,600)
      WRITE (8,100)
      WRITE (8,610) RE,L,N1S,N16
      WRITE (8,611) ISCH
      WRITE (8,612)
      WRITE (8,100)
      WRITE (8,605)
      WRITE (8,100)
      WRITE (8,685)
  685 FORMAT (1X,'VALUES OF VELOCITY IN X-DIRECTION, U:')
      WRITE (8,100)
      WRITE (8,655) (Y(J),J=1,N16,ISTEP)
      WRITE (8,100)
      DO 690 I=1,N1S
  690 WRITE (8,670) X(I),(U(I,J),J=1,N16,ISTEP)
      WRITE (8,100)
      WRITE (8,605)
      WRITE (8,600)
      WRITE (8,100)
      WRITE (8,610) RE,L,N1S,N16
      WRITE (8,611) ISCH
      WRITE (8,612)
      WRITE (8,100)
      WRITE (8,605)
      WRITE (8,100)
      WRITE (8,695)
  695 FORMAT (1X,'VALUES OF VELOCITY IN Y-DIRECTION, V:')
      WRITE (8,100)
      WRITE (8,655) (Y(J),J=1,N16,ISTEP)
      WRITE (8,100)
      DO 698 I=1,N1S
  698 WRITE (8,670) X(I),(V(I,J),J=1,N16,ISTEP)
      WRITE (8,100)
      WRITE (8,605)
      WRITE (8,600)
      WRITE (8,100)
      WRITE (8,610) RE,L,N1S,N16
      WRITE (8,611) ISCH
      WRITE (8,612)
      WRITE (8,100)
      WRITE (8,605)
      WRITE (8,100)
      WRITE (8,770)
```

NOT LEGIBLE
ILLISIBLE

```
      770 FORMAT (1X,'VALUES OF SKIN-FRICTION FACTOR,',
         ' CF:')
          WRITE (6,100)
          WRITE (6,775)
      775 FORMAT (6X,'X',14X,'CF',9X,'CF*RE')
          WRITE (6,100)
          DO 780 I=1,NIS
      780 WRITE (6,785) X(I),CF(I),CFF(I)
      785 FORMAT (E12.4,4X,2E12.4)
          WRITE (6,100)
          WRITE (6,605)
C
          RETURN
          END
End of File
```

```
      SUBROUTINE ITER2
      REAL L
      COMMON RE,L,A,B,SC,ISCH
      COMMON N1,N2,N3,N4,N5,N6,N7,N8,N9,N10
      COMMON N11,N12,N13,N14,N15,N16,N17,N18
      COMMON NY,NT,NJ1,NJ,DX128
      COMMON DX1,DX2,DX4,DX8,DX16,DX32,DX64
      COMMON ISTOR,DYP
      COMMON X(70),XC(70),Y(35),YP(35),YC(35)
      COMMON DXB(70),DXC(70),DYB(35),DYC(35)
      COMMON S(70,35),W(70,35),C(70,35)
      COMMON U(70,35),V(70,35)
      DIMENSION UC(70,35),VC(70,35),CFD(35),CN(70,35)
      DIMENSION ALPHA(70,35),BETA(70,35),GAMMA(70,35),DETA(70,35)
      DIMENSION XI(70,35),ETA(70,35)
      DIMENSION AA1(35),AA2(35),AA3(35),AA4(35),AA5(35)
      DIMENSION A1(70,35),A2(70,35),A3(70,35),A4(70,35),A5(70,35)
      DIMENSION ERC(70,35),RW(70,35),RS(70,35)
C
      WRITE (6,100)
  100 FORMAT (/)
      WRITE (6,130)
  130 FORMAT (1X,'(1) ENTER INPUT DATA FOR ITERATIONS:')
      WRITE (6,100)
      WRITE (6,131)
  131 FORMAT (1X,'DO YOU WANT TO USE DATA FROM THE FILE?')
      WRITE (6,132)
  132 FORMAT (1X,' (0=YES,1=NO)')
      READ (5,122) IGUES
  122 FORMAT (I5)
C
      IF (IGUES.EQ.0) GO TO 1001
C
      WRITE (6,133)
  133 FORMAT (1X,'INITIAL GUESSES, CC:')
      READ (5,134) CC
  134 FORMAT (F10.4)
 1001 WRITE (6,135)
  135 FORMAT (1X,'RELAXATION FACTORS, FC:')
      READ (5,134) FC
C
      WRITE (6,136)
  136 FORMAT (1X,'MAXIMUM NO. OF ITERATIONS FOR CONCENTRATION, IMAX:')
      READ (5,122) IMAX
      WRITE (6,137)
  137 FORMAT (1X,'CONVERGENCE CRITERION:')
      READ (5,112) CONV
  112 FORMAT (F10.4)
C
      WRITE (6,100)
      WRITE (6,140)
  140 FORMAT (1X,'(4) ENTER INPUT DATA FOR PRINT OUT:')
      WRITE (6,100)
      WRITE (6,141)
  141 FORMAT (1X,'NO. OF ITERATIONS FOR CONCENTRATION BEFORE ',
     *  'FIRST PRINT OUT:')
      READ (5,122) IMIN
      WRITE (6,142)
  142 FORMAT (1X,'NO. OF ITERATIONS FOR CONCENTRATION OF EACH ',
```

```
      'PRINT OUT:')
      READ (5,122) NS
      WRITE (6,144)
  144 FORMAT (1X,'ISTEP,ISTEPY:')
      READ (5,145) ISTEP,ISTEPY
  145 FORMAT (2I5)
C
C     ******************************
C     *  COMPUTE PROBLEM CONSTANTS  *
C     ******************************
C
      EE=EXP(-0.721*DX128/2./L/RE/SC)
C
      DO 505 J=2,NY
      DO 505 I=1,NT
      UC(I,J)=(S(I+1,J+1)+S(I,J+1)-S(I+1,J-1)-S(I,J-1))/4./DYC(J)
  505 CONTINUE
C
      DO 506 J=1,NY
      DO 506 I=2,NT
      VC(I,J)=-(S(I+1,J+1)+S(I+1,J)-S(I-1,J+1)-S(I-1,J))/4./DXC(I)
  506 CONTINUE
      DO 558 J=1,NY
      VC(1,J)=-(S(2,J+1)+S(2,J))/2./DXB(1)
  558 CONTINUE
C
      DO 300 J=2,NY
      DO 300 I=2,N1S
      XI(I,J)=DYC(J)/DXB(I-1)/RE/SC
  300 CONTINUE
C
      DO 310 J=2,N16
      DO 310 I=2,NT
      ETA(I,J)=DXC(I)/DYB(J-1)/RE/SC
  310 CONTINUE
      DO 313 J=2,N16
      ETA(1,J)=DXB(1)/DYB(J-1)/RE/SC
  313 CONTINUE
C
      IF (ISCH.EQ.3) GO TO 5500
      IF (ISCH.EQ.2) GO TO 3000
C
C     CENTRAL DIFFERENCING SCHEMES (C.D.S.)
C     (ALPHA=BETA=GAMMA=DETA=0)
C
      DO 360 J=1,N1S
      DO 360 I=1,N1S
      ALPHA(I,J)=0.0
      BETA(I,J)=0.0
      GAMMA(I,J)=0.0
      DETA(I,J)=0.0
  360 CONTINUE
      GO TO 5000
C
C     UPSTREAM DIFFERENCING SCHEMES (U.D.S.)
C     (ALPHA=BETA=0.5,GAMMA=DETA=0)
C
 3000 DO 370 J=1,N16
      DO 370 I=1,N1S
      ALPHA(I,J)=0.5
```

```
      BETA(I,J)=0.5
      GAMMA(I,J)=0.0
      DETA(I,J)=0.0
  370 CONTINUE
      GO TO 5000
C
 5900 DO 503 J=2,NY
      DO 503 I=2,N1S
      RV(I,J)=RE*SC*ABS(UC(I-1,J))*DXB(I-1)
  503 CONTINUE
C
      DO 508 J=2,N1S
      DO 508 I=1,NT
      RS(I,J)=RE*SC*ABS(VC(I,J-1))*DYB(J-1)
  508 CONTINUE
C
      DO 509 J=2,NY
      DO 509 I=2,N1S
C
      IF (RV(I,J).LE.0.001) GO TO 5081
      IF (RV(I,J).GT.0.001.AND.RV(I,J).LT.20.) GO TO 5083
      IF (RV(I,J).GE.20.) GO TO 5082
C
 5081 ALPHA(I,J)=0.0
      GAMMA(I,J)=0.0
      GO TO 509
C
 5082 ALPHA(I,J)=0.5
      GAMMA(I,J)=1.0
      GO TO 509
C
 5083 ALPHA(I,J)=0.5-(EXP(RV(I,J)*0.5)-1.)/(EXP(RV(I,J))-1.)
      GAMMA(I,J)=1.-RV(I,J)*EXP(RV(I,J)*0.5)/(EXP(RV(I,J))-1.)
  509 CONTINUE
C
      DO 504 J=2,N1S
      DO 504 I=1,NT
C
      IF (RS(I,J).LE.0.001) GO TO 5041
      IF (RS(I,J).GT.0.001.AND.RS(I,J).LT.20.) GO TO 5043
      IF (RS(I,J).GE.20.) GO TO 5042
C
 5041 BETA(I,J)=0.0
      DETA(I,J)=0.0
      GO TO 504
C
 5042 BETA(I,J)=0.5
      DETA(I,J)=1.0
      GO TO 504
C
 5043 BETA(I,J)=0.5-(EXP(RS(I,J)*0.5)-1.)/(EXP(RS(I,J))-1.)
      DETA(I,J)=1.-RS(I,J)*EXP(RS(I,J)*0.5)/(EXP(RS(I,J))-1.)
  504 CONTINUE
C
 5000 DO 507 J=2,NY
      DO 507 I=2,NT
      A1(I,J)=(1.-GAMMA(I,J))*XI(I,J)+0.5*(UC(I-1,J)*DYC(J))+
     ALPHA(I,J)*ABS(UC(I-1,J)*DYC(J))
      A2(I,J)=(1.-GAMMA(I+1,J))*XI(I+1,J)-0.5*(UC(I,J)*DYC(J))+
     ALPHA(I+1,J)*ABS(UC(I,J)*DYC(J))
```

NOT LEGIBLE
ILLISIBLE

```
      A3(I,J)=(ABS(UC(I,J)*DYC(J))*ALPHA(I+1,J)+ABS(UC(I-1,J)*
     DYC(J))*ALPHA(I,J)+ABS(VC(I,J)*DXC(I))*BETA(I,J+1)+
     ABS(VC(I,J-1)*DXC(I))*BETA(I,J))+((1.-GAMMA(I+1,J))*
     XI(I+1,J)+(1.-GAMMA(I,J))*XI(I,J)+(1.-DETA(I,J+1))*
     ETA(I,J+1)+(1.-DETA(I,J))*ETA(I,J))
      A4(I,J)=(1.-DETA(I,J))*ETA(I,J)+0.5*(VC(I,J-1)*DXC(I))+
     BETA(I,J)*ABS(VC(I,J-1)*DXC(I))
      A5(I,J)=(1.-DETA(I,J+1))*ETA(I,J+1)-0.5*(VC(I,J)*DXC(I))+
     BETA(I,J+1)*ABS(VC(I,J)*DXC(I))
  507 CONTINUE
C
      DO 577 J=2,NY
      AA1(J)=(1.-GAMMA(2,J))*XI(2,J)+0.5*(-UC(1,J)*DYC(J))+
     ALPHA(2,J)*ABS(-UC(1,J)*DYC(J))
      AA2(J)=(1.-GAMMA(2,J))*XI(2,J)-0.5*(UC(1,J)*DYC(J))+
     ALPHA(2,J)*ABS(UC(1,J)*DYC(J))
      AA3(J)=(ABS(UC(1,J)*DYC(J))*ALPHA(2,J)+ABS(-UC(1,J)*
     DYC(J))*ALPHA(2,J)+ABS(VC(1,J)*DXB(1))*BETA(1,J+1)+
     ABS(VC(1,J-1)*DYB(1))*BETA(1,J))+((1.-GAMMA(2,J))*
     XI(2,J)+(1.-GAMMA(2,J))*XI(2,J)+(1.-DETA(1,J+1))*
     ETA(1,J+1)+(1.-DETA(1,J))*ETA(1,J))
C     AA4(J)=(1.-DETA(1,J))*ETA(1,J)+0.5*(VC(1,J-1)*DXB(1))+
     BETA(1,J)*ABS(VC(1,J-1)*DXB(1))
      AA5(J)=(1.-DETA(1,J+1))*ETA(1,J+1)-0.5*(VC(1,J)*DXB(1))+
     BETA(1,J+1)*ABS(VC(1,J)*DXB(1))
  577 CONTINUE
C
C     ********************
C     *  INITIAL GUESSES  *
C     ********************
C
      IF (IGUES.EQ.0) GO TO 4001
C
      DO 400 J=2,NY
      DO 400 I=2,NT
      C(I,J)=CC
  400 CONTINUE
C
      IF (IGUES.EQ.1) GO TO 4002
C
 4001 DO 401 I=1,N15
  401 READ (10,402) (C(I,J),J=1,N16)
  402 FORMAT (5E12.4)
      GO TO 4003
C
C     ************************
C     *  BOUNDARY CONDITIONS  *
C     ************************
C
C     NOZZLE EXIT
C
 4002 DO 410 I=1,NJ1
      C(I,1)=0.0
  410 CONTINUE
C
C     UPPER PLATE
C
      DO 420 I=N1,NT
      C(I,1)=((DYB(1)+DYB(2))**2*C(I,2)-DYB(1)**2*C(I,3))/
     ((DYB(1)+DYB(2))**2-DYB(1)**2)
```

```
  430 CONTINUE
C
C     AXIS OF SYMMETRY
C
      DO 430 J=2,NY
C     V(1,J)=(3.*S(1,J)+S(3,J)-4.*S(2,J))/2./DX1
C     C(1,J)=(2.*C(2,J)/DXB(1)**2
C    +2.*C(1,J+1)/DYB(J)/(DYB(J)+DYB(J-1))
C    +2.*C(1,J-1)/DYB(J-1)/(DYB(J)+DYB(J-1))
C    +(C(1,J-1)-C(1,J+1))/(DYB(J)+DYB(J-1))*V(1,J)*RE*SC)
C    /(2./DXB(1)**2+2./DYB(J)/DYB(J-1))
      C(1,J)=(AA1(J)*C(2,J)+AA2(J)*C(2,J)+AA4(J)*C(1,J-1)+
     AA5(J)*C(1,J+1))/AA3(J)
  430 CONTINUE
C
C     IMPINGEMENT PLATE
C
      DO 440 I=1,N15
      C(I,N16)=1.0
  440 CONTINUE
C
C     OUTFLOW REGION
C
      DO 450 J=1,NY
      CFD(J)=1.0
      C(N15,J)=CFD(J)+(C(NT,J)-CFD(J))*EE
  450 CONTINUE
      GO TO 4004
C
 4003 DO 460 J=1,NY
      CFD(J)=1.0
  460 CONTINUE
C
C     **********************
C     *  START ITERATIONS  *
C     **********************
C
 4004 ITERC=0
      DO 5555 II=1,IMAX
C
      SUMC=0.0
C
C     SET VALUES AT N-1 LEVEL
C
      DO 500 J=1,N16
      DO 500 I=1,N15
      CN(I,J)=C(I,J)
  500 CONTINUE
C
C     CALCULATE THE VALUE OF CONCENTRATIONS ON SUBGRID 1
C
      DO 510 J=2,NY,2
      DO 510 I=3,N17,2
C
      CTEMP=(A1(I,J)*C(I-1,J)+A2(I,J)*C(I+1,J)+A4(I,J)*C(I,J-1)+
     A5(I,J)*C(I,J+1))/A3(I,J)
      C(I,J)=CN(I,J)+FC*(CTEMP-CN(I,J))
      ERC(I,J)=ABS(C(I,J)-CN(I,J))
  510 CONTINUE
C
```

```
      DO 515 J=3,N18,2
      DO 515 I=2,NT,2
C
      CTEMP=(A1(I,J)*C(I-1,J)+A2(I,J)*C(I+1,J)+A4(I,J)*C(I,J-1)+
     A5(I,J)*C(I,J+1))/A3(I,J)
      C(I,J)=CN(I,J)+FC*(CTEMP-CN(I,J))
      ERC(I,J)=ABS(C(I,J)-CN(I,J))
  515 CONTINUE
C
C     CALCULATE THE VALUE OF CONCENTRATIONS ON SUBGRID 2
C
      DO 520 J=3,N18,2
      DO 520 I=3,N17,2
C
      CTEMP=(A1(I,J)*C(I-1,J)+A2(I,J)*C(I+1,J)+A4(I,J)*C(I,J-1)+
     A5(I,J)*C(I,J+1))/A3(I,J)
      C(I,J)=CN(I,J)+FC*(CTEMP-CN(I,J))
      ERC(I,J)=ABS(C(I,J)-CN(I,J))
  520 CONTINUE
C
      DO 525 J=2,NY,2
      DO 525 I=2,NT,2
C
      CTEMP=(A1(I,J)*C(I-1,J)+A5(I,J)*C(I+1,J)+A4(I,J)*C(I,J-1)+
     A5(I,J)*C(I,J+1))/A3(I,J)
      C(I,J)=CN(I,J)+FC*(CTEMP-CN(I,J))
      ERC(I,J)=ABS(C(I,J)-CN(I,J))
  525 CONTINUE
C
C     UPDATE THE BOUNDARY CONDITIONS AT UPPER PLATE
C
      DO 560 I=N1,NT
      C(I,1)=((DYB(1)+DYB(2))**2*C(I,2)-DYB(1)**2*C(I,3))/
     ((DYB(1)+DYB(2))**2-DYB(1)**2)
      ERC(I,1)=ABS(C(I,1)-CN(I,1))
  560 CONTINUE
C
C     UPDATE THE BOUNDARY CONDITIONS AT AXIS OF SYMMETRY
C
      DO 570 J=2,NY
C     V(1,J)=(3.*S(1,J)+S(3,J)-4.*S(2,J))/2./DX1
C     CTEMP=(2.*C(2,J)/DXB(1)**2
C    +2.*C(1,J+1)/DYB(J)/(DYB(J)+DYB(J-1))
C    +2.*C(1,J-1)/DYB(J-1)/(DYB(J)+DYB(J-1))
C    +(C(1,J-1)-C(1,J+1))/(DYB(J)+DYB(J-1))*V(1,J)*RE*SC)
C    /(2./DXB(1)**2+2./DYB(J)/DYB(J-1))
      CTEMP=(AA1(J)*C(2,J)+AA2(J)*C(2,J)+AA4(J)*C(1,J-1)+
     AA5(J)*C(1,J+1))/AA3(J)
      C(1,J)=CN(1,J)+FC*(CTEMP-CN(1,J))
      ERC(1,J)=ABS(C(1,J)-CN(1,J))
  570 CONTINUE
C
C     UPDATE THE BOUNDARY CONDITIONS AT OUTFLOW REGION
C
      DO 555 J=1,NY
      C(N15,J)=CFO(J)+(C(NT,J)-CFO(J))*EE
      ERC(N15,J)=ABS(C(N15,J)-CN(N15,J))
  555 CONTINUE
C
      DO 580 J=2,NY
```

NOT LEGIBLE
ILLISIBLE

```
      DO 580 I=1,N15
      SUMC=SUMC+ABS(C(I,J)-CN(I,J))
  580 CONTINUE
C
      DO 585 I=N1,N15
      SUMC=SUMC+ABS(C(I,1)-CN(I,1))
  585 CONTINUE
C
      ITERC=ITERC+1
C
C     CONVERGENCE TEST
C
      IWRITE=0
      ERRC=SUMC/(FLOAT(N15*N18)+FLOAT(N15-NJ1))
C
      ERCMAX=0.0
      DO 591 J=2,NY
      DO 591 I=1,N15
      IF (ERC(I,J)-ERCMAX) 591,591,592
  592 ERCMAX=ERC(I,J)
  591 CONTINUE
C
      DO 593 I=N1,N15
      IF (ERC(I,1)-ERCMAX) 593,593,594
  594 ERCMAX=ERC(I,1)
  593 CONTINUE
C
      IF (ERCMAX.LT.CONV) IWRITE=1
C
      IF (IWRITE.EQ.1) GO TO 6000
C
      IPRINT=0
      KC=ITERC/NS
      IDIV=ITERC-NS*KC
C
      IF (IDIV.EQ.0) IPRINT=1
C
      IF (ITERC.LT.IMIN) IPRINT=0
C
      IF (IPRINT.EQ.0) GO TO 6001
C
C     **********************
C     *  OUTPUT STATEMENTS  *
C     **********************
C
 6000 WRITE (6,100)
      WRITE(6,600)
  600 FORMAT (1X,'****************************************************',
     *'*****************************************************',
     *'**********')
      WRITE (6,100)
      WRITE (6,610) ITERC,ERRC,ERCMAX
  610 FORMAT (1X,'VALUES OF CONCENTRATION, C, AFTER ',I4,1X,
     *'ITERATIONS WITH ERRC=',F12.8,' AND ERCMAX=',F12.8)
      WRITE (6,100)
      WRITE (6,620) (Y(J),J=1,N16,ISTEPY)
  620 FORMAT (6X,'X',11X,'Y=',F6.3,4X,'Y=',F6.3,4X,'Y=',F6.3,4X,
     *'Y=',F6.3,4X,'Y=',F6.3,4X,'Y=',F6.3,4X,'Y=',F6.3,4X,'Y=',
     *F6.3,4X,'Y=',F6.3)
      WRITE (6,100)
```

```
      DO 690 I=1,N15,ISTEP
  690 WRITE (6,640) X(I),(C(I,J),J=1,N16,ISTEPY)
  640 FORMAT (E12.4,4X,9E12.4)
C
 6001 IF (IWRITE.EQ.1) GO TO 6003
C
 5555 CONTINUE
C
 6003 WRITE (6,100)
      WRITE (6,700)
  700 FORMAT (1X,'DO YOU WANT TO STORE THE RESULTS IN THE FILE?',
     *'(0=YES,1=NO)')
      READ (5,122) ISTOR
C
      IF (ISTOR.EQ.1) GO TO 6002
C
C     STORE RESULTS IN THE FILE
C
      REWIND 9
C
      DO 710 I=1,N15
  710 WRITE (9,720) (C(I,J),J=1,N16)
  720 FORMAT (9E12.4)
C
      WRITE (6,740)
  740 FORMAT (1X,'**DONE**')
C
      IF (IWRITE.EQ.1) GO TO 6666
C
      WRITE (6,100)
 6002 WRITE (6,750)
  750 FORMAT (1X,'DO YOU WANT TO CONTINUE THIS RUN?',
     *'(0=YES,1=NO)')
      READ (5,122) IEND
C
      IF (IEND.EQ.1) GO TO 6666
C
      WRITE (6,100)
      WRITE (6,136)
      READ (5,122) IMAX
      WRITE (6,137)
      READ (5,112) CONV
      WRITE (6,135)
      READ (5,134) FC
      WRITE (6,141)
      READ (5,122) IMIN
      WRITE (6,142)
      READ (5,122) NS
      WRITE (6,144)
      READ (5,145) ISTEP,ISTEPY
C
      IF (IEND.EQ.0) GO TO 4003
C
 6666 RETURN
      END
End of file
```

```
      SUBROUTINE CALC2
      REAL L
      COMMON RE,L,A,B,SC,ISCH
      COMMON N1,N2,N3,N4,N5,N6,N7,N8,N9,N10
      COMMON N11,N12,N13,N14,N15,N16,N17,N18
      COMMON NY,NT,NJ1,NJ,DX128
      COMMON DX1,DX2,DX4,DX8,DX16,DX32,DX64
      COMMON ISTOR,DYP
      COMMON X(70),XC(70),Y(35),YP(36),YC(35)
      COMMON DXC(70),DYC(70),DYB(35),DYC(35)
      COMMON S(70,35),W(70,35),C(70,35)
      COMMON U(70,35),V(70,35)
      DIMENSION SH(70),CY1(35)
      DIMENSION SHB(70),PRO(70,35),SUMC(70),CB(70)
      DIMENSION CF(70),CFF(70)
C
C     ******************************
C     *  COMPUTE PROBLEM CONSTANTS  *
C     ******************************
C
      DO 300 J=1,N16
      CY1(J)=(EXP(A*YP(J)))/A/B
  300 CONTINUE
C
C     ******************************
C     *  CALCULATE SHERWOOD NUMBERS  *
C     ******************************
C
      DO 800 I=1,N15
      SH(I)=-((C(I,NY)-C(I,N16))*(DYB(NY)+DYB(N18))**2-
     (C(I,N18)-C(I,N16))*DYB(NY)**2)/(DYB(NY)+DYB(N18))/
     DYB(NY)/DYB(N18)
  800 CONTINUE
C
      DO 850 J=1,N16
      DO 850 I=1,N15
      PRO(I,J)=U(I,J)*C(I,J)
  850 CONTINUE
C
      DO 860 I=1,N15
      SUMC(I)=0.0
      DO 870 J=2,NY,2
      SUMC(I)=SUMC(I)+4.*PRO(I,J)/CY1(J)+2.*PRO(I,J+1)/CY1(J+1)
  870 CONTINUE
      SUMC(I)=SUMC(I)+PRO(I,1)/CY1(1)-PRO(I,N16)/CY1(N16)
      SUMC(I)=SUMC(I)*DYP/3.
      CB(I)=2.*SUMC(I)
  860 CONTINUE
C
      DO 880 I=1,N15
      IF (SH(I).LT.0.001) GO TO 888
      SHB(I)=SH(I)/(C(I,N16)-CB(I))
      GO TO 880
  888 SHB(I)=4.861/2./L
  880 CONTINUE
C
C     ******************************
C     *  STORE RESULTS IN THE FILE  *
C     ******************************
```

```
C
      DO 930 I=1,N15
  930 WRITE (11,940) X(I),SH(I),SHB(I),CB(I)
  940 FORMAT (4E12.4)
C
C     **********************
C     *  OUTPUT STATEMENTS  *
C     **********************
C
      ISCH=3
      ISTEP=2
      IF (NY.EQ.24) ISTEP=3
      WRITE (12,100)
  100 FORMAT (/)
      WRITE (12,600)
  600 FORMAT ('1',1X,'**********************************************',
     *'*******************************************************',
     *'***************')
      WRITE (12,100)
      WRITE (12,610) RE,SC,L,N15,N16
  610 FORMAT (1X,'JET REYNOLDS NUMBER =',F6.1,2X ,'SCHMIDT',
     *' NUMBER =',F6.2,2X,'JET-TO-PLATE SPACING =',F5.1,
     *16X,'NX = ',I2,2X,'NY = ',I2)
      WRITE (12,611) ISCH
  611 FORMAT (1X,'DIFFERENCING SCHEME (1=C.D.S.,2=U.D.S.,',
     *'3=U.W.D.S.) = ',I2)
      WRITE (12,612)
  612 FORMAT (1X,'INITIAL VELOCITY PROFILE = PARABOLIC')
      WRITE (12,100)
      WRITE (12,605)
  605 FORMAT (1X,'**************************************************',
     *'*******************************************************',
     *'***********')
      WRITE (12,100)
      WRITE (12,650)
  650 FORMAT (1X,'VALUES OF CONCENTRATION, C:')
      WRITE (12,100)
      WRITE (12,655) (Y(J),J=1,N16,ISTEP)
  655 FORMAT (4X,'X',11X,'Y=',F6.3,4X,'Y=',F6.3,4X,'Y=',F6.3,4X,
     *'Y=',F6.3,4X,'Y=',F6.3,4X,'Y=',F6.3,4X,'Y=',F6.3,4X,'Y=',
     *F6.3,4X,'Y=',F6.3)
      WRITE (12,100)
      DO 660 I=1,N15
  660 WRITE (12,670) X(I),(C(I,J),J=1,N16,ISTEP)
  670 FORMAT (E12.4,4X,9E12.4)
      WRITE (12,100)
      WRITE (12,605)
      WRITE (12,600)
      WRITE (12,100)
      WRITE (12,610) RE,SC,L,N15,N16
      WRITE (12,611) ISCH
      WRITE (12,612)
      WRITE (12,100)
      WRITE (12,605)
      WRITE (12,100)
      WRITE (12,770)
  770 FORMAT (1X,'VALUES OF SHERWOOD NUMBER, SH:')
      WRITE (12,100)
      WRITE (12,775)
  775 FORMAT (4X,'X',14X,'SH',13X,'SHB',14X,'CB')
```

```
      WRITE (12,100)
      DO 780 I=1,N15
  780 WRITE (12,785) X(I),SH(I),SHB(I),CB(I)
  785 FORMAT (E12.4,4X,E12.4,4X,E12.4,4X,E12.4)
      WRITE (12,100)
      WRITE (12,605)
C
      RETURN
      END
End of File
```

JET REYNOLDS NUMBER = 100.0 JET-TO-PLATE SPACING = 2.0
DIFFERENCING SCHEME (1=C.D.S.,2=U.D.S.,3=U.V.D.S.) = 3
INITIAL VELOCITY PROFILE = PARABOLIC

NX = 56 NY = 56

VOLUMETRIC FLOW RATE AT NOZZLE EXIT = 0.5000E+00
VOLUMETRIC FLOW RATE AT I=NX-1 = 0.4969E+00
VOLUMETRIC FLOW RATE AT OUTFLOW REGION = 0.4970E+00
VOLUMETRIC FLOW RATE WHEN FULLY DEVELOPED = 0.5000E+00

VALUES OF VORTICITY, W:

X	Y=-0.0	Y= 0.440	Y= 0.805	Y= 1.100	Y= 1.350	Y= 1.558	Y= 1.730	Y= 1.882	Y= 2.000
0.0	0.0	0.0	0.0	0.0	0.0	0.0	0.0	0.0	0.0
0.6250E-01	0.7500E+00	0.7319E+00	0.6908E+00	0.6142E+00	0.5026E+00	0.3716E+00	0.2328E+00	-0.1423E+00	-0.2294E+01
0.1250E+00	0.1500E+01	0.1461E+01	0.1373E+01	0.1216E+01	0.9929E+00	0.7326E+00	0.4571E+00	-0.2850E+00	-0.4409E+01
0.1875E+00	0.2250E+01	0.2178E+01	0.2026E+01	0.1784E+01	0.1455E+01	0.1072E+01	0.6656E+00	-0.4675E+00	-0.6517E+01
0.2500E+00	0.3000E+01	0.2852E+01	0.2603E+01	0.2282E+01	0.1866E+01	0.1379E+01	0.8520E+00	-0.6820E+00	-0.8290E+01
0.3125E+00	0.3750E+01	0.3396E+01	0.3010E+01	0.2651E+01	0.2202E+01	0.1642E+01	0.1012E+01	-0.8984E+00	-0.9758E+01
0.3750E+00	0.4500E+01	0.3624E+01	0.3131E+01	0.2836E+01	0.2441E+01	0.1857E+01	0.1143E+01	-0.1167E+01	-0.1088E+02
0.4375E+00	0.5250E+01	0.3328E+01	0.2913E+01	0.2822E+01	0.2579E+01	0.2023E+01	0.1243E+01	-0.1468E+01	-0.1162E+02
0.5000E+00	0.6000E+01	0.2551E+01	0.2444E+01	0.2652E+01	0.2639E+01	0.2176E+01	0.1324E+01	-0.1951E+01	-0.1190E+02
0.6250E+00	-0.1519E+01	0.9431E+00	0.1352E+01	0.2055E+01	0.2527E+01	0.2272E+01	0.1335E+01	-0.2603E+01	-0.1221E+02
0.7500E+00	-0.9876E+00	0.1840E+00	0.6992E+00	0.1553E+01	0.2340E+01	0.2266E+01	0.1101E+01	-0.3475E+01	-0.1145E+02
0.1000E+01	-0.5887E+00	-0.8504E-01	0.3596E+00	0.1188E+01	0.2163E+01	0.2141E+01	0.5656E+00	-0.4185E+01	-0.9815E+01
0.1250E+01	-0.5946E+00	-0.6957E-01	0.4638E+00	0.1170E+01	0.2073E+01	0.1890E+01	-0.1191E+00	-0.4488E+01	-0.7858E+01
0.1500E+01	-0.6956E+00	-0.1649E-01	0.6103E+00	0.1306E+01	0.1932E+01	0.1371E+01	-0.9518E+00	-0.4359E+01	-0.6285E+01
0.2000E+01	-0.9455E+00	0.8124E-01	0.8167E+00	0.1409E+01	0.1635E+01	0.6719E+00	-0.1572E+01	-0.3716E+01	-0.4336E+01
0.2500E+01	-0.1198E+01	0.2284E+00	0.1012E+01	0.1395E+01	0.1251E+01	0.5651E-01	-0.1820E+01	-0.3021E+01	-0.3135E+01
0.3000E+01	-0.1380E+01	0.4053E+00	0.1109E+01	0.1260E+01	0.8242E+00	-0.4192E+00	-0.1815E+01	-0.2389E+01	-0.2259E+01
0.3500E+01	-0.1393E+01	0.5392E+00	0.1098E+01	0.1017E+01	0.4114E+00	-0.7276E+00	-0.1658E+01	-0.1849E+01	-0.1610E+01
0.4000E+01	-0.1205E+01	0.6022E+00	0.9853E+00	0.7758E+00	0.6771E-01	-0.8748E+00	-0.1430E+01	-0.1419E+01	-0.1174E+01
0.4500E+01	-0.8467E+00	0.5932E+00	0.8147E+00	0.5273E+00	-0.1761E+00	-0.8979E+00	-0.1196E+01	-0.1104E+01	-0.8942E+00
0.5000E+01	-0.4311E+00	0.5610E+00	0.7012E+00	0.3236E+00	-0.3213E+00	-0.8475E+00	-0.9958E+00	-0.8921E+00	-0.7227E+00
0.5500E+01	-0.7885E-01	0.5207E+00	0.5745E+00	0.1748E+00	-0.3884E+00	-0.7682E+00	-0.8444E+00	-0.7625E+00	-0.6542E+00
0.6000E+01	0.1263E+00	0.4877E+00	0.4711E+00	0.7553E-01	-0.4050E+00	-0.6881E+00	-0.7303E+00	-0.6903E+00	-0.6271E+00
0.6500E+01	0.3865E+00	0.4643E+00	0.3965E+00	0.1359E-01	-0.3965E+00	-0.6198E+00	-0.6701E+00	-0.6543E+00	-0.6302E+00
0.7000E+01	0.5163E+00	0.4493E+00	0.3292E+00	-0.2329E-01	-0.3765E+00	-0.5662E+00	-0.6263E+00	-0.6101E+00	-0.6467E+00
0.7500E+01	0.5884E+00	0.4401E+00	0.2832E+00	-0.4466E-01	-0.3544E+00	-0.5260E+00	-0.5992E+00	-0.6378E+00	-0.6671E+00
0.8000E+01	0.6379E+00	0.4345E+00	0.2487E+00	-0.5694E-01	-0.3342E+00	-0.4957E+00	-0.5827E+00	-0.6105E+00	-0.6483E+00
0.8500E+01	0.6755E+00	0.4316E+00	0.2271E+00	-0.6408E-01	-0.3171E+00	-0.4757E+00	-0.5727E+00	-0.6440E+00	-0.7074E+00
0.9000E+01	0.6318E+00	0.4286E+00	0.2044E+00	-0.6835E-01	-0.3042E+00	-0.4604E+00	-0.5666E+00	-0.6494E+00	-0.7197E+00
0.9500E+01	0.7071E+00	0.4268E+00	0.1903E+00	-0.7102E-01	-0.2942E+00	-0.4503E+00	-0.5622E+00	-0.6530E+00	-0.7235E+00
0.1000E+02	0.7183E+00	0.4255E+00	0.1797E+00	-0.7281E-01	-0.2867E+00	-0.4429E+00	-0.5604E+00	-0.6558E+00	-0.7351E+00
0.1050E+02	0.7266E+00	0.4245E+00	0.1719E+00	-0.7409E-01	-0.2812E+00	-0.4376E+00	-0.5587E+00	-0.6577E+00	-0.7402E+00
0.1100E+02	0.7330E+00	0.4237E+00	0.1659E+00	-0.7507E-01	-0.2774E+00	-0.4338E+00	-0.5575E+00	-0.6590E+00	-0.7433E+00
0.1150E+02	0.7380E+00	0.4231E+00	0.1614E+00	-0.7587E-01	-0.2745E+00	-0.4311E+00	-0.5566E+00	-0.6598E+00	-0.7451E+00
0.1200E+02	0.7419E+00	0.4225E+00	0.1569E+00	-0.7670E-01	-0.2719E+00	-0.4286E+00	-0.5557E+00	-0.6604E+00	-0.7475E+00
0.1300E+02	0.7464E+00	0.4221E+00	0.1531E+00	-0.7747E-01	-0.2693E+00	-0.4266E+00	-0.5548E+00	-0.6607E+00	-0.7485E+00
0.1400E+02	0.7486E+00	0.4220E+00	0.1513E+00	-0.7797E-01	-0.2688E+00	-0.4254E+00	-0.5542E+00	-0.6608E+00	-0.7491E+00

0.1500E+02	0.7500E+00	0.4218E+00	0.1500E+00	-0.7836E-01	-0.2682E+00	-0.4247E+00	-0.5538E+00	-0.6607E+00	-0.7494E+00
0.1600E+02	0.7508E+00	0.4218E+00	0.1492E+00	-0.7862E-01	-0.2679E+00	-0.4243E+00	-0.5536E+00	-0.6607E+00	-0.7495E+00
0.1700E+02	0.7514E+00	0.4218E+00	0.1487E+00	-0.7881E-01	-0.2677E+00	-0.4240E+00	-0.5534E+00	-0.6606E+00	-0.7495E+00
0.1800E+02	0.7518E+00	0.4218E+00	0.1484E+00	-0.7894E-01	-0.2676E+00	-0.4239E+00	-0.5533E+00	-0.6606E+00	-0.7494E+00
0.1900E+02	0.7520E+00	0.4218E+00	0.1482E+00	-0.7904E-01	-0.2676E+00	-0.4238E+00	-0.5532E+00	-0.6605E+00	-0.7494E+00
0.2000E+02	0.7521E+00	0.4218E+00	0.1480E+00	-0.7912E-01	-0.2676E+00	-0.4237E+00	-0.5532E+00	-0.6605E+00	-0.7494E+00
0.2200E+02	0.7522E+00	0.4218E+00	0.14[illegible]E+00	-0.7919E-01	-0.2675E+00	-0.4237E+00	-0.5531E+00	-0.6604E+00	-0.7494E+00
0.2400E+02	0.7523E+00	0.4218E+00	0.1479E+00	-0.7922E-01	-0.2675E+00	-0.4237E+00	-0.5531E+00	-0.6604E+00	-0.7493E+00
0.2600E+02	0.7523E+00	0.4218E+00	0.1479E+00	-0.7923E-01	-0.2675E+00	-0.4237E+00	-0.5531E+00	-0.6604E+00	-0.7494E+00
0.2800E+02	0.7523E+00	0.4218E+00	0.1479E+00	-0.7924E-01	-0.2675E+00	-0.4237E+00	-0.5531E+00	-0.6604E+00	-0.7493E+00
0.3000E+02	0.7523E+00	0.4218E+00	0.1479E+00	-0.7925E-01	-0.2675E+00	-0.4237E+00	-0.5531E+00	-0.6604E+00	-0.7493E+00
0.3400E+02	0.7523E+00	0.4218E+00	0.1479E+00	-0.7925E-01	-0.2676E+00	-0.4237E+00	-0.5531E+00	-0.6604E+00	-0.7493E+00
0.3800E+02	0.7523E+00	0.4218E+00	0.1479E+00	-0.7925E-01	-0.2676E+00	-0.4237E+00	-0.5531E+00	-0.6604E+00	-0.7493E+00
0.4200E+02	0.7523E+00	0.4218E+00	0.1479E+00	-0.7925E-01	-0.2676E+00	-0.4237E+00	-0.5531E+00	-0.6604E+00	-0.7493E+00
0.5000E+02	0.7523E+00	0.4218E+00	0.1479E+00	-0.7925E-01	-0.2675E+00	-0.4236E+00	-0.5531E+00	-0.6604E+00	-0.7493E+00
0.5800E+02	0.7523E+00	0.4218E+00	0.1479E+00	-0.7925E-01	-0.2675E+00	-0.4236E+00	-0.5531E+00	-0.6604E+00	-0.7493E+00
0.6600E+02	0.7523E+00	0.4218E+00	0.1479E+00	-0.7924E-01	-0.2675E+00	-0.4237E+00	-0.5531E+00	-0.6604E+00	-0.7493E+00
0.7400E+02	0.7500E+00	0.4199E+00	0.1462E+00	-0.8067E-01	-0.2688E+00	-0.4247E+00	-0.5540E+00	-0.6611E+00	-0.7500E+00

NOT LEGIBLE
ILLISIBLE

JET REYNOLDS NUMBER = 100.0 JET-TO-PLATE SPACING = 2.0 NX = 99 NY = 9
DIFFERENCING SCHEME (1=C.D.S.,2=U.D.S.,3=U.W.D.S.) = 3
INITIAL VELOCITY PROFILE = PARABOLIC

VALUES OF STREAM-FUNCTION, S:

X	Y= 0.0	Y= 0.440	Y= 0.806	Y= 1.108	Y= 1.358	Y= 1.906	Y= 1.730	Y= 1.862	Y= 2.000
0.0	0.0	0.0	0.0	0.0	0.0	0.0	0.0	0.0	0.0
0.6250E-01	-0.9326E-01	-0.9145E-01	-0.8729E-01	-0.7867E-01	-0.6442E-01	-0.4629E-01	-0.2712E-01	-0.9608E-02	0.0
0.1250E+00	-0.1836E+00	-0.1801E+00	-0.1721E+00	-0.1554E+00	-0.1274E+00	-0.9153E-01	-0.5366E-01	-0.1895E-01	0.0
0.1875E+00	-0.2681E+00	-0.2632E+00	-0.2519E+00	-0.2281E+00	-0.1876E+00	-0.1349E+00	-0.7903E-01	-0.2776E-01	0.0
0.2500E+00	-0.3438E+00	-0.3379E+00	-0.3244E+00	-0.2951E+00	-0.2437E+00	-0.1756E+00	-0.1027E+00	-0.3582E-01	0.0
0.3125E+00	-0.4077E+00	-0.4017E+00	-0.3874E+00	-0.3548E+00	-0.2947E+00	-0.2129E+00	-0.1244E+00	-0.4294E-01	0.0
0.3750E+00	-0.4570E+00	-0.4524E+00	-0.4394E+00	-0.4061E+00	-0.3397E+00	-0.2463E+00	-0.1436E+00	-0.4897E-01	0.0
0.4375E+00	-0.4888E+00	-0.4891E+00	-0.4800E+00	-0.4486E+00	-0.3785E+00	-0.2754E+00	-0.1601E+00	-0.5379E-01	0.0
0.5000E+00	-0.5000E+00	-0.5129E+00	-0.5102E+00	-0.4826E+00	-0.4110E+00	-0.3003E+00	-0.1740E+00	-0.5727E-01	0.0
0.6250E+00	-0.5000E+00	-0.5309E+00	-0.5448E+00	-0.5252E+00	-0.4582E+00	-0.3372E+00	-0.1935E+00	-0.6143E-01	0.0
0.7500E+00	-0.5000E+00	-0.5353E+00	-0.5625E+00	-0.5548E+00	-0.4875E+00	-0.3596E+00	-0.2031E+00	-0.6143E-01	0.0
0.1000E+01	-0.5000E+00	-0.5375E+00	-0.5782E+00	-0.5776E+00	-0.5103E+00	-0.3725E+00	-0.2026E+00	-0.5709E-01	0.0
0.1250E+01	-0.5000E+00	-0.5422E+00	-0.5907E+00	-0.5972E+00	-0.5109E+00	-0.3628E+00	-0.1876E+00	-0.4914E-01	0.0
0.1500E+01	-0.5000E+00	-0.5497E+00	-0.6016E+00	-0.5906E+00	-0.4994E+00	-0.3398E+00	-0.1654E+00	-0.4033E-01	0.0
0.2000E+01	-0.5000E+00	-0.5568E+00	-0.6119E+00	-0.5796E+00	-0.4622E+00	-0.2926E+00	-0.1310E+00	-0.2965E-01	0.0
0.2500E+01	-0.5000E+00	-0.5606E+00	-0.6100E+00	-0.5529E+00	-0.4155E+00	-0.2459E+00	-0.1029E+00	-0.2209E-01	0.0
0.3000E+01	-0.5000E+00	-0.5698E+00	-0.5933E+00	-0.5119E+00	-0.3625E+00	-0.2013E+00	-0.7942E-01	-0.1635E-01	0.0
0.3500E+01	-0.5000E+00	-0.5621E+00	-0.5619E+00	-0.4605E+00	-0.3077E+00	-0.1610E+00	-0.6037E-01	-0.1200E-01	0.0
0.4000E+01	-0.5000E+00	-0.5400E+00	-0.5206E+00	-0.4052E+00	-0.2562E+00	-0.1272E+00	-0.4579E-01	-0.8867E-02	0.0
0.4500E+01	-0.5000E+00	-0.5256E+00	-0.4765E+00	-0.3532E+00	-0.2127E+00	-0.1013E+00	-0.3549E-01	-0.6784E-02	0.0
0.5000E+01	-0.5000E+00	-0.5038E+00	-0.4362E+00	-0.2997E+00	-0.1794E+00	-0.8318E-01	-0.2884E-01	-0.5533E-02	0.0
0.5500E+01	-0.5000E+00	-0.4854E+00	-0.4027E+00	-0.2766E+00	-0.1562E+00	-0.7162E-01	-0.2494E-01	-0.4846E-02	0.0
0.6000E+01	-0.5000E+00	-0.4712E+00	-0.3785E+00	-0.2511E+00	-0.1412E+00	-0.6487E-01	-0.2293E-01	-0.4549E-02	0.0
0.6500E+01	-0.5000E+00	-0.4609E+00	-0.3608E+00	-0.2377E+00	-0.1321E+00	-0.6134E-01	-0.2209E-01	-0.4478E-02	0.0
0.7000E+01	-0.5000E+00	-0.4538E+00	-0.3489E+00	-0.2278E+00	-0.1270E+00	-0.5975E-01	-0.2192E-01	-0.4533E-02	0.0
0.7500E+01	-0.5000E+00	-0.4490E+00	-0.3407E+00	-0.2217E+00	-0.1243E+00	-0.5924E-01	-0.2206E-01	-0.4617E-02	0.0
0.8000E+01	-0.5000E+00	-0.4458E+00	-0.3353E+00	-0.2178E+00	-0.1230E+00	-0.5925E-01	-0.2232E-01	-0.4719E-02	0.0
0.8500E+01	-0.5000E+00	-0.4436E+00	-0.3316E+00	-0.2155E+00	-0.1224E+00	-0.5916E-01	-0.2259E-01	-0.4810E-02	0.0
0.9000E+01	-0.5000E+00	-0.4421E+00	-0.3291E+00	-0.2140E+00	-0.1221E+00	-0.5972E-01	-0.2282E-01	-0.4883E-02	0.0
0.9500E+01	-0.5000E+00	-0.4411E+00	-0.3274E+00	-0.2129E+00	-0.1220E+00	-0.5994E-01	-0.2301E-01	-0.4938E-02	0.0
0.1000E+02	-0.5000E+00	-0.4403E+00	-0.3261E+00	-0.2122E+00	-0.1219E+00	-0.6011E-01	-0.2314E-01	-0.4977E-02	0.0
0.1050E+02	-0.5000E+00	-0.4397E+00	-0.3252E+00	-0.2117E+00	-0.1219E+00	-0.6023E-01	-0.2323E-01	-0.5004E-02	0.0
0.1100E+02	-0.5000E+00	-0.4393E+00	-0.3244E+00	-0.2113E+00	-0.1218E+00	-0.6030E-01	-0.2329E-01	-0.5022E-02	0.0
0.1150E+02	-0.5000E+00	[illegible]	-0.3239E+00	-0.2109E+00	-0.1217E+00	-0.6035E-01	-0.2333E-01	-0.5031E-02	0.0
0.1200E+02	-0.5000E+00	-0.4387E+00	-0.3231E+00	-0.2107E+00	-0.1217E+00	-0.6029E-01	-0.2337E-01	-0.5045E-02	0.0
0.1300E+02	-0.5000E+00	-0.4384E+00	-0.3229E+00	-0.2103E+00	-0.1216E+00	-0.6039E-01	-0.2335E-01	-0.5050E-02	0.0
0.1400E+02	-0.5000E+00	-0.4382E+00	-0.3226E+00	-0.2102E+00	-0.1215E+00	-0.6038E-01	-0.2339E-01	-0.5053E-02	0.0
0.1500E+02	-0.5000E+00	-0.4381E+00	-0.3224E+00	-0.2100E+00	-0.1215E+00	-0.6038E-01	-0.2339E-01	-0.5054E-02	0.0
0.1600E+02	-0.5000E+00	-0.4381E+00	-0.3223E+00	-0.2100E+00	-0.1214E+00	-0.6037E-01	-0.2339E-01	-0.5055E-02	0.0
0.1700E+02	-0.5000E+00	-0.4380E+00	-0.3223E+00	-0.2099E+00	-0.1214E+00	-0.6036E-01	-0.2339E-01	-0.5055E-02	0.0
0.1800E+02	-0.5000E+00	-0.4380E+00	-0.3222E+00	-0.2099E+00	-0.1214E+00	-0.6035E-01	-0.2338E-01	-0.5054E-02	0.0
0.1900E+02	-0.5000E+00	-0.4380E+00	-0.3222E+00	-0.2098E+00	-0.1214E+00	-0.6035E-01	-0.2339E-01	-0.5054E-02	0.0
0.2000E+02	-0.5000E+00	-0.4380E+00	-0.3222E+00	-0.2098E+00	-0.1214E+00	-0.6034E-01	-0.2338E-01	-0.5054E-02	0.0

0.2200E+02	-0.5000E+00	-0.4380E+00	-0.3222E+00	-0.2098E+00	-0.1214E+00	-0.6034E-01	-0.2339E-01	-0.5054E-02	0.0
0.2400E+02	-0.5000E+00	-0.4380E+00	-0.3221E+00	-0.2098E+00	-0.1214E+00	-0.6034E-01	-0.2338E-01	-0.5054E-02	0.0
0.2600E+02	-0.5000E+00	-0.4380E+00	-0.3221E+00	-0.2098E+00	-0.1213E+00	-0.6034E-01	-0.2338E-01	-0.5054E-02	0.0
0.2800E+02	-0.5000E+00	-0.4380E+00	-0.3221E+00	-0.2098E+00	-0.1213E+00	-0.6033E-01	-0.2338E-01	-0.5053E-02	0.0
0.3000E+02	-0.5000E+00	-0.4380E+00	-0.3221E+00	-0.2098E+00	-0.1213E+00	-0.6033E-01	-0.2338E-01	-0.5053E-02	0.0
0.3400E+02	-0.5000E+00	-0.4380E+00	-0.3221E+00	-0.2098E+00	-0.1213E+00	-0.6033E-01	-0.2338E-01	-0.5053E-02	0.0
0.3800E+02	-0.5000E+00	-0.4380E+00	-0.3221E+00	-0.2098E+00	-0.1213E+00	-0.6033E-01	-0.2338E-01	-0.5053E-02	0.0
0.4200E+02	-0.5000E+00	-0.4380E+00	-0.3221E+00	-0.2098E+00	-0.1213E+00	-0.6033E-01	-0.2338E-01	-0.5053E-02	0.0
0.5000E+02	-0.5000E+00	-0.4380E+00	-0.3221E+00	-0.2098E+00	-0.1213E+00	-0.6033E-01	-0.2338E-01	-0.5053E-02	0.0
0.5800E+02	-0.5000E+00	-0.4380E+00	-0.3221E+00	-0.2098E+00	-0.1213E+00	-0.6033E-01	-0.2338E-01	-0.5053E-02	0.0
0.6600E+02	-0.5000E+00	-0.4380E+00	-0.3221E+00	-0.2098E+00	-0.1214E+00	-0.6034E-01	-0.2338E-01	-0.5054E-02	0.0
0.7400E+02	-0.5000E+00	-0.4380E+00	-0.3222E+00	-0.2098E+00	-0.1214E+00	-0.6035E-01	-0.2339E-01	-0.5056E-02	0.0

NOT LEGIBLE
ILLISIBLE

JET REYNOLDS NUMBER = 100.0 JET-TO-PLATE SPACING = 2.0 NX = 96 NY = 25
DIFFERENCING SCHEME (1=C.D.S.,2=U.D.S.,3=U.V.D.S.) = 3
INITIAL VELOCITY PROFILE = PARABOLIC

VALUES OF VELOCITY IN X-DIRECTION, U:

X	Y=-0.0	Y= 0.440	Y= 0.805	Y= 1.108	Y= 1.358	Y= 1.566	Y= 1.730	Y= 1.882	Y= 2.000
0.0	0.0	0.0	0.0	0.0	0.0	0.0	0.0	0.0	0.0
0.6250E-01	0.0	0.7010E-02	0.1813E-01	0.4178E-01	0.7296E-01	0.1009E+00	0.1102E+00	0.1189E+00	0.0
0.1250E+00	0.0	0.1349E-01	0.3527E-01	0.8781E-01	0.1441E+00	0.1996E+00	0.2362E+00	0.2345E+00	0.0
0.1875E+00	0.0	0.1949E-01	0.4928E-01	0.1173E+00	0.2092E+00	0.2944E+00	0.3490E+00	0.3453E+00	0.0
0.2500E+00	0.0	0.2361E-01	0.5958E-01	0.1467E+00	0.2691E+00	0.3817E+00	0.4562E+00	0.4489E+00	0.0
0.3125E+00	0.0	0.2549E-01	0.6375E-01	0.1674E+00	0.3197E+00	0.4626E+00	0.5550E+00	0.5431E+00	0.0
0.3750E+00	0.0	0.2249E-01	0.6104E-01	0.1789E+00	0.3598E+00	0.5332E+00	0.6461E+00	0.6266E+00	0.0
0.4375E+00	0.0	0.1274E-01	0.5064E-01	0.1811E+00	0.3908E+00	0.5951E+00	0.7274E+00	0.6983E+00	0.0
0.5000E+00	0.0	-0.5248E-02	0.3481E-01	0.1751E+00	0.4118E+00	0.6475E+00	0.8012E+00	0.7575E+00	0.0
0.6250E+00	0.0	-0.5522E-01	-0.7234E-02	0.1489E+00	0.4322E+00	0.7261E+00	0.9160E+00	0.8352E+00	0.0
0.7500E+00	0.0	-0.9153E-01	-0.4024E-01	0.1254E+00	0.4414E+00	0.7832E+00	0.1000E+01	0.8687E+00	0.0
0.1000E+01	0.0	-0.1256E+00	-0.7144E-01	0.1102E+00	0.4631E+00	0.8538E+00	0.1067E+01	0.8424E+00	0.0
0.1250E+01	0.0	-0.1495E+00	-0.7777E-01	0.1347E+00	0.5092E+00	0.9014E+00	0.1063E+01	0.7572E+00	0.0
0.1500E+01	0.0	-0.1702E+00	-0.7370E-01	0.1811E+00	0.5736E+00	0.9356E+00	0.1010E+01	0.6459E+00	0.0
0.2000E+01	0.0	-0.1934E+00	-0.3708E-01	0.2803E+00	0.6625E+00	0.9200E+00	0.8722E+00	0.4912E+00	0.0
0.2500E+01	0.0	-0.1987E+00	0.2261E-01	0.3725E+00	0.7118E+00	0.8689E+00	0.7287E+00	0.3741E+00	0.0
0.3000E+01	0.0	-0.1792E+00	0.9595E-01	0.4467E+00	0.7197E+00	0.7800E+00	0.5905E+00	0.2820E+00	0.0
0.3500E+01	0.0	-0.1338E+00	0.1703E+00	0.4976E+00	0.6914E+00	0.6729E+00	0.4664E+00	0.2101E+00	0.0
0.4000E+01	0.0	-0.7084E-01	0.2338E+00	0.5127E+00	0.6381E+00	0.5650E+00	0.3642E+00	0.1570E+00	0.0
0.4500E+01	0.0	-0.2240E-02	0.2826E+00	0.5105E+00	0.5736E+00	0.4602E+00	0.2872E+00	0.1207E+00	0.0
0.5000E+01	0.0	0.6110E-01	0.3160E+00	0.4947E+00	0.5112E+00	0.3940E+00	0.2341E+00	0.9795E-01	0.0
0.5500E+01	0.0	0.1136E+00	0.3372E+00	0.4728E+00	0.4532E+00	0.3408E+00	0.2009E+00	0.8528E-01	0.0
0.6000E+01	0.0	0.1541E+00	0.3509E+00	0.4516E+00	0.4184E+00	0.3056E+00	0.1818E+00	0.7916E-01	0.0
0.6500E+01	0.0	0.1837E+00	0.3572E+00	0.4325E+00	0.3901E+00	0.2839E+00	0.1720E+00	0.7706E-01	0.0
0.7000E+01	0.0	0.2047E+00	0.3599E+00	0.4172E+00	0.3704E+00	0.2712E+00	0.1679E+00	0.7713E-01	0.0
0.7500E+01	0.0	0.2193E+00	0.3606E+00	0.4052E+00	0.3568E+00	0.2612E+00	0.1668E+00	0.7819E-01	0.0
0.8000E+01	0.0	0.2290E+00	0.3613E+00	0.3959E+00	0.3177E+00	0.2605E+00	0.1671E+00	0.7953E-01	0.0
0.8500E+01	0.0	0.2358E+00	0.3608E+00	0.3880E+00	0.3420E+00	0.2586E+00	0.1680E+00	0.8079E-01	0.0
0.9000E+01	0.0	0.2406E+00	0.3604E+00	0.3845E+00	0.3375E+00	0.2577E+00	0.1688E+00	0.8184E-01	0.0
0.9500E+01	0.0	0.2436E+00	0.3599E+00	0.3807E+00	0.3351E+00	0.2571E+00	0.1696E+00	0.8263E-01	0.0
0.1000E+02	0.0	0.2463E+00	0.3591E+00	0.3774E+00	0.3327E+00	0.2568E+00	0.1702E+00	0.8320E-01	0.0
0.1050E+02	0.0	0.2481E+00	[illegible]	0.3750E+00	0.3312E+00	0.2565E+00	0.1706E+00	0.8359E-01	0.0
0.1100E+02	0.0	0.2493E+00	[illegible]	0.3737E+00	0.3305E+00	0.2563E+00	0.1707E+00	0.8383E-01	0.0
0.1150E+02	0.0	[illegible]	[illegible]	0.3730E+00	0.3292E+00	0.2564E+00	0.1710E+00	0.8402E-01	0.0
0.1200E+02	0.0	0.2515E+00	[illegible]	0.3725E+00	0.3285E+00	0.2561E+00	0.1711E+00	0.8410E-01	0.0
0.1300E+02	0.0	0.2523E+00	0.3590E+00	0.3714E+00	0.3283E+00	0.2559E+00	0.1712E+00	0.8426E-01	0.0
0.1400E+02	0.0	0.2530E+00	0.3587E+00	0.3709E+00	0.3279E+00	0.2557E+00	0.1711E+00	0.8428E-01	0.0
0.1500E+02	0.0	0.2530E+00	0.3590E+00	0.3703E+00	0.3273E+00	0.2555E+00	0.1711E+00	0.8431E-01	0.0
0.1600E+02	0.0	0.2534E+00	0.3590E+00	0.3703E+00	0.3275E+00	0.2554E+00	0.1711E+00	0.8431E-01	0.0
0.1700E+02	0.0	0.2538E+00	0.3590E+00	0.3703E+00	0.3270E+00	0.2554E+00	0.1711E+00	0.8431E-01	0.0
0.1800E+02	0.0	0.2534E+00	0.3565E+00	0.3703E+00	0.3271E+00	0.2552E+00	0.1711E+00	0.8431E-01	0.0
0.1900E+02	0.0	0.2531E+00	0.3590E+00	0.3703E+00	0.3272E+00	0.2552E+00	0.1710E+00	0.8429E-01	0.0
0.2000E+02	0.0	0.2534E+00	0.3590E+00	0.3698E+00	0.3272E+00	0.2553E+00	0.1710E+00	0.8429E-01	0.0

NOT LEGIBLE
ILLISIBLE

0.2200E+02	0.0	0.2590E+00	0.3590E+00	0.3698E+00	0.3272E+00	0.2552E+00	0.1710E+00	0.8428E-01	0.0
0.2400E+02	0.0	0.2538E+00	0.3590E+00	0.3698E+00	0.3266E+00	0.2552E+00	0.1710E+00	0.8428E-01	0.0
0.2600E+02	0.0	0.2538E+00	0.3590E+00	0.3698E+00	0.3266E+00	0.2552E+00	0.1710E+00	0.8428E-01	0.0
0.2800E+02	0.0	0.2538E+00	0.3590E+00	0.3698E+00	0.3266E+00	0.2552E+00	0.1710E+00	0.8428E-01	0.0
0.3000E+02	0.0	0.2538E+00	0.3590E+00	0.3698E+00	0.3266E+00	0.2552E+00	0.1710E+00	0.8428E-01	0.0
0.3400E+02	0.0	0.2538E+00	0.3590E+00	0.3699E+00	0.3266E+00	0.2552E+00	0.1710E+00	0.8428E-01	0.0
0.3800E+02	0.0	0.2538E+00	0.3590E+00	[illegible]	0.3266E+00	0.2552E+00	0.1710E+00	0.8428E-01	0.0
0.4200E+02	0.0	0.2538E+00	0.3590E+00	0.3698E+00	0.3266E+00	0.2552E+00	0.1710E+00	0.8428E-01	0.0
0.5000E+02	0.0	0.2538E+00	0.3590E+00	0.3698E+00	0.3266E+00	0.2552E+00	0.1710E+00	0.8428E-01	0.0
0.5800E+02	0.0	0.2538E+00	0.3590E+00	0.3698E+00	0.3266E+00	0.2552E+00	0.1710E+00	0.8428E-01	0.0
0.6600E+02	0.0	0.2538E+00	[illegible]	0.3698E+00	0.3266E+00	0.2552E+00	0.1710E+00	0.8428E-01	0.0
0.7400E+02	0.0	0.2534E+00	[illegible]	0.3698E+00	0.3272E+00	0.2552E+00	0.1711E+00	0.8431E-01	0.0

NOT LEGIBLE
ILLISIBLE

JET REYNOLDS NUMBER = 100.0 JET-TO-PLATE SPACING = 2.0 NX = 95 NY = 25
DIFFERENCING SCHEME (1=C.D.S.,2=U.D.S.,3=U.V.D.S.) = 3
INITIAL VELOCITY PROFILE = PARABOLIC

VALUES OF VELOCITY IN Y-DIRECTION, V:

X	Y=-0.0	Y= 0.440	Y= 0.805	Y= 1.100	Y= 1.350	Y= 1.[illegible]	Y= 1.730	Y= 1.862	Y= 2.000
0.0	0.1500E+01	0.1486E+01	0.1416E+01	0.1274E+01	0.1042E+01	0.7478E+00	0.4388E+00	0.1559E+00	0.0
0.6250E-01	0.1477E+01	0.1441E+01	0.1377E+01	0.1243E+01	0.1019E+01	0.7322E+00	0.4283E+00	0.1516E+00	0.0
0.1250E+00	0.1406E+01	0.1374E+01	0.1317E+01	0.1195E+01	0.9854E+00	0.7092E+00	0.4152E+00	0.1452E+00	0.0
0.1875E+00	0.1289E+01	0.1262E+01	0.1218E+01	0.1118E+01	0.9304E+00	0.6726E+00	0.3922E+00	0.1350E+00	0.0
0.2500E+00	0.1126E+01	0.1108E+01	0.1094E+01	0.1014E+01	0.8568E+00	0.6240E+00	0.3630E+00	0.1214E+00	0.0
0.3125E+00	0.9141E+00	0.9160E+00	0.9200E+00	0.8880E+00	0.7[illegible]0E+00	0.5656E+00	0.3272E+00	0.1052E+00	0.0
0.3750E+00	0.6563E+00	0.6992E+00	0.7408E+00	0.7504E+00	0.6704E+00	0.5000E+00	0.2856E+00	0.8680E-01	0.0
0.4375E+00	0.3516E+00	0.4840E+00	0.5664E+00	0.6120E+00	0.5704E+00	0.4320E+00	0.2432E+00	0.6640E-01	0.0
0.5000E+00	-0.[illegible]	0.2223E+00	0.2456E+00	0.4245E+00	0.4251E+00	0.3296E+00	0.1781E+00	0.4075E-01	0.0
0.6250E+00	0.[illegible]	0.8960E-01	0.2032E+00	0.2888E+00	0.3060E+00	0.2372E+00	0.1164E+00	0.1664E-01	0.0
0.7500E+00	0.0	0.1760E-01	0.8907E-01	0.1317E+00	0.1380E+00	0.9440E-01	0.2427E-01	-0.1160E-01	0.0
0.1000E+01	0.0	0.1520E-01	0.5640E-01	0.6480E-01	0.4600E-01	0.6400E-02	-0.3100E-01	-0.2459E-01	0.0
0.1250E+01	0.0	0.2440E-01	0.4680E-01	0.2600E-01	-0.2180E-01	-0.6560E-01	-0.7440E-01	-0.3310E-01	0.0
0.1500E+01	0.0	0.2387E-01	0.2813E-01	-0.1013E-01	-0.6493E-01	-0.9360E-01	-0.7547E-01	-0.2594E-01	0.0
0.2000E+01	0.0	0.1890E-01	0.8400E-02	-0.3780E-01	-0.8390E-01	-0.9390E-01	-0.6250E-01	-0.1844E-01	0.0
0.2500E+01	0.0	0.8000E-02	-0.1850E-01	-0.6770E-01	-0.9970E-01	-0.9130E-01	-0.5158E-01	-0.1330E-01	0.0
0.3000E+01	0.0	-0.6500E-02	-0.4810E-01	-0.9220E-01	-0.1078E+00	-0.8490E-01	-0.4253E-01	-0.1009E-01	0.0
0.3500E+01	0.0	-0.2380E-01	-0.7270E-01	-0.1067E+00	-0.1063E+00	-0.7410E-01	-0.3383E-01	-0.7483E-02	0.0
0.4000E+01	0.0	-0.37[illegible]E-01	-0.8540E-01	-0.1073E+00	-0.9500E-01	-0.5970E-01	-0.2488E-01	-0.5216E-02	0.0
0.4500E+01	0.0	-0.4220E-01	-0.8440E-01	-0.95[illegible]E-01	-0.7600E-01	-0.4402E-01	-0.1695E-01	-0.3244E-02	0.0
0.5000E+01	0.0	-0.3900E-01	-0.7120E-01	-0.76[illegible]E-01	-0.[illegible]E-01	0.29[illegible]E-01	-0.1055E-01	-0.1938E-02	0.0
0.5500E+01	0.0	-0.3200E-01	-0.5770E-01	-0.56[illegible]E-01	0.3920E-01	-0.1811E-01	-0.5110E-02	-0.9740E-03	0.0
0.6000E+01	0.0	-0.2450E-01	-0.4250E-01	-0.38[illegible]E-01	-0.2410E-01	-0.1028E-01	-0.2850E-02	-0.3600E-03	0.0
0.6500E+01	0.0	-0.1740E-01	-0.2970E-01	-0.2550E-01	-0.1420E-01	-0.5120E-02	-0.1010E-02	-0.2600E-04	0.0
0.7000E+01	0.0	-0.1190E-01	-0.2010E-01	-0.1600E-01	-0.7800E-02	-0.2100E-02	-0.3000E-04	0.1390E-03	0.0
0.7500E+01	0.0	-0.8000E-02	-0.1350E-01	-0.1000E-01	-0.4000E-02	-0.5000E-03	0.4000E-03	0.1960E-03	0.0
0.8000E+01	0.0	-0.5400E-02	-0.9100E-02	-0.6200E-02	-0.1900E-02	0.2200E-03	0.5300E-03	0.1930E-03	0.0
0.8500E+01	0.0	-0.3700E-02	-0.6200E-02	-0.3800E-02	-0.9000E-03	0.4700E-03	0.5000E-03	0.1640E-03	0.0
0.9000E+01	0.0	-0.2500E-02	-0.4200E-02	-0.2500E-02	-0.4000E-03	0.4800E-03	0.4200E-03	0.1293E-03	0.0
0.9500E+01	0.0	-0.1800E-02	-0.3000E-02	-0.1800E-02	-0.2000E-03	0.3900E-03	0.3200E-03	0.9400E-04	0.0
0.1000E+02	0.0	-0.1400E-02	-0.2200E-02	-0.1200E-02	-0.2000E-03	0.2900E-03	0.2200E-03	0.6600E-04	0.0
0.1050E+02	0.0	-0.1000E-02	-0.1700E-02	-0.9000E-03	-0.1000E-03	0.1900E-03	0.1500E-03	0.4500E-04	0.0
0.1100E+02	0.0	-0.7000E-03	-0.1300E-02	-0.8000E-03	-0.1000E-03	0.1200E-03	0.1000E-03	0.3000E-04	0.0
0.1150E+02	0.0	-0.6000E-03	-0.1000E-02	-0.6000E-03	-0.1000E-03	0.9000E-04	0.8000E-04	0.2700E-04	0.0
0.1200E+02	0.0	-0.4000E-03	-0.6667E-03	-0.4000E-03	0.6668E-04	0.2667E-04	0.3333E-04	0.1067E-04	0.0
0.1300E+02	0.0	-0.2500E-03	-0.4000E-03	-0.2500E-03	-0.9998E-04	-0.4999E-05	0.9999E-05	0.399[illegible]E-05	0.0
0.1400E+02	0.0	-0.1500E-03	-0.2500E-03	-0.1500E-03	-0.4998E-04	-0.4299E-05	0.4999E-05	0.200[illegible]E-05	0.0
0.1500E+02	0.0	-0.5001E-04	-0.1500E-03	-0.1000E-03	-0.5001E-04	-0.5001E-05	-0.0	0.1000E-05	0.0
0.1600E+02	0.0	-0.4998E-04	-0.4999E-04	-0.4998E-04	-0.5001E-04	-0.1000E-04	-0.0	0.4992E-06	0.0
0.1700E+02	0.0	-0.4999E-04	-0.5001E-04	-0.4998E-04	-0.0	-0.9999E-05	-0.4998E-05	-0.4992E-06	0.0
0.1800E+02	0.0	-0.0	-0.5001E-04	-0.5001E-04	-0.0	-0.4999E-05	-0.4999E-05	-0.4992E-06	0.0
0.1900E+02	0.0	-0.0	-0.0	-0.5001E-04	-0.0	-0.5001E-05	-0.0	-0.0	0.0
0.2000E+02	0.0	-0.0	-0.0	-0.0	-0.0	-0.3334E-05	-0.0	-0.0	0.0

0.2200E+02	0.0	-0.0	-0.2500E-04	-0.0	-0.0	-0.0	-0.0	-0.0	0.0
0.2400E+02	0.0	-0.0	-0.2500E-04	-0.0	-0.2500E-04	-0.0	-0.0	-0.0	0.0
0.2600E+02	0.0	-0.0	-0.0	-0.0	-0.2500E-04	-0.2500E-05	-0.0	-0.2500E-06	0.0
0.2800E+02	0.0	-0.0	-0.0	-0.0	-0.0	-0.2500E-05	-0.0	-0.2500E-06	0.0
0.3000E+02	0.0	-0.0	-0.0	-0.0	-0.0	-0.0	-0.0	-0.0	0.0
0.3400E+02	0.0	-0.0	-0.0	-0.0	-0.0	-0.0	-0.0	-0.0	0.0
0.3800E+02	0.0	-0.0	-0.0	-0.0	-0.0	-0.0	-0.0	-0.0	0.0
0.4200E+02	0.0	-0.0	-0.0	-0.0	-0.0	-0.0	-0.0	-0.0	0.0
0.5000E+02	0.0	-0.0	-0.0	-0.0	-0.0	-0.0	-0.0	-0.0	0.0
0.5800E+02	0.0	-0.0	-0.0	-0.0	0.6251E-05	0.6249E-06	-0.0	0.6263E-07	0.0
0.6600E+02	0.0	-0.0	0.6251E-05	-0.0	0.6251E-05	0.1250E-05	0.6249E-06	0.1877E-06	0.0
0.7400E+02	0.0	-0.0	0.1877E-04	-0.0	-0.6251E-05	0.1255E-05	0.1878E-05	0.3125E-06	0.0

NOT LEGIBLE
ILLISIBLE

JET REYNOLDS NUMBER = 100.0 JET-TO-PLATE SPACING = 2.0 NX = 99 NY = 25
DIFFERENCING SCHEME (1=C.D.S.,2=U.D.S.,3=U.V.D.S.) = 3
INITIAL VELOCITY PROFILE = PARABOLIC

VALUES OF SKIN-FRICTION FACTOR, CF:

X	CF	CF*RE
0.0	-0.0	0.0
0.6250E-01	0.4588E-01	0.4588E+01
0.1250E+00	0.8990E-01	0.8990E+01
0.1875E+00	0.1303E+00	0.1303E+02
0.2500E+00	0.1658E+00	0.1658E+02
0.3125E+00	0.1952E+00	0.1952E+02
0.3750E+00	0.2176E+00	0.2176E+02
0.4375E+00	0.2324E+00	0.2324E+02
0.5000E+00	0.2380E+00	0.2380E+02
0.6250E+00	0.2442E+00	0.2442E+02
0.7500E+00	0.2290E+00	0.2290E+02
0.1000E+01	0.1983E+00	0.1983E+02
0.1250E+01	0.1592E+00	0.1592E+02
0.1500E+01	0.1257E+00	0.1257E+02
0.2000E+01	0.8672E-01	0.8672E+01
0.2500E+01	0.6270E-01	0.6270E+01
0.3000E+01	0.4518E-01	0.4518E+01
0.3500E+01	0.3239E-01	0.3239E+01
0.4000E+01	0.2352E-01	0.2352E+01
0.4500E+01	0.1788E-01	[illegible]
0.5000E+01	0.1465E-01	[illegible]
0.5500E+01	0.1358E-01	[illegible]
0.6000E+01	0.1255E-01	[illegible]
0.6500E+01	0.1260E-01	[illegible]
0.7000E+01	0.1293E-01	0.1293E+01
0.7500E+01	0.1336E-01	0.1336E+01
[illegible]	0.1377E-01	0.1377E+01
[illegible]	0.1411E-01	0.1411E+01
[illegible]	0.1437E-01	0.1437E+01
0.9500E+01	0.1457E-01	0.1457E+01
0.1000E+02	0.1471E-01	0.1471E+01
0.1050E+02	0.1480E-01	0.1480E+01
0.1100E+02	0.1487E-01	0.1487E+01
[illegible]	0.1491E-01	0.1491E+01
[illegible]	0.1495E-01	0.1495E+01
0.1300E+02	0.1497E-01	0.1497E+01
0.1400E+02	0.1498E-01	0.1498E+01
0.1500E+02	0.1499E-01	0.1499E+01
0.1600E+02	0.1499E-01	0.1499E+01
0.1700E+02	0.1499E-01	0.1499E+01
0.1800E+02	0.1499E-01	0.1499E+01
0.1900E+02	0.1499E-01	0.1499E+01
0.2000E+02	0.1499E-01	0.1499E+01

NOT LEGIBLE
ILLISIBLE

0.2200E+02	0.1499E-01	0.1499E+01
0.2400E+02	0.1499E-01	0.1499E+01
0.2600E+02	0.1499E-01	0.1499E+01
0.2800E+02	0.1499E-01	0.1499E+01
0.3000E+02	0.1499E-01	0.1499E+01
0.3400E+02	0.1499E-01	0.1499E+01
0.3800E+02	0.1499E-01	0.1499E+01
0.4200E+02	0.1499E-01	0.1499E+01
0.5000E+02	0.1499E-01	0.1499E+01
0.5800E+02	0.1499E-01	0.1499E+01
0.6500E+02	0.1499E-01	0.1499E+01
0.7400E+02	0.1500E-01	0.1500E+01

****

JET REYNOLDS NUMBER = 100.0 SCHMIDT NUMBER = 2.74 JET-TO-PLATE SPACING = 2.0 NX = 56 NY = 25
DIFFERENCING SCHEME (1=C.D.S.,2=U.D.S.,3=U.V.D.S.) = 3
INITIAL VELOCITY PROFILE = PARABOLIC

****

VALUES OF CONCENTRATION, C:

X	Y=-0.0	Y= 0.440	Y= 0.805	Y= 1.106	Y= 1.358	Y= 1.566	Y= 1.739	Y= 1.882	Y= 2.000
0.0	0.0	-0.9908E-07	-0.3313E-06	-0.3944E-06	-0.2921E-06	-0.1876E-06	0.7149E-07	0.3261E-01	0.1000E+01
0.6250E-01	0.0	0.3033E-07	0.1490E-06	0.2483E-06	0.2435E-06	0.1830E-06	0.2702E-06	0.3325E-01	0.1000E+01
0.1250E+00	0.0	0.4185E-06	0.1590E-05	0.2176E-05	0.1850E-05	0.1235E-05	0.8661E-06	0.3517E-01	0.1000E+01
0.1875E+00	0.0	0.4044E-05	0.1181E-04	0.1295E-04	0.8971E-05	0.4844E-05	0.2371E-05	0.3835E-01	0.1000E+01
0.2500E+00	0.0	0.3565E-04	0.7882E-04	0.7151E-04	0.4052E-04	0.1725E-04	0.6103E-05	0.4281E-01	0.1000E+01
0.3125E+00	0.0	0.2686E-03	0.4552E-03	0.3407E-03	0.1605E-03	0.5459E-04	0.1452E-04	0.4907E-01	0.1000E+01
0.3750E+00	0.0	0.1565E-02	0.1980E-02	0.1274E-02	0.5141E-03	0.1445E-03	0.3091E-04	0.5715E-01	0.1000E+01
0.4375E+00	0.0	0.6157E-02	0.5942E-02	0.3479E-02	0.1271E-02	0.3124E-03	0.5848E-04	0.6763E-01	0.1000E+01
0.5000E+00	0.1632E-01	0.1430E-01	0.1187E-01	0.7254E-02	0.2919E-02	0.7262E-03	0.1445E-03	0.8809E-01	0.1000E+01
0.6250E+00	0.2447E-01	0.2284E-01	0.2029E-01	0.1370E-01	0.5738E-02	0.1447E-02	0.4286E-03	0.1205E+00	0.1000E+01
0.7500E+00	0.2544E-01	0.2402E-01	0.2221E-01	0.1793E-01	0.8257E-02	0.2055E-02	0.2521E-02	0.1794E+00	0.1000E+01
0.1000E+01	0.2577E-01	0.2395E-01	0.2173E-01	0.1956E-01	0.9573E-02	0.2382E-02	0.1182E-01	0.2586E+00	0.1000E+01
0.1250E+01	0.2609E-01	0.2179E-01	0.2023E-01	0.1918E-01	0.9193E-02	0.3292E-02	0.3289E-01	0.3393E+00	0.1000E+01
0.1500E+01	0.2636E-01	0.2350E-01	0.2001E-01	0.1716E-01	0.8282E-02	0.9792E-02	0.7975E-01	0.4343E+00	0.1000E+01
0.2000E+01	0.2675E-01	0.2303E-01	0.1855E-01	0.1482E-01	0.1037E-01	0.2964E-01	0.1537E+00	0.5281E+00	0.1000E+01
0.2500E+01	0.2732E-01	0.2244E-01	0.1670E-01	0.1438E-01	0.1805E-01	0.6185E-01	0.2341E+00	0.6019E+00	0.1000E+01
0.3000E+01	0.2801E-01	0.2212E-01	0.1662E-01	0.1751E-01	0.3235E-01	0.1066E+00	0.3162E+00	0.6619E+00	0.1000E+01
0.3500E+01	0.2899E-01	0.2270E-01	0.1919E-01	0.2549E-01	0.5725E-01	0.1614E+00	0.3947E+00	0.7106E+00	0.1000E+01
0.4000E+01	0.3058E-01	0.2495E-01	0.2452E-01	0.3848E-01	0.8855E-01	0.2213E+00	0.4645E+00	0.7492E+00	0.1000E+01
0.4500E+01	0.3170E-01	0.2896E-01	0.3207E-01	0.5516E-01	0.1240E+00	0.2791E+00	0.5218E+00	0.7785E+00	0.1000E+01
0.5000E+01	0.3390E-01	0.3326E-01	0.4054E-01	0.7330E-01	0.1593E+00	0.3120E+00	0.5653E+00	0.7996E+00	0.1000E+01
0.5500E+01	0.3615E-01	0.3633E-01	0.4800E-01	0.9076E-01	0.1909E+00	0.3700E+00	0.5963E+00	0.8141E+00	0.1000E+01
0.6000E+01	0.3765E-01	0.4001E-01	0.5641E-01	0.1062E+00	0.2167E+00	0.3991E+00	0.6174E+00	0.8238E+00	0.1000E+01
0.65[illegible]+01	0.3883E-01	0.4258E-01	0.6279E-01	0.1180E+00	0.2369E+00	0.4205E+00	0.6318E+00	0.8304E+00	0.1000E+01
0.7000E+01	0.4035E-01	0.4476E-01	0.6814E-01	0.1296E+00	0.2525E+00	0.4358E+00	0.6422E+00	0.8352E+00	0.1000E+01
0.7500E+01	0.4119E-01	0.4567E-01	0.7268E-01	0.1384E+00	0.2649E+00	0.4477E+00	0.6504E+00	0.8391E+00	0.1000E+01
0.8000E+01	0.4233E-01	0.4841E-01	0.7662E-01	0.1460E+00	0.2754E+00	0.4578E+00	0.6575E+00	0.8425E+00	0.1000E+01
0.8500E+01	0.4348E-01	0.5065E-01	0.8010E-01	0.1527E+00	0.2848E+00	0.4670E+00	0.6641E+00	0.8457E+00	0.1000E+01
0.9000E+01	0.4450E-01	0.5164E-01	0.8309E-01	0.1590E+00	0.2935E+00	0.4756E+00	0.6704E+00	0.8487E+00	0.1000E+01
0.9500E+01	0.4585E-01	0.5322E-01	0.8666E-01	0.1650E+00	0.3019E+00	0.4839E+00	0.6764E+00	0.8516E+00	0.1000E+01
0.1000E+02	0.4710E-01	0.5480E-01	0.8976E-01	0.1708E+00	0.3100E+00	0.4920E+00	0.6822E+00	0.8544E+00	0.1000E+01
0.1050E+02	0.4838E-01	0.5641E-01	0.9284E-01	0.1765E+00	0.3179E+00	0.4997E+00	0.6877E+00	0.8570E+00	0.1000E+01
0.1100E+02	0.4968E-01	0.5804E-01	0.9[illegible]E-01	0.1822E+00	0.3255E+00	0.5072E+00	0.6930E+00	0.8595E+00	0.1000E+01
0.1150E+02	0.5107E-01	0.5971E-01	0.9[illegible]E-01	0.1877E+00	0.3330E+00	0.5142E+00	0.6979E+00	0.8618E+00	0.1000E+01
0.1200E+02	0.5316E-01	0.6274E-01	0.1017E+00	0.1959E+00	0.3436E+00	0.5242E+00	0.7048E+00	0.8651E+00	0.1000E+01
0.1300E+02	0.5615E-01	0.6576E-01	0.1100E+00	0.2066E+00	0.3560E+00	0.5363E+00	0.7130E+00	0.8689E+00	0.1000E+01
0.1400E+02	0.5935E-01	0.6979E-01	0.1165E+00	0.2168E+00	0.3693E+00	0.5473E+00	0.7204E+00	0.8724E+00	0.1000E+01
0.1500E+02	0.6274E-01	0.7382E-01	0.1231E+00	0.2271E+00	0.3810E+00	0.5571E+00	0.7271E+00	0.8755E+00	0.1000E+01
0.1600E+02	0.6532E-01	0.7605E-01	0.1298E+00	0.2369E+00	0.3921E+00	0.5667E+00	0.7333E+00	0.8784E+00	0.1000E+01
0.1700E+02	0.7011E-01	0.8219E-01	0.1368E+00	0.2465E+00	0.4025E+00	0.5754E+00	0.7389E+00	0.8810E+00	0.1000E+01
0.1800E+02	0.7410E-01	0.8709E-01	0.1434E+00	0.2559E+00	0.4123E+00	0.5834E+00	0.7442E+00	0.8834E+00	0.1000E+01
0.1900E+02	0.7827E-01	0.9188E-01	0.1503E+00	0.2650E+00	0.4217E+00	0.5910E+00	0.7491E+00	0.8857E+00	0.1000E+01
0.2000E+02	0.8495E-01	0.9943E-01	0.1607E+00	0.2781E+00	0.4347E+00	0.6013E+00	0.7557E+00	0.8888E+00	0.1000E+01

NOT LEGIBLE
ILLISIBLE

0.2200E+02	0.8493E-01	0.1100E+00	0.1748E+00	0.2946E+00	0.4506E+00	0.6137E+00	0.7636E+00	0.8824E+00	0.1000E+01
0.2400E+02	0.1047E+00	0.1211E+00	0.1884E+00	0.3103E+00	0.4653E+00	0.6250E+00	0.7707E+00	0.8957E+00	0.1000E+01
0.2600E+02	0.1184E+00	0.1326E+00	0.2021E+00	0.3253E+00	0.4789E+00	0.6353E+00	0.7772E+00	0.8987E+00	0.1000E+01
0.2800E+02	0.1265E+00	0.1444E+00	0.2156E+00	0.3396E+00	0.4916E+00	0.6448E+00	0.7832E+00	0.9014E+00	0.1000E+01
0.3000E+02	0.1433E+00	0.1625E+00	0.2355E+00	0.3597E+00	0.5090E+00	0.6577E+00	0.7913E+00	0.9051E+00	0.1000E+01
0.3400E+02	0.1679E+00	0.1870E+00	0.2612E+00	0.3846E+00	0.5299E+00	0.6730E+00	0.8008E+00	0.9094E+00	0.1000E+01
0.3800E+02	0.1923E+00	0.2117E+00	0.2862E+00	0.4078E+00	0.5490E+00	0.6868E+00	0.8093E+00	0.9133E+00	0.1000E+01
0.4200E+02	0.2289E+00	0.2483E+00	0.3217E+00	0.4397E+00	0.5747E+00	0.7051E+00	0.8206E+00	0.9185E+00	0.1000E+01
0.5000E+02	0.2765E+00	0.2953E+00	0.3661E+00	0.4783E+00	0.6050E+00	0.72[illegible]E+00	0.8337E+00	0.9244E+00	0.1000E+01
0.5800E+02	0.3221E+00	0.3401E+00	0.4076E+00	0.5135E+00	0.6323E+00	0.7497E+00	0.8454E+00	0.9298E+00	0.1000E+01
0.6600E+02	0.3654E+00	0.3825E+00	0.4464E+00	0.5461E+00	0.6573E+00	0.7631E+00	0.8560E+00	0.9346E+00	0.1000E+01
0.7400E+02	0.4089E+00	0.4248E+00	0.4843E+00	0.5772E+00	0.6807E+00	0.7793E+00	0.8659E+00	0.9391E+00	0.1000E+01

....

NOT LEGIBLE
ILLISIBLE

JET REYNOLDS NUMBER = 100.0 SCHMIDT NUMBER = 2.74 JET-TO-PLATE SPACING = 2.0 NX = 95 NY = 25
DIFFERENCING SCHEME (1=C.D.S.,2=U.D.S.,3=U.V.D.S.) = 3
INITIAL VELOCITY PROFILE = PARABOLIC

VALUES OF SHERWOOD NUMBER, SH:

X	SH	SHB	CB
0.0	0.1384E+02	0.1384E+02	0.0
0.6250E-01	0.1378E+02	0.1385E+02	0.5000E-02
0.1250E+00	0.1361E+02	0.1375E+02	0.1013E-01
0.1875E+00	0.1334E+02	0.1354E+02	0.1821E-01
0.2500E+00	0.1297E+02	0.1324E+02	0.2030E-01
0.3125E+00	0.1254E+02	0.1287E+02	0.2543E-01
0.3750E+00	0.1203E+02	0.1241E+02	0.3072E-01
0.4375E+00	0.1145E+02	0.1189E+02	0.3627E-01
0.5000E+00	0.1062E+02	0.1103E+02	0.4305E-01
0.6250E+00	0.8604E+01	0.1013E+02	0.5231E-01
0.7500E+00	0.8298E+01	0.8877E+01	0.6526E-01
0.1000E+01	0.7005E+01	0.7620E+01	0.8068E-01
0.1250E+01	0.5944E+01	0.6560E+01	0.9394E-01
0.1500E+01	0.4933E+01	0.5563E+01	0.1132E+00
0.2000E+01	0.4043E+01	0.4643E+01	0.1292E+00
0.2500E+01	0.3383E+01	0.3349E+01	0.1431E+00
0.3000E+01	0.2858E+01	0.3382E+01	0.1548E+00
0.3500E+01	0.2440E+01	0.2919E+01	0.1643E+00
0.4000E+01	0.2114E+01	0.2551E+01	0.1712E+00
0.4500E+01	0.1870E+01	0.2269E+01	0.1759E+00
0.5000E+01	0.1693E+01	0.2063E+01	0.1794E+00
0.5500E+01	0.1572E+01	0.1922E+01	0.1824E+00
0.6000E+01	0.1431E+01	0.1871E+01	0.1857E+00
0.6500E+01	0.1434E+01	0.1768E+01	0.1892E+00
0.7000E+01	0.1393E+01	0.1727E+01	0.1932E+00
0.7500E+01	0.1361E+01	0.1696E+01	0.1975E+00
0.8000E+01	0.1330E+01	0.1667E+01	0.2020E+00
0.8500E+01	0.1303E+01	0.1642E+01	0.2065E+00
0.9000E+01	0.1280E+01	0.1621E+01	0.2111E+00
0.9500E+01	0.1256E+01	0.1602E+01	0.2156E+00
0.1000E+02	0.1231E+01	0.1579E+01	0.2200E+00
0.1050E+02	0.1210E+01	0.1561E+01	0.2244E+00
0.1100E+02	0.1188E+01	0.1540E+01	0.2287E+00
0.1150E+02	0.1165E+01	0.1518E+01	0.2329E+00
0.1200E+02	0.1135E+01	0.1496E+01	0.2412E+00
0.1300E+02	0.1106E+01	0.1463E+01	0.2472E+00
0.1400E+02	0.1077E+01	0.1445E+01	0.25[illegible]E+00
0.1500E+02	0.1049E+01	0.1422E+01	0.2626E+00
0.1600E+02	0.1020E+01	0.1412E+01	0.2701E+00
0.1700E+02	0.1003E+01	0.1395E+01	0.2773E+00
0.1800E+02	0.9859E+00	0.1378E+01	0.2845E+00
0.1900E+02	0.9576E+00	0.1366E+01	0.2915E+00
0.2000E+02	0.8398E+00	0.1346E+01	0.3017E+00

0.[illegible]E+02	0.9108E+00	0.1329E+01	0.3140E+00
0.2400E+02	0.8787E+00	0.1307E+01	0.3275E+00
0.2600E+02	0.8562E+00	0.1297E+01	0.3398E+00
0.2800E+02	0.8299E+00	0.1280E+01	0.3519E+00
0.3000E+02	0.8018E+00	0.1271E+01	0.3692E+00
0.3400E+02	0.7629E+00	0.1253E+01	0.3912E+00
0.3800E+02	0.7308E+00	0.1243E+01	0.4122E+00
0.4200E+02	0.6888E+00	0.1234E+01	0.4419E+00
0.5000E+02	0.6360E+00	0.1220E+01	0.4785E+00
0.5800E+02	0.5940E+00	0.1219E+01	0.5126E+00
0.6600E+02	0.5548E+00	0.1218E+01	0.5443E+00
0.7400E+02	0.5172E+00	0.1217E+01	0.5751E+00

21. APPENDIX G : LISTINGS OF NUMERICAL RUNS

The listings of all numerical runs of which the results are used for studying the flow and mass transfer characteristics due to a confined laminar impinging two-dimensional jet are given in Tables 21.1, 21.2 and 21.3 for L=2, 4 and 12, respectively. Numerical runs with an initial parabolic velocity profile at the nozzle exit are studied for all three different jet-to-plate spacings. Numerical runs with an initial flat velocity profile at the nozzle exit are studied for the case of L=4 only.

TABLE 21.1 : NUMERICAL RUNS FOR L=2

b_1 = 0.75

Re_b	RUN NO.	nx	ny	DIFFERENCING SCHEME	NOZZLE EXIT PROFILE
1	2B1	55	25	U.W.D.S.	PARABOLIC
100	2B100	55	25	U.W.D.S.	PARABOLIC
	2U100	55	25	U.D.S.	PARABOLIC
200	2B200	55	25	U.W.D.S.	PARABOLIC
	2U200	55	25	U.D.S.	PARABOLIC
300	2B300	55	25	U.W.D.S.	PARABOLIC
	2U300	55	25	U.D.S.	PABABOLIC
400	2B400	55	25	U.W.D.S.	PARABOLIC
	2U400	55	25	U.D.S.	PARABOLIC

TABLE 21.2 : NUMERICAL RUNS FOR L=4

$b_1 = 0.25$

Re_b	RUN NO.	nx	ny	DIFFERENCING SCHEME	NOZZLE EXIT PROFILE
1	4B1	55	25	U.W.D.S.	PARABOLIC
	4F1	55	25	U.W.D.S.	FLAT
100	4B100	55	25	U.W.D.S.	PARABOLIC
	4U100	55	25	U.D.S.	PARABOLIC
	4F100	55	25	U.W.D.S.	FLAT
200	4B200	55	25	U.W.D.S.	PARABOLIC
	4U200	55	25	U.D.S.	PARABOLIC
	4F200	55	25	U.W.D.S.	FLAT
300	4B300	55	25	U.W.D.S.	PARABOLIC
	4U300	55	25	U.D.S.	PARABOLIC
	4F300	55	25	U.W.D.S.	FLAT
400	4B400	55	25	U.W.D.S.	PARABOLIC
	4U400	55	25	U.D.S.	PARABOLIC
	4F400	55	25	U.W.D.S.	FLAT

TABLE 21.2 (CONTINUED)

b_1 = 0.75

Re_b	RUN NO.	nx	ny	DIFFERENCING SCHEME	NOZZLE EXIT PROFILE
100	4Q100	55	25	U.W.D.S.	PARABOLIC
	4W100	55	25	U.D.S.	PARABOLIC
200	4Q200	55	25	U.W.D.S.	PARABOLIC
	4W200	55	25	U.D.S.	PARABOLIC
300	4Q300	55	25	U.W.D.S.	PARABOLIC
	4W300	55	25	U.D.S.	PARABOLIC
400	4Q400	55	25	U.W.D.S.	PARABOLIC
	4W400	55	25	U.D.S.	PARABOLIC

TABLE 21.3 : NUMERICAL RUNS FOR L=12

b_1 = 0.075

Re_b	RUN NO.	nx	ny	DIFFERENCING SCHEME	NOZZLE EXIT PROFILE
1	12B1	55	25	U.W.D.S.	PARABOLIC
100	12B100	67	25	U.W.D.S.	PARABOLIC
	12U100	67	25	U.D.S.	PARABOLIC
200	12B200	67	25	U.W.D.S.	PARABOLIC
	12U200	67	25	U.D.S.	PARABOLIC
300	12B300	67	25	U.W.D.S.	PARABOLIC
	12U300	67	25	U.D.S.	PABABOLIC
400	12B400	69	25	U.W.D.S.	PARABOLIC
	12U400	69	25	U.D.S.	PARABOLIC